# Bone and Tooth Microstructure in Extinct and Extant Mammals and Implications for Growth and Life History Evolution, with an Emphasis on Cervids as a Case Study

---

**Dissertation**
**zur**
**Erlangung der naturwissenschaftlichen Doktorwürde**
**(Dr. sc. nat.)**
**vorgelegt der**
**Mathematisch-naturwissenschaftlichen Fakultät**
**der**
**Universität Zürich**
**von**

**Christian Kolb**

**aus**
**Deutschland**

**Promotionskomitee**
**Prof. Dr. Marcelo R. Sánchez-Villagra**
**(Leitung der Dissertation und Vorsitz)**
**PD Dr. Torsten M. Scheyer**
**Prof. Dr. Arpat Ozgul**
**Dr. Loïc Costeur (Gutachter)**

**Zürich, 2016**

**To my family**

# BONE AND TOOTH MICROSTRUCTURE IN EXTINCT AND EXTANT MAMMALS AND IMPLICATIONS FOR GROWTH AND LIFE HISTORY EVOLUTION, WITH AN EMPHASIS ON CERVIDS AS A CASE STUDY

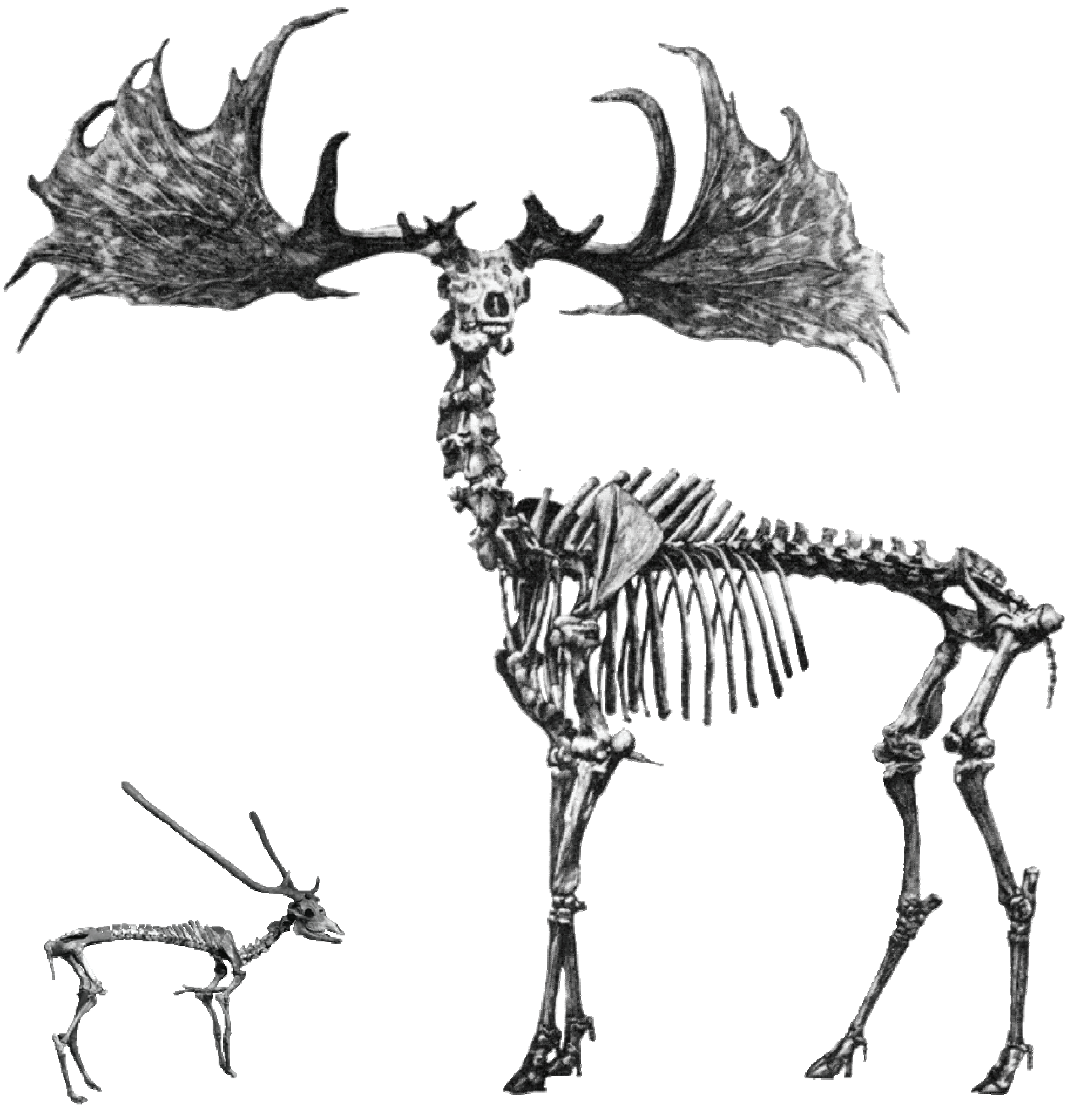

Christian Kolb

Universität Zürich, 2016

Title page image:

Extreme size variation within fossil cervids, exemplified by the insular dwarf deer *Candiacervus* sp. II and the giant deer *Megaloceros giganteus*.

Sources: van der Geer et al. (2006), Gould (1974)

# CONTENTS

## Acknowledgements

There are many people I am indebted to since they helped me finishing this dissertation in different ways. First of all, I thank my supervisor Prof. Dr. Marcelo R. Sánchez-Villagra for his continuous support, enthusiasm, encouragement, and veritable interest in my work. Not least because of fruitful discussions and constructive criticism raised by him, the success and kind of this dissertation became possible. PD Dr. Torsten M. Scheyer is thanked for his constant sustainment and good advice and Prof. Hugo Bucher for being an encouraging director. Further I would like to thank the Schweizerischer Nationalfonds (SNF), the Forschungskredit of the University of Zurich, and the Deutscher Akademischer Austauschdienst (DAAD) for financial support. Many thanks for his advice go to Prof. Arpat Ozgul (Institut für Evolutionsbiologie und Umweltwissenschaften, Universität Zürich, Switzerland), the third member of my committee. Dr. Loïc Costeur (Naturhistorisches Museum Basel, Switzerland) is thanked for reviewing this dissertation.

Cordial thanks go to co-authors/colleagues for granting access to collections for histological sampling, fruitful discussions, and important advice: Adrian M. Lister and Emma Bernard (Natural History Museum, London, UK), John de Vos (Naturalis, Leiden, The Netherlands), Gertrud E. Rössner (Bayerische Staatssammlung, München, Germany), Nigel T. Monaghan (National Museum of Ireland, Dublin), Frank Zachos and Alexander Bibl (Naturhistorisches Museum Wien, Austria), Christian Stauffer (Wildnispark Zürich, Switzerland), Renate Lücht and Heiner Luttman (Zoologisches Institut der Universität Kiel, Germany), Marianne Haffner and Barbara Oberholzer (Zoologisches Museum der Universität Zürich, Switzerland), Heinz Furrer, Christian Klug, and Winand Brinkmann (Paläontologisches Institut und Museum, Universität Zürich, Switzerland (PIMUZ)), Loïc Costeur (Naturhistorisches Museum Basel), George Lyras (Museum of Paleontology and Geology, University of Athens, Greece), Hiroyuki Taruno (Osaka Museum of Natural History, Japan), Ebru Albayrak (MTA Natural History Museum, Ankara, Turkey), Christine Argot, Christine Lefèvre, and Joséphine Lesur (Muséum National d'Histoire Naturelle, Paris, France), Christiane Funk (Museum für Naturkunde, Berlin), and Analia M. Forasiepi (CONICET, Mendoza, Argentina).

I also would like to thank the following co-authors/colleagues for scientific and methodological collaboration as well as helpful advice: Eli Amson (Museum für Naturkunde, Berlin, Germany), Concepcion Azorit (University of Jaen, Spain), Kristof Veitschegger (PIMUZ), Alexandra A. E. van der Geer (Naturalis, Leiden, The Netherlands), Shoji Hayashi (Osaka Museum of Natural History, Japan), Margaretha A. J. Schlingemann (Leiden

University, The Netherlands), Pierre-Olivier Antoine (Institut des Sciences de l'Evolution-Montpellier, France), Hatem Alkadhi (UniversitätsSpital Zürich), Alexandra Houssaye (Muséum National d'Histoire Naturelle, Paris, France), Valentin Fischer (Géologie, Université de Liège, Belgium), P. Martin Sander (Steinmann-Institut, Universität Bonn, Germany), and Jasmina Hugi (PIMUZ).
The collaboration with all these persons was my pleasure and an honour.

Many thanks go to Heike Götzmann for administrative support and Heinrich Walter for IT sustainment. I thank Vivien Jaquier, Fiona Straehl, Madeleine Geiger, and Sarah Bolliger (all PIMUZ) for help with the preparation of thin sections and Stephan Spiekman (Leiden University, The Netherlands) and Philipp Münst (University of Zurich, Switzerland) for preliminary data acquisition and analysis. Ashley Latimer (PIMUZ) and Cathy Ridgway are thanked for English corrections in chapter 2. Alexandra Wegmann, Markus Hebeisen, Rosi Roth, Jérôme Gapany, and Sabine Schenk (all PIMUZ) are thanked for various support.

During the course of my dissertation I had the luck to share offices with great colleagues and friends who helped me through difficult times and I would like to thank them heartily for their support, encouragement, understanding, and many fruitful discussions on not only our scientific projects but also, family, friends, beer, football, and everything under the sun: James Neenan, Juan Carrillo, Ashley Latimer, Gabriel Aguirre Fernandez, and Madeleine Geiger. Many thanks also go to all the other members of the PIMUZ that shared their time in and outside the institute with me and my family. Moreover, I would like to thank all my friends from outside the PIMUZ for their sustainment and encouragement.

There is no doubt that all this would not have been possible with the incredible sustainment, understanding, and encouragement I received from my family: My wife Melanie, my daughter Theresa who was born during the course of this dissertation, my mother Marianne, my father Günter who sadly passed away during the course of this dissertation, and my brother Alexander and his family. I hereby would like to thank them from my deepest heart for everything.

## Summary

Since pioneering works in the middle of the 19th century, our knowledge of the histology of hard tissues of mammals has much increased. It has been demonstrated that bone and tooth histological traits correlate with biological variables and provide reliable estimates of growth and life history patterns in mammals. The variation of the key trait body size within clades of this group is common, especially if we consider extinct species. The developmental and life history changes behind this evolutionary pattern are a rich subject of investigation. This dissertation aims at investigating bone and tooth microstructure as markers of such changes.

In chapters 1.7 and 2, the knowledge and methods on synapsid (modern mammals as well as extinct ancestors and close relatives) bone microstructure and palaeohistology were systematically reviewed. Potential future research fields and techniques were discussed. Synapsid bone shows a large variety of bone tissues: Woven-fibred bone (disorganised), parallel-fibred bone, lamellar bone (arranged in thin layers), and fibrolamellar bone (mixture of woven-fibred and parallel-fibred/lamellar bone). New bone histological data on two extant marsupial species and of several extinct mainland and island placental mammals are presented. The bone cortex of extant marsupials consists of mainly parallel-fibred bone with a varying orientation of vascular canals. *Hippopotamus minor*, an extinct dwarf island hippopotamid from the Late Pleistocene (~126 –12 kya) of Cyprus, shows fibrolamellar bone with a reticular (anastomosing) to plexiform (circumferential with radial connections) arrangement of vascular canals. *Mikrotia magna*, an extinct island rodent from the Late Miocene (~12–5 Mya) of Gargano, shows parallel-fibred primary bone with reticular vascularisation whereas another extinct island rodent, the dormouse *Leithia* sp. from the Pleistocene (~2.6-0.012 Mya) of Sicily, displays lamellar primary bone and a high amount of remodelling. The bone cortex of one continental and three island species of the extinct lagomorph *Prolagus* is characterised mainly by parallel-fibred primary bone with varying orientation of vascular canals. *Paraceratherium* sp. from the Late Oligocene (~28-23 Mya) of Turkey, the extinct giant rhinocerotoid, is represented by dense Haversian bone. *Sinomegaceros yabei*, the extinct Japanese giant deer from the Late Pleistocene, is characterised by high growth rates. Bone histological and skeletochronological (based on growth mark analysis) traits of sampled island mammals in comparison to mainland relatives suggest the presence of various modes of life history modifications on islands to depend on factors of island evolution such as island size, distance from mainland, time of evolution, climate, and phylogeny.

# SUMMARY

Deer (Cervidae) represent an ideal case study for exploring body size and life history evolution, as they are characterised by a rich fossil record, a generally well-known phylogeny, and exceptional examples of body size evolution. In chapter 3, the hard tissue histology of eight deer species, including the illustrative genus *Candiacervus* with two dwarfed morphotypes from the Pleistocene of Crete, and the extinct giant deer *Megaloceros giganteus*, both closely related to the recent fallow deer, *Dama dama*, was examined. Long bones of all deer species sampled mainly possess primary plexiform fibrolamellar bone indicating a comparable mode of growth. Dwarf *Candiacervus* are characterised by low absolute growth rates, *Megaloceros giganteus* by high rates, and *Dama dama* by intermediate to low ones. The small, basal deer from the Early Miocene (~23-16 Mya), *Procervulus praelucidus*, shows the lowest growth rates recorded. Growth rates as derived by Sander & Tückmantel (2003) plotted against the anteroposterior bone diameter as a proxy for body mass indicate three groups: A group showing low growth rates, including dwarf *Candiacervus* and *Procervulus,* an intermediate group with *Capreolus capreolus* (roe deer) and *Muntiacus muntjak* (Indian muntjac), and one with high growth rates including *Megaloceros giganteus*, *Alces alces* (elk), *Cervus elaphus* (red deer), and *Dama dama*. Dwarf *Candiacervus* and *Procervulus praelucidus* indicate late attainment of skeletal maturity. Two senile *Megaloceros* specimens revealed, after tooth cementum analysis, ages of 16 and 19 years whereas two old dwarf *Candiacervus* specimens gave ages of 12 and 18 years. In an allometric (in relation to body size) context, dwarf *Candiacervus* therefore had an extended lifespan compared to deer of similar body size. After comparison with other clades of mammals, it is concluded that various modes of skeletal tissue modification in evolution are linked with changes in size and life history that have occurred in parallel.

In chapter 4, the histological dataset on cervids presented in chapter 3 was expanded. The long bone histology of the extinct "basal" deer *Dicrocerus elegans* and *Euprox* sp. from the Miocene (~23-5 Mya) was examined. Those species together with growth rates of the extinct Japanese giant deer, *Sinomegaceros yabei*, were included in the dataset of chapter 3 and ancestral growth rates among cervids and their correlation with body size were estimated. *Dicrocerus* shows a relatively high growth rate for its body size and attainment of skeletal maturity after five years. The growth rate condition found in *Procervulus* and *Euprox* is different and documents diversity in life history evolution of Miocene cervids.

Scaling of skeletal elements in relation to size is a fundamental question of biology. By broad sampling of a wide range of body sizes, previous examinations have discovered general principles. However, for understanding scaling patterns of bones, it is essential to consider effects of confounding factors related to different lifestyles. In chapter 5, cervids, comprising various body sizes in contrast to a relatively uniform lifestyle, were comprehensively sampled and the mid-diaphyseal structure of their long bones was studied. Compactness parameters do not scale allometrically in cervid long bones. However, femoral cross-sectional shape scales positively allometric. This points towards greater directional bending rigidity in large-sized taxa. Relative cortical thickness (P) is more constrained in large-sized taxa. Therefore, it is concluded that tubular bones of large-sized terrestrial animals are more intensively selected for an energy-saving mid-diaphyseal structure since the P parameter is known to be centred around a mass-saving biomechanical optimum.

**Keywords**: Mammals, Palaeohistology, Body size, Life history, Island evolution, Bone tissue, Cementum analysis, Cervids, Marsupialia, Rodentia, *Prolagus*, *Hippopotamus*, *Deinogalerix*, *Paraceratherium*

## Zusammenfassung

Seit bahnbrechenden Arbeiten in der Mitte des 19. Jahrhunderts hat unser Wissen über die Histologie von Hartgeweben stark zugenommen. Es ist gezeigt worden, dass knochen- und zahnhistologische Merkmale mit biologischen Grössen korrelieren und verlässliche Schätzungen von Wachstum und Lebenszyklusmustern innerhalb der Säugetiere liefern. Die Veränderlichkeit des Schlüsselmerkmals Körpergrösse innerhalb von Säugetiergruppen ist verbreitet, vor allem bei der Betrachtung ausgestorbener Arten. Die Entwicklungs- und Lebenszyklusveränderungen hinter diesem evolutionären Muster stellen ein umfassendes Forschungsgebiet dar. Diese Dissertation hat zum Ziel, die Mikrostruktur von Knochen und Zähnen als Anzeiger solcher Veränderungen zu untersuchen.

In den Kapiteln 1.7 und 2 wurde bezüglich des gegenwärtigen Stands des Wissens und der Methodik zur Knochenmikrostruktur und Paläohistologie von Synapsiden (moderne Säugetiere sowie ausgestorbene Vorfahren und nahe Verwandte) Rückschau gehalten. Potentiell zukunftsträchtige Forschungsgebiete und Techniken wurden diskutiert. Der Knochen von Synapsiden zeigt eine grosse Vielfalt von Knochengeweben: Faserknochen (ungeordnet), parallelfaseriger Knochen, lamellärer Knochen (in dünnen Lagen angeordnet) und fibrolamellärer Knochen (Mischung aus Faserknochen und parallelfaserigem/lamellärem Knochen). Neue knochenhistologische Daten von zwei lebenden Beuteltierarten und mehreren ausgestorbenen Festland- und Inselsäugerarten werden präsentiert. Die Knochenrinde heute lebender Beuteltiere besteht hauptsächlich aus parallelfaserigem Knochen mit unterschiedlichen Orientierungen der Gefässkanäle. *Hippopotamus minor*, ein ausgestorbenes, verzwergtes Inselflusspferd aus dem Jungpleistozän (vor ca. 126000–12000 Jahren), zeigt fibrolamellären Knochen mit einer retikulären (verflechtet) bis plexiformen (umlaufend mit radiären Verbindungen) Anordnung von Gefässkanälen. *Mikrotia magna*, ein ausgestorbenes Inselnagetier aus dem Obermiozän (vor ca. 12–5 Millionen Jahren) von Gargano, zeigt parallelfaserigen Knochen mit retikulärer Gefässversorgung während ein weiterer ausgestorbener Inselnager, der Bilch *Leithia* sp. aus dem Pleistozän (vor ca. 2.6-0.012 Millionen Jahren) von Sizilien, lamellären Primärknochen und einen hohen Anteil an Knochenumbau zeigt. Die Knochenrinde von einer kontinentalen und drei Inselarten des ausgestorbenen Hasenartigen (Lagomorpha) *Prolagus* wird hauptsächlich durch parallelfaserigen Primärknochen mit unterschiedlicher Orientierung von Gefässkanälen charakterisiert. *Paraceratherium* sp. aus dem Oberoligozän (vor ca. 28-23 Millionen Jahren) der Türkei, der ausgestorbene, riesige Nashornartige (Rhinocerotoidea), wird in seiner Knochenrinde von dichtem Havers‘schem Knochen repräsentiert. *Sinomegaceros yabei,* der

ausgestorbene japanische Riesenhirsch aus dem Oberpleistozän, wird durch hohe Wachstumsraten charakterisiert. Knochenhistologische und skelettochronologische (basierend auf der Analyse der Wachstumsmarken) Merkmale der beprobten Inselsäugetiere im Vergleich mit deren Festlandsverwandten zeigen an, dass das Vorhandensein von unterschiedlichen Arten von Lebenszyklusveränderungen auf Inseln abhängig von inselevolutiven Faktoren wie Inselgrösse, Distanz zum Festland, Evolutionszeit, Klima, und Phylogenie (Stammesgeschichte) ist.

Hirsche (Cervidae) stellen eine ideale Fallstudie dar um die Evolution von Körpergrösse und Lebenszyklus zu erforschen, da sie durch einen reichen Fossilbericht, eine generell wohlbekannte Phylogenie und aussergewöhnliche Beispiele von Körpergrössenevolution charakterisiert sind. In Kapitel 3 wurde die Hartgewebshistologie von acht Hirscharten einschliesslich der anschaulichen Gattung *Candiacervus* mit zwei verzwergten Morphotypen aus dem Pleistozän von Kreta, und des ausgestorbenen Riesenhirsches *Megaloceros giganteus*, beide nahe verwandt mit dem heute lebenden Damhirsch, *Dama dama*, untersucht. Langknochen aller beprobten Hirscharten besitzen hauptsächlich primären plexiformen, fibrolamellären Knochen, der eine vergleichbare Art zu wachsen anzeigt. Zwerg-*Candiacervus* sind durch niedrige, absolute Wachstumsraten charakterisiert, *Megaloceros giganteus* durch hohe und *Dama dama* durch mittlere bis niedrige Raten. Der kleine, “ursprüngliche” Hirsch aus dem Untermiozän (vor ca. 23-16 Millionen Jahren), *Procervulus praelucidus*, zeigt die niedrigsten verzeichneten Wachstumsraten. Sander & Tückmantel (2003) folgende Wachstumsraten, aufgetragen gegen den anteroposterioren (vorne-hinten) Knochendurchmesser als ein Näherungswert für Körpermasse, zeigen drei Gruppen an: Eine Gruppe, die niedrige Wachstumsraten einschliesslich Zwerg-*Candiacervus* und *Procervulus* zeigt, eine mittlere Gruppe mit *Capreolus capreolus* (Reh) und *Muntiacus muntjak* (Indischer Muntjak), und eine mit hohen Raten einschliesslich *Megaloceros giganteus*, *Alces alces* (Elch), *Cervus elaphus* (Rothirsch), und *Dama dama*. Zwerg-*Candiacervus* und *Procervulus* zeigen ein spätes Erreichen der skelettalen Reife an. Zwei alte *Megaloceros*-Exemplare offenbarten nach einer Zahnzementanalyse Alter von 16 und 19 Jahren, während zwei alte Zwerg-*Candiacervus*-Exemplare Alter von 12 und 18 Jahren anzeigten. In einem allometrischen (im Verhältnis zur Körpergrösse) Kontext hatten Zwerg-*Candiacervus* daher eine verlängerte Lebensspanne verglichen mit anderen Hirschen ähnlicher Körpergrösse. Nach dem Vergleich mit anderen Säugetiergruppen wird geschlussfolgert, dass verschiedene Arten von

Skelettgewebsveränderungen im Verlauf der Evolution mit Veränderungen der Grösse und des Lebenszyklus verbunden sind, welche sich parallel ereignet haben.

In Kapitel 4 wurde der histologische Datensatz der Hirsche, welcher in Kapitel 3 präsentiert wird, erweitert. Die Knochenhistologie der ausgestorbenen, ursprünglichen Hirsche *Dicrocerus elegans* und *Euprox* sp. aus dem Miozän (vor ca. 23-5 Millionen Jahren) wurde untersucht. Diese Arten, zusammen mit Wachstumsraten des ausgestorbenen japanischen Riesenhirsches, *Sinomegaceros yabei*, wurden in den Datensatz von Kapitel 3 eingeschlossen und die ursprünglichen Wachstumsraten und deren Korrelation mit der Körpergrösse innerhalb der Hirsche wurden abgeschätzt. *Dicrocerus* zeigt relativ hohe Wachstumsraten für seine Körpergrösse und ein Erreichen der skelettalen Reife nach fünf Jahren. Die Beschaffenheit der Wachstumsrate in *Procervulus* und *Euprox* ist unterschiedlich und dokumentiert die Vielfältigkeit der Evolution des Lebenszyklus der miozänen Hirsche.

Die Skalierung von Skelettelementen im Verhältnis zur Körpergrösse ist eine fundamentale Frage der Biologie. Durch die breite Beprobung einer weiten Spanne an Körpergrössen haben vorherige Untersuchungen allgemeine Prinzipien entdeckt. Jedoch um die Skalierungsmuster von Knochen zu verstehen, ist es wesentlich die Effekte von verfälschenden Einflüssen entsprechend unterschiedlicher Lebensweisen zu berücksichtigen. In Kapitel 5 wurden die Hirsche, welche verschiedene Körpergrössen im Gegensatz zu einer relativ einheitlichen Lebensweise zeigen, beprobt, und die Struktur des mittleren Knochenschaftes ihrer Langknochen wurde untersucht. Kompaktheitsparameter skalieren nicht allometrisch in Hirschlangknochen. Jedoch skaliert der Querschnittsdurchmesser der Oberschenkelknochen positiv allometrisch. Dies weist auf eine grössere gerichtete Biegefestigkeit in gross gewachsenen Taxa hin. Die relative Dicke der Knochenrinde (P) ist niedriger in gross gewachsenen Taxa. Daher wird geschlussfolgert, dass Röhrenknochen von gross gewachsenen Landtieren stärker nach energiesparenden Strukturen des mittleren Knochenschaftes selektiert werden, da der P-Parameter dafür bekannt ist, dass er um ein Masse einsparendes, biomechanisches Optimum zentriert ist.

**Schlüsselwörter**: Säugetiere, Paläohistologie, Körpergrösse, Lebenszyklus, Inselevolution, Knochengewebe, Zementanalyse, Hirsche, Marsupialia, Rodentia, *Prolagus*, *Hippopotamus*, *Deinogalerix*, *Paraceratherium*

# CHAPTER 1

# INTRODUCTION

# 1 Introduction

## 1.1 Body size and island evolution

Body size is a key trait of organisms (e.g. Schmidt-Nielsen 1984, Bonner 2006). The fossil record presents spectacular examples of body size evolution, such as the largest insects (giant dragonflies of the Late Palaeozoic; Dudley 1998), the largest terrestrial animals ever, the sauropod dinosaurs (Sander et al. 2011), and the largest mammal that ever walked the earth, the rhinocerotoid *Paraceratherium* (Antoine et al. 2008).

Island settings present body size anomalies that are among the most spectacular phenomena in nature, including plants as well as animals (Lomolino 2010, 2012). Following island isolation, several lineages of mammals have evolved remarkable changes in body size (Foster 1964, Lomolino 1985, Lomolino et al. 2013), including among others dwarf hippopotamuses, elephants, deer (Figure 1), and giant rabbits (van der Geer et al. 2010). This phenomenon was already reported by Forsyth Major in 1902. Van Valen (1973) considered this pattern general enough to label it the "Island Rule", which is now described as a graded trend from gigantism in small species to dwarfism in large species (Lomolino 1985, 2005), but exceptions have been documented (Meiri et al. 2008). Various authors have explored and reviewed this topic since then (e.g. Benton et al. 2010, van der Geer et al. 2010, van der Geer 2014, Lomolino et al. 2012, 2013).

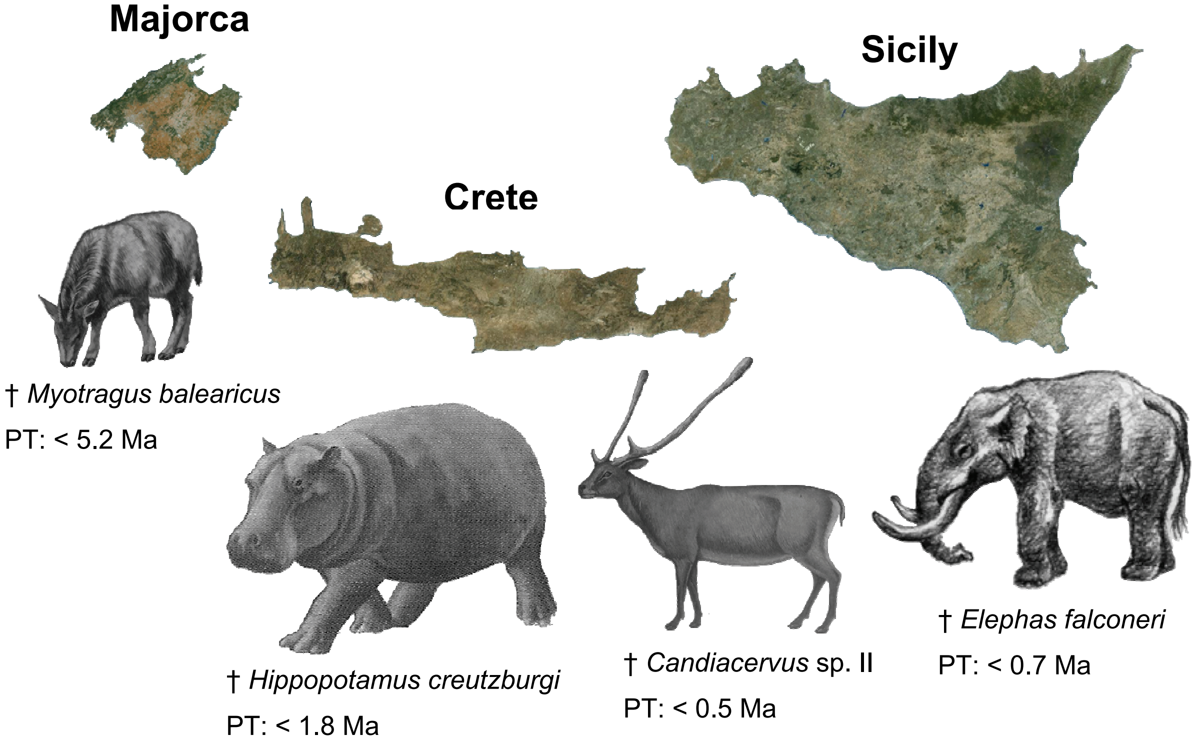

**Figure 1:** Islands (to scale) and examples of their Plio-Pleistocene dwarf mammals. Note the extreme long persistence time (PT) of the bovid *Myotragus* on Majorca in comparison to other island mammals such as *Hippopotamus* and *Candiacervus* from Crete and *Elephas* from Sicily (sources: Benton et al. 2010, van der Geer et al. 2009, 2010, www.google.ch/maps).

The degree of body size change decreases from species of extreme, ancestral (mainland) size to those of intermediate ancestral size, and has been accordingly called "graded" (Lomolino et al. 2012). Insular body size changes associated to the island rule potentially offer insights into essential factors driving biodiversity in general, i.e. mainland and island communities. As a consequence, not only causal explanations of island patterns but also those of body size evolution on the mainland can be explored. Although the optimum is predicted to vary with the bauplan and trophic strategy of the species studied, the body size of extant mammals on isolated islands converges on a relatively narrow range of intermediate sizes (about 100 to 500 g), and is therefore hypothesized to be optimal for mammals (Lomolino 2005, Lomolino et al. 2012). Ecological interactions seem to play a central role in driving body size diversification in lineages on the mainland over evolutionary time, in many cases following Cope's rule (e.g. Alroy 1998, Kingsolver and Pfennig, 2004). Potentially fast reversals in this trend on islands seem not to be only related to isolation or limited area and resources, but also to their impoverished faunas (Millien 2006, Lomolino et al. 2012), i.e. ecological character displacement and character release (Simberloff et al. 2000, Grant and Grant 2006). This ecological release hypothesis predicts that the direction and magnitude of body size evolution, and the underlying selection forces should be dependent on the size and trophic strategies of both the species under study and those species with which they interact (Lomolino et al. 2012; Figure 2). Lomolino et al. (2012) discussed several other hypotheses on insular body size evolution to be complementary, as elaborated below.

More isolated islands should be colonised by a subset of source populations biased in favour of the larger individuals and larger species since larger individuals should have greater physiological endurance and dispersal capacities. This theory is called the immigrant selection-thrifty genotype hypothesis (Figure 2) and predicts that the body size of insular populations of especially small species (more limited by dispersal distances) should increase with island isolation (Neel 1962, Bindon and Baker 1997, Lomolino 1985). The resource limitation hypothesis (Figure 2) predicts selection for smaller individuals on islands because resource requirements tend to increase with body size, whereas area and total productivity of islands are more limited, and densities of many island populations are higher.

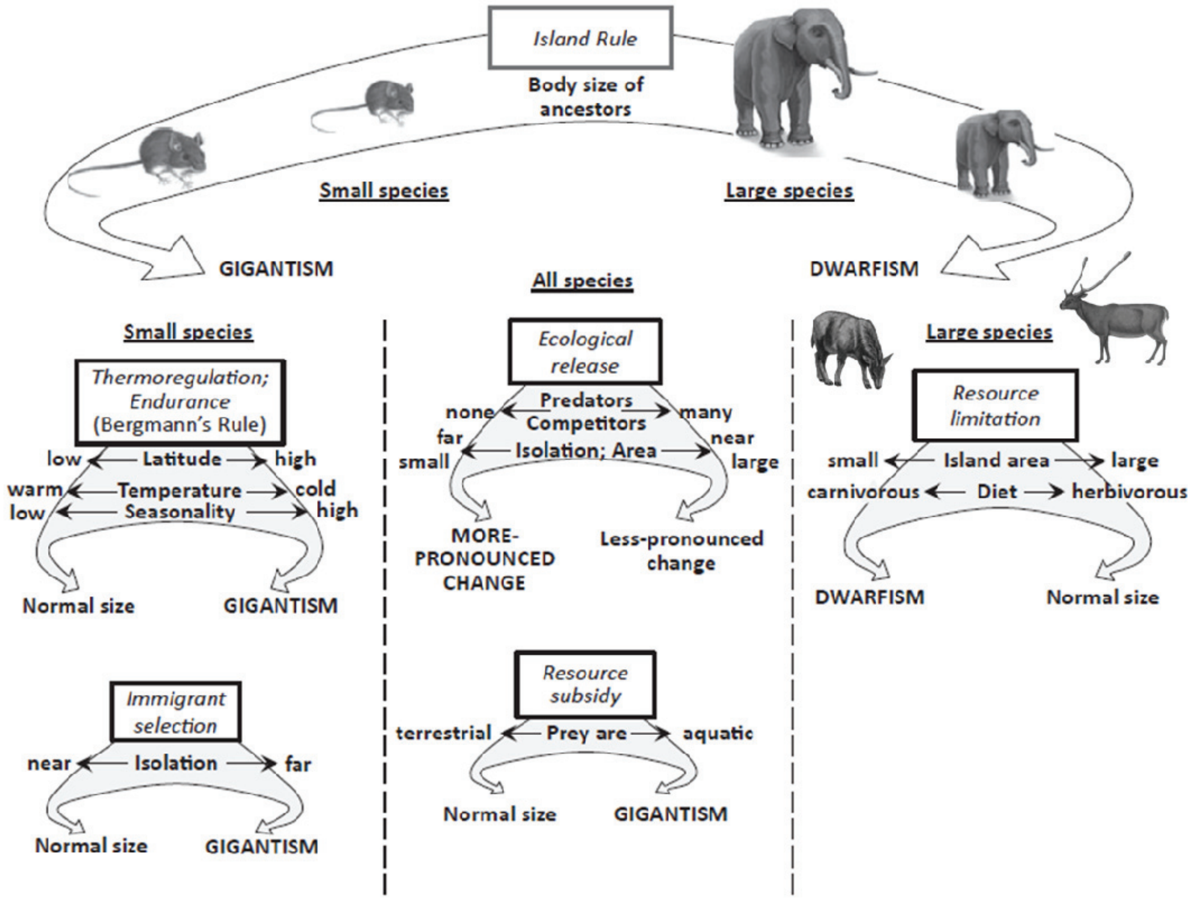

**Figure 2:** The "Island Rule" and its effects. Selective forces (in rectangles), associated variables (below), and predicted effects (below the arrows) on islands (modified from Lomolino et al. 2012).

For larger species, this selection should be most intense since their resource requirements are more likely to approach carrying capacities of the island studied. The influence of diet and habitat is expected to be high, i.e. smaller sizes in terrestrial carnivores than in herbivores, larger sizes in island species that feed on aquatic prey such as otters and bears (Lomolino et al. 2012). The most familiar ecogeographic rule is probably Bergmann's rule (Bergmann, 1847; Figure 2), stating that body size of mammals and other vertebrates increases with latitude, since larger mammals have an advantage in cold climates for more insulation (thermoregulation) and greater energy stores (endurance) (Calder 1974, McNab 2002).

Within the compound interplay of variables influencing patterns of island evolution as described above, ecological release and/or resource limitation amplified by isolation time are discussed to be the main selective forces (Figure 2; Palkovacs 2003, Köhler et al. 2009, van der Geer et al. 2010, Lomolino et al. 2012, 2013). In line with Lomolino et al. (2012), McClain et al. (2013) found the island rule to be a complex phenomenon driven by interacting intrinsic and extrinsic mechanisms and that the pattern of size shifts reflects multiple processes.

## 1.2 Hard tissue palaeohistology – a tool for decipherment of life histories

Palaeohistology of hard tissues is a powerful tool to understand the mechanisms of life-history and size evolution on islands. This is also the case for fossil mainland lineages displaying significant body size changes such as 'dwarf ' and 'giant' sauropod (Erickson et al. 2001, Sander and Andrassy 2006, Sander et al. 2011) and tyrannosaurid (Erickson et al. 2004) dinosaurs, as well as early synapsids (Chinsamy-Turan 2012a, Huttenlocker and Botha-Brink 2014).

Fossil mammalian bone microstructure can reveal life history traits and therefore inform about developmental schedules in extinct species (Padian and Lamm 2013). In general, mammalian bone exhibits high rates of tissue deposition in juveniles, whereas after onset of maturity a decrease in growth rate occurs, resulting in deposition of highly organised bone tissue (Garcia-Martinez et al. 2011, Chinsamy-Turan 2012b, Marin-Moratalla et al. 2013). Counting lines of arrested growth (LAGs) provides the means to estimate minimum individual ages. Chapter 2 gives an extensive review on the current knowledge in the field of bone palaeohistology.

Unlike bone, dental cementum usually lacks resorption and displays the more complete growth record. Therefore, it is a more accurate source for estimating individual ages and longevity in mammals (Klevezal 1996; as summarised and discussed in section 1.6 below).

## 1.3 Cervids – an ideal case study clade

With 19 genera and 51 species (Grubb 2005) the Cervidae (cervids) are a diverse clade within the Cetartiodactyla. They first appear in the Early Miocene, reached North America in the Late Miocene and entered South America in the late Pliocene or Early Pleistocene (Janis and Scott 1987). Today, cervids are distributed worldwide and are found in a wide variety of habitats, from the arctic tundra to tropical forests (Groves 2007, Vaughan et al. 2015).

The Cervidae are pecoran ruminants with paired frontal outgrowths consisting of a perennial proximal pedicle that carries temporary, distal and more or less regularly cast branched antlers (Janis and Scott 1987, Azanza et al. 2013). As typical faunal components, cervids are in general continuously documented in the fossil record and cover a rather uniform lifestyle but a wide range of body sizes, from ca. 10 kg for *Pudu puda* (Tacutu et al. 2013) to ca. 600 kg for *Alces alces* (Franzmann 1981). Spectacular cases of body size reduction on islands are documented within cervids (Lister 1989, van der Geer et al. 2010). *Candiacervus,* an endemic and extinct clade of deer, presents a remarkable example of island evolution in the

Pleistocene of Crete, including 'dwarfed' species which evolved from the megacerine clade (Megacerini) of partially giant forms (de Vos 1979, 1984, Vislobokova 2012, 2013; see chapter 3). Moreover, phylogenetic relationships of cervids are in general well resolved (e.g. Lister et al. 2005, Gilbert et al. 2006, Hassanin et al. 2012, see chapters 3 and 4). For their rich fossil record, the well-known phylogeny and exceptional examples of body size evolution, deer represent an ideal case study clade for exploring signals and mechanisms of body size and life history evolution as well as function.

## 1.4 Aims and overview

A major aim of evolutionary biology is to understand how organisms have changed in geological time and how natural selection operates. Palaeohistology is an important tool in this endeavour, as it provides data to decode the life history of fossil animals from conception to death (e.g. Ricqlès 1976a, Padian and Lamm 2013; see also chapter 2). Estimation of age and maturity, deciphering of developmental and growth patterns, as well as understanding of activity and reproductive cycles are the main goals of palaeohistology. By integrating data on extant and extinct mammals gained by histological studies, this dissertation aims at providing insights into growth and life history evolution of mainland and island species.

During the last two decades, the interest in mammalian palaeohistology increased dramatically. Since the first recorded research efforts in this subject in 1849 (Quekett 1849a, b), it has been subsequently shown that mammalian bone consists of a large variety of bone tissues and vascularisation patterns which correlate with several biological variables such as age and growth rate (Ricqlès 1976a, Padian 2011). Chapter 2 systematically reviews the knowledge on cynodont and mammalian bone tissue and its applications. Potential future research fields are discussed. New data on extant marsupials and several extinct continental and island placental mammals are presented. It is suggested that various modes of bone histological modification and life history evolution on islands underlie factors such as island size, distance from mainland, and time of evolution.

In chapter 3, body size and life history variation and underlying mechanisms within cervids are explored by methods of bone and dental histology. Dwarfed morphotypes of *Candiacervus*, i.e. *C. ropalophorus* and *C.* sp. II from the Pleistocene of Crete (de Vos 1979, 1984) and the extinct giant deer *Megaloceros giganteus*, both in a clade together with recent *Dama dama* (Lister et al. 2005), constitute ideal case study taxa. Additionally, other mainland cervids are investigated, focusing on bone microstructure in growth series of various long bones and dental histology. Based on rest lines in tooth cementum of first molars of old individuals, longevity estimates are made. The relation between body weight and bone growth rates, as attained by histological analysis for studying growth patterns across cervids and for putting life history data into an allometric context, is investigated. Similar patterns of bone tissue and vascularisation, and therefore a comparable mode of growth across the eight deer species examined, are discovered. Dwarf *Candiacervus* are characterised by low absolute growth rates whereas *Megaloceros giganteus* displays high rates. The Miocene small stem cervid *Procervulus praelucidus* shows the lowest rates recorded. In an allometric context, *Candiacervus* indicates an extended lifespan compared to deer of similar body size. Therefore, it is concluded that changes in size and life history have occurred in parallel in evolution, with various modes of skeletal tissue modification.

In chapter 4, the bone histology and life history of further stem cervids, i.e. *Dicrocerus elegans* (Azanza 1993) and *Euprox* sp. (Gentry et al. 1999) from the Miocene of Europe and those of *Sinomegaceros yabei* from the Pleistocene of Japan (Vislobokova 2013) are investigated. These taxa are included within the dataset of chapter 3 and diversity in life history traits of Miocene cervids is found. The bone cortex of *Dicrocerus* indicates a relatively high growth rate in relation to its body size therefore presenting a different condition than observed in *Procervulus* and *Euprox*.

An essential question in biology is how bone scales to body size. General principles of bone scaling have been discovered in the past by studying a wide range of body sizes (e.g. Alexander et al. 1979, Houssaye et al. 2016). It is essential however, to understand the factors influencing the scaling of bones in relation to different lifestyles. Cervids comprise various body sizes but a relatively uniform lifestyle (Geist 1998). Chapter 5 comprehensively explores the cervid mid-diaphyseal structure of long bones and finds that bone compactness does not scale with allometry. However, the relative thickness of the cortex (P), an indicator of a mass-saving biomechanical optimum, is found to be more constrained in large-sized cervids. Therefore, it is concluded that tubular bones of large-sized terrestrial animals are more intensively selected for an energy saving mid-diaphyseal structure. Moreover, femoral cross-sectional shape scales positively allometric pointing towards greater directional bending rigidity in large-sized taxa.

Additional publications representing an area of my research work that is methodologically related to the main chapters of this thesis are appended to this dissertation. They discuss the bone histology and its palaeobiological implications of a group of extinct marine reptiles, the ichthyosaurs. With their strongly re-shaped body outline including numerous adaptations to a marine lifestyle, the Ichthyosauria were a group of Mesozoic

(Early Triassic – Late Cretaceous) reptiles lacking any modern descendants. Since ichthyosaur fossils occur in excellent preservation worldwide and in abundance, they offer unique opportunities to get insights into the palaeobiology of a long extinct and specialised group of reptiles (Sander 2000a). In appendix 1, a bone histological examination of an ontogenetic series of the basal ichthyosaur *Mixosaurus* is performed for the first time. Growth marks and periosteal fibrolamellar bone indicating high growth rates are found, and that small, Triassic ichthyosaurs already had relatively high metabolic rates, as had been suggested for post-Triassic, derived forms (Buffrénil and Mazin 1990; Motani 2010).

Ichthyosaurs display a wide range of morphologies illustrating diverse marine ecological grades (McGowan and Motani 2003). The anatomical diversity found in ichthyosaurs is expected to match the histological characteristics in their long bones and provide information on locomotor abilities and physiology. In appendix 2, bone histological traits in stylopod bones of various ichthyosaur taxa are analysed. The finds confirm the previous assumptions of high growth rates in ichthyosaurs. Moreover, the occurrence of two remodelling types is described for the first time. Questions about definitions of microanatomical specialisations are raised and the difficulties in determining their occurrence within ichthyosaurs are demonstrated.

## 1.5 Thesis outline

In this thesis I present all chapters subsequent to chapter 1 as fully-formatted and published in peer-reviewed journals (chapters to 2 to 4, and appendix 1 and 2) or in manuscript form (chapter 5). Authors, publication details, and author contributions are provided at the beginning of each chapter whereas supplementary material is provided at the end of each chapter. The following sections lead towards the main chapters of the thesis by addressing new methodological aspects of palaeohistology (1.6) and by reviewing the current knowledge on the bone histology of basal synapsids (1.7).

## 1.6 Excursion: Dental histology in fossil mammals – A method for visualising growth marks in cementum

The histology of teeth provides useful data to investigate patterns and mechanisms of life history evolution (Klevezal 1996). In general, three recording structures are present in recent and fossil tetrapod teeth: enamel, dentin, and cementum (Klevezal 1996, Ungar 2010).

The existing dental tissues differ in chemistry, morphology, and function (Hillson 2005). Klevezal (1996) emphasised the importance of bones but especially teeth as histological recording structures in mammals. Unlike enamel and dentin, root cementum (Figure 3) continues deposition during the whole life of an individual due to compensation of crown wear and is promoting the fixation of a tooth in its alveolus. Since cementum, both acellular and cellular, is formed by cells (cementoblasts) which cover the root from the outside, layers formed later are closer to the outer part of the root. Cellular as well as acellular cementum is divided into strongly mineralised layers called rest or incremental lines.

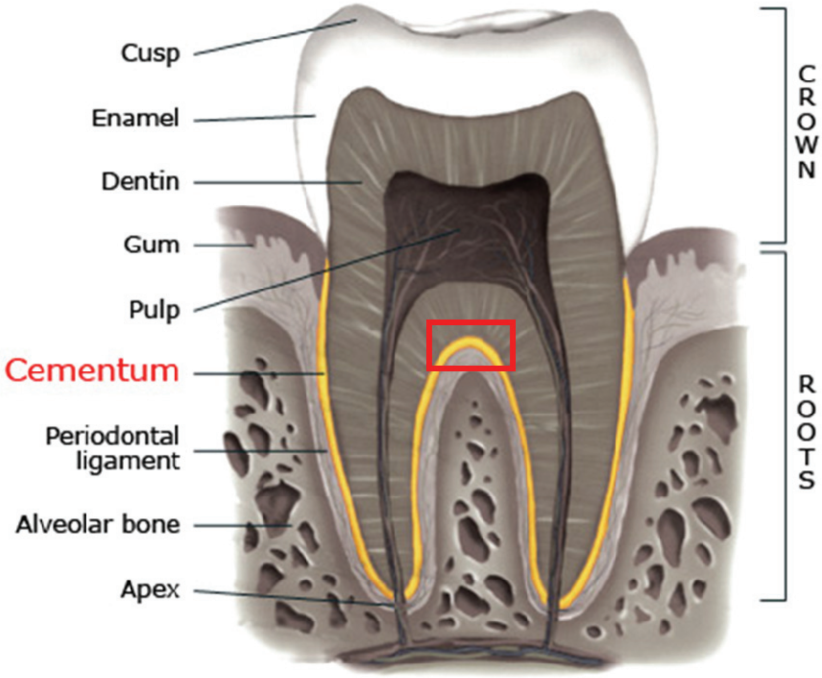

**Figure 3:** Diagram of a human cheek tooth (longitudinal cross section). Red rectangle: Interroot pad of cementum (modified from www.studiodentaire.com).

Tooth cementum as a recording structure offers a life long period of registration and persistence of the growth record. Therefore it is considered as being the most accurate method for age determination in mammals, becoming an essential tool for biological sciences as well as domestic lifestock and wildlife management serving to understand mammal populations in terms of life span, mortality, herd growth, and reaction to ecological factors (see Klevezal 1996 for an overview). Applications of this have been made for example in humans (e.g. Meinl et al. 2008), bears (e.g. Mundy and Fuller, 1964, Willey 1974), and ruminants (Low and Cowan 1963; Reimers and Nordby 1968; Lundervold et al. 2003; Rolandsen et al. 2008). In 1992, Liebermann and Meadow reviewed the current knowledge of development, histology and function of cementum in connection to incremental line formation in *Gazella gazella*. Aitken (1975) (*Capreolus capreolus*), Ohtaishi et al. (1990) (*Cervus albirostris*), and Azorit et al. (2003) (*Cervus elaphus*) determined absolute ages by cementum analysis and correlated them with tooth wear stages. In dental cementum of red deer (*Cervus elaphus hispanicus*), Azorit et al. (2002a) showed that two growth marks are formed per year – a wide mark during spring-summer, called the growth layer, and a thin rest line resulting from decreased growth rate in winter. Therefore, the sequence and appearance of growth layers is regular and seasonal. Azorit et al. (2004) assessed the age at which the first growth layer and the first rest line appear in cementum of incisors, molars, and canines in the Spanish red deer. Moreover, they explained how to interpret growth marks in cementum for age determination. The lower first molar is the first permanent tooth to erupt showing the most complete growth record. The first rest line in the lower first molar is deposited at an age of 6 months.

The value of cementum analysis is widely acknowledged in archaeozoology (e.g. Saxon & Higham 1969, Spiess 1976, Burke & Castanet 1995) although tooth cementum is potentially poorly or only incompletely preserved in fossil specimens (Figure 4).

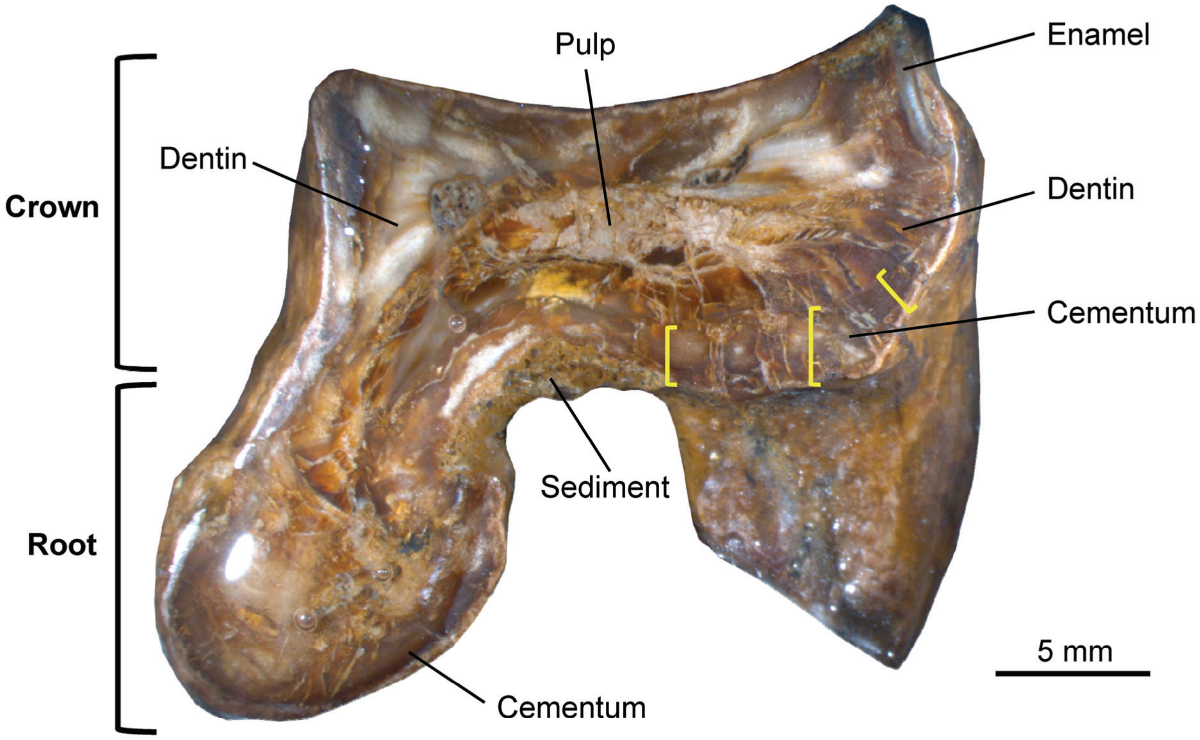

Figure 4: Polished longitudinal section additionally wetted with glycerine of an upper molar of an undetermined Late Miocene macraucheniid South American ungulate. Please note that in the cementum, rest lines were probably obliterated by permineralisation/recrystallisation processes. Yellow brackets mark observable upper (cementum-dentin junction) and lower margins of the cementum pad. (Photo: E. Amson)

Determination of individual ages by cementum analysis is a powerful tool of palaeontology for deciphering the biology and life history of extinct mammals. Debeljak (1996) introduced a technique for cementum analysis in fossil cave bears. By etching ground tooth roots with 15-

25% phosphoric acid and staining with gentianae violet, rest lines in cementum became clearly visible. Jordana et al. (2012) determined 27 years as potential lifespan (longevity) in the island bovid *Myotragus balearicus* from the Balearic Islands by cementum analysis using standard thin sectioning techniques. Aaris-Sorensen & Liljegren (2004) determined an individual age of 23 years for a specimen of the giant deer *Megaloceros giganteus*. Chritz et al. (2009) addressed questions of life history seasonality and successfully applied cementum analysis for *Megaloceros*. Their data indicated that ages of individuals ranged from 6.5 to 14 years. Molars were sectioned across lophs by Chritz et al. using a diamond-tipped saw and were then waterpolished to expose the cementum pad below the crown of each tooth. Polished pieces were observed under a light-reflecting dissecting microscope and annuli (growth layers) were counted by eye.

For the thesis presented here, cementum analysis was applied in several fossil cervid species. Here, I present a protocol and recommendations about a time-saving combination of known palaeohistological methods also applicable to other groups of fossil mammals such as macrauchenid South American ungulates (Figures 4, 6). Debeljak (1996) used phosphoric acid and staining in fossil specimens for achieving high visibility of cementum lines, I applied fine polishing for that purpose.

First, it was essential to choose tooth and cutting plane as expected to present the most complete growth record and distinctness of rest lines. Cervid specimens sampled for the current study, were longitudinally cut through the interroot cementum pad of the lower first molar (Figure 5, Figure 8 of chapter 3; Azorit et al. 2002b). First, teeth and the upper mandibular areas were coated with one layer of Araldite® (XW 396 and Hardener XW 397). After drying of the first layer (24 hours) the lower mandibular area was coated as well with Araldite®. For the drying process, specimens were mounted in plasticine. In case specimens were stable enough, cutting with a diamond-tipped saw as next step was performed (the finer the sawing blade used, the lower the loss of material). Otherwise the mandible was coated with Technovit® (Powder 5071 and Universal Liquid) without covering the lower area of the teeth in order to make identification of the right cutting plane possible. In case suitable for reasons of time and/or method, the second layer of Araldite® can be substituted by a layer of Technovit® (Figure 5). Technovit® can in turn be substituted by thermoplastic (Friendly Plastic®) and is especially useful for collection visits with a lack of time and in absence of a fume hood (see below). Thermoplastic can be repeatedly melted with hot water (ideally around 60 ˚C) or a hairdryer, as it melts and hardens very fast.

**Figure 5:** Longitudinal cut of lower mandible/first molar of *Megaloceros giganteus* (PIMUZ A/V 2235). A) Lingual view of the anterior part of the left mandible. B) View on the polished mandibular/dental surface. Araldite® (transparent) and Technovit® (green) coating and additional embedding of cutting surface. The cementum area was polished to a grain size of 8000.

In case preservation of specimens was stable enough (most cases), the cementum area could be directly polished under use of water with polishing papers ideally in the following order (from rough to fine): 240, 400, 600, 1500, 1800, 4000, 8000 and higher if required. In case of brittle preservation, cutting surfaces had to be impregnated with Araldite® 2020.

Finally, cementum analysis was performed with a light-reflecting binocular microscope under usage of different light conditions for identification of rest lines. A Leica DFC 420 °C digital camera was used for taking micrographs. In cases of inhomogeneous preservation of specimens and mobilisation of hard particles during the grinding and polishing process, it can be difficult to achieve the desired polishing effect. In those cases the use of glycerine helps detecting rest lines in cementum (Figures 4, 6).

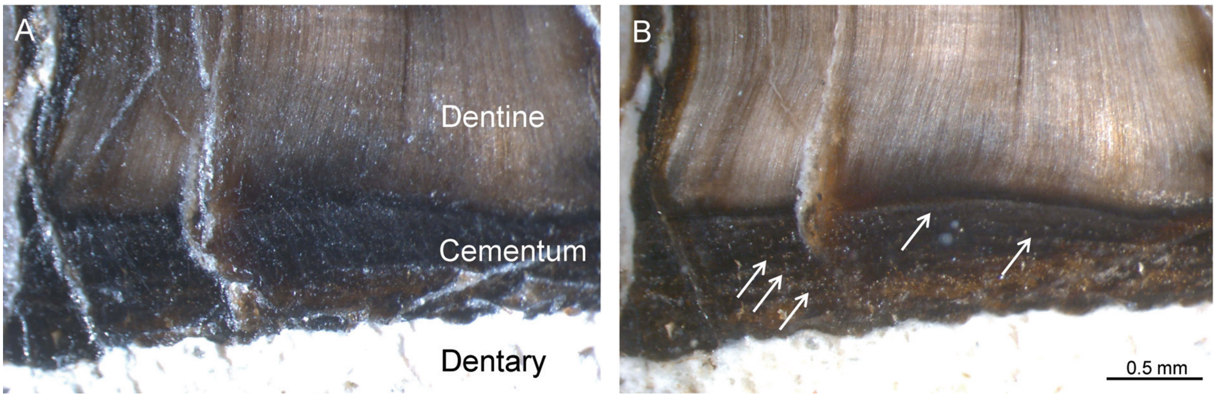

**Figure 6:** The glycerine effect. Polished longitudinal section of the upper first molar of the Early Miocene macraucheniid *Theosodon garrettorum* (PIMUZ A/V 4662) photographed without (A) and with (B) the use of glycerine. Please note that in (B) rest lines (white arrows) within the cementum are visible.

## 1.7 Bone histology of non-cynodont synapsids – a review

The following sections synthesise the current knowledge on the bone histology of major groups of early synapsids and lead the reader towards chapter 2. Comments of the reviewers of the original submission to the journal were addressed, see acknowledgements in chapter 2.

*Non-therapsid synapsids*- More than 320 Myr ago during the Carboniferous, reptilian-grade amniotes and synapsids, the lineage leading to mammals including "basal" forms such as edaphosaurids and sphenacodontids (Figure 7), diverged (Huttenlocker and Rega 2012). Because of their phylogenetic position, the understanding of the evolution and structure of their skeleton is essential, since the anamniote-amniote transition was accompanied by the transition from a mainly amphibious to a terrestrial biomechanical regime and life cycle (Romer 1957, 1958, Germain and Laurin 2005). In order to decipher essential life history parameters and especially thermophysiology in basal synapsids, several authors studied the microstructure of their long bones and neural spines comparing them to extant mammals and birds (Enlow and Brown 1957, Enlow and Brown 1958, Peabody 1961, Warren 1963, Ricqlès 1974a, Ricqlès 1976a, Bennett & Ruben 1986, see also Huttenlocker and Rega 2012). Cyclic and regularly lamellated ("lamellar-zonal") bone tissues in early edaphosaurids and sphenacodontids revealed similarity in bone tissue type to extant reptiles and amphibians (Ricqlès 1974a, b, Ricqlès 1976a, Enlow 1969). Huttenlocker (2008) noted bone histological differences between sphenacodontids and edaphosaurids. Sphenacodontids show fibrolamellar (see also Shelton et al. 2013) or parallel-fibred bone, whereas edaphosaurids are mainly characterised by lamellar-zonal bone. In conclusion, "basal" synapsids display a histological organisation that is suggestive of representing the whole range of slow to fast growth (Huttenlocker and Rega 2012; Shelton et al. 2013). Peabody (1961) and Warren (1963) showed the occurrence and skeletochronological relevance of growth marks in Palaeozoic synapsids, while Ricqlès (1969, 1972, 1974a, 1974b, 1975, 1976a, 1976b) studied several basal synapsid taxa in a series of publications. Vickaryous and Sire (2009) reviewed the integumentary skeleton of tetrapods and mentioned varanopid osteoderms to have a block-like morphology, organised into multiple transverse rows in the cervical and pectoral regions. They described synapsid osteoderms to consist of parallel-fibred or lamellar bone with limited amounts of unmineralised fibrous connective tissue. Bone compactness profiles are used in more recent publications to infer habitat and ecology (e.g. Germain and Laurin 2005, Kriloff et al. 2008). Growth and mechanics of unusual skeletal structures are discussed by Rega et al. (2005), Huttenlocker et al. (2010), and Huttenlocker et al. (2011).

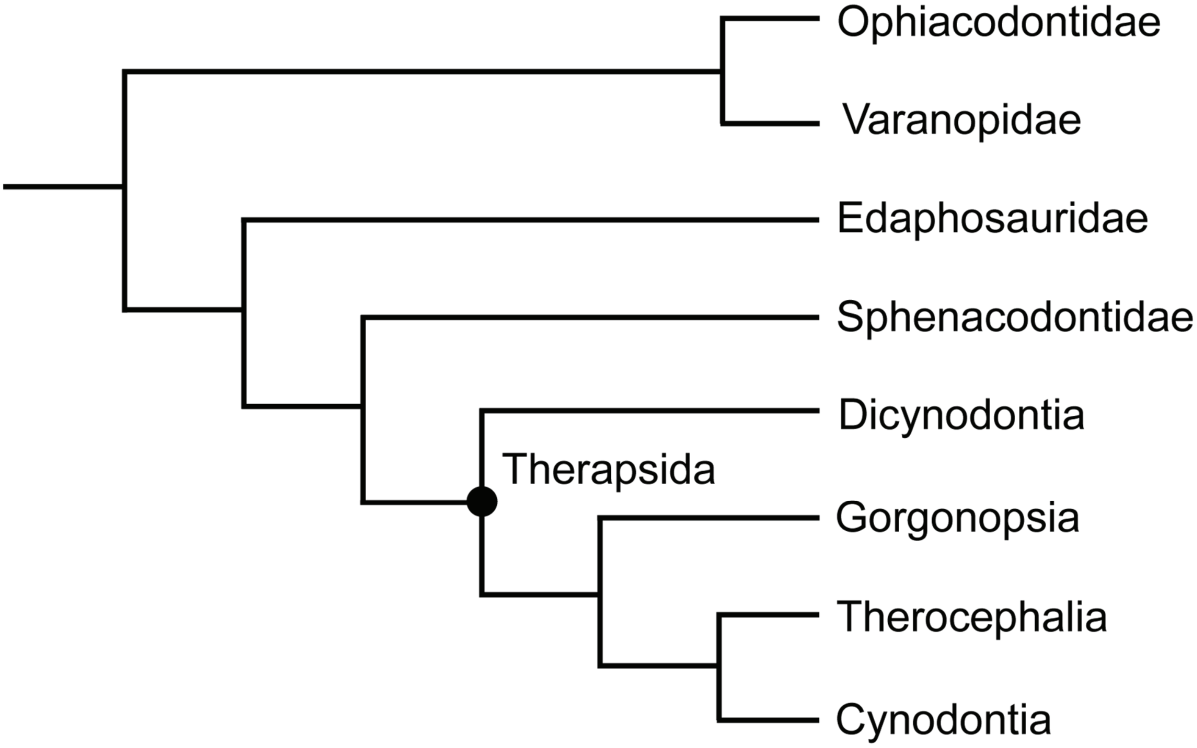

**Figure 7:** Phylogeny of major synapsid clades focussing on groups discussed, based on Rubidge & Sidor (2001), Benson (2012), and Brink & Reisz (2014).

Laurin and Buffrénil (2015) studied the histology and compactness of ophiacodontid bone tissue. *Clepsydrops collettii*, a Late Carboniferous ophiacodontid, displayed a thin, compact cortex lacking a medullary spongiosa, therefore suggesting a terrestrial lifestyle. An optimisation of inferred lifestyle of other early stegocephalians (based on bone microanatomy) indicated that the first amniotes were terrestrial. The Early Permian *Ophiacodon uniformis* showed a thicker cortex with few resorption cavities and bone trabeculae surrounding the free medullary cavity, thus indicating a possibly secondary amphibious lifestyle. Shelton and Sander (2015) showed the existence of highly vascularised fibrolamellar bone in *Ophiacodon* by sampling an ontogenetic series of humeri and additional femora, and therefore providing evidence for fast skeletal growth. Hence, they suggested to set the evolutionary origin of modern mammalian endothermy and high skeletal growth rates back to the Early Permian.

*Dicynodontia* – A large amount of studies on therapsid histology deals with dicynodont long bones, cranial bones, and ribs. Early work on the bone histology of several dicynodont genera has been performed by Nopcsa and Heidsieck (1933), Gross (1934), Enlow and Brown (1957), Enlow (1969), Ricqlès (1972, 1975, 1976a). More recent work contributed essentially to a better understanding of general dicynodont histology, containing studies on isolated bones of several individuals, several skeletal elements of one individual or dicynodont biomechanics (e.g. Chinsamy and Rubidge 1993, Ray and Chinsamy 2004, Ray et al. 2005, Green et al. 2010, Ray et al. 2010, Botha-Brink and Angielczyk 2010, Jasinoski et al. 2010a, Jasinoski et al. 2010b, Green 2012, Nasterlack et al. 2012, Ray et al. 2012). All authors agree on the fact that dicynodonts share primary bone tissue that consists of mainly fibrolamellar bone with a plexiform to laminar arrangement of vascular canals, suggesting overall fast rates of growth and metabolism high metabolic demands. Uninterrupted fibrolamellar bone in early ontogenetic stages and annuli, as well as LAGs only appearing during later stages of ontogeny (50 % of adult size), characterise several dicynodont taxa (Ray and Chinsamy 2004, Botha-Brink and Angielczyk 2010; see also Ray et al. 2012). The occurrence of parallel-fibred bone in the periphery of the cortex indicates a decrease in growth rate suggesting onset of reproductive maturity (e.g. Castanet and Baez 1991, Sander 2000b, Chinsamy-Turan 2012b). Peripheral rest lines in a few genera suggest asymptotic growth (Green et al. 2010). For some taxa it was possible to determine ontogenetic stages by bone histological features (Ray and Chinsamy 2004, Ray et al. 2005, Ray et al. 2010). Most dicynodonts are characterised by a thick bone cortex independent of body size suggesting a fossorial life style or digging habits (Botha-Brink and Angielczyk 2010), whereas the life style of some taxa remains unclear (Germain and Laurin 2005, Ray et al. 2010, Nasterlack et al. 2012).

*Gorgonopsia and Therocephalia* – Compared to other non-mammalian synapsids see above and chapter 2), sampling of the Middle to Late Permian carnivorous gorgonopsians and the Permotriassic therocephalians has been more limited (Ray et al. 2004, Chinsamy-Turan and Ray 2012, Sigurdsen et al. 2012, Huttenlocker and Botha-Brink 2013, Huttenlocker and Botha-Brink 2014). The earliest contributions on gorgonopsian and therocephalian bone histology were performed by Ricqlès (1969, 1975, 1978). He found fibrolamellar bone in two therocephalian species and in the long bones of five gorgonopsian taxa with partially thick compacta and mainly longitudinal vascularisation. The histological traits found suggested differential growth rates between a basal therocephalian from the Middle Permian of South Africa and a more derived Late Permian whaitsiid therocephalian. Because of comparatively higher vascularisation in the radius of the whaitsiid, Ricqlès (1969) suggested that therocephalians might have grown at higher rates later in their phylogeny. Recently, Huttenlocker and Botha-Brink (2014) performed a phylogenetic survey of limb bone histology in therocephalians from the Middle Permian through the Middle Triassic of the Karoo Basin, South Africa. They sampled eighty limb bones representing eleven genera of therocephalians using skeletal growth, including cortical vascularity and mean primary osteon diameters as histological indicators, and assessed for correlations with other biologically significant variables (e.g. size and robustness). Smaller-bodied descendants tended to have lower vascularity than their phylogenetically larger-bodied ancestors. Bone wall thickness tended to be high in early therocephalians and lower in gracile-limbed baurioid therocephalians. However, clade-level patterns deviated from previously studied within-lineage patterns (e.g. *Moschorhinus* displayed higher vascularity in the Triassic than in the Permian despite its smaller size). Therefore, Huttenlocker and Botha-Brink (2014) argued for a synergistic model of size reductions for Triassic therocephalians, influenced by within-lineage heterochronic shifts in survivor taxa and phylogenetically inferred survival of small-bodied taxa that had evolved short growth durations.

## References

Aaris-Sorensen, K., and R. Liljegren. 2004. Late Pleistocene remains of giant deer (*Megaloceros giganteus* Blumenbach) in Scandinavia: chronology and environment. Boreas 33:61-73.

Aitken, R. J. 1975. Cementum layers and tooth wear as criteria for ageing roe deer (*Capreolus capreolus*). Journal of Zoology 175:15-28.

Alexander, R. M., A. S. Jayes, G. M. O. Maloiy, and E. M. Wathuta. 1979. Allometry of the limb bones of mammals from shrews (*Sorex*) to elephant (*Loxodonta*). Journal of Zoology 189:305-314.

Alroy, J. 1998. Evolution in North American fossil mammals. Cope’s rule and the dynamics of body mass. Science 280:731-734.

Antoine, P.-O., L. Karadenizli, G. Sarac, and S. Sen. 2008. A giant rhinocerotoid (Mammalia, Perissodactyla) from the Late Oligocene of north-central Anatolia (Turkey). Zoological Journal of the Linnean Society 152:581-592.

Azanza, B. 1993. Sur la nature des appendices frontaux des cervidés (Artiodactyla, Mammalia) du Miocène inférieur et moyen. Remarques sur leur systématique et leur phylogénie. Comptes Rendus de l'Académie des Sciences Paris, Ser. II 316:1163-1169.

Azanza, B., G. E. Rössner, and E. Ortiz-Jaureguizar. 2013. The early Turolian (late Miocene) Cervidae (Artiodactyla, Mammalia) from the fossil site of Dorn-Dürkheim 1 (Germany) and implications on the origin of crown cervids. Palaeobiodiversity and Palaeoenvironments 93:217-258.

Azorit, C., J. Muñoz-Cobo, and M. Analla. 2002a. Seasonal deposition of cementum in first lower molars from *Cervus elaphus hispanicus*. Mammalian Biology 67:243-245.

Azorit, C., M. Analla, J. Hervas, R. Carrasco, and J. Muñoz-Cobo. 2002b. Growth marks observation: preferential techniques and teeth for ageing of Spanish red deer (*Cervus elaphus hispanicus*). Anatomia Histologia Embryologia-Journal of Veterinary Medicine Series C 31(5):303-307.

Azorit, C., M. Analla, R. Carrasco, and J. Muñoz-Cobo. 2003. Determinación de edad por desgaste dental en el ciervo ibérico (*Cervus elaphus hispanicus*). Boletín de la Real Sociedad Española de Historia Natural. Sección Biológica 98(1-4):123-134.

Azorit, C., J. Muñoz-Cobo, J. Hervas, and M. Analla. 2004. Aging through growth marks in teeth of Spanish red deer. Wildlife Society Bulletin 32(3):702-710.

Bennett, A. F., and A. J. Ruben. 1986. The matabolic and thermoregulatory status of therapsids. Pp. 207-218. *In* N. Hotton, P. D. MacLean, J. J. Roth, and E. C. Roth, eds. The ecology and biology of mammal-like reptils. Smithsonian Institution Press, Washington.

Benson, R. B. J. 2012. The global interrelationships of basal synapsids: cranial and postcranial morphological partitions suggest different topologies. Journal of Systematic Palaeontology 10:601-624.

Benton, M. J., Z. Csiki, D. Grigorescu, R. Redelstorff, P. M. Sander, K. Stein, and D. B. Weishampel. 2010. Dinosaurs and the island rule: The dwarfed dinosaurs from Hateg Island. Palaeogeography Palaeoclimatology Palaeoecology 293(3-4):438-454.

Bergmann, C. 1847. Über die Verhältnisse der Wärmeökonomie der Thiere zu ihrer Grösse. Göttinger Studien 3:595-708.

Bindon, J. R., and P. T. Baker. 1997. Bergmann's Rule and the Thrifty Genotype. American Journal of Physical Anthropology 104:201-210.

Bonner, J. T. 2006. Why size matters: from bacteria to blue whales. Princeton University Press, Princeton.

Botha-Brink, J., and K. D. Angielczyk. 2010. Do extraordinarily high growth rates in Permo-Triassic dicynodonts (Therapsida, Anomodontia) explain their success before and after the end-Permian extinction? Zoological Journal of the Linnean Society 160:341-365.

Brink, K. S., and R. R. Reisz. 2014. Hidden dental diversity in the oldest terrestrial apex predator *Dimetrodon*. Nature Communications 5:3269.

Buffrénil, V. de, and J. M. Mazin. 1990. Bone histology of the ichthyosaurs: comparative data and functional interpretation. Paleobiology 16:435-447.

Burke, A., and J. Castanet. 1995. Histological observations of cementum growth in horse teeth and their application to archaeology. Journal of Archaeological Science 22:479-493.

Calder, W. A. 1974. Consequences of body size for avian energetics. Pp. 86-151. *In* R. A. Paynter Jr., ed. Avian energetics. Nuttal Ornithology Club, Cambridge.

Castanet, J., and M. Baez. 1991. Adaptation and evolution in Gallotia lizards from the Canary Islands: age, growth, maturity and longevity. Amphibia-Reptilia 12:81-102.

Chinsamy-Turan, A., ed. 2012a. Forerunners of mammals: radiation, histology, biology. Indiana University Press, Bloomington.

Chinsamy-Turan, A. 2012b. Microstructure of bones and teeth of nonmammalian therapsids. Pp. 65-88. *In* A. Chinsamy-Turan, ed. Forerunners of mammals: radiation, histology, biology. Indiana University Press, Bloomington.

Chinsamy-Turan, A., and S. Ray. 2012. Bone histology of some therocephalians and gorgonopsians, and evidence of bone degradation by fungi. *In* A. Chinsamy-Turan, ed. Forerunners of mammals: radiation, histology, biology. Indiana University Press, Bloomington.

Chinsamy, A., and B. S. Rubidge. 1993. Dicynodont (Therapsida) bone histology: phylogenetic and physiological implications. Palaeontologia Africana 30:97-102.

Chritz, K. L., G. J. Dyke, A. Zazzo, A. M. Lister, N. T. Monaghan, and J. D. Sigwart. 2009. Palaeobiology of an extinct Ice Age mammal: Stable isotope and cementum analysis of giant deer teeth. Palaeogeography Palaeoclimatology Palaeoecology 282(1-4):133-144.

Debeljak, I. 1996. A simple preparation technique of cave bear teeth for age determination by cementum increments. Revue de Paléobiologie 15(1):105-108.

de Vos, J. 1979. The endemic Pleistocene deer of Crete. Proceedings of the Koninklijke Akademie van Wetenschappen (Series B) 82(1):59-90.

de Vos, J. 1984. The endemic Pleistocene deer of Crete. North-Holland Publishing Company, Amsterdam.

Dudley, R. 1998. Atmospheric oxygen, giant paleozoic insects and the evolution of aerial locomotor performance. The Journal of Experimental Biology 201:1043-1050.

Enlow, D. H. 1969. The bone of reptiles. Pp. 45-80. *In* C. Gans, A. d. A. Bellairs, and T. S. Parsons, eds. Biology of the Reptilia. Vol. 1 Morphology A. Academic Press, London.

Enlow, D. H., and S. O. Brown. 1957. A comparative histological study of fossil and recent bone tissues. Part II. Texas Journal of Science 9:186-214.

Enlow, D. H., and S. O. Brown. 1958. A comparative histological study of fossil and recent bone tissues. Part III. Texas Journal of Science 10:187-230.

Erickson, G. M., K. Curry Rogers, and S. A. Yerby. 2001. Dinosaurian growth patterns and rapid avian growth rates. Nature 412:429-433.

Erickson, G. M., P. J. Makovicky, P. J. Currie, M. A. Norell, S. A. Yerby, and C. A. Brochu. 2004. Gigantism and comparative life-history parameters of tyrannosaurid dinosaurs. Nature 430:772-775.

Forsyth Major, C. I. 1902. On the pigmy hippopotamus form the Pleistocene of Cyprus. Proceeding of the Zoological Society of London 2(1,2):238-239,107-112.

Foster, J. B. 1964. Evolution of mammals on islands. Nature 202:234-235.

Franzmann, A. W. 1981. *Alces alces*. Mammalian Species 154:1-7.

Gentry, A. W., G. E. Rössner, and E. P. J. Heizmann. 1999. Suborder Ruminantia. Pp. 225-258. *In* G. E. Rössner, and K. Heissig, eds. The Miocene land mammals of Europe. Verlag Dr. Friedrich Pfeil, München.

Grubb, P. 2005. Order Artiodactyla. *In* D. E. Wilson, and M. R. DeeAnn, eds. Mammal species of the world: a taxonomic and geographic reference. Johns Hopkins University Press, Baltimore.

Garcia-Martinez, R., N. Marin-Moratalla, X. Jordana, and M. Köhler. 2011. The ontogeny of bone growth in two species of dormice: Reconstructing life history traits. Comptes Rendus Palevol 10(5-6):489-498.

Geist, V. 1998. Deer of the world: their evolution, behaviour, and ecology. Stackpole Books, Mechanicsburg.

Gentry, A. W., G. E. Rössner, and E. P. J. Heizmann. 1999. Suborder Ruminantia. Pp. 225-258. *In* G. E. Rössner, and K. Heissig, eds. The Miocene land mammals of Europe. Verlag Dr. Friedrich Pfeil, München.

Germain, D., and M. Laurin. 2005. Microanatomy of the radius and lifestyle in amniotes (Vertebrata, Tetrapoda). Zoologica Scripta 34:335-350.

Gilbert, C., A. Ropique, and A. Hassanin. 2006. Mitochondrial and nuclear phylogenies of Cervidae (Mammalia, Ruminantia): Systematics, morphology, and biogeography. Molecular Phylogenetics and Evolution 40:101-117.

Gould, S. J. 1974. The origin and function of 'bizarre' structures: antler size and skull size in the 'Irish Elk', *Megaloceros giganteus*. Evolution 28(2 ):191-220.

Grant, P. R., and R. Grant. 2006. Evolution of character displacement in Darwin's finches. Science 313:224-226.

Green, J. L. 2012. Bone and dental histology of Late Triassic dicynodonts from North America. Pp. 179-196. *In* A. Chinsamy-Turan, ed. Forerunners of mammals: radiation, histology, biology. Indiana University Press, Bloomington.

Green, J. L., M. H. M. H. Schweitzer, and E.-T. Lamm. 2010. Limb bone histology and growth in *Placerias hesternus* (Therapsida: Anomodontia) from the Upper Triassic of North America. Palaeontology 53:347-364.

Gross, W. 1934. Die Typen des mikroskopischen Knochenbaues bei fossilen Stegocephalen und Reptilien. Zeitschrift für Anatomie und Enwicklungsgeschichte 103:731-764.

Groves, C. P. 2007. Family Cervidae. Pp. 249-256. *In* D. R. Prothero, and S. E. Foss, eds. The evolution of artiodactyls. Johns Hopkins University Press, Baltimore.

Grubb, P. 2005. Order Artiodactyla. Pp. 637-723. *In* D. E. Wilson, and M. R. DeeAnn, eds. Mammal species of the world: a taxonomic and geographic reference. Johns Hopkins University Press, Baltimore.

Hassanin, A., F. Delsuc, A. Ropiquet, C. Hammer, B. J. van Vuuren, C. Matthee, M. Ruiz-Garcia, F. Catzeflis, V. Areskoug, T. T. Nguyen, and A. Couloux. 2012. Pattern and timing of diversification of Cetartiodactyla (Mammalia, Laurasiatheria), as revealed by a comprehensive analysis of mitochondrial genomes. Comptes Rendus Biologies 335:32-50.

Hillson, S. 2005. Teeth. Cambridge University Press, Cambridge.

Houssaye, A., K. Waskow, S. Hayashi, A. H. Lee, and J. R. Hutchinson. 2016. Biomechanical evolution of solid bones in large animals: a microanatomical investigation. Biological Journal of the Linnean Society 117(2):350-371.

Huttenlocker, A. K. 2008. Comparative osteohistology of hyperelongate neural spines in basal synapsids (Vertebrata: Amniota): Growth and mechanical considerations. MSc thesis. California State University San Bernardino.

Huttenlocker, A. K., and J. Botha-Brink. 2013. Body size and growth patterns in the therocephalian *Moschorhinus kitchingi* (Therapsida: Eutheriodontia) before and after the end-Permian extinction in South Africa. Paleobiology 39:253–277.

Huttenlocker, A. K., and J. Botha-Brink. 2014. Bone microstructure and the evolution of growth patterns in Permo-Triassic therocephalians (Amniota, Therapsida) of South Africa. PeerJ 2:e325:1-31.

Huttenlocker, A. K., and E. Rega. 2012. The paleobiology and bone microstructure of pelycosaurian-grade synapsids. Pp. 91-119. *In* A. Chinsamy-Turan, ed. Forerunners of mammals: radiation, histology, biology. Indiana University Press, Bloomington.

Huttenlocker, A. K., D. Mazierski, and R. R. Reisz. 2011. Comparative osteohistology of hyperelongate neural spines in the Edaphosauridae (Amniota: Synapsida). Palaeontology 54:573-590.

Huttenlocker, A. K., E. Rega, and S. S. Sumida. 2010. Comparative anatomy and osteohistology of hyperelongate neural spines in the sphenacodontids *Sphenacodon* and *Dimetrodon* (Amniota: Synapsida). Journal of Morphology 271:1407-1421.

Janis, C. M., and K. M. Scott. 1987. The interrelationships of higher ruminant families: with special emphasis on the members of the Cervoidea. American Museum Novitates 2893:1-85.

Jasinoski, S. C., E. J. Rayfield, and A. Chinsamy. 2010a. Functional implications of dicynodont cranial suture morphology. Journal of Morphology 271:705-728.

Jasinoski, S. C., E. J. Rayfield, and A. Chinsamy. 2010b. Mechanics of the scarf premaxilla-nasal suture in the snout of *Lystrosaurus*. Journal of Vertebrate Paleontology 30:1283-1288.

Jordana, X., N. Marín-Moratalla, D. DeMiguel, T. M. Kaiser, and M. Köhler. 2012. Evidence of correlated evolution of hypsodonty and exceptional longevity in endemic insular mammals. Proceedings of the Royal Society of London B: Biological Sciences 279(1741):3339-3346.

Kingsolver, J. G., and D. W. Pfennig. 2004. Individual-level selection as a cause of Cope's Rule of phyletic size increase. Evolutionary Theory 58(7):1608-1612.

Klevezal, G. A. 1996. Recording structures of mammals. Determination of age and reconstruction of life history. A.A.Balkema, Rotterdam/Brookfield.

Köhler, M., and S. Moyà-Solà 2009. Physiological and life history strategies of a fossil large mammal in a resource-limited environment. Proceedings of the National Academy of Sciences of the United States of America 106(48):20354-20358.

Kriloff, A., D. Germain, A. Canoville, P. Vincent, M. Sache, and M. Laurin. 2008. Evolution of bone microanatomy of the tetrapod tibia and its use in palaeobiological inference. Journal of Evolutionary Biology 21:807-826.

Laurin, M., and V. De Buffrénil. 2015. Microstructural features of the femur in early ophiacodontids: a reappraisal of ancestral habitat use and lifestyle of amniotes C. R. Palevol.

Liebermann, D. E., and R. H. Meadow. 1992. The biology of cementum increments (with an archaeological application). Mammal Review 22(2):57-77.

Lister, A. M. 1989. Rapid dwarfing of red deer on Jersey in the last interglacial. Nature 342:539-542.

Lister, A. M., C. J. Edwards, D. A. W. Nock, M. Bunce, I. A. van Pijlen, D. G. Bradley, M. G. Thomas, and I. Barnes. 2005. The phylogenetic position of the "giant deer" *Megaloceros giganteus*. Nature 438(7069):850-853.

Lomolino, M. V. 1985. Body size of mammals on islands: the island rule re-examined. American Naturalist 125:310–316.

Lomolino, M. V. 2005. Body size evolution in insular vertebrates: generality of the island rule. Journal of Biogeography 32:1683–1699.

Lomolino, M. V. 2010. Four Darwinian themes on the origin, evolution and preservation of island life. Journal of Biogeography 37:985–994.

Lomolino, M. V., D. F. Sax, M. R. Palombo, and A. van der Geer. 2012. Of mice and mammoths: evaluations of causal explanations for body size evolution in insular mammals. Journal of Biogeography 39:842-854.

Lomolino, M. V., A. A. van der Geer, G. A. Lyras, M. R. Palombo, D. F. Sax, and R. Rozzi. 2013. Of mice and mammoths: generality and antiquity of the island rule. Journal of Biogeography 40:1427–1439.

Low, W. A., and I. M. Cowan. 1963. Age determination of deer by annular structure of dental cementum. The Journal of Wildlife Management 27(3):466-471.

Lundervold, M., R. Langvatn, and E. J. Milner-Gulland. 2003. A comparison of age estimation methods for the saiga antelope *Saiga tatarica*. Wildlife Biology 9:219-227.

Marin-Moratalla, N., X. Jordana, and M. Köhler. 2013. Bone histology as an approach to providing data on certain key life history traits in mammals: Implications for conservation biology. Mammalian Biology 78:422-429.

McClain, C. R., P. A. P. Durst, A. G. Boyer, and C. D. Francis. 2013 Unravelling the determinants of insular body size shifts. Biology Letters 9:20120989.

McGowan, C., and R. Motani. 2003. Ichthyopterygia. Handbook of Paleoherpetology, Part 8. Verlag Dr. Friedrich Pfeil, München.

McNab, B. K. 2002. The physiological ecology of vertebrates: a view from energetics. Cornell University Press, Ithaca.

Meinl, A., C. D. Huber, S. Tangl, G. M. Gruber, M. Teschler-Nicola, and G. Watzek. 2008. Comparison of the validity of three dental methods for the estimation of age at death. Forensic Science International 178:96–105.

Meiri, S., N. Cooper, and A. Purvis. 2008. The island rule: made to be broken? Proceedings of the Royal Society, Series B 275:141-148.

Millien, V. 2006. Morphological evolution is accelerated among island mammals. PLoS Biology 4(10):e321. 1863-1868.

Motani, R. 2010. Warm-blooded "sea dragons"? Science 328:1361-1362.

Mundy, K. R. D., and W. A. Fuller. 1964. Age determination in the grizzly bear. The Journal of Wildlife Management 28(4):863-866.

Nasterlack, T., A. Canoville, and A. Chinsamy. 2012. New insights into the biology of the Permian genus *Cistecephalus* (Therapsida, Dicynodontia). Journal of Vertebrate Paleontology 32:1396-1410.

Neel, J. V. 1962. Diabetes mellitus: a ''thrifty'' genotype rendered detrimental by ''progress''? American Journal of Human Genetics 14:353-362.

Nopcsa, F. v., and E. Heidsieck. 1933. On the histology of the ribs of immature and half-grown trachodont dinosaurs. Proceedings of the Zoological Society of London 1:221-223.

Ohtaishi, N., K. Kaji, S. Miura, and J. Wu. 1990. Age determination of the white-lipped deer *Cervus albirostris* by dental cementum and molar wear. Journal of the Mammalogical Society of Japan 15(1):15-24.

Padian, K. 2011. Vertebrate palaeohistology then and now: A retrospective in the light of the contributions of Armand de Ricqles. Comptes Rendus Palevol 10(5-6):303-309.

Padian, K., and E.-T. Lamm, eds. 2013. Bone histology of tetrapods. University of California Press, Berkeley, Los Angeles.

Palkovacs, E. P. 2003. Explaining adaptive shifts in body size on islands: a life history approach. Oikos 103:37-44.

Peabody, F. E. 1961. Annual growth zones in living and fossil vertebrates. Journal of Morphology 108:11-62.

Quekett, J. T. 1849a. On the intimate structure of bone as composing the skeleton in the four great classes of animals, viz., mammals, birds, reptiles, and fishes, with some remarks on the great value of the knowledge of such structure in determining the affinities of minute fragments of organic remains. Transactions of the Microscopical Society of London 2:46-58.

Quekett, J. T. 1849b. Additional observations on the intimate structure of bone. Transactions of the Microscopical Society of London 2:59-64.

Ray, S., and A. Chinsamy. 2004. *Diictodon feliceps* (Therapsida, Dicynodontia): bone histology, growth, and biomechanics. Journal of Vertebrate Paleontology 24:180-194.

Ray, S., S. Bandyopadhyay, and R. Appana. 2010. Bone histology of a kannemeyeriid dicynodont *Wadiasaurus*: palaeobiological implications. Pp. 73-89. *In* S. Bandyopadhyay, ed. New aspects of mesozoic biodiversity. Springer, Heidelberg.

Ray, S., J. Botha, and A. Chinsamy. 2004. Bone histology and growth patterns of some nonmammalian therapsids. Journal of Vertebrate Paleontology 24:634-648.

Ray, S., J. Botha-Brink, and A. Chinsamy-Turan. 2012. Dicynodont growth dynamics and lifestyle adaptations. Pp. 121-146. *In* A. Chinsamy-Turan, ed. Forerunners of mammals: radiation, histology, biology. Indiana University Press, Bloomington.

Ray, S., A. Chinsamy, and S. Bandyopadhyay. 2005. *Lystrosaurus murrayi* (Therapsida, Dicynodontia): bone histology, growth and lifestyle adaptations. Palaeontology 48:1169-1185.

Rega, E., S. S. Sumida, K. Noriega, C. Pell, and A. Lee. 2005. Evidence-based paleopathology I: ontogenetic and functional implications of dorsal sails in *Dimetrodon*. Journal of Vertebrate Paleontology 25(3):103A.

Reimers, E., and Ø. Nordby. 1968. Relationship between age and tooth cementum layers in Norwegian reindeer. The Journal of Wildlife Management 32(4 ):957-961.

Ricqlès, A. de. 1969. Recherches palèohistologiques sur les os longs des tetrapodes. II.- Quelques observations sur la structure des os longs des thériodontes. Annales de Paléontologie 55:1-52.

Ricqlès, A. de. 1972. Recherches palèohistologiques sur les os longs des tetrapodes. III.- Titanosuchiens, dinocéphaliens et dicynodontes. Annales de Paléontologie (Vertébrés) 58:17-46.

Ricqlès, A. de 1974a. Evolution of endothermy: histological evidence. Evolutionary Theory 1(2):51-80.

Ricqlès, A. de 1974b. Recherches paléohistologiques sur les os longs des tétrapodes. IV. - Éothériodontes et pélycosaures. Annales de Paléontologie 60:1-56.

Ricqlès, A. d. 1975. Recherches paléohistologiques sur les os longs des tétrapodes VII. - Sur la classification, la signification fonctionnelle et l'histoire des tissus oseux des tétrapodes. Première partie, structures. Annales de Paléontologie 61:49-129.

Ricqlès, A. de 1976a. On bone histology of fossil and living reptiles, with comments on its functional and evolutionary significance. Pp. 123-150. *In* A. Bellairs, and C. B. Cox, eds. Morphology and biology of reptiles. Academic Press, London and New York.

Ricqlès, A. de. 1976b. Recherches paléohistologiques sur les os longs des tétrapodes. VII. - Sur la classification, la signification fonctionnelle et l'histoire des tissus osseux des tétrapodes. Deuxième partie. Fonctions: considérations fonctionnelles et physiologiques. Annales de Paléontologie 62:71-126.

Ricqlès, A. de. 1978. Recherches paléohistologiques sur les os longs des tétrapodes. VII. — Sur la classification, la signification fonctionnelle et l'histoire des tissus osseux des tétrapodes. Troisième partie. IV.-Les problèmes du déterminisme des types de tissus osseux. Annales de Paléontologie 64:153-184.

Rolandsen, C. M., E. J. Solberg, M. Heim, F. Holmstrøm, M. I. Solem, and B. E. Sæther. 2008. Accuracy and repeatability of moose (*Alces alces*) age as estimated from dental cement layers. European Journal of Wildlife Research 54:6-14.

Romer, A. S. 1957. Origin of the amniote egg. Scientific monthly 85:57-63.

Romer, A. S. 1958. Tetrapod limbs and early tetrapod life. Evolution 12:365-369.

Rubidge, B. S., and C. A. Sidor. 2001. Evolutionary patterns among Permo-Triassic therapsids. Annual Review of Ecology and Systematics 32:449-480.

Sander, P. M. 2000a. Ichthyosauria: their diversity, distribution, and phylogeny. Paläontologische Zeitschrift 74:1-35.

Sander, P. M. 2000b. Long bone histology of the Tendaguru sauropods: implications for growth and biology. Paleobiology 26:466-488.

Sander, P. M., and P. Andrassy. 2006. Lines of arrested growth and long bone histology in Pleistocene large mammals from Germany: What do they tell us about dinosaur physiology? Palaeontographica Abteilung A 277:143-159.

Sander, P. M., A. Christian, M. Clauss, R. Fechner, C. T. Gee, E.-A. Griebeler, H.-C. Gunga, J. Hummel, H. Mallison, S. F. Perry, H. Preuschoft, O. W. M. Rauhut, K. Remes, T. Tütken, O. Wings, and U. Witzel. 2011. Biology of the sauropod dinosaurs: the evolution of gigantism. Biological Reviews 86:117-155.

Saxon, A., and C. F. W. Higham. 1969. A new research method for economic prehistorians. American Antiquity 34(3):303-311.

Schmidt-Nielsen, K. 1984. Scaling: why is animal size so important? Cambridge University Press, Cambridge.

Shelton, C., and P. M. Sander. 2015. *Ophiacodon* long bone histology: the earliest occurrence of FLB in the mammalian stem lineage. PeerJ PrePrints 3:e1262.

Shelton, C. D., P. M. Sander, K. Stein, and H. Winkelhorst. 2013. Long bone histology indicates sympatric species of Dimetrodon (Lower Permian, Sphenacodontidae). Earth and Environmental Science Transactions of the Royal Society of Edinburgh 103:1-20.

Sigurdsen, T., A. K. Huttenlocker, S. P. Modesto, T. Rowe, and R. Damiani. 2012. Reassessment of the morphology and paleobiology of the therocephalian *Tetracynodon darti* (Therapsida), and the phylogenetic relationships of Baurioidea. Journal of Vertebrate Paleontology 32:1113-1134.

Simberloff, D., T. Dayan, C. Jones, and G. Ogura. 2000. Character displacement and release in the small Indian mongoose, *Herpestes javanicus*. Ecology 81:2086-2099.

Spiess, A. 1976. Determining season of death of archaeological fauna by analysis of teeth. Arctic 29(1):53-55.

Tacutu, R., T. Craig, A. Budovsky, D. Wuttke, G. Lehmann, D. Taranukha, J. Costa, V. E. Fraifeld, and J. P. de Magalhaes. 2013. Human Ageing Genomic Resources: Integrated databases and tools for the biology and genetics of ageing. Nucleic Acids Research 41(D1):D1027-D1033.

Ungar, P. S. 2010. Mammal teeth: origin, evolution, and diversity. Johns Hopkins University Press, Baltimore.

van der Geer, A., J. de Vos, G. Lyras, and M. Dermitzakis. 2006. New data on the Pleistocene Cretan deer *Candiacervus* sp. II (Cervinae, Mammalia). Courier Forschungsinstitut Senckenberg 256:131-137.

van der Geer, A., J. De Vos, M. Dermitzakis, and G. Lyras. 2009. Hoe dieren op eilanden evolueren. Natuurwetenschap & Techniek, Diemen.

van der Geer, A., G. Lyras, J. de Vos, and M. Dermitzakis. 2010. Evolution of island mammals. Adaptation and extinction of placental mammals on islands. Wiley-Blackwell, Sussex.

van der Geer, A. A. E. 2014. Parallel patterns and trends in functional structures in extinct island mammals. Integrative Zoology 9:167–182.

van Valen, L. M. 1973. Pattern and the balance of nature. Evolutionary Theory 1:31-49.

Vaughan, T. A., J. M. Ryan, and N. J. Czaplewski. 2015. Mammalogy. Sixth Edition. Saunders College Publishing, Philadelphia.

Vickaryous, M. K., and J. Y. Sire. 2009. The integumentary skeleton of tetrapods: origin, evolution, and development. Journal of Anatomy 214:441-464.

Vislobokova, I. A. 2012. Giant deer: origin, evolution, role in the biosphere. Paleontological Journal 46(7):643-775.

Vislobokova, I. A. 2013. Morphology, taxonomy, and phylogeny of megacerines (Megacerini, Cervidae, Artiodactyla). Paleontological Journal 47(8):833-950.

Warren, J. W. 1963. Growth zones in the skeleton of recent and fossil vertebrates. PhD. University of California, Los Angeles.

Willey, C. H. 1974. Aging black bears from first premolar tooth sections. The Journal of Wildlife Management 38(1):97-100.

# CHAPTER 2

## Mammalian bone palaeohistology: a survey and new data with emphasis on island forms

Authors: Kolb C., Scheyer T. M., Veitschegger K., Forasiepi A. M., Amson E., van der Geer A. A. E., van den Hoek Ostende L. W., Hayashi S., Sánchez-Villagra M. R.

Publication: 2015, *PeerJ,* 3:e1358

Contributions: CK designed the study/experiments, performed the experiments, and wrote the majority of the manuscript, MRS-V designed the study/experiments and wrote parts of the manuscript, KV, AMF, and EA wrote parts of the manuscript and performed the experiments, CK, TMS, KV, AMF, and EA collected and analysed histological data, AMF, AAEVDG, LWVDHO provided material, CK and EA prepared figures/tables, CK, EA, KV, and AMF took micrographs, all authors contributed to the final interpretation and editing of the manuscript. All authors read and approved the final manuscript.

# Mammalian bone palaeohistology: a survey and new data with emphasis on island forms

Christian Kolb[1], Torsten M. Scheyer[1], Kristof Veitschegger[1],
Analia M. Forasiepi[2], Eli Amson[1], Alexandra A.E. Van der Geer[3,4],
Lars W. Van den Hoek Ostende[3], Shoji Hayashi[5] and
Marcelo R. Sánchez-Villagra[1]

[1] Paläontologisches Institut und Museum, Universität Zürich, Zürich, Switzerland
[2] Consejo Nacional de Investigaciones Científicas y Técnicas, Instituto Argentino de Nivología, Glaciología y Ciencias Ambientales, Centro Científico y Tecnológico, Mendoza, Argentina
[3] Department of Geology, Naturalis Biodiversity Center, Leiden, The Netherlands
[4] Department of Historical Geology and Palaeontology, National and Kapodistrian University of Athens, Zografou, Greece
[5] Osaka Museum of Natural History, Osaka, Japan

## ABSTRACT

The interest in mammalian palaeohistology has increased dramatically in the last two decades. Starting in 1849 via descriptive approaches, it has been demonstrated that bone tissue and vascularisation types correlate with several biological variables such as ontogenetic stage, growth rate, and ecology. Mammalian bone displays a large variety of bone tissues and vascularisation patterns reaching from lamellar or parallel-fibred to fibrolamellar or woven-fibred bone, depending on taxon and individual age. Here we systematically review the knowledge and methods on cynodont and mammalian bone microstructure as well as palaeohistology and discuss potential future research fields and techniques. We present new data on the bone microstructure of two extant marsupial species and of several extinct continental and island placental mammals. Extant marsupials display mainly parallel-fibred primary bone with radial and oblique but mainly longitudinal vascular canals. Three juvenile specimens of the dwarf island hippopotamid *Hippopotamus minor* from the Late Pleistocene of Cyprus show reticular to plexiform fibrolamellar bone. The island murid *Mikrotia magna* from the Late Miocene of Gargano, Italy displays parallel-fibred primary bone with reticular vascularisation and strong remodelling in the middle part of the cortex. *Leithia* sp., the dormouse from the Pleistocene of Sicily, is characterised by a primary bone cortex consisting of lamellar bone and a high amount of compact coarse cancellous bone. The bone cortex of the fossil continental lagomorph *Prolagus oeningensis* and three fossil species of insular *Prolagus* displays mainly parallel-fibred primary bone and reticular, radial as well as longitudinal vascularisation. Typical for large mammals, secondary bone in the giant rhinocerotoid *Paraceratherium* sp. from the Late Oligocene of Turkey is represented by dense Haversian bone. The skeletochronological features of *Sinomegaceros yabei*, a large-sized deer from the Pleistocene of Japan closely related to *Megaloceros*, indicate a high growth rate. These examples and the synthesis of existing data show the potential of bone microstructure to reveal essential information on life history evolution. The bone tissue and the skeletochronological data of the sampled island species suggest

Submitted 2 June 2015
Accepted 7 October 2015
Published 22 October 2015

Corresponding author
Christian Kolb,
christian.kolb@pim.uzh.ch

Academic editor
John Hutchinson

Additional Information and Declarations can be found on page 32

DOI 10.7717/peerj.1358

**How to cite this article** Kolb et al. (2015), Mammalian bone palaeohistology: a survey and new data with emphasis on island forms. **PeerJ 3:e1358; DOI 10.7717/peerj.1358**

the presence of various modes of bone histological modification and mammalian life history evolution on islands to depend on factors of island evolution such as island size, distance from mainland, climate, phylogeny, and time of evolution.

**Subjects** Evolutionary Studies, Paleontology, Histology
**Keywords** Mammals, Palaeohistology, Island evolution, Bone tissue, *Mikrotia*, *Paraceratherium*, *Hippopotamus minor*, *Leithia*, *Sinomegaceros*, *Prolagus*

## INTRODUCTION

Histology of fossil bones (e.g., *Ricqlès, 1976a*; *Padian, 2011*) provides data to investigate life history variables such as age, sexual maturity, growth patterns, and reproductive cycles. Research on fossil vertebrate hard tissues dates back to the 19th century, when it was recognised that bones and teeth are commonly very well preserved at the histological level (*Quekett, 1849a*; *Quekett, 1849b*). Since then, several descriptive surveys of different tetrapod taxa, including mammals, have been published (e.g., *Schaffer, 1890*; *Enlow & Brown, 1958*; *Ricqlès, 1976a*; *Ricqlès, 1976b*; *Klevezal, 1996*; *Marín-Moratalla et al., 2014*; *Prondvai et al., 2014*). The study of the microstructure of highly mineralised components such as blood vessel arrangement (*De Boef & Larsson, 2007*) and tissue types in bones as well as teeth (e.g., *Kolb et al., 2015*) provides information on growth patterns and remodelling processes of hard tissues in extinct vertebrates (see also *Scheyer, Klein & Sander, 2010*; *Chinsamy-Turan, 2012a*; *Padian & Lamm, 2013* for summaries).

Mammals are a well-known group of vertebrates with a well-documented fossil record. However, until recent years and apart from a few seminal papers (*Gross, 1934*; *Enlow & Brown, 1958*; *Warren, 1963*; *Klevezal, 1996*), mammalian bone histology received little attention by biologists and palaeontologists alike compared to dinosaurs and non-mammalian synapsids (e.g., *Horner, Ricqlès & Padian, 1999*; *Sander et al., 2004*; *Chinsamy-Turan, 2012a*; see also *Padian, 2013* for a review on *Chinsamy-Turan, 2012a*).

The present contribution summarises the main aspects about the current state of knowledge on mammalian palaeohistology without omitting some of the relevant non-mammalian contributions, presents new finds on several extant and extinct species from diverse clades, and discusses perspectives in this field of research. Bone histological traits of extinct island mammals sampled for the present study are described and implications for island evolution are discussed. Literature dealing with pathologies in mammalian bone is omitted since this goes beyond the scope of this synthesis.

### Bone tissue types

In synapsids, three main types of bone matrix are distinguished. *Woven-fibred bone* shows highly disorganised collagen fibres of different sizes being loosely and randomly arranged. *Parallel-fibred bone* consists of tightly packed collagen fibrils arranged in parallel. *Lamellar bone* shows the highest spatial organisation. It consists of thin layers (lamellae) of closely packed collagen fibres. Both parallel-fibred and lamellar bone are indicative of relatively low growth rates (*Francillon-Vieillot et al., 1990*; *Huttenlocker, Woodward & Hall, 2013*). *Bromage et al. (2009)* confirmed that lamellar bone is an incremental tissue, with one lamella formed in the species-specific time dependency of the formation of long-period increments (striae of Retzius) in enamel. The authors also showed a negative correlation between osteocyte density in bone and body mass and thus suggested a central autonomic regulatory control mechanism to the coordination of organismal life history and body mass. This demonstrates the relevance of bone histology for understanding physiological mechanisms in extant and extinct vertebrates.

A bone complex composed of a woven-fibred bone matrix in which osteonal lamellar bone infills the space between woven bone and primary vascular canals, is defined as *fibrolamellar bone* (Figs. 1B, 1C, 1E and 1F) (*Ricqlès, 1974*; *Stein & Prondvai, 2014*) or fibrolamellar complex (FLC; *Ricqlès, 1975*; *Ricqlès et al., 1991*; *Margerie, Cubo & Castanet, 2002*; *Prondvai et al., 2014*). According to its vascular orientation, three main types of fibrolamellar bone are distinguished: *Laminar bone* shows an almost uniform circumferential orientation of vascular canals. In case circumferential canals are connected by radial ones forming a dense anastomosing network, the pattern is called *plexiform* (Figs. 1B, 1C, 1E and 1F). An anastomosing network showing random organisation with oblique orientations is defined as reticular. Moreover, a radial arrangement of vascular canals is called *radiating* or *radial bone* (*Francillon-Vieillot et al., 1990*; *Chinsamy-Turan, 2012b*; *Huttenlocker, Woodward & Hall, 2013*).

Amprino identified for the first time a relationship between bone tissue type and growth rate in vertebrates, what is now called "Amprino's rule" (*Amprino, 1947*; see also *Lee et al., 2013*). *Stein & Prondvai (2014)* found, by investigating longitudinal thin sections of sauropod long bones, that the amount of woven bone in the primary complex has been largely overestimated (e.g., *Klein & Sander, 2008*), questioning former arguments on the biology and life history of sauropod dinosaurs. Similarly, *Kolb et al. (2015)* showed, via longitudinal thin sections, that in the giant deer *Megaloceros giganteus* the amount of woven-fibred bone within the fibrolamellar complex (FLC) is easily overestimated as well.

## Growth marks and skeletochronology

Different types of growth marks in the bone cortex are distinguished in the osteohistological literature. They are deposited cyclically, usually occurring within lamellar or parallel-fibred bone. All kinds of growth marks indicate a change in growth rate or a complete arrest of growth.

In all groups of mammals thin, semitranslucent to opaque bands, termed lines of arrested growth (LAGs, see also *Huttenlocker, Woodward & Hall, 2013*), occur (*Morris, 1970*; *Frylestam & Schantz, 1977*; *Buffrénil, 1982*; *Chinsamy, Rich & Vickers-Rich, 1998*; *Klevezal, 1996*; *Castanet et al., 2004*; *Köhler et al., 2012*). It has repeatedly been confirmed and is now widely accepted that LAGs are deposited annually (e.g., *Castanet & Smirina, 1990*; *Buffrénil & Castanet, 2000*; *Castanet, 1994*; *Marangoni et al., 2009*; *Chinsamy-Turan, 2012b*) and independently of metabolic rate and climatic background (*Köhler et al., 2012*;

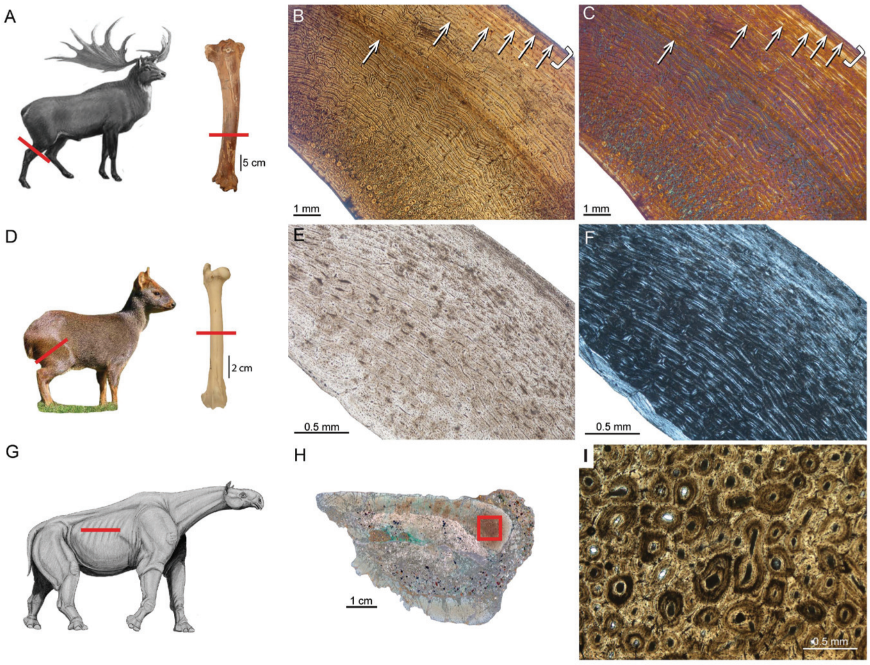

**Figure 1 Typical mammalian bone tissue as observed in large mammals such as cervids.** Red bars indicate area and plane of sectioning. Histological images (B), (E), and (I) in linear polarised light, (C) in crossed polarised light and with additional use of lambda compensator, and (F) in crossed polarised light. (A) Life reconstruction of the cervid *Megaloceros giganteus* ("Knight Megaloceros" by Charles R. Knight, courtesy of the American Museum of Natural History via Wikimedia Commons—http://commons.wikimedia.org). (B, C) Bone cortex of an adult tibia of *Megaloceros giganteus* specimen NMING:F21306/14 displaying an endosteal lamellar layer (innermost part of the cortex) and reticular as well as plexiform fibrolamellar primary bone with growth marks. Note that the primary bone is pervaded by secondary Haversian systems in the inner third of the bone cortex. White arrows indicate lines of arrested growth. Occurrence of LAGs indicated by black/white arrows and the outer circumferential layer (OCL) by white brackets. (D) Photograph of *Pudu puda* ("Pudupuda hem 8 FdoVidal Villarr 08Abr06-PhotoJimenez," courtesy of Jaime E. Jimenez via Wikimedia Commons—http://commons.wikimedia.org). (E, F) Bone cortex of an adult femur of *Pudu puda* specimen NMW 60135 displaying an endosteal lamellar layer and mainly plexiform fibrolamellar bone. (G) Reconstruction of *Paraceratherium* ("Indricotherium11," Courtesy of Dmitry Bogdanov via Wikimedia Commons—http://commons.wikimedia.org). (H) Cross-section of a rib of *Paraceratherium* sp. specimen MTA-TTM 2006-1209. Red rectangle indicates area of dense Haversian bone magnified in (I).

Huttenlocker, Woodward & Hall, 2013) and therefore they can be used for age estimations, estimates of age at sexual or skeletal maturity, and growth rate analysis.

Castanet et al. (2004) studied LAGs in long bones, mandibles, and tooth cementum (M2 and M3) of captive specimens of known aged mouse lemur, *Microcebus murinus*. The 43 male and 23 female specimens sampled ranged from juveniles to 11-year-old adults, for which LAG counts and ages correlated best in the tibiae. In individuals older than seven years the correlation decreased, leading to an age underestimation of three to four years and demonstrating limitations of skeletochronology in long bones (see also Klevezal, 1996; Castanet, 2006). Additionally, animals exposed to an artificially accelerated photoperiodic regimen (a 10-month cycle) show a higher number of LAGs than animals of the same true age in which a yearly photoperiod is maintained. According to that, there is strong evidence that photoperiodicity is an essential factor for the deposition of LAGs rather than environmental factors (see also Woodward, Padian & Lee, 2013).

Köhler et al. (2012) additionally demonstrated that the annual formation of LAGs is present throughout ruminants and that a cyclic arrest of growth in bone is mainly triggered by hormonal cues rather than environmental stresses. By confirming seasonal deposition of LAGs throughout ruminants, the general occurrence of LAGs in homeothermic endotherms has been confirmed, precluding the use of lines of arrested growth as an indicator of ectothermy (Köhler et al., 2012).

Different kinds of processes in the cortex potentially remove parts of the growth record and may erase early LAGs. One of those processes is the substitution of primary bone tissue by secondary bone tissue in areas where resorption previously occurred. Secondary bone can appear as *Haversian bone* (Fig. 1I) consisting of clustered Haversian systems responding to damage such as microcracks, or around the medullary cavity forming endosteal lamellar bone in response to ontogenetic changes in bone shape, i.e., bone drift (Enlow, 1962).

Several approaches to retrocalculate the lost information have been attempted and there are two ways of retrocalculating missing years. First, in case an appropriate ontogenetic growth series sampling is not available, it is possible to perform arithmetic estimates of the missing intervals, applied first for dinosaurs (e.g., Sander & Tückmantel, 2003; Horner & Padian, 2004; Erickson et al., 2004). The second approach is the superimposition of thin sections of long bones of different ontogenetic stages, again applied first for dinosaurs (e.g., Horner, Ricqlès & Padian, 2000; Bybee, Lee & Lamm, 2006; Lee & Werning, 2008; Erickson, 2014; see also Woodward, Padian & Lee, 2013 for more methodological details).

Marín-Moratalla, Jordana & Köhler (2013) were the first to apply the superimposition method to mammals using anteroposterior diameters of successive growth rings in five antelope (*Addax*) femora of different ages. They found that the first LAG in adult specimens fits the second growth cycle of juveniles, indicating that the first LAG is lost by resorption throughout ontogeny. This allowed estimates of age at death by counting all the rest lines in the bone cortex and increasing the LAG count by one. Additionally, it was possible to estimate age at sexual maturity. When an animal reaches maturity it is indicated by the deposition of a narrow layer of avascular lamellar bone, called the *outer circumferential layer* (OCL, Ponton et al., 2004; Figs. 1B and 1C), and also referred to as the *external fundamental system* (EFS, *sensu* Horner, Ricqlès & Padian, 1999; see also Woodward, Padian & Lee, 2013). Given that Cormack (1987) uses the term "outer circumferential lamellae" (p. 305), we follow Ponton et al. (2004) in using the term outer circumferential layer (OCL) instead of EFS. Marín-Moratalla, Jordana & Köhler (2013) and Jordana et al. (in press) interpreted the transition from the FLC to the OCL to represent attainment of reproductive maturity in ruminants, since maturity estimates correlated well with individual tooth eruption and wear stages, as well as life history data. Therefore, the authors could show that in ruminants it is possible to determine age at reproductive maturity and death. Maturity estimates based on the occurrence of the OCL in a recent study by *Kolb et al. (2015)* on extant cervids showed bone microstructure corresponding well with the timing of the attainment of skeletal maturity.

## MATERIAL AND METHODS

In order to contribute to a more complete picture of mammalian palaeohistology, long bones of the following additional mammalian taxa, including several taxa of extinct insular mammals, were sampled. Characteristics of bone histology of the following taxa are either poorly or not at all documented in the literature (Table 1): the extant white-eared opossum *Didelphis albiventris* and the thick-tailed opossum *Lutreolina crassicautada*, the giant deer *Megaloceros giganteus* from the Late Pleistocene of Ireland, the Asian giant deer *Sinomegaceros yabei* from the Late Pleistocene of Japan, the extant southern pudu *Pudu puda*, the Cyprus dwarf hippopotamid *Hippopotamus minor* from the Late Pleistocene of Cyprus, the dormouse *Leithia* sp. from the Pleistocene of Sicily, the giant hornless rhinocerotoid *Paraceratherium* sp. from the Late Oligocene of Turkey, the continental pika *Prolagus oeningensis* from the Middle Miocene of La Grive, France, and the Sardinian pika *Prolagus sardus* from the Late Pleistocene. From the Late Miocene of Gargano, Italy, the following material was sampled: the galericine insectivore *Deinogalerix* sp., the giant murid *Mikrotia magna*, as well as the giant pikas *Prolagus apricenicus* and *Prolagus imperialis*. Ontogenetic stages in long bones have been determined by the state of epiphyseal fusion (*Habermehl, 1985*).

Following standard procedures, bones were coated and impregnated with epoxy resin (Araldite or Technovit) prior to sawing and grinding. Long bones were transversely sectioned at the mid-shaft where the growth record is most complete (e.g., *Sander & Andrassy, 2006*; *Kolb et al., 2015*). A tibia of *Megaloceros giganteus* was also sampled by using a diamond-studded core drill, with sampled cores being subsequently processed (*Sander & Andrassy, 2006*; *Stein & Sander, 2009*). Sections were observed in normal transmitted and cross-polarised light using a Leica DM 2500 M compound microscope equipped with Leica DFC 420 C digital camera. Phylogeny was produced using Mesquite 3.02© (*Maddison & Maddison, 2015*) and redrawn using Adobe Illustrator CS5©.

### Approval information

We thank Naturalis Biodiversity Center, Leiden, the Netherlands, Loïc Costeur (Naturhistorisches Museum Basel, Switzerland), George Lyras (Museum of Paleontology and Geology, University of Athens, Greece), Nigel Monaghan (National Museum of Ireland, Natural History), Hiroyuki Taruno (Osaka Museum of Natural History, Japan), Frank Zachos and Alexander Bibl (Naturhistorisches Museum Wien, Austria), Pierre-Olivier Antoine (Institut des Sciences de l'Evolution-Montpellier, France), and Ebru Albayrak, (MTA Natural History Museum, The General Directorate of Mineral Research and Exploration, Ankara, Turkey) for approving sampling of specimens for histological study.

**Table 1** **Material used in this study.** Specimens sampled in this study with ontogenetic stage, geological age, locality of death/fossil site, and specimen number.

| Species | Object | Ontogenetic stage | Geological age; locality | Specimen number |
|---|---|---|---|---|
| *Didelphis albiventris* | Femur | adult | La Plata, Argentina | PIMUZ A/V 5279 |
| ” | ” | adult | ” | PIMUZ A/V 5277 |
| ” | ” | adult | Ingeniero Mashwitzt, Argentina | PIMUZ A/V 5276 |
| ” | ” | adult | Ranchos, Argentina | PIMUZ A/V 5278 |
| *Lutreolina crassicautada* | ” | adult | Mar de Ajo, Argentina | PIMUZ A/V 5275 |
| ” | ” | adult | La Plata, Argentina | PIMUZ A/V 5274 |
| *Leithia* sp. | Tibia | adult | Pleistocene; Grotta di Maras, Sicily | NMB G 2160 |
| *Mikrotia magna* | Femur | adult | Late Miocene; Sono Giovo, Gargano | RGM.792083 |
| ” | ” | adult | ” | RGM.792084 |
| ” | ” | adult | ” | RGM.792085 |
| ” | ” | adult | ” | RGM.792086 |
| *Prolagus apricenicus* | Femur | adult | Late Miocene; San Giovannino, Gargano | RGM.792087 |
| ” | ” | adult | ” | RGM.792088 |
| ” | ” | adult | ” | RGM.792089 |
| ” | ” | adult | ” | RGM.792090 |
| ” | ” | adult | ” | RGM.792091 |
| ” | ” | adult | ” | RGM.702092 |
| ” | Humerus | adult | ” | RGM.792093 |
| ” | ” | adult | ” | RGM.792094 |
| ” | ” | adult | ” | RGM.792095 |
| *Prolagus imperialis* | Femur | adult | ” | RGM.792096 |
| ” | ” | adult | ” | RGM.792097 |
| ” | ” | adult | ” | RGM.792098 |
| ” | ” | adult | ” | RGM.792099 |
| ” | ” | adult | ” | RGM.792100 |
| ” | ” | adult | ” | RGM.792101 |
| ” | Humerus | juvenile | ” | RGM.792102 |
| ” | ” | adult | ” | RGM.792103 |
| ” | ” | adult | ” | RGM.792104 |
| *Prolagus sardus* | Femur | juvenile | Late Pleistocene; Monte San Giovanni, Sardinia | NMB Ty. 4974 |
| ” | ” | adult | ” | NMB Ty. 4977 |
| ” | ” | adult | Late Pleistocene; Grotta Nicolai, Sardinia | NMB Ty.12656 |
| ” | ” | adult | ” | NMB Ty.12657 |
| ” | ” | adult | Late Pleistocene; Isola di Tavolara, Sardinia | NMB Ty.12658 |
| ” | ” | adult | ” | NMB Ty.12659 |
| *Prolagus oeningensis* | Femur | juvenile | Middle Miocene; La Grive, France | PIMUZ A/V 4532 |
|  | ” | adult |  | PIMUZ A/V 4532 |
| ” | ” | adult | ” | PIMUZ A/V 4532 |
| ” | Humerus | adult | ” | PIMUZ A/V 4532 |
| ” | ” | adult | ” | PIMUZ A/V 4532 |
| *Megaloceros giganteus* | Tibia | adult | Late Pleistocene; Baunmore Townland, Rep. of Ireland | NMING:F21306/14 |

(*continued on next page*)

Table 1 (*continued*)

| **Species** | **Object** | **Ontogenetic stage** | **Geological age; locality** | **Specimen number** |
|---|---|---|---|---|
| *Sinomegaceros yabei* | Tibia | juvenile | Late Pleistocene; Kumaishi-do Cave, Miyama, Hachiman-cho, Gujo City, Gifu Prefecture, Japan | OMNH QV-4067 |
| " | Tibia | adult | " | OMNH QV-4068 |
| " | Femur | juvenile | " | OMNH M-087 |
| " | Femur | adult | " | OMNH QV-4062 |
| *Pudu puda* | Femur | adult | Tiergarten Schönbrunn, Vienna, Austria | NMW 60135 |
| *Hippopotamus minor* | " | juvenile | Late Pleistocene; Kissonerga, Cyprus | CKS 110/B |
| " | " | juvenile | " | CKS 122/B |
| " | " | subadult | " | CKS 117 |
| " | Tibia | adult | " | CKS 215 |
| *Paraceratherium* sp. | Rib | adult | Late Oligocene; Gözükizilli, Turkey | MTA-TTM 2006-1209 |
| *Deinogalerix* sp. | Femur | adult | Late Miocene; Gervasio 1, Gargano, Italy | RGM.178017 |
| " | Humerus | adult | Late Miocene; Chiro 20E, Foggia, Gargano, Italy | RGM.425360 |

**Notes.**

**Institutional Abbreviations:** CKS, Cyprus Kissonerga collection of the University of Athens; MTA, Natural History Museum, The General Directorate of Mineral Research and Exploration, Ankara, Turkey; NMB, Naturhistorisches Museum Basel, Switzerland; NMING, National Museum of Ireland—Natural History; NMW, Naturhistorisches Museum Wien, Austria; OMNH, Osaka Museum of Natural History, Japan; PIMUZ, Paläontologisches Institut und Museum, Universität Zürich, Switzerland; RGM, Rijksmuseum voor Geologie en Mineralogie (now Netherlands Centre for Biodiversity Leiden).

## MAMMALIAN BONE HISTOLOGY—WORKS BEFORE 1935

The initial contribution on the bone palaeohistology of mammals was performed by Quekett (1849a), Quekett (1849b) and Quekett (1855) as part of comprehensive studies dealing with the bone cortex of not only mammals but also fish, reptiles, and birds. He described the tissue from mammalian long bones including an extinct rhinocerotid and equid, the extinct giant deer *Megaloceros giganteus*, the extinct proboscidean *Mastodon*, fossils of xenarthrans such as *Megatherium*, and humans. Quekett (1849a), Quekett (1849b) and Quekett (1855) described in these taxa Haversian canals, bony laminae, bone-cells, and canaliculi as well as a the typical three layered composition of cranial bones, ribs, and scapulae displaying a diploe structure within two thin compact layers. Later, Aeby (1878) concentrated on taphonomical effects and compared bone tissue of reptiles, birds, and mammals. Then, Kiprijanoff (1881) illustrated the bone cortex of the sperm whale (*Physeter macrocephalus*) in a comparative study of fossil material from Russia. Schaffer (1890) described the bone tissue of several mammals, including sirenians from the Eocene, Oligocene, and Miocene (*Halitherium*), a proboscidean from the Miocene (*Mastodon*), an undetermined fossil cetacean, and artiodactyls (an undetermined artiodactyl referred to an antelope and *Hippopotamus*, both from the Pliocene). Schaffer also investigated Artiodactyla (*Sus scrofa, Capreolus*), Carnivora (*Ursus spelaeus*), Rodentia (*Arvicola*), as well as undetermined long and skull bones, all from the Pleistocene. Foote (1911a) and Foote (1911b) examined in a comprehensive study the femoral bone cortex of extant amphibians, birds, and mammals including marsupials, rodents, lagomorphs, carnivorans, 'ungulates', and primates. Nopcsa & Heidsieck (1934) studied reptile bones and the ribs of sirenians (*Halitherium*). In his comparative work, *Gross (1934)* studied the bone cortex of the proboscidean *Mammuthus*.

## BONE HISTOLOGY OF EXTINCT AND EXTANT CYNODONT CLADES

### Non-mammalian cynodonts

Cynodonts represent the last major synapsid lineage to appear in Earth history with mammals as living representatives. Many articles have been published on non-mammalian cynodont histology in recent years (e.g., *Ricqlès, 1969*; *Botha & Chinsamy, 2000*; *Botha & Chinsamy, 2004*; *Botha & Chinsamy, 2005*; *Ray, Botha & Chinsamy, 2004*; *Chinsamy & Abdala, 2008*; *Botha-Brink, Abdala & Chinsamy, 2012*; *Chinsamy-Turan, 2012b*). Fibrolamellar bone is present to a varying degree in all cynodonts. Considerable variation in vascular density and orientation and the presence/absence of growth marks such as LAGs are evident. When observed within the phylogenetic context, there is an overall increase in bone deposition rate. This is indicated by an increasing prevalence of highly vascularised fibrolamellar bone in phylogenetically later cynodonts (*Botha-Brink, Abdala & Chinsamy, 2012*). Several factors are proposed to influence the microstructure and therefore responsible for the aforementioned variability: phylogeny, biomechanics, ontogeny, body size, lifestyle preferences, and environmental influences (*Cubo et al., 2005*; *Kriloff et al., 2008*; *Botha-Brink, Abdala & Chinsamy, 2012*). *Padian (2013)* emphasised that the correlation between fibrolamellar bone and high growth rates, and endothermy is still valid, although fibrolamellar bone is known to occur in rare cases in ectothermic reptiles such as crocodiles and turtles.

### Multituberculata and early mammals

Histological studies of multituberculates (see Fig. 2 for mammalian groups discussed below) and in general stem mammals are scarce. *Enlow & Brown (1958)* described a section of a mandible from *Ptilodus*. Its cortex consisted of lamellar bone with a central region of indistinct and unorganised lamellae, in which lacunae and cell spaces as well as radial vascular canals were present. Morphological studies have suggested different kinds of locomotion within the group (saltatorial, fossorial, scansorial, and arboreal; *Kielan-Jaworowska, Cifelli & Luo, 2004*), which might be reflected in the microstructure of the appendicular bones. *Chinsamy & Hurum (2006)* compared the bone tissue from long bones and one rib of multituberculates, Morganucodon, and early mammals. They showed that *Morganucodon* and multituberculates (*Kryptobataar*, *Nemegtbataar*) were characterised by fibrolamellar/woven-fibred bone at early stages of ontogeny and later on by parallel-fibred or lamellar bone. Their findings pointed towards relatively high growth rates compared to the late Mesozoic eutherians *Zalambdalestes* and *Barunlestes* with periodic growth pauses as indicated by the occurrence of LAGs. Comparisons of morganucodontid and early mammalian bone microstructure with that of non-mammalian cynodonts, extant monotremes, and placentals indicated significant differences in the rate of osteogenesis in the various groups. The authors concluded multituberculates and Mesozoic eutherians

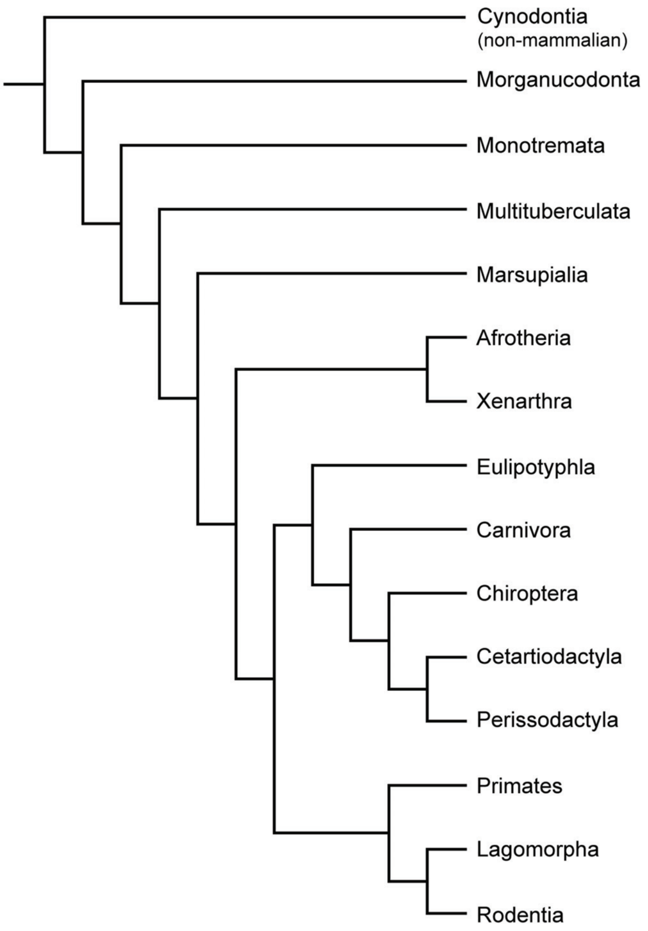

Figure 2 **Phylogeny of Cynodontia focussing on groups discussed, based on *Luo & Wible (2005)*, *Luo (2011)*, *Meredith et al. (2011)* and *O'Leary et al. (2013)*.** Notoungulates and Pantodonta are not included given their controversial systematic position.

to have had slower growth rates than modern monotremes and placentals and that the sustained, uninterrupted bone formation among multituberculates may have been an adaptive attribute prior to the K–Pg event, but that a flexible growth strategy implying periodic growth pauses of the early eutherians was more advantageous thereafter.

## Monotremata

Monotremes are represented today by three genera (*Ornithorynchus*, *Tachyglossus*, and *Zaglossus*) each with specialized skeletal morphology. Their poor fossil record includes material from Australia and South America (*Pascual et al., 1992*; *Musser & Archer, 1998*; *Musser, 2003*). Accordingly, the bone histology of monotremes has been scarcely studied.

*Enlow & Brown (1958)* were the first to describe sections of long bones and ribs of *Platypus* and *Echidna*. *Chinsamy & Hurum (2006)* described the femoral bone tissue of *Ornithorhynchus* as being a mixture of woven-fibred bone with lamellar bone deposits. Additionally, large parts of the compacta consisted of compacted coarse cancellous bone. The type of vascularisation and the orientation of the vascular channels varied from simple blood vessels with longitudinal, circular and radial orientations to primary osteons with longitudinal and reticular arrangements. Only isolated secondary osteons were present.

## Marsupialia

Despite marsupials being the second most diverse group of living mammals, so far their bone histology is poorly studied. Early contributions are those of *Foote (1911a)*, *Enlow & Brown (1958)* and *Singh, Tonna & Gandel (1974)* on the marsupial *Didelphis*. Our study of new samples of the white-eared opossum *Didelphis albiventris* and the latrine opossum *Lutreolina crassicaudata* (Table 1) essentially confirms their observations.

The bone cortex of long bones from *Didelphis* is characterised by a compacta surrounding the medullary cavity. The bone matrix is dominated by parallel-fibred bone (Figs. 3A–3C). Towards the inner part, the amount of woven-fibred bone increases (Fig. 3C). In most specimens remodelling is restricted to isolated secondary osteons as described by *Enlow & Brown (1958)*. Inner and outer circumferential layers are present. The inner circumferential layer consists of lamellar bone. The outer circumferential layer is dominated by parallel-fibred bone. The thickness of this layer varies between specimens. Except in one specimen with one LAG, no LAGs are present in the analysed specimens. The bone cortex is well vascularised throughout (see also *Enlow & Brown, 1958*), with an irregular pattern, i.e., radial, oblique, but mainly longitudinal primary vascular canals. *Lutreolina* shows a primary bone matrix that is dominated by parallel-fibred bone with simple primary longitudinal and radial to oblique vascular canals (Figs. 3D–3F). Remodelled areas are characterised by partially oblique secondary osteons (Fig. 3F). The inner circumferential layer is thin and formed by lamellar bone. The outer circumferential layer is, if present, formed by parallel-fibred bone. LAGs are not developed. The vascularity is less dense than in *Didelphis*. The combination of parallel-fibred bone with low vascularisation suggests slow apposition rates (*Chinsamy-Turan, 2012b*; *Huttenlocker, Woodward & Hall, 2013*).

## Xenarthra

Early contributions on xenarthran bone histology are *Quekett (1849a)*, *Quekett (1855)*and *Enlow & Brown (1958)*. Because dermal armour is an outstanding feature of xenarthrans, several studies focussed on the histology of osteoderms (e.g., *Wolf, 2007*; *Wolf, 2008*; *Chávez-Aponte et al., 2008*; *Hill, 2006*; *Vickaryous & Hall, 2006*; *Krmpotic et al., 2009*; *Vickaryous & Sire, 2009*; *Wolf, Kalthoff & Martin Sander, 2012*; *Da Costa Pereira et al., 2012*). These data, shed light on soft tissue structures of extinct xenarthrans, their phylogenetic relationships, and their functional morphology. The most detailed study up to date dealing with xenarthran long bone histology was performed by *Straehl et al. (2013)* (but see also *Ricqlès, Taquet & Buffrénil, 2009*). Straehl and colleagues sampled 67 long bones of 19 genera and 22 xenarthran species and studied bone microstructure as well as bone

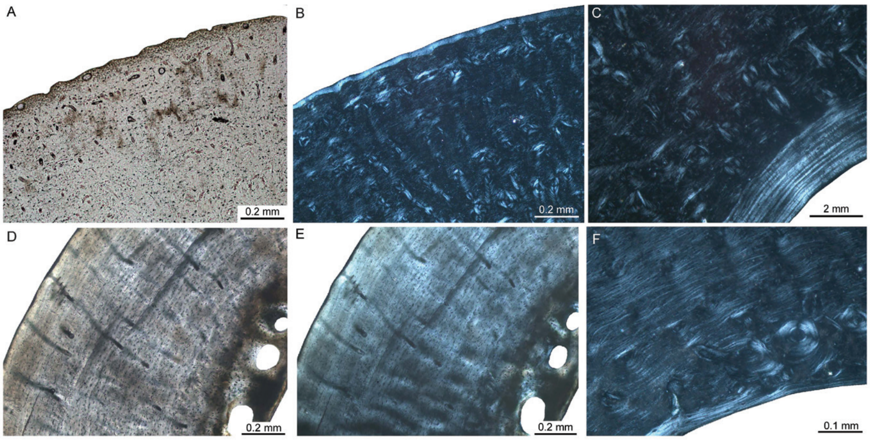

**Figure 3 Femoral bone cortex of marsupials.** Histological images (A) and (D) in linear polarised light and (B), (C), (E), and (F) in crossed polarised light. (A, B) Outer bone cortex of adult *Didelphis albiventris* specimen PIMUZ A/V 5279. Note the occurrence of simple primary longitudinal vascular canals and primary osteons in mainly parallel-fibred bone tissue. (C) Inner bone cortex of the same specimen displaying a distinct endosteal lamellar layer. (D, E) Bone cortex of adult *Lutreolina crassicautada* specimen PIMUZ A/V 5275. (F) Inner cortex of same specimen. Note the occurrence of primary longitudinal vascular canals and primary osteons as well as Haversian systems within the parallel-fibred bone.

compactness trends. Primary bone tissue consists of a mixture of woven, parallel-fibred, and lamellar bone. Irregularly shaped vascular canals show longitudinal, reticular, or radial orientation. Anteaters are the only sampled taxa showing laminar orientation. Armadillo long bones are characterised by obliquely oriented secondary osteons in transverse sections, reflecting their complex morphology. LAGs are common in xenarthrans although being restricted to the outermost part of the bone cortex in armadillo long bones. Moreover, cingulates (armadillos and closely relative extinct taxa) show lower bone compactness than pilosans (sloths) and an allometric relationship between humeral and femoral compactness. Straehl and colleagues emphasise that remodelling is more developed in larger taxa as indicated by dense Haversian bone in adult specimens and discuss increased loading as a possible cause. Amson et al. (2014) assessed the timing of acquisition of osteosclerosis (increase in bone compactness) and pachyostosis (increase in bone volume) in long bones and ribs of the aquatic sloth *Thalassocnus* from the Neogene of Peru as the main osteohistological modifications of terrestrial tetrapods returning to water. They showed that such modifications can occur during a short geological time span, i.e., *ca* 4 Ma. Furthermore, the strongly remodelled nature of xenarthran bone histology allowed the reassignment of a rib previously ascribed to a sirenian to the aquatic sloth (Amson et al., 2015).

## Afrotheria

Early contributions on the bone histology of afrotherians are Aeby (1878) and Schaffer (1890) on sirenians and proboscideans, Nopcsa & Heidsieck (1934) on sirenians, Vanderhoof (1937), Enlow & Brown (1958), Kaiser (1960), Mitchell (1963) and Mitchell

*(1964)* on sirenians and desmostylians, and *Ezra & Cook (1959)* as well as *Cook, Brooks & Ezra-Cohn (1962)* on elephantids. *Ricqlès & Buffrénil (1995)* described pachyosteosclerosis in the sirenian *Hydrodamalis gigas*. *Buffrénil et al. (2008)* and *Buffrénil et al. (2010)* studied the ribs of 15 extant and extinct sirenian species representing 13 genera, one desmostylian, and 53 specimens of 42 extant species of terrestrial, aquatic, or amphibious mammals. In those studies, primary bone tissue in young specimens is constituted by fibrolamellar bone, whereas with increasing age, parallel-fibred bone tissue with longitudinal vascular canals and frequent LAGs is deposited. The authors showed that pachyostosis is subsequently regressed during evolution of the clade. In contrast, only by the end of the Eocene, osteosclerosis was fully developed. Furthermore, Buffrénil et al. argued that variable degrees of pachyostosis and osteosclerosis in extinct and extant sirenians were caused by similar heterochronic mechanisms bearing on the timing of osteoblast activity. *Hayashi et al. (2013)* analysed the histology of long bones, ribs, and vertebrae of four genera of desmostylians (usually considered as tethytherians, but see *Cooper et al., 2014*) and 108 specimens of extant taxa (ribs: 19 taxa, humeri: 62 taxa, femora: 16 taxa, vertebrae: 11 taxa) with various phylogenetic positions and ecologies by using thin sections and CT-scan data. Primary bone tissue in desmostylians consisted of parallel-fibred bone with multiple LAGs. By comparisons with extant mammals, they found that *Behemetops* and *Palaeoparadoxia* show osteosclerosis, *Ashoroa* pachyosteosclerosis (i.e., a combination of increase in bone volume and compactness), while *Desmostylus* shows an osteoporotic-like pattern (i.e., decrease in bone compactness) instead. Since it is known from extant mammals that increasing bone mass provides hydrostatic buoyancy and body trim control suitable for passive swimmers and shallow divers, whereas spongy bones are associated with hydrodynamic buoyancy control in active swimmers, they concluded that all desmostylians achieved an essentially aquatic lifestyle. However, the basal taxa *Behemotops*, *Paleoparadoxia*, and *Ashoroa* could be interpreted as shallow water swimmers hovering slowly or walking on the bottom, whereas the more derived taxon *Desmostylus* was a more active swimmer. The study has therefore shown that desmostylians are the second mammalian group after cetaceans to show a shift from bone mass increase to decrease during their evolutionary history.

As several tethytherian taxa are aquatic, the question of the ancestral lifestyle of the clade was raised. A femur and a humerus of the Eocene proboscidean *Numidotherium* were sampled by *Mahboubi et al. (2014)*. These authors recognised "large medullar cavities" (p. 506), which were considered suggestive of terrestrial habits. However, the illustrations provided by *Mahboubi et al. (2014)* show no opened medullary cavity, and trabecular bone occupies most of the cross-sectional area (labelled "medullary bone" by *Mahboubi et al., 2014*: Fig. 4).

*Sander & Andrassy (2006)* described the bone tissue of long bones from *Mammuthus primigenius* as laminar fibrolamellar bone. Due to poor preservation of the fossil bone tissue, the authors were not able to definitely confirm the occurrence of LAGs. The valuable study of *Curtin et al. (2012)* dealt with two aspects of bone histology. First, they described for the first time the bone tissue of fifteen bones (femora and tibiae) of eleven specimens of late-term-fetal, neonatal, and young juvenile extant and extinct elephantids representing

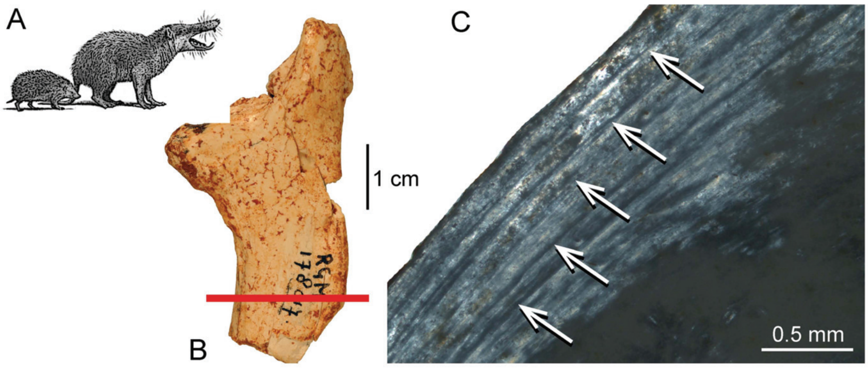

**Figure 4 Histological features of the femur of *Deinogalerix* sp.** (A) Life reconstruction of *Deinogalerix koenigswaldi* in comparison to the extant hedgehog *Erinaceus* (modified from Agustí & Antón, 2002). (B) Adult right femur (specimen RGM.178017) in anterior view. Red bar indicates area and plane of sectioning. (C) Lateral bone cortex in crossed polarised light showing parallel-fibred bone and 5 LAGs. Occurrence of LAGs indicated by white arrows.

four species, including the insular dwarf mammoth *Mammuthus exilis* from the Late Pleistocene of Santa Rosa Island of the Californian Channel Islands. The bone tissue they found was predominantly laminar fibrolamellar bone. Remarkable was a distinct change in tissue microstructure marking the boundary between prenatal and postnatal bone deposition, i.e., a higher amount of large longitudinal vascular canals suggesting slightly higher postnatal growth rates. Secondly, besides histological thin sections, Curtin and colleagues employed synchrotron microtomography (SR-μCT) for noninvasively obtaining high-resolution image-"slices." They showed that, in comparison to histological sectioning, the SR-μCT data lack shrinkage, distortion or loss of tissue, as is usually the case in histological sections. However, they stated that the quality of histological detail observable is by far superior in histological thin sections. The virtual microtomography enabled the authors to rank specimens by ontogenetic stage and quantified vascular patterns. They showed that bones of the Columbian mammoth, *M. columbi* had the thickest and largest number of laminae, whereas the insular dwarf mammoth, *M. exilis*, was characterised by its variability in that regard. The authors concluded that, qualitatively, patterns of early bone growth in elephantids are similar to those of juveniles of other tetrapods, including dinosaurs.

## Notoungulata

Notoungulates are an extinct, largely diverse, endemic group of Cenozoic South American mammals, ecologically similar to current hoofed ungulates. Only four taxa (*Toxodon*, *Nesodon*, *Mesotherium*, and *Paedotherium*) were subject to histological studies (*Ricqlès, Taquet & Buffrénil, 2009*; *Forasiepi et al., 2015*; *Tomassini et al., 2014*) from the more than 150 species recognised in the group. The bone samples were characterised by a well-vascularised compact cortex with mostly longitudinal vascular canals. Few irregularly oriented canals could be found. Osteocyte lacunae were large and very abundant.

Haversian bone was recorded in *Toxodon*, *Nesodon*, and *Mesotherium*. This is a common feature in mammalian bone (*Enlow & Brown, 1958*), probably caused by increased loading in large-bodied species as discussed by *Straehl et al. (2013)* for xenarthrans. Areas of primary bone matrix were visible between secondary osteons, which displayed a mostly parallel-fibred to lamellar organisation. Localized areas of woven bone characterised by round osteocyte lacunae were also present. The most external layer of the cortex consisted of parallel-fibred bone with very few secondary osteons and was in clear contrast to the heavily remodelled inner cortex. The study of *Tomassini et al. (2014)* on the palaeohistology of hemimandibles of *Paedotherium bonaerense* from the early Pliocene of Argentina discussed the processes affecting fossil remains before and after burial.

## Pantodonta

Pantodonts are an extinct group of mammals that comprised large-bodied, heavily built omnivores and herbivores from the Paleocene and Eocene of Laurasia. Only one study (*Enlow & Brown, 1958*) examined their bone histology. A rib of the Eocene pantodont *Coryphodon* showed primary lamellar bone with longitudinal vascularisation.

## Laurasiatheria—Eulipotyphla

The comprehensive work of *Enlow & Brown (1958)* was the first contribution on eulipotyphlan bone histology. They described the primary bone tissue of a *Talpa* tibia and a *Sorex* mandible as almost completely avascular lamellar bone. A humerus and radius from a juvenile showed in their outer cortex a "disorganised" (*Enlow & Brown, 1958*: p. 190) structure called it, being accompanied by oblique, radial, circumferential or longitudinal simple vascular canals). *Klevezal (1996)* discussed eulipotyphlan histology by emphasising growth marks (LAGs) in the bone cortex of mandibles and their value for skeletochronology. *Meier et al. (2013)* studied the bone compactness of humeri from eleven extant and eight fossil talpid species and two non-talpid species. They could not detect any pattern of global compactness related to biomechanical specialization, phylogeny, or size and concluded that at this small size the overall morphology of the humerus plays a predominant role in absorbing load. *Morris (1970)* evaluated the applicability of LAGs in extant hedgehog mandibles and found high correlation between age and LAG count.

In the giant galericine "hedgehog" *Deinogalerix* from the palaeoisland of Gargano (Table 1), Italy, the bone tissue at the inner layer of femur RGM.178017 and humerus RGM.425360 is characterised by parallel-fibred bone, whereas the outer layer and the trabecular bone is composed of lamellar bone (Figs. 4A–4C). In the bone cortex, simple longitudinal vascular canals and primary osteons are present. Primary bone tissue is partially replaced by secondary osteons. In a femur corresponding to an adult individual, five LAGs can be distinguished (Fig. 4C) indicating a minimum age of five years.

## Chiroptera

*Enlow & Brown (1958)* described the primary bone tissue in chiropterans as lamellar bone surrounding a non-cancellous medullary cavity. *Klevezal (1996)* described the presence of LAGs in chiropteran bone tissue. *Herdina et al. (2010)* described the bone tissue of the baculum from three *Plecotus* species as lamellar bone surrounding a small medullary cavity similar to the arrangement of a Haversian system whereas the ends of the bone consisted of woven-fibred bone.

## Perissodactyla

*Enlow & Brown (1958)*, *Sander & Andrassy (2006)*, *Cuijpers (2006)*, and *Hillier & Bell (2007)* described long bones and ribs of fossil and extant equids as being primarily plexiform fibrolamellar with longitudinal vascular canals, accompanied by extensive remodelling including the occurrence of dense Haversian bone. *Zedda et al. (2008)* found much Haversian tissue in extant horses and cattle. Osteons of the horse were more numerous and composed of a higher number of well-defined lamellae when compared to those of cattle. Diameter, perimeter, and area of osteons and Haversian canals were always higher in horses than in cattle and this pattern was related to their different locomotor behaviour. However, *Hillier & Bell (2007)* found non-significant differences between Haversian canals of horses and cattle. *Enlow & Brown (1958)* additionally described a stratified, circumferential pattern of vascular canals in a mandible of a Miocene chalicothere (*Moropus*), i.e., laminar fibrolamellar bone tissue *sensu* *Francillon-Vieillot et al. (1990)*. The authors demonstrated an identical pattern of bone tissues and vascular canals in several ribs of fossil tapirs from the Eocene. *Sander & Andrassy (2006)* described bone tissue of tibiae of Late Pleistocene woolly rhinocerotid (*Coelodonta antiquitatis*). They found predominantly laminar fibrolamellar bone as primary bone type besides a high amount of Haversian bone. *Ricqlès, Taquet & Buffrénil (2009)* described the distribution of primary and secondary bone as well as vascularisation in thin sections of several extant and extinct perissodactyls including chalicotheres. *Cooper et al. (2014)* considered anthracobunids as stem-perissodactyls, and concluded osteosclerosis in limb bones and ribs of anthracobunids to be consistent with the occupation of shallow-water habitats. *Martinez-Maza et al. (2014)* analysed the bone tissue of humeri, femora, tibiae and metapodials of the equid *Hipparion concudense* from the upper Miocene site of Los Valles de Fuentidueña (Spain) and showed that the number of growth marks is similar across the different limb bones. They distinguished four age groups and determined that *Hipparion concudense* tended to reach skeletal maturity during its third year of life. *Martinez-Maza et al. (2014)* identified ontogenetic changes in bone structure and growth rate and distinguished three histological stages of ontogeny corresponding to immature, subadult, and adult individuals. *Nacarino-Meneses, Jordana & Köhler (in press)* studied an ontogenetic series of *Equus hemionus* (Asiatic wild ass). They analysed growth marks in femora of different ontogenetic stages. Bone tissue types and vascular canal orientation varied both during ontogeny and within a cross-section. Skeletochronology generally fitted previous age estimates from dental eruption patterns. A wild adult female attained skeletal maturity at the age of four, a wild male at five years of age.

A rib of the giant rhinocerotoid *Paraceratherium* sp. (Fig. 1G and Table 1) from the Late Oligocene of Turkey displays dense Haversian bone (Fig. 1I), whereas the bone cortex is heavily recrystallised and does not allow observations on primary bone.

## Cetartiodactyla

*Enlow & Brown (1958)* gave a comprehensive overview on the bone histology of artiodactyls. The Miocene artiodactyls *Merycoidodon* and *Leptomeryx* showed in mandibles, maxillas, and ribs a reticular pattern of primary vascularisation next to secondary Haversian tissue. Extant taxa showed essentially plexiform fibrolamellar bone in long bones and reticular bone tissue in skull bones and mandibles. *Singh, Tonna & Gandel (1974)* studied the long bone tissue of a mature specimen of the blue duiker *Cephalophus manticola*, and two perinatal specimens of the Indian sambar *Cervus unicolor* and the reindeer *Rangifer tarandus*. Whereas *Cephalophus* showed primary longitudinal vascularisation, the perinatal cervids revealed a reticular pattern of vascular canals. Plexiform fibrolamellar bone (Figs. 1B, 1C, 1E and 1F) was confirmed as primary bone tissue in artiodactyls in subsequent publications (*Klevezal, 1996*; *Horner, Ricqlès & Padian, 1999*; *Cuijpers, 2006*; *Sander & Andrassy, 2006*; *Hillier & Bell, 2007*; *Köhler et al., 2012*; *Marín-Moratalla, Jordana & Köhler, 2013*; *Kolb et al., 2015*; *Jordana et al., in press*). *Marín-Moratalla et al. (2014)* identified the primary bone tissue in bovids as laminar to plexiform. They studied 51 femora representing 27 ruminant species in order to determine the main intrinsic or extrinsic factors shaping the vascular and cellular network of fibrolamellar bone. Specifically, the authors examined the correlation of certain life history traits in bovids, i.e., body mass at birth and adulthood as well as relative age at reproductive maturity. Quantification of vascular orientation and vascular and cell densities revealed that there is no correlation with broad climatic categories or life history. Instead, the authors found correlation with body mass since larger bovids showed more circular canals and lower cell densities than did smaller bovids. *Mitchell & Sander (2014)* suggested a three front model consisting of an apposition front, a Haversian substitution front, and a resorption front, and applied this model successfully to a humerus of red deer *Cervus elaphus*. They found moderate apposition and remodelling as well as slow resorption in the red deer specimen. *Hofmann, Stein & Sander (2014)* examined the lamina thickness in bone tissue (LD) in sauropodomorph dinosaurs and 17 mammalian taxa, including artiodactyls and perissodactyls. They found that LD is relatively constrained within the groups and that mean mammalian LD differs significantly from mean sauropodomorph LD. In suids, LD was higher than in other mammals. The authors therefore concluded that laminar vascular architecture is most likely determined by a combination of structural, functional as well as vascular supply and physiological causes.

For the present study, the bone cortex of one small (CKS 110/B), one intermediate (CKS 122/B), and one large juvenile (subadult; CKS 117) of the extinct Pleistocene dwarf hippopotamid of Cyprus, *Hippopotamus minor* (also called *Phanourios minor*, see *Van der Geer et al., 2010*), were examined (Table 1). In the juvenile femora the bone tissue is characterised by reticular to plexiform fibrolamellar bone with an endosteal, inner circumferential layer consisting of lamellar bone (Fig. 5). The bone is generally highly vascularised with primary longitudinal vascular canals and primary osteons towards the outer part of the cortex. There are no Haversian systems in the small juvenile (Fig. 5B), although their content increases during ontogeny and is highest in the subadult specimen. Although heavily recrystallized, an adult tibia of *Hippopotamus minor* shows

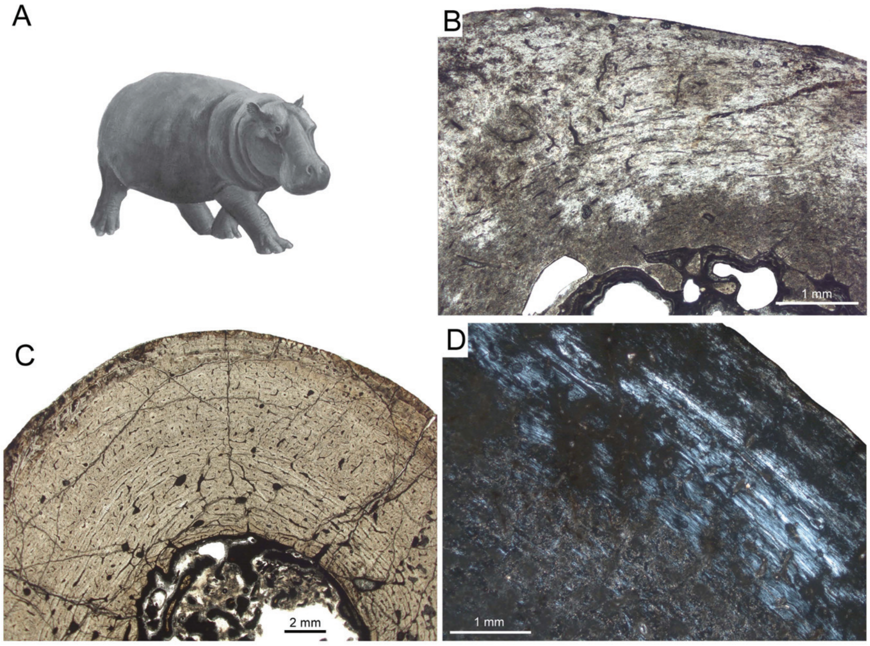

**Figure 5 Bone cortex of *Hippopotamus minor* femora.** (A) Life reconstruction (from *Van der Geer et al., 2010*; drawing: Alexis Vlachos) of another Mediterranean dwarf hippopotamid from the Middle Pleistocene of Crete. Since no life reconstruction of *Hippopotamus minor* is available, we here show the one of *Hippopotamus creutzburgi*. Histological images (B), and (C) in linear polarised light, (D) in crossed polarised light. (B) Small juvenile specimen CKS 110/B. (C) Intermediate sized juvenile specimen CKS 122/B showing reticular to plexiform vascularised bone. Note that the middle part mainly consists of reticular bone. (D) Outer bone cortex of large juvenile specimen CKS 117 showing mainly parallel-fibred bone. Black and grey areas indicate zones of recrystallisation due to diagenetic alteration of bone tissue.

strong remodelling with partially dense Haversian bone occurring from the inner to the outermost part of the cortex. Towards the outer cortex of the subadult femur (Fig. 5D) and typically for large mammals, the amount of parallel-fibred bone within the fibrolamellar complex increases, indicating a decrease in growth rate.

Another taxon sampled for the current study is *Sinomegaceros yabei* (Table 1), which is, as *Megaloceros*, a large-sized megacerine deer. Although a thorough description is prevented by the suboptimal preservation of the specimens, some of their histological features can be described here. The primary bone of the inner cortex is highly vascularised, being formed by fibrolamellar tissue with a mostly plexiform vascularisation. The outer cortex is in turn weakly vascularised. The adult femur OMNH QV-4062 features seven LAGs (Fig. 6), with a 2.57 mm thick second growth zone, which is even greater than the extreme values found in the elk, *Alces* and *Megaloceros* (*Kolb et al., 2015*), and which indicates, as in the latter taxa, a high growth rate.

Several authors focused on the bone histology of cetaceans and sirenians for their peculiar aquatic lifestyle. *Enlow & Brown (1958)* described the primary bone tissue of

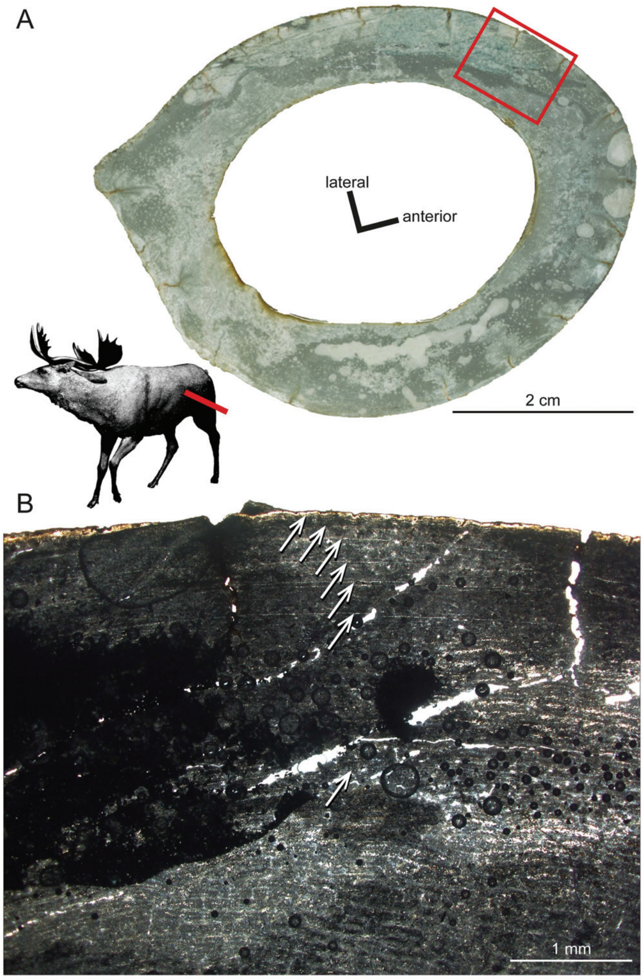

**Figure 6** **Histological features of *Sinomegaceros yabei*, the megacerine deer from the Pleistocene of Japan.** Histological images in linear polarised light of an adult femur (OMNH QV-4062) depicting (A) the whole cross-section and (B) a close-up of the outer cortex. The red bar in (A) localises the approximated position of the section on the life reconstruction (courtesy of Hirokazu Tokugawa), and the red rectangle indicates the area of the close-up. (B) Note that seven LAGs are visible, as indicated by white arrows.

skull bones and vertebrae of the porpoise (*Phocoena phocoena*) as featuring a reticular vascularisation with a high amount of remodelling including the occurrence of dense Haversian bone. Buffrénil and colleagues studied the microstructure of bone tissue from baleen whales in several works. They found annually deposited well-defined LAGs in mandibular bone tissue of the common porpoise, *Phocoena phocoena* (*Buffrénil, 1982*). The humeral bone tissue of the common dolphin (*Delphinus delphis*) shows a cancellous texture without an open medullary cavity and during ontogeny more bone eroded than deposited, indicating an osteoporotic-like process (*Buffrénil & Schoevaert, 1988*). *Buffrénil & Casinos (1995)*, by using standard microscopic methods, and *Zylberberg et al. (1998)*, by using scanning and transmission electron microscopy, studied the rostrum of the extant Blainville's beaked whale *Mesoplodon densirostris*, demonstrating a high density because of hypermineralised tissue with longitudinal fibres in dense Haversian bone. *Buffrénil, Dabin & Zylberberg (2004)* demonstrated that the petro-tympanic bone complex in common dolphins consists of reticular to laminar fibrolamellar bone, initially being deposited as loose spongiosa with hypermineralised tissue and without Haversian remodelling. Two Eocene archaeocete taxa featured pachyostosis with hyperostosis (excessive bone growth) of the periosteal cortex very similar to the condition present in some sirenians (*Buffrénil et al., 1990*). The comparative study by *Gray et al. (2007)* analysed the ribs of ten specimens representing five extinct cetacean families from the Eocene as they made their transition from a terrestrial/semiaquatic to an obligate aquatic lifestyle over a 10-million-year period. The authors compared those data to nine genera of extant mammals, amongst them modern dolphins, and found profound changes in microstructure involving a shift in bone function. The mechanisms of osteogenesis were flexible enough to accommodate the shift from a typical terrestrial form to one presenting osteosclerosis and pachyosteosclerosis, and then to osteoporosis in the first quarter of the evolutionary history of cetaceans. The limb bones and ribs of *Indohyus*, a taxon closely related to cetaceans, featured osteosclerosis, and considered indicative of the use of bottom-walking as swimming mode (*Thewissen et al., 2007*; *Cooper et al., 2012*). *Ricqlès, Taquet & Buffrénil (2009)* published the description of a rediscovered collection of thin sections from the 19th century French palaeontologist Paul Gervais including sections of cetacean bones. The most recent study on the bone microstructure of cetaceans is the one of *Houssaye, Muizon & Gingerich (2015)* analysing the bone microstructure of ribs and vertebrae of 15 archaeocete specimens, i.e., Remingtonocetidae, Protocetidae, and Basilosauridae using microtomography and virtual thin-sectioning (i.e., CT scanning). They found bone mass increase in ribs and femora, whereas vertebrae are essentially spongeous. Humeri changed from compact to spongeous whereas femora in basilosaurids became, once spurious for locomotion, reduced, displaying strong osteosclerosis. The authors concluded that Remingtonocetidae and Protocetidae probably swam in shallow water, whereas basilosaurids, for their osseous specializations similar to those of modern cetaceans, are considered capable of active swimming in the open-sea.

### Creodonta

As it is the case for many other vertebrate taxa, *Enlow & Brown (1958)* are still the only workers who analysed the "creodonts," mammalian predators from the Paleogene and Early Neogene of North America, Africa, and Eurasia. Bone tissue from mandibles, ribs, and long bones consists of primary lamellar bone with longitudinal/radial vascularisation and secondary Haversian tissue, generally similar to the bone tissue found in modern carnivorans.

### Carnivora

Enlow & Brown (1958) studied the mandible bone tissue of *Ursus* and found primary reticular bone and secondary dense Haversian bone, whereas a rib showed only dense Haversian bone. In the outer part, the bone cortex of *Ursus* consisted of plexiform bone. Chinsamy, Rich & Vickers-Rich (1998) found several LAGs in the zonal bone cortex of the polar bear. Hayashi et al. (2013) reported that the polar bear (*Ursus maritimus*) has microanatomical features close to those of active swimmers in its limb bones, particularly in the humerus. The microanatomy of the femur is intermediate between aquatic and terrestrial taxa, despite its morphological features, which do not show particular adaptation for swimming. However, *U. maritimus* long bones still display a true medullary cavity. The authors suggested that this result, notably the apparently stronger adaptation of the humerus for an aquatic mode of life, is probably linked to its swimming style because *U. maritimus* uses the forelimbs as the main propulsors during swimming.

*Mephitis* (skunk), *Procyon* (raccoon), *Mustela* (badger), *Felis* (cat), *Canis* (dog), and *Urocyon* (fox) all possess reticular and radial primary bone (Enlow & Brown, 1958). However, the bone cortex of adult specimens in these taxa was dominated by secondary Haversian bone. The outer cortex of *Canis* was composed of primary plexiform bone tissue. The mongoose (*Herpestes*) showed in its femur primary longitudinal vascularised bone devoid of Haversian remodelling whereas the bone cortex of the American mink (*Neovison vison*) was composed of reticular and Haversian bone.

Singh, Tonna & Gandel (1974) found in felids and mustelids lamellar bone with radial to longitudinal vascularisation. Klevezal & Kleinenberg (1969) found annual LAGs in the bone cortex of carnivorans. Several works dealt with the accuracy of LAGs in carnivorans in comparison to dental histology as a tool of age determination: Johnston & Beauregard (1969) (*Vulpes*), Pascal & Delattre (1981) (*Mustela*), King (1991) (*Mustela*), Klevezal (1996) (*Mustela*, *Martes*), Pascal & Castanet (1978) (*Felis*). The outcome was always in favour of dental cementum analysis. Buffrénil & Pascal (1984) concluded that in mink mandibles the deposition of LAGs is not strictly annual by using fluorescein and alizarin labelling.

The long bones of *Valenictus*, a Pliocene walrus (Odobenidae), were described as being osteosclerotic (Deméré, 1994). Nakajima & Endo (2013) and Nakajima, Hirayama & Endo (2014) analysed humeral microanatomy of multiple carnivore taxa including terrestrial, semi-aquatic and fully-aquatic taxa. The authors used CT-scans and found variations of bone organisation in the centre of bone ossification and in the humeral head among carnivorans including different modes of life. Cancellousness in the centre of bone ossification is relatively low in the semiaquatic taxa like the sea otter and is relatively high both in terrestrial taxa like the wolverine and highly aquatic taxa such as the southern elephant seal. Trabeculae in humeral heads are fine and well-organised in terrestrial to semi-aquatic taxa, while trabeculae from aquatic taxa are rather coarse and randomly oriented.

### Euarchontoglires–Rodentia

Early contributions to rodent bone histology were made by Foote (1911a), Enlow & Brown (1958) as well as Singh, Tonna & Gandel (1974). More recent works are by Klevezal (1996) on rest lines and age determination, *Martiniaková et al. (2005)* on rat bone histology, and *Garcia-Martinez et al. (2011)* on the bone histology of dormice. The bone tissue of rodents mainly consists of lamellar or parallel-fibred bone with reticular, radial or longitudinal vascularisation as primary bone tissue. Development of Haversian systems is rare. *Geiger et al. (2013)* studied the bone cortex of a femur of the giant caviomorph *Phoberomys pattersoni* from the Miocene of Trinidad, and found it to be composed of lamellar-zonal bone. The sampled specimen showed alternating layers of compacted coarse cancellous bone and parallel-fibred/lamellar primary bone with a reticulum-like structure. The authors reported Haversian tissue absent. *Montoya (2014)* examined the bone microstructure of the extant subterranean rodent *Bathyergus suillus* (Bathyergidae). The author found thickening compacta during ontogeny in contrast to cursorial and bipedal mammals. Females of *Bathyergus suillus* displayed a wide variation of microanatomical parameters with resorptive activity already from juvenile ontogenetic stages.

The femoral bone cortex of *Mikrotia magna*, a giant insular murine rodent from the Late Miocene former island of Gargano (Italy; Table 1), consists merely of compact bone. The bone matrix of the middle part of the cortex is dominated by parallel-fibred bone with poor longitudinal but mainly reticular vascularisation being pervaded by mainly irregularly shaped and obliquely oriented secondary osteons (Figs. 7A–7C), producing a distinct disorganised pattern (*Enlow & Brown, 1958*). Additionally, delimited areas of fibrolamellar bone occur within the middle cortex. The inner and outer parts of the cortex are formed by lamellar bone with poor longitudinal but mainly radial vascularisation. The thickness of those parts varies throughout the circumference of the bone cortex and between samples, and intercalated thin layers consisting of woven-fibred bone are present. All the samples display LAGs. In the adult femur RGM.792085, four to five LAGs were counted. Resorption cavities are present close to the medullary cavity.

Thin sections of the femur of the dormouse *Leithia* sp. from the Pleistocene of Sicily (Table 1) are characterised by a compact cortex. The primary bone matrix, which is only present in the outermost periosteal part of the cortex, was formed by avascular lamellar bone. The rest of the cortex consists of compact coarse cancellous bone displaying thick layers of endosteal lamellar bone with poor longitudinal to radial vascularisation and areas of endosteal infilling of intertrabecular spaces with lamellar bone (Figs. 7D–7F; *Enlow, 1962*; *Francillon-Vieillot et al., 1990*; *Prondvai et al., 2012*). The compact coarse cancellous bone is in turn invaded by mainly irregularly shaped and obliquely oriented secondary osteons. LAGs are absent in the sampled specimen. Large resorption cavities and small areas of fibrolamellar bone occur.

## Lagomorpha

For this study four different species of ochotonids (*Prolagus*) were investigated (Table 1). One mainland form (*Prolagus oeningensis* from La Grive France) and three island forms: the giant species *Prolagus sardus* (Sardinia, Italy) (Fig. 8A) and *P. imperialis* along with *P. apricenicus*, both from Gargano, Italy. Generally, the bone cortex of the femur and the humerus of *Prolagus* is compact. It is characterised by a bone matrix changing from

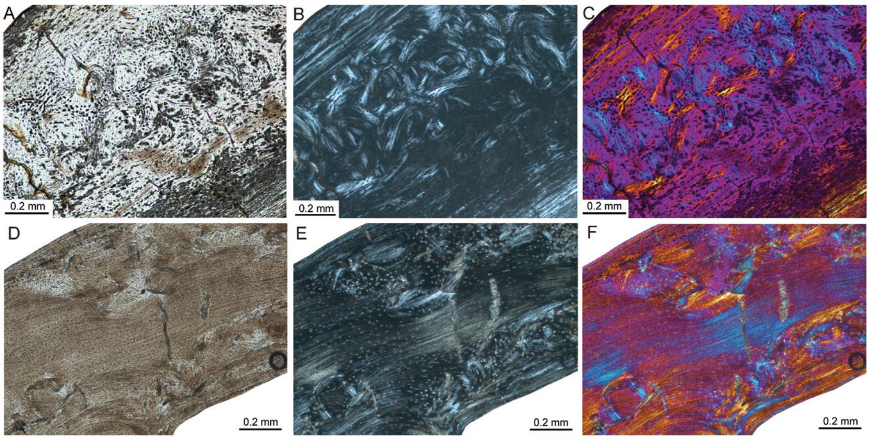

**Figure 7 Bone histology of fossil island rodents.** Histological images (A) and (D) in linear polarised light, (B) and (E) in crossed polarised light, and (C) and (F) in crossed polarised light with additional use of lambda compensator. (A–C) Adult *Mikrotia* sp. femur (specimen RGM.792085) showing disorganised, mainly parallel-fibred/lamellar bone in its centre. (D–F) Adult femur of *Leithia* sp. specimen NMB G 2160 displaying a mainly compacted coarse cancellous cortex of endosteal lamellar bone with areas of trabecular infilling and remodelling. Please note that periosteal lamellar bone is only present close to the bone surface.

fibrolamellar to parallel-fibred into lamellar bone from the inner cortex towards the OCL (Figs. 8B–8F). An endosteal lamellar layer is present. In most specimens the fibrolamellar or parallel-fibred bone is partly pervaded by mainly irregularly shaped and obliquely oriented secondary osteons, producing the "subendosteal layer of Haversian-like bone" *sensu Pazzaglia et al.* (*2015*: Fig. 6B). The primary bone cortex is in general weakly vascularised. Within the primary fibrolamellar and parallel-fibred bone, primary and simple longitudinal vascular canals as well as radial and reticular vascular canals occur and are arranged in an irregular manner. LAGs indicating minimum ages are present in some adult specimens. *Prolagus oeningensis* (Figs. 8B and 8C) has a maximum number of three LAGs, *Prolagus apricenicus* a maximum of two LAGs, and *Prolagus imperialis* as well as *Prolagus sardus* each have a maximum of five (Figs. 8D–8F). Femora from juvenile *Prolagus oeningensis* (PIMUZ A/V 4532) and *Prolagus sardus* (NMB Ty. 4974; Fig. 8E) as well as a humerus from a juvenile *Prolagus imperialis* (RGM.792102) are characterised in the inner and middle part of the cortex by longitudinal, radial, and reticular vascularised fibrolamellar bone with a high amount of woven bone. Towards the bone surface, the amount of parallel-fibred bone increases and the vascularisation changes into longitudinal simple and primary vascular canals. Primary bone tissue in juveniles is already invaded by mainly irregularly shaped and obliquely oriented secondary osteons in the inner and middle part of the cortex. Our observations on lagomorph bone histology essentially agree with *Foote*'s (*1911a*) and *Enlow & Brown*'s (*1958*) observations on lagomorphs. The same is the case for the study of *Pazzaglia et al. (2015)*, who studied rabbit (*Oryctolagus cuniculus*) femora of different ontogenetic stages via micro CT-scanning. However, what they call

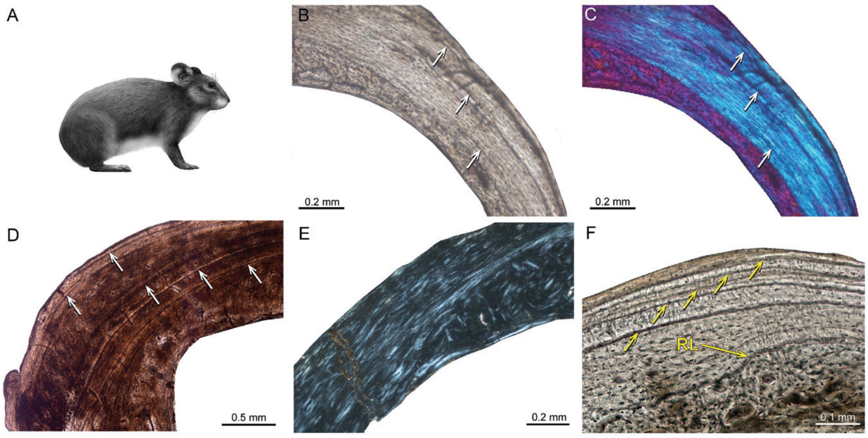

**Figure 8 Bone histology of fossil ochotonids.** (A) Life reconstruction of *Prolagus sardus* ("Prolagus3," courtesy of Wikimedia Commons—http://commons.wikimedia.org). Histological images (B), (D), (F) in linear polarised light, (C) in crossed polarised light with additional use of lambda compensator, and (E) in crossed polarised light. (B, C) Lateral cortex of adult *Prolagus oeningensis* femur PIMUZ A/V 4532 showing fibrolamellar bone partially pervaded by irregular secondary osteons in the inner part and mainly parallel-fibred bone in the middle and outer part as well as three LAGs. (D) Lateral cortex of adult *Prolagus imperialis* femur RGM.792096 displaying an identical pattern of bone tissue but five LAGs. (E) Posteromedial cortex of juvenile *Prolagus sardus* femur NMB Ty. 4974 showing an area of fibrolamellar bone with a high amount of woven-fibred bone in the inner part and an increasing amount of parallel-fibred bone in the middle and outer part of the cortex. (F) Outer anterolateral cortex of adult *Prolagus sardus* femur NMB Ty.12659 displaying five LAGs. Note that the line in the lower third of the cortex is a resorption line (RL) and not a LAG. Occurrence of LAGs indicated by white or yellow arrows.

laminar respectively plexiform bone tissue is not in agreement with the nomenclature of *Francillon-Vieillot et al. (1990)* used by us, i.e., longitudinal, radial, and reticular vascularisation. *Moncunill-Solé et al. (in press)* provided mass estimates of 350 g for the extinct continental *Prolagus* cf. *calpensis*, and 280–600 g for *Prolagus apricenicus* based on femoral measurements. Bone histological analysis suggests a longevity for *Prolagus apricenicus* of at least seven years (five years more than in our sample of *P. apricenicus*). Again, the bone histological traits observed in *Moncunill-Solé et al. (in press)* are essentially in agreement with our findings in *Prolagus*.

### Primates

Again, *Enlow & Brown (1958)* were the first to describe the bone tissue of extinct primates by sampling a mandible of the fossil Paleocene *Plesiolestes* and long bones of modern primates. The authors described primary bone tissue formed by lamellar bone. Vascularisation was mainly characterised by longitudinal primary vascular canals. Remodelling was locally abundant and the organisation of Haversian bone was dense in some areas of the bone cortex. Those observations have been confirmed by the comparative studies of *Cuijpers (2006)* and *Hillier & Bell (2007)* as well as in the conceptual studies of *Bromage et al.* (*2009*; see also above) and *Castanet* (*2006*; see also above). *Castanet et al.* (*2004*; see also above) found the inner and thicker part of the bone cortex of *Microcebus* formed by parallel-fibred bone containing primary blood vessels and scarce primary osteons. In contrast, the outer part of the cortex is not vascularised. *Crowder & Stout (2012)* have compiled a book covering the current utilisation of histological analysis of bones and teeth within the field of anthropology, including the biology and growth of bone, histomorphological analysis, and age determination. Extensive literature on hominoids, especially on bone pathologies in *Homo sapiens*, exists. To remain within the scope of this work, we cite here only some examples of those publications specific to this area. *Martínez-Maza, Rosas & García-Vargas (2006)* and *Martinez-Maza et al. (2011)* analysed bone surfaces under the reflected light and scanning electron microscope in order to decipher modelling and remodelling patterns in extant hominine facial skeletons and mandibles as well as in Neanderthal mandibles, explaining specific morphological traits. *Schultz & Schmidt-Schultz (2014)* examined fossil human bone and reviewed the methods and techniques of light microscopy, scanning electron microscopy, and the advantages of polarisation microscopy for palaeoanthropology. In this context it is noteworthy that the estimation of individual age in anthropology is carried out by mainly two methods (*Schultz & Schmidt-Schultz, 2014*): (1) the histomorphometric method (HMM) and (2) the histomorphologic method (HML). The HMM method is applied primarily to long bones (e.g., *Kerley, 1965*; *Drusini, 1987*) and is based upon the frequencies of osteons (Haversian systems), fragmented osteons (interstitial lamellae), non-Haversian canals, and the percentage of the external circumferential lamellae. The HML method is based upon the morphology (presence, size, shape, development) of external and internal circumferential lamellae, osteons, fragmented osteons, and non-Haversian canals (e.g., *Schultz, 1997*). *Skinner et al. (2015)* studied the pattern of trabeculae distributions of metacarpals in *Australopithecus africanus* and Pleistocene hominins. They found a 'human-like' pattern, considered to be consistent with tool use. *Ryan & Shaw (2015)* quantified the proximal femur trabecular bone structure using micro-CT data from 31 extant primate taxa (229 individuals) and four distinct archaeological human populations (59 individuals) representing sedentary agriculturalists and mobile foragers. Trabecular bone variables indicate that the forager populations had significantly higher bone volume fraction, thicker trabeculae, and lower relative bone surface area compared with the two agriculturalist groups. The authors did not find any significant differences between agriculturalist and forager populations for trabecular spacing, number, or degree of anisotropy. Ryan & Shaw concluded there was a correspondence between human behaviour and bone structure in the proximal femur, indicating that more highly mobile human populations have trabecular bone structure similar to what would be expected for wild non-human primates of the same body mass, thus emphasising the importance of physical activity and exercise for bone health and the attenuation of age-related bone loss.

## SELECTED CONTRIBUTIONS ON MAMMALIAN HISTOLOGY

Many excellent papers on mammalian histology have appeared over the years, and we cannot discuss all of them. However, we feel that a number of these deserve a more detailed evaluation as they address important aspects of applications of palaeohistological work. *Enlow & Brown*'s (*1958*) outstanding comparative work on mammalian bone histology is not further mentioned in this section, since it is repeatedly discussed above.

*Klevezal & Kleinenberg (1969)* were the first to recognise the presence and importance of rest lines in the bone cortex of mammals for skeletochronological studies (see also *Chinsamy-Turan, 2005*). In their work, which was originally published in Russian in 1967, they found that in mammals, unlike the zonal bone forming in reptiles, the recording part including LAGs is the outer or periosteal zone (see also above). *Klevezal (1996)* found that rest lines are not formed from the first year of life in every mammalian taxon. Therefore, she suggested a variable correction factor for different mammalian taxa and concluded that the best structures for recording growth and age are dentine and especially cementum (*Klevezal, 1996*). In her detailed and comprehensive study of recording structures in mammals, she found that the growth rate of a particular structure can change according to the growth rate of the whole organism and that seasonal changes of growth intensity of an animal as a whole determine the formation of growth layers. *Klevezal (1996)* argued that changes in humidity, not temperature, may play a role as a seasonal factor in growth.

*Sander & Andrassy (2006)* described the occurrence of LAGs in 21 long bones (mainly tibiae and metatarsals) of herbivorous mammals from the Late Pleistocene of Germany comprising the extinct giant deer *Megaloceros giganteus*, the red deer *Cervus elaphus*, the reindeer *Rangifer tarandus*, the extinct bovids *Bos primigenius* and *Bison priscus*, the equid *Equus* sp., the extinct rhinocerotid *Coelodonta antiquitatis*, and the extinct elephantid *Mammuthus primigenius*. All samples showed fibrolamellar bone and a varying degree of remodelling and most of the long bones displayed LAGs. The authors questioned the argument that LAGs in dinosaur bone indicate ectothermy because of the frequently found LAGs in endothermic animals.

*Köhler & Moyà-Solà (2009)* examined the long-bone histology of *Myotragus*, a Plio-Pleistocene bovid from the Balearic Islands. They found lamellar-zonal tissue throughout the cortex, a trait exclusive to ectothermic reptiles. According to Köhler and colleagues, *Myotragus* grew unlike any other mammal but similar to crocodiles, i.e., at slow and flexible rates, ceased growth periodically, and attained somatic maturity late after twelve years. The authors concluded that this developmental pattern indicates that *Myotragus*, much like extant reptiles, synchronized its metabolic requirements with fluctuating resource levels.

*Kolb et al. (2015)* performed a histological analysis of long bones and teeth representing eleven extinct and extant cervid taxa, amongst them the dwarf island morphotypes of *Candiacervus* from the Late Pleistocene of Crete and the giant deer *Megaloceros giganteus*, both in a clade together with fallow deer (*Dama dama*) among extant species. Bone tissue types observed were similar, indicating a comparable mode of growth across the eight species examined, with long bones mainly possessing primary plexiform fibrolamellar bone (Figs. 1B, 1C, 1E and 1F). Dwarf *Candiacervus* were characterised by low growth rates, *Megaloceros* by high rates, and the lowest recorded rates were those of the Miocene small stem cervid *Procervulus praelucidus*. It should be noted that *Sinomegaceros yabei*, sampled for the present study, features a very thick second growth zone, which suggests a high growth rate, comparable to that of the closely related *Megaloceros*. Skeletal maturity estimates (see also above) indicated late attainment in sampled *Candiacervus* and *Procervulus*. Tooth cementum analysis of first molars of two senile *Megaloceros giganteus* specimens revealed ages of 16 and 19 years whereas two old dwarf *Candiacervus* specimens gave ages of 12 and 18 years. *Kolb et al. (2015)* concluded that the bone histological condition found in *Candiacervus* had features in common with that of *Myotragus* (*Köhler & Moyà-Solà, 2009*), but was achieved with a lesser modification of bone tissue and suggested various modes of life history and size evolution among island mammals. *Amson et al. (in press)* examined further 'stem-cervid' bone histology in describing that of other Miocene taxa, *Dicrocerus elegans* and *Euprox* sp. With their inclusion in the dataset of *Kolb et al. (2015)*, they estimated ancestral growth rates among cervids, and studied their correlation with body size. The skeletochronology of *Dicrocerus* and *Euprox* suggested relatively high and intermediate growth rates respectively for their body sizes, differing from the condition of *Procervulus*, and hence documenting diversity in the life history traits of Miocene cervids.

*Dumont et al. (2013)* documented the microstructure of vertebral centra using 2D histomorphometric analyses of vertebral centra from 98 therian mammal species that cover the main size ranges and locomotor adaptations known in therian taxa. The authors extracted eleven variables relative to the development and geometry of trabecular networks from CT scan mid-sagittal sections. Random taxon reshuffling and squared change parsimony indicated a phylogenetic signal in the majority of the variables. Furthermore, based on those variables, it was possible to determine three categories of locomotion among the sampled taxa: (a) terrestrial + flying + digging + amphibious forms, (b) coastal oscillatory aquatic taxa, and (c) pelagic oscillatory aquatic forms represented by oceanic cetaceans. Dumont and colleagues concluded that, when specific size increases, the length of trabecular networks, as well as trabecular proliferation, increase with positive allometry. They found that, by using six structural variables, locomotion mode can be predicted with a 97.4% success rate for terrestrial forms, 66.7% for coastal oscillatory, and 81.3% for pelagic oscillatory.

## DISCUSSION ON BONE HISTOLOGY OF ISLAND MAMMALS

Within our overview, we have a large sample of insular mammals. Islands have their own set of rules when it comes down to evolution (*Van der Geer et al., 2010*; *Lomolino et al., 2012*; *Lomolino et al., 2013*), and in the following we explore to what extent insular evolution may effect bone histology.

Three juvenile specimens of the dwarf island hippopotamid *Hippopotamus minor* from the Late Pleistocene of Cyprus show reticular to plexiform fibrolamellar bone, which does not indicate an island-specific pattern of bone growth or life history but a mode of growth similar to continental artiodactyl relatives instead. The bone cortex of the dormouse *Leithia* sp. from the Pleistocene of Sicily is characterised by primary lamellar bone and a high amount of compact coarse cancellous bone. *Mikrotia magna*, the giant island rodent from the Late Miocene of Gargano, Italy shows in the middle part of the cortex parallel-fibred bone with reticular vascularisation and mainly irregularly shaped and obliquely oriented secondary osteons. The inner and outer parts of the cortex are formed by lamellar bone. Garcia-Martinez et al. (2011) did not find compact coarse cancellous bone in their sample of extant dormice. The high amount of compact coarse cancellous bone and therefore strong inward growth (Enlow, 1962) in our *Leithia* sp. specimen might point towards an island specific modification of bone tissue. However, sampling of more specimens in order to confirm this observation is necessary. The composition of bone tissues found in *Mikrotia magna* is in general similar to the one encountered in extant murid rodents (Foote, 1911a; Enlow & Brown, 1958; Enlow, 1962; Singh, Tonna & Gandel, 1974; Martiniaková et al., 2005). The partially high amount of remodelling encountered in *Mikrotia* is likely related to high individual ages. In the bone cortex of three fossil species of insular giant *Prolagus* and the fossil continental lagomorph *Prolagus oeningensis* are mainly parallel-fibred bone and reticular, radial as well as longitudinal vascularisation indicating a similarity of bone histological arrangements in continental and island species of rodents and lagomorphs.

The highest age found in *Prolagus sardus* and *P. imperialis* of five years are well within the known longevities of extant ochotonids such as *Ochotona princeps* (seven years in captivity) and *O. hyperborean* (9.4 years in captivity) (Tacutu et al., 2013). Moncunill-Solé et al. (in press) suggested a longevity for *Prolagus apricenicus* of at least seven years (five years more than in our sample of *P. apricenicus*). Based on the predictions by the body mass inferred, Moncunill-Solé et al. (in press) suggested a move to the slow end of the fast-slow continuum (maturing later and fewer offspring) in *Prolagus apricenicus*. A minimal individual age deduced from growth marks in the bone tissue of *Deinogalerix* specimen RGM 178017 lies also well within the known longevities for extant erinaceids such as *Erinaceus europaeus* (11.7 years in captivity), *E. concolor* (seven years in captivity), and *E. amurensis* (9.4 years in captivity). Longevity data for extant galericines are not yet available (Tacutu et al., 2013).

The insular dwarf bovid *Myotragus balearicus* from Majorca showed an important decrease in bone growth rate and an evolution towards a slow life history, i.e., delayed maturity and long lifespan (Köhler & Moyà-Solà, 2009; Köhler, 2010; Jordana & Köhler, 2011; Jordana et al., 2012; Moncunill-Solé et al., in press; but see Raia, Barbera & Conte (2003) for an opposite case of life history modification in Sicilian dwarf elephants). The authors suggest these findings to be trends for island mammals in agreement with MacArthur & Wilson (1967), as well as life history theory (Stearns, 1992) and that the degree of these modifications depends on multiple factors such as island size, distance from mainland, climate, phylogeny, time of evolution and others (see also Moncunill-Solé et al., 2014). *Myotragus* dwelt on Majora for 5.2 Ma and therefore underwent an exceptionally long time of evolution (Van der Geer et al., 2010) and resource limitation (Köhler & Moyà-Solà, 2009). A similarly high degree of bone histological and life history modification as described by Köhler & Moyà-Solà (2009) for *Myotragus* in comparison to continental artiodactyls has not been recorded for the insular mammals *Deinogalerix* sp., *Hippopotamus minor*, *Leithia* sp., *Mikrotia magna*, or for several species of *Prolagus* in comparison to their mainland relatives.

A variable degree of modification in bone tissue and life history could be related to shorter persistence times and different island size (*Lomolino et al., 2012*; *Lomolino et al., 2013*; *Kolb et al., 2015*), in line with *Austad & Fischer (1991)*, *McNab (1994)*, *McNab (2002)*, *McNab (2010)*, *Raia, Barbera & Conte (2003)*, *Curtin et al. (2012)* and *Kolb et al. (2015)*.

## CONCLUSIONS

A large variety of bone tissues and vascularisation patterns is encountered in mammalian bone reaching from lamellar or parallel-fibred to fibrolamellar or woven-fibred bone, largely depending on taxon and individual age. A plexiform to laminar organisation of vascular canals within fibrolamellar bone is typically found in taxa containing large-bodied species such as non-mammalian cynodonts, laurasiatherians, and afrotherians. The deposition of Haversian systems throughout ontogeny of non-mammalian cynodonts and mammals is common. Table 2 gives a summary on general patterns of bone histological features encountered in major cynodont clades.

We suggest the presence of various modes of bone histological modification and mammalian life history evolution on islands depending on factors of island evolution such as island size, distance from mainland, climate, phylogeny, and time of evolution. Further bone histological comparisons and sampling of more specimens as well as species of fossil insular endemics and their mainland relatives within an ontogenetic framework would contribute significantly to the knowledge of the ecology of past island ecosystems.

## FUTURE RESEARCH FIELDS

### New technologies

3D reconstructions attained by virtual image analysis gain increasing importance for palaeontological research at the anatomical, microanatomical, and even histological levels (*Sanchez et al., 2012*; *Clément & Geffard-Kuriyama, 2010*; *Curtin et al., 2012*; see also *Ricqlès, 2011*). The potential advantages of virtual imaging as a method are evident: firstly, specimens are not damaged by invasive sampling. Secondly, a third dimension, usually achieved by time consuming serial sectioning or preparation of orthogonally oriented thin sections, is easily realizable. Thirdly, virtual imaging techniques allow continuous "zooming" from the histological to the micro- and macronatomical levels of structural organisation. High resolution synchrotron virtual histology provides new 3D insights into the submicron-scale histology of fossil and extant bones. This is based on the development of new data acquisition strategies, pink-beam configurations, and improved processing tools (*Sanchez et al., 2012*). Nevertheless, for the high resolution optical properties of a polarisation microscope and its applications for identification and analysis of bone microstructure, as well as for the comparatively low amount of financial resources needed, traditional thin sections are far from being completely replaced by virtual imaging techniques. Moreover, new statistical methods allow extraction of phylogenetic signals from bone microstructures and of high specimen numbers (*Laurin, 2004*; *Laurin, Girondot*

**Table 2** **Summary of histological traits of non-mammalian cynodonts and major mammalian clades (based on material sampled and references cited in the current study).** The terminology follows *Francillon-Vieillot et al. (1990)*.

| Histological traits | Non-mammalian cynodonts | Multituberculata and early mammals | Monotremata | Marsupialia | Euarchontoglires | Laurasiatheria | Afrotheria | Xenarthra |
|---|---|---|---|---|---|---|---|---|
| Main primary bone tissue types | fibrolamellar, parallel-fibred, lamellar | fibrolamellar, parallel-fibred, lamellar | fibrolamellar, lamellar | fibrolamellar, parallel-fibred, lamellar | lamellar or parallel-fibred | fibrolamellar | fibrolamellar | fibrolamellar |
| Main vascularisation patterns | plexiform, laminar, longitudinal, reticular, radial | longitudinal, radial, reticular | longitudinal, radial, reticular, laminar | longitudinal, radial | longitudinal, reticular, radial | longitudinal, reticular, radial, laminar, plexiform | circumferential, longitudinal, reticular, laminar, plexiform | longitudinal, reticular, radial |
| Lines of arrested growth | present | present | not documented | present | present | present | present | present |
| Remodelling | Haversian bone | not documented | Haversian bone | Haversian bone | Haversian bone | Haversian bone | Haversian bone | Haversian bone |

*& Loth, 2004*; *Cubo et al., 2008*). In addition to a phylogenetic signal, bone tissues are also influenced by biomechanical and ecological signals (*Cubo et al., 2005*; *Cubo et al., 2008*; *Laurin, Girondot & Loth, 2004*; *Laurin, 2004*; *Ricqlès & Cubo, 2010*; *Hayashi et al., 2013*). Here too, the advances in high performance computers and software open possibilities to investigate the variability in bone tissues by taking multiple factors into account. The creation of histological databases will soon be necessary due to an increasing number of palaeohistological publications and growing collections of thin sections (*Ricqlès, Castanet & Francillon-Vieillot, 2004*; *Ricqlès, Taquet & Buffrénil, 2009*; *Bromage, 2006*; *Kriloff et al., 2008*; *Scheyer, 2009–2015*; *Canoville & Laurin, 2010*; *O'Leary & Kaufman, 2012*).

### Extant vertebrate biology

Actualistic models are essential for the interpretation of fossil hard tissues in every sense, no matter if developmental and life historical, histophysiological, morphological, ecological, or systematic. Living animals present the basis for inferring palaeobiological conclusions and this has already been performed in several bone histological works (e.g., *Canoville & Laurin, 2010*; *Köhler et al., 2012*; *Marín-Moratalla, Jordana & Köhler, 2013*; *Marín-Moratalla et al., 2014*; *Kolb et al., 2015*).

In regard to deciphering life history signals, the actualistic approach is fundamental and will become increasingly more so (e.g., *Köhler et al., 2012*; *Marín-Moratalla, Jordana & Köhler, 2013*; *Marín-Moratalla et al., 2014*; *Kolb et al., 2015*). Life history variables such as annual growth rate, skeletal/sexual maturity, and longevity and their signal in bone microstructure help to understand palaeobiology not only of fossil mammals but also of tetrapods in general. It is possible to use bone histology to quantify growth rates and vascularisation or cellular density in mammals as a relative proxy for growth rate (*Curtin et al., 2012*; *Kolb et al., 2015*; *Marín-Moratalla, Jordana & Köhler, 2013*; *Marín-Moratalla et al., 2014*; *Jordana et al., in press*), whereby the existing literature on the paleobiology of dinosaurs has been used as a starting point. However, not every methodological approach used for dinosaurs is applicable or relevant for mammals (e.g., *Erickson, Curry Rogers & Yerby, 2001*; *Griebeler, Klein & Sander, 2013*; *Kolb et al., 2015*). No one stated it better than Armand de Ricqlès: "The possibilities of using bone histology of extant vertebrates for various fundamental or applied research, whether on life history traits, ecology, or microevolution, are simply boundless." (*Ricqlès, 2011*).

## ACKNOWLEDGEMENTS

Alexandra Wegmann and Fiona Straehl are thanked for their help with the bone histological preparation, Madeleine Geiger for the fruitful discussions (all Palaeontological Institute of the University of Zurich (PIMUZ), Switzerland), and Ashley Latimer (PIMUZ) and Cathy Ridgway for English corrections. Likewise, we thank Xavier Jordana and P. Martin Sander for their thorough and critical reviews, which helped greatly to improve the manuscript.

## ADDITIONAL INFORMATION AND DECLARATIONS

### Funding

This study was funded by the SNSF (3100A0-133032/1 and 31003A-149605 to MRS-V; 31003A-149506 to TMS), the Forschungskredit of the University of Zurich (No. 8264 to CK) and the JSPS KAKENHI (26800270 Grant-in-Aid for Young Scientists B to SH). The research of AVDG was co-financed by the European Union (European Social Fund) and Greek national funds through the Operational Program "Education and Lifelong Learning" of the National Strategic Reference Framework (NSRF)-Research Funding Program: THALIS–UOA "Island biodiversity and cultural evolution" (MIS375910, KA:70/3/11669). The funders had no role in study design, data collection and analysis, decision to publish, or preparation of the manuscript.

### Grant Disclosures

The following grant information was disclosed by the authors:
SNSF: 3100A0-133032/1, 31003A-149605, 31003A-149506.
Forschungskredit of the University of Zurich: 8264.
JSPS KAKENHI: 26800270 Grant-in-Aid for Young Scientists B.
European Union (European Social Fund) and Greek national funds: MIS375910, KA:70/3/11669.

### Competing Interests

Shoji Hayashi is an employee of Osaka Museum of Natural History.

### Author Contributions

- Christian Kolb conceived and designed the experiments, performed the experiments, analyzed the data, wrote the paper, prepared figures and/or tables, reviewed drafts of the paper, took micrographs.
- Torsten M. Scheyer analyzed the data, reviewed drafts of the paper.
- Kristof Veitschegger and Analia M. Forasiepi performed the experiments, analyzed the data, wrote the paper, reviewed drafts of the paper, took micrographs.
- Eli Amson performed the experiments, analyzed the data, wrote the paper, prepared figures and/or tables, reviewed drafts of the paper, took micrographs.
- Alexandra A.E. Van der Geer, Lars W. Van den Hoek Ostende and Shoji Hayashi reviewed drafts of the paper.
- Marcelo R. Sánchez-Villagra conceived and designed the experiments, contributed reagents/materials/analysis tools, wrote the paper, reviewed drafts of the paper.

### Animal Ethics

The following information was supplied relating to ethical approvals (i.e., approving body and any reference numbers):

Naturalis Biodiversity Center, Leiden, the Netherlands, Loïc Costeur (Naturhistorisches Museum Basel, Switzerland), George Lyras (Museum of Paleontology and Geology, University of Athens, Greece), Nigel Monaghan (National Museum of Ireland, Natural History), Hiroyuki Taruno (Osaka Museum of Natural History, Japan), Frank Zachos and Alexander Bibl (Naturhistorisches Museum Wien, Austria), Pierre-Olivier Antoine (Institut des Sciences de l'Evolution-Montpellier, France), and Ebru Albayrak (MTA Natural History Museum, The General Directorate of Mineral Research and Exploration, Ankara, Turkey) approved sampling of specimens for histological study.

## REFERENCES

**Aeby C. 1878.** Das histologische Verhalten fossilen Knochen- und Zahngewebes. *Archiv für Mikroskopische Anatomie* **15**:371–382 DOI 10.1007/BF02933858.

**Agustí J, Antón M. 2002.** *Mammoths, sabertooths and hominids*. New York: Columbia University Press.

**Amprino R. 1947.** La structure du tissu osseux envisagee comme l'expression de différences dans la vitesse de l'accroissement. *Archives de Biologie* **58**:315–330.

**Amson E, Kolb C, Scheyer TM, Sánchez-Villagra MR.** Growth and life history of middle Miocene deer (Mammalia, Cervidae) based on bone histology. *Comptes Rendus Palevol* In Press DOI 10.1016/j.crpv.2015.07.001.

**Amson E, Muizon C de, Domning DP, Argot C, Buffreìnil V de. 2015.** Bone histology as a clue for resolving the puzzle of a dugong rib in the Pisco Formation, Peru. *Journal of Vertebrate Paleontology* **35(3)**:e922981 DOI 10.1080/02724634.2014.922981.

**Amson E, Muizon C de, Laurin M, Argot C, Buffrénil V de. 2014.** Gradual adaptation of bone structure to aquatic lifestyle in extinct sloths from Peru. *Proceedings of the Royal Society B* **281**:1–6 DOI 10.1098/rspb.2014.0192.

**Austad SN, Fischer KE. 1991.** Mammalian aging, metabolism, and ecology: evidence from the bats and marsupials. *Journal of Gerontology* **46**:B47–B53 DOI 10.1093/geronj/46.2.B47.

**Botha J, Chinsamy A. 2000.** Growth patterns deduced from the bone histology of the cynodonts *Diademodon* and *Cynognathus*. *Journal of Vertebrate Paleontology* **20**:705–711 DOI 10.1671/0272-4634(2000)020[0705:GPDFTB]2.0.CO;2.

**Botha J, Chinsamy A. 2004.** Growth and life habits of the Triassic cynodont *Trirachodon*, inferred from bone histology. *Acta Palaeontologica Polonica* **49**:619–627.

**Botha J, Chinsamy A. 2005.** Growth patterns of *Thrinaxodon liorhinus*, a non-mammalian cynodont from the Lower Triassic of South Africa. *Palaeontology* **48**:385–394 DOI 10.1111/j.1475-4983.2005.00447.x.

**Botha-Brink J, Abdala F, Chinsamy A. 2012.** The radiation and osteohistology of nonmammaliaform cynodonts. In: Chinsamy-Turan A, ed. *Forerunners of mammals: radiation, histology, biology*. Bloomington: Indiana University Press, 223–246.

**Bromage TG. 2006.** *Donald H. Enlow digital image library. Available at http://www.nyu.edu/dental/enlow/* (accessed 13 May 2015).

**Bromage TG, Lacruz RS, Hogg R, Goldman HM, McFarlin SC, Warshaw J, Dirks W, Perez-Ochoa A, Smolyar I, Enlow DH, Boyde A. 2009.** Lamellar bone is an incremental tissue reconciling enamel rhythms, body size, and organismal life history. *Calcified Tissue International* **84**:388–404 DOI 10.1007/s00223-009-9221-2.

**Buffrénil V de. 1982.** Données préliminaires sur la présence de lignes d'arret de croissance périostiques dans la mandibule du marsouin commun, *Phocoena phocoena* (L.), et leur utilisation comme indicateur de l'age. *Canadian Journal of Zoology* **60**:2557–2567 DOI 10.1139/z82-328.

**Buffrénil V de, Astibia H, Pereda Suberbiola X, Berreteaga A. 2008.** Variation in bone histology of middle Eocene sirenians from western Europe. *Geodiversitas* **30**:425–432.

**Buffrénil V de, Canoville A, D'Anastasio R, Domning DP. 2010.** Evolution of sirenian pachyosteosclerosis, a model-case for the study of bone structure in aquatic tetrapods. *Journal of Mammalian Evolution* **17**:101–120 DOI 10.1007/s10914-010-9130-1.

**Buffrénil V de, Casinos A. 1995.** Observations histologiques sur le rostre de *Mesoplodon densirostris* (Mammalia, Cetacea, Ziphiidae): le tissu osseux le plus dense connu. *Annales des Sciences Naturelles, Zoologie, Paris, 13e Série* **16**:21–36.

**Buffrénil V de, Castanet J. 2000.** Age estimation by skeletochronology in the Nile monitor (*Varanus niloticus*), a highly exploited species. *Journal of Herpetology* **34**:414–424 DOI 10.2307/1565365.

**Buffrénil V de, Dabin W, Zylberberg L. 2004.** Histology and growth of the cetacean petro-tympanic bone complex. *Journal of Zoology* **262**:371–381 DOI 10.1017/S0952836903004758.

**Buffrénil V de, Pascal B. 1984.** Croissance et morphogenèse postnatales de la mandibule du vison (*Mustela vison*, Schreiber): données sur la dynamique et l'interprétation fonctionnelle des dépots osseux mandibulaires. *Canadian Journal of Zoology* **62**:2026–2037 DOI 10.1139/z84-297.

**Buffrénil V de, Ricqlès AD, Ray CE, Domning DP. 1990.** Bone histology of the ribs of the archaeocetes (Mammalia: Cetacea). *Journal of Vertebrate Paleontology* **10**:455–466 DOI 10.1080/02724634.1990.10011828.

**Buffrénil V de, Schoevaert D. 1988.** On how the periosteal bone of the delphinid humerus becomes cancellous: ontogeny of a histological specialization. *Journal of Morphology* **198**:149–164 DOI 10.1002/jmor.1051980203.

**Bybee PJ, Lee AH, Lamm ET. 2006.** Sizing the Jurassic theropod dinosaur *Allosaurus*: assessing growth strategy and evolution of ontogenetic scaling of limbs. *Journal of Morphology* **267**:347–359 DOI 10.1002/jmor.10406.

**Canoville A, Laurin M. 2010.** Evolution of humeral microanatomy and lifestyle in amniotes, and some comments on palaeobiological inferences. *Biological Journal of the Linnean Society* **100**:384–406 DOI 10.1111/j.1095-8312.2010.01431.x.

**Castanet J. 1994.** Age estimation and longevity in reptiles. *Gerontology* **40**:174–192 DOI 10.1159/000213586.

**Castanet J. 2006.** Time recording in bone microstructures of endothermic animals; functional relationships. *Comptes Rendus Palevol* **5**:629–636 DOI 10.1016/j.crpv.2005.10.006.

**Castanet J, Croci S, Aujard F, Perret M, Cubo J, De Margerie E. 2004.** Lines of arrested growth in bone and age estimation in a small primate: *Microcebus murinus*. *Journal of Zoology* **263**:31–39 DOI 10.1017/S0952836904004844.

**Castanet J, Smirina EM. 1990.** Introduction to the skeletochronological method in amphibians and reptiles. *Annales des Sciences Naturelles, Zoologie* **11**:191–196.

**Chávez-Aponte EO, Alfonzo-Hernández I, Finol HJ, Barrios NCE, Boada-Sucre A, Carrillo-Briceño JD. 2008.** Histologia y ultraestructura de los osteodermos fosiles de *Glyptodon clavipes* y *Holmesina* sp. (Xenarthra: Cingulata). *Interciencia* **33**:616–619.

**Chinsamy A, Abdala F. 2008.** Palaeobiological implications of the bone microstructure of South American traversodontids (Therapsida: Cynodontia). *South African Journal of Science* **104**:225–230.

**Chinsamy A, Hurum JH. 2006.** Bone microstructure and growth patterns of early mammals. *Acta Palaeontologica Polonica* **51**:325–338.

**Chinsamy A, Rich T, Vickers-Rich P. 1998.** Polar dinosaur bone histology. *Journal of Vertebrate Paleontology* **18**:385–390 DOI 10.1080/02724634.1998.10011066.

**Chinsamy-Turan A. 2005.** *The microstructure of dinosaur bone: deciphering biology with fine scale techniques*. Baltimore: Johns Hopkins University Press.

**Chinsamy-Turan A. 2012a.** Forerunners of mammals: radiation, histology, biology. In: *Life of the past*. Bloomington: Indiana University Press, 352.

**Chinsamy-Turan A. 2012b.** Microstructure of bones and teeth of nonmammalian therapsids. In: Chinsamy-Turan A, ed. *Forerunners of mammals: radiation, histology, biology*. Bloomington: Indiana University Press, 65–88.

**Clément G, Geffard-Kuriyama D. 2010.** Imaging and 3D in palaeontology and palaeoanthropology. *Comptes Rendus Palevol* **9**:259–264 DOI 10.1016/j.crpv.2010.09.001.

**Cook SF, Brooks ST, Ezra-Cohn HE. 1962.** Histological studies on fossil bone. *Journal of Paleontology* **36**:483–494.

**Cooper LN, Seiffert ER, Clementz M, Madar SI, Bajpai S, Hussain ST, Thewissen JGM. 2014.** Anthracobunids from the middle eocene of India and Pakistan are stem perissodactyls. *PLoS ONE* **9**:e109232 DOI 10.1371/journal.pone.0109232.

**Cooper LN, Thewissen JGM, Bajpai S, Tiwari BN. 2012.** Postcranial morphology and locomotion of the Eocene raoellid *Indohyus* (Artiodactyla: Mammalia). *Historical Biology* **24**:279–310 DOI 10.1080/08912963.2011.624184.

**Cormack DH. 1987.** *Ham's histology*. Philadelphia: J.B. Lippincott Company.

**Crowder C, Stout S. 2012.** *Bone histology: an anthropological perspective*. Boca Raton: CRC Press.

**Cubo J, Legendre P, Ricqlès A de, Montes L, Margerie E de, Castanet J, Desdevise Y. 2008.** Phylogenetic, functional and structural components of variation in bone growth rate in amniots. *Evolution and Development* **10**:217–227 DOI 10.1111/j.1525-142X.2008.00229.x.

**Cubo J, Ponton F, Laurin M, Margerie E de, Castanet J. 2005.** Phylogenetic signal in bone microstructure of sauropsids. *Systematic Biology* **54**:562–574 DOI 10.1080/10635150591003461.

**Cuijpers A. 2006.** Histological identification of bone fragments in archaeology: telling humans apart from horses and cattle. *International Journal of Osteoarchaeology* **16**:465–480 DOI 10.1002/oa.848.

**Curtin AJ, Macdowell AA, Schaible EG, Roth L. 2012.** Noninvasive histological comparison of bone growth patterns among fossil and extant neonatal elephantids using synchrotron radiation X-ray microtomography. *Journal of Vertebrate Paleontology* **32**:939–955 DOI 10.1080/02724634.2012.672388.

**Da Costa Pereira PVLG, Victer GD, Porpino KDO, Bergqvist LP. 2012.** Osteoderm histology of Late Pleistocene cingulates from the intertropical region of Brazil. *Acta Palaeontologica Polonica* **59**:543–552 DOI 10.4202/app.2011.0117.

**De Boef M, Larsson HCE. 2007.** Bone microstructure: quantifying bone vascular orientation. *Canadian Journal of Zoology* **85**:63–70 DOI 10.1139/z06-195.

**Deméré TA. 1994.** Two new species of fossil walruses (Pinnipedia: Odobenidae) from the upper Pliocene San Diego Formation, California. *Proceedings of the San Diego Society of Natural History* **29**:77–98.

**Drusini AZ. 1987.** Refinement of two methods for the histomorphometric determination of age in human bone. *Zeitschrift für Morphologie und Anthropologie* **77**:167–176.

**Dumont M, Laurin M, Jacques F, Pellé E, Dabin W, Buffrénil V de. 2013.** Inner architecture of vertebral centra in terrestrial and aquatic mammals: a two-dimensional comparative study. *Journal of Morphology* **274**:570–584 DOI 10.1002/jmor.20122.

**Enlow DH. 1962.** A study of the postnatal growth and remodeling of bone. *American Journal of Anatomy* **110**:79–101 DOI 10.1002/aja.1001100202.

**Enlow DH, Brown SO. 1958.** A comparative histological study of fossil and recent bone tissues. Part III. *Texas Journal of Science* **10**:187–230.

**Erickson GM. 2014.** On dinosaur growth. *Annual Review of Earth and Planetary Sciences* **42**:675–697 DOI 10.1146/annurev-earth-060313-054858.

**Erickson GM, Curry Rogers K, Yerby SA. 2001.** Dinosaurian growth patterns and rapid avian growth rates. *Nature* **412**:429–433 DOI 10.1038/35086558.

**Erickson GM, Makovicky PJ, Currie PJ, Norell MA, Yerby SA, Brochu CA. 2004.** Gigantism and comparative life-history parameters of tyrannosaurid dinosaurs. *Nature* **430**:772–775 DOI 10.1038/nature02699.

**Ezra HC, Cook SF. 1959.** Histology of mammoth bone. *Science* **129**:465–466 DOI 10.1126/science.129.3347.465-a.

**Foote JS. 1911a.** The comparative histology of femoral bones. *Transactions of the American Microscopical Society* **30**:87–140 DOI 10.2307/3221427.

**Foote JS. 1911b.** Preliminary notice. *Transactions of the American Microscopical Society* **30**:326–327 DOI 10.2307/3221427.

**Forasiepi AM, Cerdeño E, Bond M, Schmidt GI, Naipauer M, Straehl FR, Martinelli AG, Garrido AC, Schmitz MD, Crowley JL. 2015.** New toxodontid (Notoungulata) from the Early Miocene of Mendoza, Argentina. *Paläontologische Zeitschrift* **89(3)**:611–634 DOI 10.1007/s12542-014-0233-5.

**Francillon-Vieillot H, Buffrénil V de, Castanet J, Géraudie J, Meunier FJ, Sire JY, Ricqlès A de. 1990.** Microstructure and mineralization of vertebrate skeletal tissues. In: Carter JG, ed. *Skeletal biomineralization: patterns, processes and evolutionary trends*. New York: Van Nostrand Reinhold, 471–530.

**Frylestam B, Schantz T von. 1977.** Age determination of European hares based on periosteal growth lines. *Mammal Review* **7**:151–154 DOI 10.1111/j.1365-2907.1977.tb00367.x.

**Garcia-Martinez R, Marin-Moratalla N, Jordana X, Köhler M. 2011.** The ontogeny of bone growth in two species of dormice: reconstructing life history traits. *Comptes Rendus Palevol* **10**:489–498 DOI 10.1016/j.crpv.2011.03.011.

**Geiger M, Wilson LAB, Costeur L, Sánchez R, Sánchez-Villagra MR. 2013.** Diversity and body size in giant caviomorphs (Rodentia) from the Northern Neotropics—study of femoral variation. *Journal of Vertebrate Paleontology* **33**:1449–1456 DOI 10.1080/02724634.2013.780952.

**Gray NM, Kainec K, Madar S, Tomko L, Wolfe S. 2007.** Sink or Swim? Bone density as a mechanism for buoyancy control in early cetaceans. *Anatomical Record* **290**:638–653 DOI 10.1002/ar.20533.

**Griebeler EM, Klein N, Sander PM. 2013.** Aging, maturation and growth of sauropodomorph dinosaurs as deduced from growth curves using long bone histological data: an assessment of methodological constraints and solutions. *PLoS ONE* **8**:e67012 DOI 10.1371/journal.pone.0067012.

**Gross W. 1934.** Die Typen des mikroskopischen Knochenbaues bei fossilen Stegocephalen und Reptilien. *Zeitschrift für Anatomie und Enwicklungsgeschichte* **103**:731–764 DOI 10.1007/BF02118752.

**Habermehl K-H. 1985.** *Altersbestimmung bei Wild- und Pelztieren—Möglichkeiten und Methoden—Ein praktischer Leitfaden für Jäger, Biologen und Tierärzte.* Hamburg, Berlin: Verlag Paul Parey.

**Hayashi S, Houssaye A, Nakajima Y, Chiba K, Ando T, Sawamura H, Inuzuka N, Kaneko N, Osaki T. 2013.** Bone inner structure suggests increasing aquatic adaptations in Desmostylia (Mammalia, Afrotheria). *PLoS ONE* **8**:e59146 DOI 10.1371/journal.pone.0059146.

**Herdina AN, Herzig-Straschil B, Hilgers H, Metscher BD, Plenk HJ. 2010.** Histomorphology of the penis bone (baculum) in the gray long-eared bat *Pleocotus austriacus* (Chiroptera, Vespertilionidae). *The Anatomical Record* **293**:1248–1258 DOI 10.1002/ar.21148.

**Hill RV. 2006.** Comparative anatomy and histology of xenarthran osteoderms. *Journal of Morphology* **267**:1441–1460 DOI 10.1002/jmor.10490.

**Hillier ML, Bell LS. 2007.** Differentiating human bone from animal bone: a review of histological methods. *Journal of Forensic Sciences* **52**:249–263 DOI 10.1111/j.1556-4029.2006.00368.x.

**Hofmann R, Stein K, Sander PM. 2014.** Constraints on the lamina density of laminar bone architecture of large-bodied dinosaurs and mammals. *Acta Palaeontologica Polonica* **59**:287–294 DOI 10.4202/app.2012.0149.

**Horner JR, Padian K. 2004.** Age and growth dynamics of *Tyrannosaurus rex*. *Proceedings of the Royal Society of London B* **271**:1875–1880 DOI 10.1098/rspb.2004.2829.

**Horner JR, Ricqlès A de, Padian K. 1999.** Variation in dinosaur skeletochronology indicators: implications for age assessment and physiology. *Paleobiology* **25**:295–304.

**Horner JR, Ricqlès A de, Padian K. 2000.** Long bone histology of the hadrosaurid dinosaur *Maiasaura peeblesorum*: growth dynamics and physiology based on an ontogenetic series of skeletal elements. *Journal of Vertebrate Paleontology* **20**:115–129 DOI 10.1671/0272-4634(2000)020[0115:LBHOTH]2.0.CO;2.

**Houssaye APT, Muizon C de, Gingerich PD. 2015.** Transition of Eocene whales from land to sea: evidence from bone microstructure. *PLoS ONE* **10**:e0118409 DOI 10.1371/journal.pone.0118409.

**Huttenlocker AK, Woodward HN, Hall BK. 2013.** The biology of bone. In: Padian K, Lamm E-T, eds. *Histology of fossil tetrapods—Advancing methods, analysis and interpretation*. Berkeley, Los Angeles, London: University of California Press, 13–34.

**Johnston DH, Beauregard M. 1969.** Rabies epidemiology in Ontario. *Bulletin of the Wildlife Disease Association* **5**:357–370 DOI 10.7589/0090-3558-5.3.357.

**Jordana X, Köhler M. 2011.** Enamel microstructure in the fossil bovid *Myotragus balearicus* (Majorca, Spain): implications for life-history evolution of dwarf mammals in insular ecosystems. *Palaeogeography, Palaeoclimatology, Palaeoecology* **300**:59–66 DOI 10.1016/j.palaeo.2010.12.008.

**Jordana X, Marín-Moratalla N, DeMiguel D, Kaiser TM, Köhler M. 2012.** Evidence of correlated evolution of hypsodonty and exceptional longevity in endemic insular mammals. *Proceedings of the Royal Society of London B: Biological Sciences* **279**:3339–3346 DOI 10.1098/rspb.2012.0689.

**Jordana X, Marín-Moratalla N, Moncunill-Solè B, Nacarino-Meneses C, Köhler M.** Ontogenetic changes in the histological features of zonal bone tissue of ruminants: a quantitative approach. *Comptes Rendus Palevol* In Press.

**Kaiser HE. 1960.** Untersuchungen zur vergleichenden Osteologie der fossilen und rezenten Pachyostosen. *Palaeontographica Abteilung A* **114**:113–196.

**Kerley ER. 1965.** The microscopic determination of age in human bone. *American Journal of Physical Anthropology* **23**:149–163 DOI 10.1002/ajpa.1330230215.

**Kielan-Jaworowska Z, Cifelli RL, Luo XZ. 2004.** *Mammals from the age of dinosaurs: origins, evolution, and structure*. New York: Columbia University Press.

**King CM. 1991.** A review of age determination methods for the stoat *Mustela erminea*. *Mammal Review* **21**:31–49 DOI 10.1111/j.1365-2907.1991.tb00286.x.

**Kiprijanoff W. 1881.** Studien über die fossilien Reptilien Russlands. I. Theil. Gattung *Ichthyosaurus* König. *Mémoires de l'Académie des Sciences de St-Pétersbourg, VIIe Série Tome XXVIII* **8**:1–103.

**Klein N, Sander PM. 2008.** Ontogenetic stages in the long bone histology of sauropod dinosaurs. *Paleobiology* **34**:247–263 DOI 10.1666/0094-8373(2008)034[0247:OSITLB]2.0.CO;2.

**Klevezal GA. 1996.** *Recording structures of mammals. Determination of age and reconstruction of life history*. Rotterdam/Brookfield: A.A. Balkema.

**Klevezal GA, Kleinenberg SE. 1969.** *Age determination of mammals from annual layers in teeth and bones*. Jerusalem: Israel Program of Scientific Translations.

**Köhler M. 2010.** Pérez-Mellado V, Ramon C, eds. *Fast or slow? The evolution of life history traits associated with insular dwarfing*. 261–280.

**Köhler M, Marín-Moratalla N, Jordana X, Aanes R. 2012.** Seasonal bone growth and physiology in endotherms shed light on dinosaur physiology. *Nature* **487**:358–361 DOI 10.1038/nature11264.

**Köhler M, Moyà-Solà S. 2009.** Physiological and life history strategies of a fossil large mammal in a resource-limited environment. *Proceedings of the National Academy of Sciences of the United States of America* **106**:20354–20358 DOI 10.1073/pnas.0813385106.

**Kolb C, Scheyer TM, Lister AM, Azorit C, De Vos J, Schlingemann MAJ, Rössner GE, Monaghan NT, Sánchez-Villagra MR. 2015.** Growth in fossil and extant deer and implications for body size and life history evolution. *BMC Evolutionary Biology* **15**:1–15 DOI 10.1186/s12862-015-0295-3.

**Kriloff A, Germain D, Canoville A, Vincent P, Sache M, Laurin M. 2008.** Evolution of bone microanatomy of the tetrapod tibia and its use in palaeobiological inference. *Journal of Evolutionary Biology* **21**:807–826 DOI 10.1111/j.1420-9101.2008.01512.x.

**Krmpotic CM, Ciancio MR, Barbeito CG, Mario RC, Carlini AA. 2009.** Osteoderm morphology in recent and fossil euphractine xenarthrans. *Acta Zoologica* **90**:339–351 DOI 10.1111/j.1463-6395.2008.00359.x.

**Laurin M. 2004.** The evolution of body size. Cope's rule and the origin of amniotes. *Systematic Biology* **53**:594–622 DOI 10.1080/10635150490445706.

**Laurin M, Girondot M, Loth M-M. 2004.** The evolution of long bone microanatomy and lifestyle in lissamphibians. *Palaeobiology* **30**:589–613 DOI 10.1666/0094-8373(2004)030<0589:TEOLBM>2.0.CO;2.

**Lee AH, Huttenlocker AK, Padian K, Woodward HN. 2013.** Analysis of growth rates. In: Padian K, Lamm E-T, eds. *Bone histology of fossil tetrapods*. Berkeley: University of California Press, 217–251.

**Lee AH, Werning S. 2008.** Sexual maturity in growing dinosaurs does not fit reptilian growth models. *Proceedings of the National Academy of Sciences of the United States of America* **105**:582–587 DOI 10.1073/pnas.0708903105.

**Lomolino MV, Sax DF, Palombo MR, Van der Geer AA. 2012.** Of mice and mammoths: evaluations of causal explanations for body size evolution in insular mammals. *Journal of Biogeography* **39**:842–854 DOI 10.1111/j.1365-2699.2011.02656.x.

**Lomolino MV, Van der Geer AA, Lyras GA, Palombo MR, Sax DF, Rozzi R. 2013.** Of mice and mammoths: generality and antiquity of the island rule. *Journal of Biogeography* **40**:1427–1439 DOI 10.1111/jbi.12096.

**Luo XZ. 2011.** Developmental patterns in mesozoic evolution of mammal ears. *Annual Review of Ecology, Evolution, and Systematics* **42**:355–380 DOI 10.1146/annurev-ecolsys-032511-142302.

**Luo ZX, Wible JR. 2005.** A Late Jurassic digging mammal and early mammalian diversification. *Science* **308**:103–107 DOI 10.1126/science.1108875.

**MacArthur RH, Wilson EO. 1967.** *The theory of island biogeography*. Princeton: Princeton University Press.

**Maddison WP, Maddison DR. 2015.** *Mesquite: a modular system for evolutionary analysis*. Version 3.02. *Available at http://mesquiteproject.org*.

**Mahboubi S, Bocherens H, Scheffler M, Benammi M, Jaeger JJ. 2014.** Was the Early Eocene proboscidean *Numidotherium koholense* semi-aquatic or terrestrial? Evidence from stable isotopes and bone histology. *Comptes Rendus Palevol* **13**:501–509 DOI 10.1016/j.crpv.2014.01.002.

**Marangoni F, Schaefer E, Cajade R, Tejedo M. 2009.** Growth mark formation and chronology of two neotropical anuran species. *Journal of Herpetology* **43**:546–550 DOI 10.1670/08-230R1.1.

**Margerie E de, Cubo J, Castanet J. 2002.** Bone typology and growth rate: testing and quantifying 'Amprino's rule' in the mallard (*Anas platyrhynchus*). *Comptes Rendus Biologies* **325**:221–230 DOI 10.1016/S1631-0691(02)01429-4.

**Marín-Moratalla N, Cubo J, Jordana X, Moncunill-Solè B, Köhler M. 2014.** Correlation of quantitative bone histology data with life history and climate: a phylogenetic approach. *Biological Journal of the Linnean Society* **112**:678–687 DOI 10.1111/bij.12302.

**Marín-Moratalla N, Jordana X, Köhler M. 2013.** Bone histology as an approach to providing data on certain key life history traits in mammals: implications for conservation biology. *Mammalian Biology* **78**:422–429.

**Martinez-Maza C, Alberdi MT, Nieto-Diaz M, Prado JL. 2014.** Life history traits of the Miocene *Hipparion concudense* (Spain) inferred from bone histological structure. *PLoS ONE* **9**:e103708 DOI 10.1371/journal.pone.0103708.

**Martínez-Maza C, Rosas A, García-Vargas S. 2006.** Bone paleohistology and human evolution. *Journal of Anthropological Sciences* **84**:33–52.

**Martinez-Maza C, Rosas A, Garcia-Vargas S, Estalrrich A, De la Rasilla M. 2011.** Bone remodelling in Neanderthal mandibles from the El Sidron site (Asturias, Spain). *Biology Letters* **7**:593–596 DOI 10.1098/rsbl.2010.1188.

**Martiniaková M, Grosskopf B, Vondráková M, Omelka R, Fabiš M. 2005.** Observation of the microstructure of rat cortical bone tissue. *Scripta Medica* **78**:45–50.

**McNab B. 1994.** Resource use and the survival of land and freshwater vertebrates on oceanic islands. *The American Naturalist* **144**:643–660 DOI 10.1086/285698.

**McNab BK. 2002.** Minimizing energy expenditure facilitates vertebrate persistence on oceanic islands. *Ecological Letters* **5**:693–704 DOI 10.1046/j.1461-0248.2002.00365.x.

**McNab BK. 2010.** Geographic and temporal correlations of mammalian size reconsidered: a resource rule. *Oecologia* **164**:13–23 DOI 10.1007/s00442-010-1621-5.

**Meier PS, Bickelmann C, Scheyer TM, Koyabu D, Sánchez-Villagra MR. 2013.** Evolution of bone compactness in extant and extinct moles (Talpidae): exploring humeral microstructure in small fossorial mammals. *BMC Evolutionary Biology* **13**:55 DOI 10.1186/1471-2148-13-55.

**Meredith RW, Janecka J, Gatesy J, Ryder OA, Fisher CA, Teeling EC, Goodbla A, Eizirik E, Simão TLL, Stadler T, Rabosky DL, Honeycutt RL, Flynn JJ, Ingram CM, Steiner C, Williams TL, Robinson TJ, Burk-Herrick A, Westerman M, Ayoub NA, Springer MS, Murphy WJ. 2011.** Impacts of the Cretaceous terrestrial revolution and KPg extinction on mammal diversification. *Science* **334**:521–524 DOI 10.1126/science.1211028.

**Mitchell EDJ. 1963.** Brachydont desmostylian from Miocene of San Clemente Island, California. *Bulletin of the Southern California Academy of Science* **62**:192–201.

**Mitchell EDJ. 1964.** Pachyostosis in desmostylids [Abstract 214]. *The Geological Society of America Special Paper* **76**.

**Mitchell J, Sander PM. 2014.** The three-front model: a developmental explanation of long bone diaphyseal histology of Sauropoda. *Biological Journal of the Linnean Society* **112**:765–781 DOI 10.1111/bij.12324.

**Moncunill-Solé B, Jordana X, Marín-Moratalla N, Moyà-Solà S, Köhler M. 2014.** How large are the extinct giant insular rodents? New body mass estimations from teeth and bones. *Integrative Zoology* **9**:197–212 DOI 10.1111/1749-4877.12063.

**Moncunill-Solé B, Orlandi-Oliverasa G, Jordana X, Rook L, Köhler M.** First approach of the life history of *Prolagus apricenicus* (Ochotonidae, Lagomorpha) from Terre Rosse sites (Gargano, Italy) using body mass estimation and paleohistological analysis. *Comptes Rendus Palevol* In Press.

**Montoya GA. 2014.** Bone microstructure of the subterranean rodent *Bathyergus suillus* (Rodentia: Bathyergidae). Master's thesis, University of Cape Town, South Africa.

**Morris P. 1970.** A method for determining absolute age in the hedgehog. *Journal of Zoology* **161**:277–281 DOI 10.1111/j.1469-7998.1970.tb02043.x.

**Musser AM. 2003.** Review of the monotreme fossil record and comparison of palaeontological and molecular data. *Comparative Biochemistry and Physiology Part A* **136**:927–942 DOI 10.1016/S1095-6433(03)00275-7.

**Musser AM, Archer M. 1998.** New information about the skull and dentary of the Miocene *Platypus obdurodon dicksoni*, and a discussion of ornithorhynchid relationships. *Philosophical Transactions of the Royal Society of London B* **353**:1063–1079 DOI 10.1098/rstb.1998.0266.

**Nacarino-Meneses C, Jordana X, Köhler M.** First approach to bone histology and skeletochronology of *Equus hemionus*. *Comptes Rendus Palevol* In Press.

**Nakajima Y, Endo H. 2013.** Comparative humeral microanatomy of terrestrial, semiaquatic, and aquatic carnivorans using micro-focus CT scans. *Mammal Study* **38**:1–8 DOI 10.3106/041.038.0101.

**Nakajima Y, Hirayama R, Endo H. 2014.** Turtle humeral microanatomy and its relationship to lifestle. *Biological Journal of the Linnean Society* **112**:719–734 DOI 10.1111/bij.12336.

**Nopcsa F von, Heidsieck E. 1934.** Über eine pachyostotische Rippe aus der Kreide Rügens. *Acta Zoologica* **15**:431–455 DOI 10.1111/j.1463-6395.1934.tb00661.x.

**O'Leary MA, Bloch JI, Flynn JJ, Gaudin TJ, Giallombardo A, Giannini NP, Goldberg SL, Kraatz BP, Luo Z-X, Meng J, Ni X, Novacek MJ, Perini FA, Randall ZS, Rougier GW, Sargis EJ, Silcox MT, Simmons NB, Spaulding M, Velazco PM, Weksler M, Wible JR, Cirranello AL. 2013.** The placental mammal ancestor and the post-K-Pg radiation of placentals. *Science* **339**:662–667 DOI 10.1126/science.1229237.

**O'Leary MA, Kaufman SG. 2012.** MorphoBank 3.0: web application for morphological phylogenetics and taxonomy. *Available at http://www.morphobank.org* (accessed 6 May 2015).

**Padian K. 2011.** Vertebrate palaeohistology then and now: a retrospective in the light of the contributions of Armand de Ricqles. *Comptes Rendus Palevol* **10**:303–309 DOI 10.1016/j.crpv.2011.02.001.

**Padian K. 2013.** Book review: forerunners of mammals: radiation, histology, biology. *Journal of Vertebrate Paleontology* **33**:1250–1251 DOI 10.1080/02724634.2013.763814.

**Padian K, Lamm E-T. 2013.** *Bone histology of tetrapods.* Berkeley, Los Angeles: University of California Press, 285.

**Pascal M, Castanet J. 1978.** Méthodes de la détermination de l'age chez le chat haret des iles Kerguelen. *Terre et Vie* **32**:529–554.

**Pascal M, Delattre P. 1981.** Comparaison des différentes méthodes de la détermination de l'age individuel chez le vison (*Mustela vison* Schreber). *Canadian Journal of Zoology* **59**:202–211 DOI 10.1139/z81-034.

**Pascual R, Archer M, Jaureguizar EO, Prado JL, Godthelp H, Hand SJ. 1992.** First discovery of monotremes in South America. *Nature* **356**:704–706 DOI 10.1038/356704a0.

**Pazzaglia UE, Sibilia V, Congiu T, Pagani F, Ravanelli M, Zarattini G. 2015.** Setup of a bone aging experimental model in the rabbit comparing changes in cortical and trabecular bone: morphological and morphometric study in the femur. *Journal of Morphology* **276(7)**:733–747 DOI 10.1002/jmor.20374.

**Ponton F, Elzanowski A, Castanet J, Chinsamy A, Margerie E de, Ricqlès A de, Cubo J. 2004.** Variation of the outer circumferential layer in the limb bones of birds. *Acta Ornithologica* **39**:21–24 DOI 10.3161/068.039.0210.

**Prondvai E, Stein K, 0si A, Sander PM. 2012.** Life history of *Rhamphorhynchus* inferred from bone histology and the diversity of pterosaurian growth strategies. *PLoS ONE* **7**:e31392 DOI 10.1371/journal.pone.0031392.

**Prondvai E, Stein KHW, Ricqlès A de, Cubo J. 2014.** Development-based revision of bone tissue classification: the importance of semantics for science. *Biological Journal of the Linnean Society* **112**:799–816 DOI 10.1111/bij.12323.

**Quekett JT. 1849a.** On the intimate structure of bone as composing the skeleton in the four great classes of animals, viz., mammals, birds, reptiles, and fishes, with some remarks on the great value of the knowledge of such structure in determining the affinities of minute fragments of organic remains. *Transactions of the Microscopical Society of London* **2**:46–58 DOI 10.1111/j.1365-2818.1849.tb05102.x.

**Quekett JT. 1849b.** Additional observations on the intimate structure of bone. *Transactions of the Microscopical Society of London* **2**:59–64 DOI 10.1111/j.1365-2818.1849.tb05103.x.

**Quekett JT. 1855.** *Descriptive and illustrated catalogue of the histological series contained in the museum of the Royal College of Surgeons of England. Volume II. Structure of the skeleton of vertebrate animals.* London: Taylor and Francis.

**Raia P, Barbera C, Conte M. 2003.** The fast life of a dwarfed giant. *Evolutionary Ecology* **17**:293–312 DOI 10.1023/A:1025577414005.

**Ray S, Botha J, Chinsamy A. 2004.** Bone histology and growth patterns of some nonmammalian therapsids. *Journal of Vertebrate Paleontology* **24**:634–648 DOI 10.1671/0272-4634(2004)024[0634:BHAGPO]2.0.CO;2.

**Ricqlès A de. 1969.** Recherches palèohistologiques sur les os longs des tetrapodes. II.- Quelques observations sur la structure des os longs des thériodontes. *Annales de Paléontologie* **55**:1–52.

**Ricqlès A de. 1974.** Evolution of endothermy: histological evidence. *Evolutionary Theory* **1**:51–80.

**Ricqlès A de. 1975.** Recherches paléohistologiques sur les os longs des tétrapodes VII. - Sur la classification, la signification fonctionnelle et l'histoire des tissus oseux des tétrapodes. Première partie, structures. *Annales de paléontologie* **61**:51–129.

**Ricqlès A de. 1976a.** On bone histology of fossil and living reptiles, with comments on its functional and evolutionary significance. In: Bellairs A, Cox CB, eds. *Morphology and biology of reptiles*. London and New York: Academic Press, 123–150.

**Ricqlès A de. 1976b.** Recherches paléohistologiques sur les os longs des tétrapodes. VII. - Sur la classification, la signification fonctionnelle et l'histoire des tissus osseux des tétrapodes. Deuxième partie. Fonctions: considérations fonctionnelles et physiologiques. *Annales de Paléontologie* **62**:71–126.

**Ricqlès A de. 2011.** Vertebrate palaeohistology: past and future. *Comptes Rendus Palevol* **10**:509–515 DOI 10.1016/j.crpv.2011.03.013.

**Ricqlès A de, Buffrénil V de. 1995.** Sur la présence de pachyostéosclerosis chez la rhytine de Steller (*Rhytina* (*Hydrodamalis*) *gigas*), sirénian rézent éteint. *Annales des Sciences Naturelles, Zoologie, Paris, 13e Série* **16**:47–53.

**Ricqlès A de, Castanet J, Francillon-Vieillot H. 2004.** The "message" of bone tissue in Palaeoherpetology. *Italian Journal of Zoology* **71(Supplement 2)**:3–12 DOI 10.1080/11250000409356599.

**Ricqlès A de, Cubo J. 2010.** Le problème de la causalité complexe aux sources de la relation structuro-fonctionnelle : 1/généralités, 2/l'exemple du tissu osseux. In: Gayon J, Ricqlès AD, eds. *Les Fonctions: des organismes aux artefacts*. Paris: PUF, 179–188.

**Ricqlès A de, Meunier FJ, Castanet J, Francillon-Vieillot H. 1991.** Comparative microstructure of bone. In: Hall BK, ed. *Bone volume 3: bone matrix and bone specific products*. Boca Raton: CRC Press, 1–78.

**Ricqlès A de, Taquet P, Buffrénil V de. 2009.** Rediscovery of Paul Gervais' paleohistological collection. *Geodiversitas* **31**:943–971 DOI 10.5252/g2009n4a943.

**Ryan TM, Shaw CN. 2015.** Gracility of the modern *Homo sapiens* skeleton is the result of decreased biomechanical loading. *Proceedings of the National Academy of Sciences of the United States of America* **112**:372–377 DOI 10.1073/pnas.1418646112.

**Sanchez S, Ahlberg P, Trinajstic K, Mirone A, Tafforeau P. 2012.** Three dimensional synchrotron virtual paleohistology: a new insight into the world of fossil bone microstructures. *Microscopy and Microanalysis* **18**:1095–1105 DOI 10.1017/S1431927612001079.

**Sander PM, Andrassy P. 2006.** Lines of arrested growth and long bone histology in Pleistocene large mammals from Germany: what do they tell us about dinosaur physiology? *Palaeontographica Abteilung A* **277**:143–159.

**Sander PM, Klein N, Buffetaut E, Cuny G, Suteethorn V, Le Loeuff J. 2004.** Adaptive radiation in sauropod dinosaurs: bone histology indicates rapid evolution of giant body size through acceleration. *Organisms, Diversity & Evolution* **4**:165–173 DOI 10.1016/j.ode.2003.12.002.

**Sander PM, Tückmantel C. 2003.** Bone lamina thickness, bone apposition rates, and age estimates in sauropod humeri and femora. *Paläontologische Zeitschrift* **77**:161–172 DOI 10.1007/BF03004566.

**Schaffer J. 1890.** Über den feineren Bau fossiler Knochen. In: *Sitzungsberichte der Kaiserlichen Akademie der Wissenschaften, Mathematisch-Naturwissenschaftliche Classe XCVIII. Band. Hefte I bis X. Abtheilung III*. 319–382.

**Scheyer TM. 2009–2015.** Palaeohistology. In: Sánchez-Villagra MR, ed. *Developmental—palaeontology net*. Zurich: Palaeontological Institute of the University of Zurich. *Available at http://www.developmental-palaeontology.net/palaeohistology/index.php* (accessed 1 June 2015).

**Scheyer TM, Klein N, Sander PM. 2010.** Developmental palaeontology of Reptilia as revealed by histological studies. *Seminars in Cell & Developmental Biology* **21**:462–470 DOI 10.1016/j.semcdb.2009.11.005.

**Schultz M. 1997.** Microscopic investigation of excavated skeletal remains: a contribution to paleopathology and forensic medicine. In: Haglund WD, Sorg MH, eds. *Forensic taphonomy The postmortem fate of human remains*. Boca Raton/New York/London/Tokyo: CRC Press, 201–222.

**Schultz M, Schmidt-Schultz TH. 2014.** Microscopic research on fossil human bone. In: Henke W, Tattersall I, eds. *Handbook of paleoanthropology*. 2nd edition. Heidelberg/New York: Springer, 983–998.

**Singh IJ, Tonna EA, Gandel CP. 1974.** A comparative histological study of mammalian bone. *Journal of Morphology* **144**:421–438 DOI 10.1002/jmor.1051440404.

**Skinner MM, Stephens NB, Tsegai ZJ, Foote AC, Nguyen NH, Gross T, Pahr DH, Hublin J-J, Kivell TL. 2015.** Human-like hand use in *Australopithecus africanus*. *Science* **347**:395–399 DOI 10.1126/science.1261735.

**Stearns SC. 1992.** *The evolution of life histories*. Oxford: Oxford University Press.

**Stein K, Prondvai E. 2014.** Rethinking the nature of fibrolamellar bone: an integrative biological revision of sauropod plexiform bone formation. *Biological Reviews* **89(1)**:24–47 DOI 10.1111/brv.12041.

**Stein K, Sander M. 2009.** Histological core drilling: a less destructive method for studying bone histology. In: *First annual fossil preparation and collections symposium*. Petrified Forest: Petrified Forest National Park, 69–80.

**Straehl FR, Scheyer TM, Forasiepi AM, MacPhee RD, Sánchez-Villagra MR. 2013.** Evolutionary patterns of bone histology and bone compactness in xenarthran mammal long bones. *PLoS ONE* **8**:e69275 DOI 10.1371/journal.pone.0069275.

**Tacutu R, Craig T, Budovsky A, Wuttke D, Lehmann G, Taranukha D, Costa J, Fraifeld VE, De Magalhaes JP. 2013.** Human ageing genomic resources: integrated databases and tools for the biology and genetics of ageing. *Nucleic Acids Research* **41**:D1027–D1033 DOI 10.1093/nar/gks1155.

**Thewissen JGM, Cooper LN, Clementz MT, Bajpai S, Tiwari BN. 2007.** Whales originated from aquatic artiodactyls in the Eocene epoch of India. *Nature* **450**:1190–1194 DOI 10.1038/nature06343.

**Tomassini RL, Montalvo CI, Manera T, Visconti G. 2014.** Mineralogy, geochemistry, and paleohistology of Pliocene mammals from the Monte Hermoso Formation (Argentina). *Paedotherium bonaerense* (Notoungulata, Hegetotheriidae) as a case study. *Ameghiniana* **51**:385–395 DOI 10.5710/AMGH.01.07.2014.2737.

**Van der Geer A, Lyras G, De Vos J, Dermitzakis M. 2010.** *Evolution of island mammals. Adaptation and extinction of placental mammals on islands*. Sussex: Wiley-Blackwell.

**Vanderhoof VL. 1937.** A study of the Miocene sirenian *Desmostylus*. *University of California Publications in the Geological Sciences* **24**:169–262.

**Vickaryous MK, Hall BK. 2006.** Osteoderm morphology and development in the nine-banded armadillo, *Dasypus novemcinctus* (Mammalia, Xenarthra, Cingulata). *Journal of Morphology* **267**:1273–1283 DOI 10.1002/jmor.10475.

**Vickaryous MK, Sire JY. 2009.** The integumentary skeleton of tetrapods: origin, evolution, and development. *Journal of Anatomy* **214**:441–464 DOI 10.1111/j.1469-7580.2008.01043.x.

**Warren JW. 1963.** Growth zones in the skeleton of recent and fossil vertebrates. PhD, University of California.

**Wolf D. 2007.** Osteoderm histology of extinct and recent Cingulata and Phyllophaga (Xenarthra, Mammalia): implications for systematics and biomechanical adaptation. *Hallesches Jahrbuch für Geowissenschaften Beiheft* **23**:145–151.

**Wolf D. 2008.** Osteoderm histology of the Cingulata (Xenarthra, Mammalia): implications for systematics [Abstract 161A]. *Journal of Vertebrate Paleontology* **28**.

**Wolf D, Kalthoff DC, Martin Sander PM. 2012.** Osteoderm histology of the Pampatheriidae (Cingulata, Xenarthra, Mammalia): implications for systematics, osteoderm growth, and biomechanical adaptation. *Journal of Morphology* **273**:388–404 DOI 10.1002/jmor.11029.

**Woodward HN, Padian K, Lee AH. 2013.** Skeletochronology. In: Padian K, Lamm E-T, eds. *Histology of fossil tetrapods—advancing methods, analysis and interpretation*. Berkeley, Los Angeles, London: University of California Press, 195–215.

**Zedda M, Lepore G, Manca P, Chisu V, Farina V. 2008.** Comparative bone histology of adult horses and cows. *Journal of Veterinary Medicine Series C* **37**:442–445.

**Zylberberg L, Traub W, Buffrénil V de, Allizard F, Arad T, Weiner S. 1998.** Rostrum of a toothed whale: ultrastructural study of a very dense bone. *Bone* **23**:241–247 DOI 10.1016/S8756-3282(98)00101-X.

# CHAPTER 3

## Growth in fossil and extant deer and implications for body size and life history evolution

Authors: Kolb C., Scheyer T. M., Lister A. M., Azorit C., de Vos J., Schlingemann M. A. J., Rössner G. E., Monaghan N. T., Sánchez-Villagra M. R.

Publication: 2015, *BMC Evolutionary Biology,* 15:19.

Contributions: CK and MRS-V designed the study/experiments and wrote the manuscript, CK, TMS, MAJS and CA collected and analysed histological data, CK and MAJS performed the experiments, CK prepared figures/tables and took micrographs, JDV, AML, NTM, and GER provided material and taxonomic/stratigraphical information, and all authors contributed to the final interpretation and editing of the manuscript. All authors read and approved the final manuscript.

Kolb *et al. BMC Evolutionary Biology* (2015) 15:19
DOI 10.1186/s12862-015-0295-3

BMC
Evolutionary Biology

**RESEARCH ARTICLE** **Open Access**

# Growth in fossil and extant deer and implications for body size and life history evolution

Christian Kolb[1*], Torsten M Scheyer[1], Adrian M Lister[2], Concepcion Azorit[3], John de Vos[4], Margaretha AJ Schlingemann[5], Gertrud E Rössner[6], Nigel T Monaghan[7] and Marcelo R Sánchez-Villagra[1]

## Abstract

**Background:** Body size variation within clades of mammals is widespread, but the developmental and life-history mechanisms by which this variation is achieved are poorly understood, especially in extinct forms. An illustrative case study is that of the dwarfed morphotypes of *Candiacervus* from the Pleistocene of Crete versus the giant deer *Megaloceros giganteus*, both in a clade together with *Dama dama* among extant species. Histological analyses of long bones and teeth in a phylogenetic context have been shown to provide reliable estimates of growth and life history patterns in extant and extinct mammals.

**Results:** Similarity of bone tissue types across the eight species examined indicates a comparable mode of growth in deer, with long bones mainly possessing primary plexiform fibrolamellar bone. Low absolute growth rates characterize dwarf *Candiacervus* sp. II *and C. ropalophorus* compared to *Megaloceros giganteus* displaying high rates, whereas *Dama dama* is characterized by intermediate to low growth rates. The lowest recorded rates are those of the Miocene small stem cervid *Procervulus praelucidus*. Skeletal maturity estimates indicate late attainment in sampled *Candiacervus* and *Procervulus praelucidus*. Tooth cementum analysis of first molars of two senile *Megaloceros giganteus* specimens revealed ages of 16 and 19 years whereas two old dwarf *Candiacervus* specimens gave ages of 12 and 18 years.

**Conclusions:** There is a rich histological record of growth across deer species recorded in long bones and teeth, which can be used to understand ontogenetic patterns within species and phylogenetic ones across species. Growth rates *sensu* Sander & Tückmantel plotted against the anteroposterior bone diameter as a proxy for body mass indicate three groups: one with high growth rates including *Megaloceros*, *Cervus*, *Alces*, and *Dama*; an intermediate group with *Capreolus* and *Muntiacus*; and a group showing low growth rates, including dwarf *Candiacervus* and *Procervulus*. Dwarf *Candiacervus*, in an allometric context, show an extended lifespan compared to other deer of similar body size such as *Mazama* which has a maximum longevity of 12 years in the wild. Comparison with other clades of mammals reveals that changes in size and life history in evolution have occurred in parallel, with various modes of skeletal tissue modification.

**Keywords:** Island evolution, Pleistocene, Cervidae, *Candiacervus*, *Megaloceros*, Bone histology, Cementum analysis, Growth rates, Longevity, Skeletal maturity

## Background

Several lineages of mammals have evolved remarkable changes in body size following island isolation [1-3], including among others dwarf hippopotamuses, elephants, and deer, and giant rabbits [4-6]. These patterns are the result of complex interplay of multiple variables, including resource limitation and ecological release [5,7-9]. To understand the mechanisms of life-history and size evolution on islands but also in cases of significant body size changes in mainland lineages, histology of hard tissues is a powerful tool, as has been demonstrated for 'dwarf' and 'giant' sauropod [10-12] and tyrannosaurid [13] dinosaurs, as well as early synapsids [14,15] among fossil forms.

A remarkable example of island evolution is found in the Pleistocene of Crete, where an endemic clade of deer, *Candiacervus*, including 'dwarfed' species, evolved from the megacerine clade (Megacerini) of larger forms [16-19].

---

* Correspondence: christian.kolb@pim.uzh.ch
[1] Paläontologisches Institut und Museum der Universität Zürich, Karl Schmid-Strasse 4, CH-8006 Zürich, Switzerland
Full list of author information is available at the end of the article

Despite of the unresolved nature of megacerine phylogeny [20], the small *Candiacervus* morphotypes must have undergone size reduction since all their postulated mainland sister-groups are significantly larger (e.g. *Praemegaceros spp.* with shoulder heights ranging from 0.9 m to 1.50 m [18,19] or *Cervus peloponnesiacus* with a shoulder height of just slightly less than one metre [21]. The kind of dwarfism we observe in *Candiacervus* has been described as autapomorphic nanism by [22]. *Candiacervus* shows diversity in size, as six size classes of deer have been distinguished [16,17]. The smallest morphotype, *C. ropalophorus*, reached a shoulder height of about 40 cm, *C.* sp. II one of about 60 cm, and the largest one reached a height of about 1.65 m [23]. This phenomenon has been interpreted as a case of adaptive radiation [24]. In the Middle to Late Pleistocene, Crete was characterized by dense forest as well as jagged rocks with several intermediate kinds of environments, in which such a radiation could have occurred [5]. Here we study *Candiacervus ropalophorus* and *C.* sp. II, as these two size classes are small and are represented by growth series we could sample. '*Candiacervus* sp. II' may be a composite of three morphotypes of similar size [17].

Representing the other extreme of size with a shoulder height of up to 2 m [20], *Megaloceros giganteus* has been a subject of extensive debates on evolutionary processes [20,25,26]. It is best known from fossil occurrences in Ireland from 11 to 12,000 BP [27] years ago and from possessing the largest antlers of any fossil or living species. *Megaloceros* was widespread in Europe and western Asia for 400,000 years and morphological and molecular analyses have supported a close relationship with fallow deer, *Dama dama* [20,28] (Figure 1a). The fossil record of deer is long and complex, and *Procervulus praelucidus* from the Early Miocene of Germany represents a stem taxon that can help to reconstruct the evolution of life history features in deer [29] (Figure 1a).

In order to enhance reproductive success life history traits can be selected by adjusting the developmental schedule to match environmental conditions [36]. Bone microstructure can reveal such traits in mammals, which generally exhibit bone matrices indicative of high rates of tissue deposition in juveniles, whereas after onset of maturity a decrease in bone growth rate occurs resulting in deposition of highly organized bone tissue [37-39]. Lines of arrested growth (LAGs) form from the first year of an individual's postnatal life as a result of annual cessation of bone growth [40,41]. Counting these LAGs therefore provides the means to estimate minimum individual ages [40]. However, there can be decoupling of the number of LAGs in long bones and the actual age of old individuals leading to underestimation of individual ages [42]. Dental cementum is a more accurate source for estimating longevity in mammals, due to its usual absence of resorption [43] and more complete growth record, as shown by studies on growth marks in living species, including deer of known age [43,44]. For example, using cementum analysis in molars, 99% of a sample of 51 Spanish red deer could be aged within a one year confidence interval [45].

Palaeohistology previously led to the discovery in the island goat *Myotragus balearicus* from the Late Pleistocene of the Balearic Islands, of a 'reptile'-like growth pattern consisting of lamellar-zonal bone throughout the cortex [46]. *Myotragus* was therefore hypothesized to have grown at low but variable rates and to have ceased its growth cyclically. Our investigation of *Candiacervus* and of relevant mainland cervids, focusing on bone microstructure in growth series of various long bones, and dental histology in old adults, serves to examine whether the pattern of growth of *Myotragus* is general among island artiodactyls. Longevity estimates, based on the rest lines in the first molar of old individuals, were made. The first molar is the first permanent tooth to erupt [45], showing the most complete growth record in deer. In order to further examine growth patterns across cervids and to put life history data attained by histological analyses into an allometric context, we investigated the relation between body weight and growth rates [47-49].

## Methods

A total of 51 long bones, six phalanges, four lower first molars and two upper first molars of *Candiacervus* sp. II and *Candiacervus ropalophorus*, 14 long bones and five lower first molars of *Megaloceros giganteus*, and 13 long bones and 2 lower first molars of *Procervulus praelucidus* were sampled (Table 1, see also Additional file 1: Methods). Sixteen long bones and two lower first molars of *Dama dama*, and one femur each of *Muntiacus muntjak*, *Cervus elaphus* and *Alces alces*, were sampled for comparison. Of *Capreolus capreolus* one femur and one metacarpal were sampled. Following standard procedures, the bones were coated and impregnated with epoxy resin (Araldite or Technovit) prior to sawing and grinding. Long bones were transversely sectioned at mid-shaft where the growth record is most complete [e.g. 10]. For cementum analysis jaws were longitudinally cut through the cementum interroot pad of the lower first molar and surfaces were impregnated with epoxy resin and finally ground and polished. Long bones of *Megaloceros giganteus* were also sampled by using a diamond-studded core drill, with sampled cores being subsequently processed [10,50]. Sections were observed in normal transmitted and cross-polarized light using a Leica DM 2500 M composite microscope equipped with Leica DFC 420 C digital camera. Since there are no remarkable differences in the bone tissue of the two *Candiacervus* morphotypes

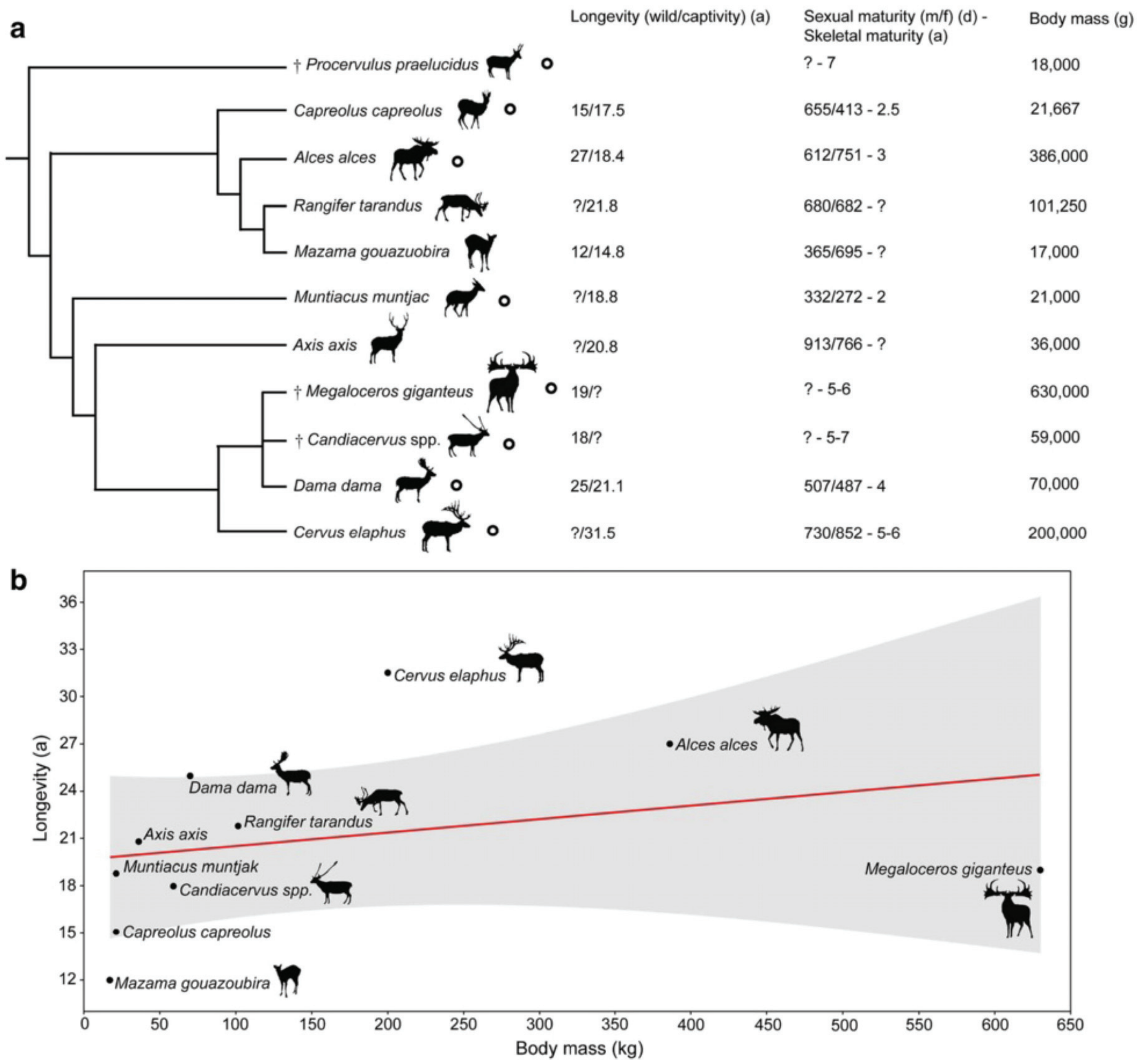

**Figure 1 Cervid phylogeny and life history. a)** Phylogenetic relationships, maximal recorded life expectancy, onset of maturity, and average adult body mass of *Candiacervus*, *Megaloceros*, and relatives based on [17,20,23,28-35]. Cervid species studied are indicated by black circles. The trichotomy of the fallow deer (*Dama*) and its extinct relatives illustrates the unresolved nature of this well-supported clade. Body mass values are average. **b)** Linear regression relating maximum recorded longevity to body mass in cervids, and observed maxima within available samples of fossil species. Shaded region represents the 95% confidence interval. In cases in which unambiguous longevity data for wild animals were not available, data of captive specimens have been used.

sampled, they are treated together here. Polished tooth surfaces were observed using a Leica MZ 165 and MZ 125 reflected-light microscope.

For quantification of growth rates, distances between LAGs, i.e. growth zones were measured with Leica IM 50 Image Manager®, and annual growth rates per day were calculated [51] by dividing growth zones by the number of days per growth period and year. The estimate of number of days per growth period, i.e. 260 days, is based on [41]. Growth period intervals (275–245 days) [41] and a 365 day growth period have been taken into account as well (Additional file 2). Since growth zone thickness may vary considerably within the cortex of one bone, all measurements have been performed along the anteroposterior axis in the anterior quadrant of each section, whereas micrographs presented in this work have been taken from the best preserved and histologically most informative areas. Growth zone measurements were performed for femora and tibiae since they are the most informative long bones in cervids

**Table 1 Material used in this study**

| Species | Object | Ontogenetic stage | Locality | Specimen number |
|---|---|---|---|---|
| *Candiacervus ropalophorus* | Femur | adult | Gerani 4, Crete (Greece) | PIMUZ A/V 5195 |
| " | " | adult | " | PIMUZ A/V 5202 |
| " | " | perinatal | " | PIMUZ A/V 5207 |
| " | " | perinatal | " | PIMUZ A/V 5206 |
| " | Tibia | adult | " | PIMUZ A/V 5188 |
| " | " | adult | " | PIMUZ A/V 5189 |
| " | " | juvenile | " | PIMUZ A/V 5208 |
| " | " | juvenile | " | PIMUZ A/V 5193 |
| " | " | perinatal | " | PIMUZ A/V 5191 |
| " | " | perinatal | " | PIMUZ A/V 5194 |
| " | Metatarsus | adult | " | PIMUZ A/V 5192 |
| " | " | juvenile | " | PIMUZ A/V 5254 |
| " | " | perinatal | " | PIMUZ A/V 5205 |
| " | Humerus | adult | " | PIMUZ A/V 5190 |
| " | " | perinatal | " | PIMUZ A/V 5187 |
| " | " | perinatal | " | PIMUZ A/V 5203 |
| " | Radius | adult | " | PIMUZ A/V 5186 |
| " | " | adult | " | PIMUZ A/V 5199 |
| " | " | perinatal | " | PIMUZ A/V 5200 |
| " | Ulna | perinatal | " | PIMUZ A/V 5255 |
| " | Metacarpus | adult | " | PIMUZ A/V 5197 |
| " | " | juvenile | " | PIMUZ A/V 5198 |
| " | Lower M1 | adult | " | PIMUZ A/V 5196 |
| *Candiacervus* sp. II | Femur | adult | Liko, Crete (Greece) | PIMUZ A/V 5218 |
| " | " | juvenile | " | PIMUZ A/V 5219 |
| " | " | perinatal | " | PIMUZ A/V 5244 |
| " | " | perinatal | " | PIMUZ A/V 5245 |
| " | Tibia | adult | " | PIMUZ A/V 5222 |
| " | " | juvenile | " | PIMUZ A/V 5220 |
| " | " | perinatal | " | PIMUZ A/V 5221 |
| " | " | perinatal | " | PIMUZ A/V 5234 |
| " | Metatarsus | adult | " | PIMUZ A/V 5240 |
| " | " | adult | " | PIMUZ A/V 5212 |
| " | " | juvenile | " | PIMUZ A/V 5213 |
| " | " | juvenile | " | PIMUZ A/V 5223 |
| " | " | perinatal | " | PIMUZ A/V 5224 |
| " | Humerus | adult | " | PIMUZ A/V 5231 |
| " | " | juvenile | " | PIMUZ A/V 5236 |
| " | " | perinatal | " | PIMUZ A/V 5237 |
| " | Radius | adult | " | PIMUZ A/V 5232 |
| " | " | adult | " | PIMUZ A/V 5233 |
| " | " | juvenile | " | PIMUZ A/V 5230 |
| " | " | perinatal | " | PIMUZ A/V 5211 |
| " | " | perinatal | " | PIMUZ A/V 5257 |

**Table 1 Material used in this study** *(Continued)*

| | | | | |
|---|---|---|---|---|
| " | " | perinatal | " | PIMUZ A/V 5214 |
| " | Ulna | adult | " | PIMUZ A/V 5215 |
| " | " | juvenile | " | PIMUZ A/V 5225 |
| " | " | perinatal | " | PIMUZ A/V 5226 |
| " | Metacarpus | adult | " | PIMUZ A/V 5246 |
| " | " | juvenile | " | PIMUZ A/V 5247 |
| " | " | perinatal | " | PIMUZ A/V 5209 |
| " | " | perinatal | " | PIMUZ A/V 5210 |
| " | 1st Phalange | adult | " | PIMUZ A/V 5238 |
| " | " | juvenile | " | PIMUZ A/V 5239 |
| " | " | perinatal | " | PIMUZ A/V 5216 |
| " | 2nd Phalange | adult | " | PIMUZ A/V 5217 |
| " | " | juvenile | " | PIMUZ A/V 5235 |
| " | " | perinatal | " | PIMUZ A/V 5227 |
| " | Rib | adult | " | PIMUZ A/V 5228 |
| " | Lower M1 | adult | " | PIMUZ A/V 5229 |
| " | " | adult | " | PIMUZ A/V 5243 |
| " | Upper M1 | senescent (18 years) | " | PIMUZ A/V 5241 |
| " | " | adult | " | PIMUZ A/V 5242 |
| *Candiacervus* sp. | Lower M1 | senescent (12 years) | Bate cave, Crete (Greece) | PV M 82318 (NHML) |
| *Procervulus praelucidus* | Femur | adult | Wintershof-West, Germany | BSPG 1937 II 23226 |
| " | " | adult | " | BSPG 1937 II 23227 |
| " | " | juvenile | " | BSPG 1937 II 23228 |
| " | " | juvenile | " | BSPG 1937 II 23229 |
| " | Tibia | adult | " | BSPG 1937 II 23230 |
| " | " | adult | " | BSPG 1937 II 23231 |
| " | " | juvenile | " | BSPG 1937 II 23232 |
| " | Humerus | adult | " | BSPG 1937 II 23233 |
| " | " | adult | " | BSPG 1937 II 23234 |
| " | Radius | adult | " | BSPG 1937 II 23235 |
| " | " | adult | " | BSPG 1937 II 23236 |
| " | " | adult | " | BSPG 1937 II 23237 |
| " | " | adult | " | BSPG 1937 II 23238 |
| " | Lower M1 | adult | " | BSPG 1937 II 12002 |
| " | " | adult | " | BSPG 1937 II 12040 |
| *Megaloceros giganteus* | Femur | adult | Craddanstown Rep. of Ireland | NMING:F7937/4 |
| " | " | adult | Baunmore Townland, Rep. of Ireland | NMING:F21306/13 |
| " | Tibia | adult | Ballyragget, Rep. of Ireland | NMING:F22655/34 |
| " | " | adult | Buttevant, Rep. of Ireland | NMING:F22534/5 |
| " | " | adult | Baunmore Townland, Rep. of Ireland | NMING:F21306/14 |
| " | Metatarsus | adult | North Sea sediments | PIMUZ A/V 5256 |
| " | " | adult | Baunmore Townland, Rep. of Ireland | NMING:F21306/19 |
| " | " | adult | Buttevant, Rep. of Ireland | NMING:F22534/6 |
| " | Humerus | adult | Ballyragget, Rep. of Ireland | NMING:F22655/37 |
| " | " | adult | Buttevant, Rep. of Ireland | NMING:F22534/2 |

**Table 1 Material used in this study** *(Continued)*

| | | | | |
|---|---|---|---|---|
| " | Radius-Ulna | adult | Ballyragget, Rep. of Ireland | NMING:F22655/36 |
| " | " | adult | Buttevant, Rep. of Ireland | NMING:F22534/3 |
| " | Metacarpus | adult | Ballyragget, Rep. of Ireland | NMING:F22655/31 |
| " | " | adult | Buttevant, Rep. of Ireland | NMING:F22534/4 |
| " | Lower M1 | senescent (19 years) | Brühl (Schwetzingen), Deutschland | PIMUZ A/V 2235 |
| " | " | senescent (16 years) | Kent'scavern, Torquay, UK | PV OR 16800 (NHML) |
| " | " | senescent (n.a.) | Wyhlen, Germany | BSPG 1957 I 398 |
| " | " | adult | Rath, Rep. of Ireland | NMING:F22654 |
| " | " | adult | Craddanstown, Rep. of Ireland | NMING:F7937/5 |
| *Dama dama* | Femur | adult (wild) | Schrevenborn, Germany | ZIUK 9630 |
| " | " | adult (captive) | Wildnispark Zürich, Switzerland | PIMUZ A/V 5248 |
| " | " | adult (captive) | " | PIMUZ A/V 5248 |
| " | " | juvenile (captive) | " | PIMUZ A/V 5249 |
| " | Tibia | adult (wild) | Schrevenborn, Germany | ZIUK 9630 |
| " | " | adult(captive) | WildnisparkZürich, Switzerland | PIMUZ A/V 5248 |
| " | " | adult (captive) | " | PIMUZ A/V 5248 |
| " | " | juvenile (captive) | " | PIMUZ A/V 5249 |
| " | Humerus | adult (wild) | Schrevenborn, Germany | ZIUK 9630 |
| " | " | adult (captive) | Wildnispark Zürich, Switzerland | PIMUZ A/V 5248 |
| " | " | adult (captive) | " | PIMUZ A/V 5248 |
| " | " | juvenile (captive) | " | PIMUZ A/V 5249 |
| " | Radius-Ulna | adult (wild) | Schrevenborn, Germany | ZIUK 9630 |
| " | " | adult (captive) | Wildnispark Zürich, Switzerland | PIMUZ A/V 5248 |
| " | " | adult (captive) | " | PIMUZ A/V 5248 |
| " | " | juvenile (captive) | " | PIMUZ A/V 5249 |
| " | Lower M1 | adult (wild) | Schrevenborn, Germany | ZIUK 9630 |
| " | " | adult (captive) | Wildnispark Zürich, Switzerland | PIMUZ A/V 5248 |
| *Capreolus capreolus* | Femur | adult (wild) | Schrevenborn, Germany | ZIUK 9872 |
| " | Metatarsus | juvenile (wild) | Hittnau, Switzerland | PIMUZ A/V 5251 |
| *Muntiacus muntjak* | Femur | adult (captive) | Tierpark Hagenbeck, Hamburg, Germany | ZIUK 7994 |
| *Cervus elaphus* | " | adult (wild) | Barmstedt, Germany | ZIUK 23517 |
| *Alces alces* | " | adult (wild) | Norway | ZMUZ 20242 |

Specimens used in this study with ontogenetic stage, locality of death/fossil site, specimen number and thin section number.
Institutional Abbreviations: **BSPG** Bayerische Staatssammlung für Paläontologie und Geologie, Munich, Germany; **NBC** Netherlands Centre for Biodiversity Leiden, The Netherlands; **NHML** Natural History Museum London, UK; **NMING** National Museum of Ireland - Natural History; **PIMUZ** Paläontologisches Institut und Museum, Universität Zürich, Switzerland; **ZIUK** Zoologisches Institut der Universität Kiel, Germany; **ZMUZ** Zoologisches Museum der Universität Zürich, Switzerland.

(see also Additional file 1: Methods). For growth rate graphs Microsoft Office Excel 2010© has been used. Regression analyses (ordinary least squares) for average and growth rates *sensu* Sander & Tückmantel [51] were performed using Past3.0 [52]. All graphs have been redrawn using Adobe Illustrator CS5©.

## Results and discussion

### Histological description of primary bone

Newborn dwarf *Candiacervus* (*C. ropalophorus* and *C.* sp. II) exhibit fibrolamellar bone with a high amount of woven-fibred bone as primary tissue (Figure 2a). In the inner cortex, vascularization tends to be reticular, whereas in the middle and outer cortex vascularization has a plexiform pattern. With increasing age, the amount of vascularisation and woven bone decreases, with the former changing from a plexiform to laminar organisation in the middle and outer cortex, whereas the amount of lamellar or parallel-fibred bone within the fibrolamellar matrix increases (Figure 2a-c). The outermost layer of the outer cortex in adult *Candiacervus* sampled is composed of a narrow layer of avascular lamellar bone, called the outer

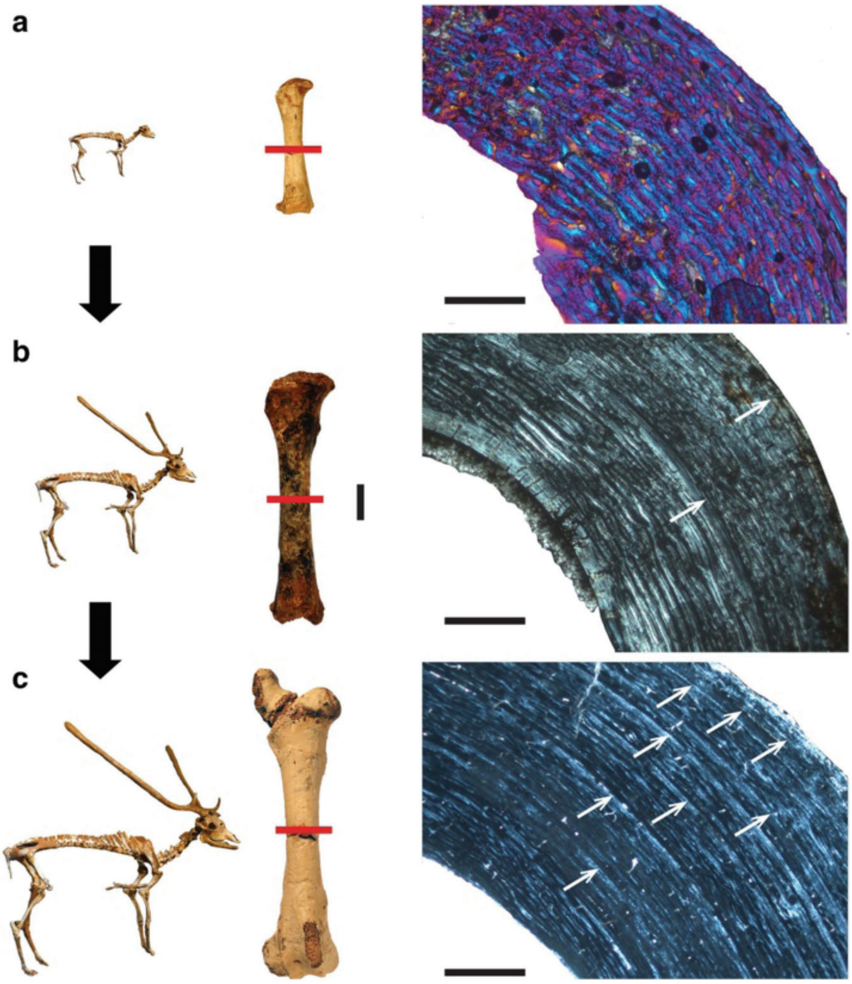

**Figure 2 Histological growth series of dwarf deer femora with skeletal reconstructions [55] and specimens sampled (anterior view).** Red bars indicate plane of sectioning. *Candiacervus* sp. II under crossed polarised light (xpl). **a)** Bone cortex of a perinatal specimen (PIMUZ A/V 5244) showing a mainly plexiform arrangement of vascular canals with a high amount of woven-fibred bone (violet areas; additional use of lambda compensator). Scale bar, 0.5 mm. **b)** Juvenile specimen (PIMUZ A/V 5219). Scale bars, 20 mm (femora all to scale), 1 mm (bone cortex). **c)** Adult specimen (PIMUZ A/V 5218). Note the increasing amount of parallel-fibred bone (bright areas) and the occurrence of lines of arrested growth (LAGs, white arrows) throughout ontogeny. Scale bar, 1 mm.

circumferential layer (OCL) [53] in this work and also referred to as external fundamental system (EFS, e.g. *sensu* [42], see also [54]). We prefer the term outer circumferential layer for being more descriptive than the term external fundamental system. An inner circumferential layer [38] is well developed in all adult femora. Long bones of *Candiacervus* indicate, based on growth line counts, minimum ages of about two years for the juveniles sampled.

Adult *Megaloceros*, *Dama*, *Cervus*, and *Alces* show in all sampled long bones a similar arrangement of bone tissue types to each other. Vascularisation in the outer part of the cortex is partly longitudinal, whereas in dwarf *Candiacervus*, *Procervulus*, and *Muntiacus* it changes directly from plexiform/laminar to avascular in the outer circumferential layer. This is evidently a feature separating large and intermediate from small-sized deer, including dwarf *Candiacervus*. Moreover, the density of vascular canals is higher in intermediate-sized and larger deer compared to smaller taxa (Figure 3a-c, see also Additional file 1: Table S2 and Figure S1). Because it is a juvenile specimen and still shows less vascularisation than the adult *Dama* and *Megaloceros*, specimen BSPG 1937 II 23227 is especially illustrative concerning the low amount of vascularization in the small sized cervid *Procervulus* (Figure 3a-c).

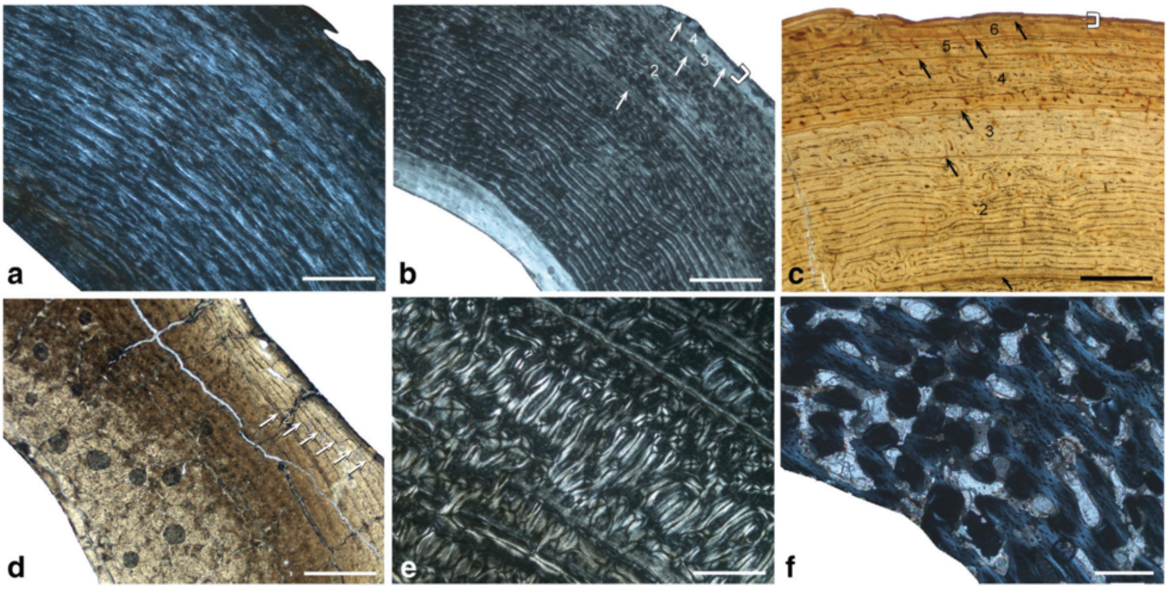

**Figure 3 Cervid bone tissue and growth marks.** Increasing femoral vascularisation **(a-c)** accompanied by increasing body size in a) juvenile *Procervulus* specimen BSPG 1937 II 23227, medial cortex (xpl; scale bar, 0.5 mm), **b)** adult *Dama* specimen ZIUK 9630, medial cortex (xpl; scale bar, 1 mm), and **c)** adult *Megaloceros* specimen NMING: F21306/13 under plane polarised light, anterior cortex (ppl, scale bar 1 mm). Note the low amount of vascularisation in the fibrolamellar bone of the juvenile *Procervulus*. Occurrence of LAGs indicated by black/white arrows and the outer circumferential layer by white brackets. Numbers indicate growth zones. Bone surfaces at the top, medullary cavities at bottom left. **d)** Tibia of adult *Candiacervus* sp. II (PIMUZ A/V 5222) showing Haversian bone in the inner part of the posterior cortex (bright area) and plexiform fibrolamellar bone in the middle part (lpl; scale bar, 1 mm). Occurrence of LAGs indicated by white arrows. Bone surface at top right, medullary cavity at bottom left. **e)** Radiating fibrolamellar bone in a metacarpal of adult *Megaloceros giganteus* (NMING:F22534/4, xpl; scale bar, 0.5 mm). **f)** First phalange of perinatal *Candiacervus* sp. II (PIMUZ A/V 5216) showing reticular vascularisation of mainly woven-fibred bone (xpl; scale bar, 0.2 mm).

A longitudinal section of a *Megaloceros* femur confirms the low amount of woven-fibred bone in plexiform bone tissue [56] (Figure 4a,b). However, since woven-fibred bone is present, we follow [57] in using the term fibrolamellar bone. In general, the bone tissue found in the femora and humeri gives a similar picture. The differences in the amount of vascularisation observed in dwarf *Candiacervus* and large/intermediate sized cervids are less obvious in the humeri than those seen in the femora. Unlike *Candiacervus* (Figure 3d), tibiae of *Dama* and *Megaloceros* show areas of radiating fibrolamellar bone interdigitating with the otherwise plexiform bone tissue. In general, adult radii of all sampled deer have a similar arrangement of bone tissue types, i.e. plexiform fibrolamellar bone with a varying amount of Haversian bone. The amount of woven bone of perinatal ulnae of dwarf *Candiacervus* is high in the inner cortex.

Similarity of bone tissue types in *Candiacervus*, *Megaloceros*, and *Capreolus* shows a comparable mode of growth in the metapodials. A remarkable difference

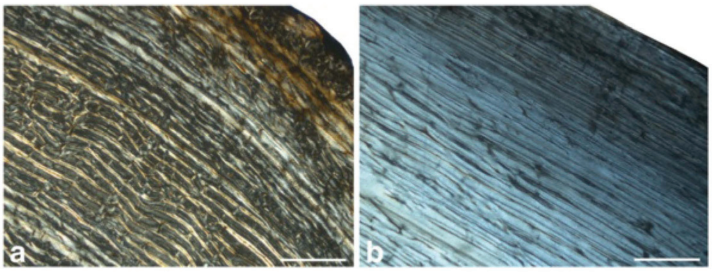

**Figure 4 Bone cortex of *Megaloceros giganteus*.** Femur (NMING: F21306/13) in transverse **(a)** and longitudinal **(b)** section under crossed polarised light (bone surface top right). Note the low amount of woven fibred bone (dark areas) in the longitudinal section.

distinguishing adult *Megaloceros* from *Candiacervus* is the occurrence of layers of radiating fibrolamellar bone (Figure 3e) in the middle and outer cortex of *Megaloceros*. The inner circumferential layer is relatively thicker in *Megaloceros* than in *Candiacervus*.

Phalanges of newborn *Candiacervus* specimens show fibrolamellar bone with reticular vascularisation (Figure 3f). During ontogeny, the vascular organisation becomes plexiform, but with increasing age this is replaced by increasing amounts of poorly vascularised lamellar/parallel-fibred bone in the sub-periosteal region.

### Secondary bone and remodelling processes

Perinatal specimens of *Candiacervus* show no signs of bone remodelling. In general, resorption of primary bone and deposition of secondary osteons in cervid long bones starts in juveniles (Figure 5a). Large areas of Haversian bone in adults indicate strong bone remodelling during ontogeny. Apart from the femora, which have a mainly circular outline in cross section, Haversian bone is most dense where the curvature of the cortex is greatest, but in all long bones and specimens the area most affected by remodelling is the posterior area of the cortex.

In the femora, remodelling starts in the juvenile *Candiacervus* specimens with scattered secondary osteons in the middle cortex, mainly in its posterior part. Adult femora of all deer species sampled show strong remodelling (i.e. Haversian bone) in the posterior part, obscuring the growth record in this area of the bone. Remodelling is strongest in the cortical area of the linea aspera.

Similar to the femora, remodelling in the humeri of juvenile specimens of *Candiacervus* and *Dama* starts in the middle zone of the medial part of the cortex (Figure 5a). Adult humeri of all deer groups sampled show more remodelling than the femora. Nevertheless, the amount of remodelling is low enough to leave a sufficient growth record.

Tibiae of juvenile *Candiacervus* and *Dama* start being remodelled mainly in the medial and lateral parts of the middle and inner cortex, leading to the deposition of dense Haversian bone (Figure 3d). In rare cases, dense Haversian bone is also found in the outermost part of the cortex in *Megaloceros*. Again, however, the amount of remodelling is low enough to leave a sufficient growth record.

Haversian bone in juvenile radii of *Candiacervus* and *Dama* indicates an early onset of secondary remodelling in the inner cortex. Strong remodelling in adult radii of *Candiacervus*, *Dama*, and *Megaloceros*, especially in the posterior area of the inner cortex, obscures the growth record to a large degree in these bones.

Ulnae of all juvenile deer species sampled are already remodelled to a high degree, especially in the inner cortex surrounding the medullary cavity, indicated by dense Haversian bone. Adult ulnae are strongly remodelled leaving only small areas of primary bone tissue in the posterior part of the cortex. During ontogeny, the medullary cavity shifts to the anterior area of the cortex being subsequently closed by the deposition of endosteal lamellar bone which is in turn subsequently replaced by dense Haversian bone (Figure 5b). Due to this strong remodelling of the ulnae in all deer species sampled, and since only small areas of primary plexiform bone tissue are left in the bone cortex, skeletochronological interpretations are not feasible.

Remodelling in metapodials begins with the development of Haversian bone in the inner cortex and is already strongly developed in juvenile specimens. In all specimens, the area most affected by remodelling is the posterior area of the cortex. Adult deer metapodials are strongly remodelled, occupying about half of the cortex and obliterating

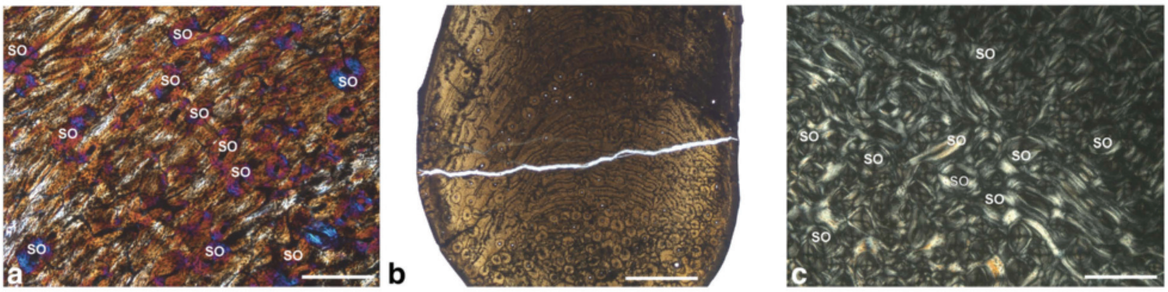

**Figure 5 Cervid bone remodelling. a)** Humerus of juvenile *Candiacervus* sp.II specimen PIMUZ A/V 5236 (xpl, lambda compensator, scale bar 0.5 mm). Note the scattered secondary osteons (SO). **b)** Ulna of adult *Candiacervus* sp. II specimen PIMUZ A/V 5215 (lpl, scale bar 1 mm) displaying plexiform fibrolamellar bone (centre) and dense Haversian bone (bottom). Note that the medullary cavity (bottom) has been subsequently closed by the deposition of endosteal lamellar bone which was in turn replaced by secondary Haversian bone. Anterior at the bottom. **c)** Dense Haversian bone in a metacarpal of adult *Megaloceros giganteus* specimen NMING: F22534/4 (xpl, scale bar 0.5 mm).

the growth record by development of dense Haversian bone (Figure 5c).

### Skeletochronology and growth mark analysis

Cyclical growth patterns have been observed in many extant artiodactyls [41]. However, in mammals bone resorption and remodelling may occur throughout ontogeny and LAG counts and age are apparently decoupled in old individuals [40,42,43]. Therefore, individual ages are often underestimated by bone histological studies, making cementum analysis a crucial tool in order to study longevity in fossil cervids (see also Additional file 1: Discussion).

LAGs are present in all deer taxa sampled. Femora, tibiae, and humeri of adult specimens show, due to relatively low remodelling, the highest LAG counts. The maximum LAG counts seen in adult femora are eight in dwarf *Candiacervus* (n = 3, Figure 2c), six in *Dama* (n = 2), and 10 in *Megaloceros* (n = 2).

In order to quantify growth rates in the sampled deer taxa, we measured non-remodelled cortical growth zones until the "virtual end of circumferential bone growth" [42]. Growth marks in the outermost part of the bone cortex, not giving a signal because of similarity and diminutiveness of growth zone thickness, have been omitted. It has recently been shown that in antelope (*Addax nasomaculatus*) femora the first LAG is resorbed during ontogeny [39]. Ruminants such as antelopes and cervids show similar long bone morphology as well as similar arrangement of bone tissue types, bone remodelling, and resorption patterns [41,58]. Superimposition of sections of femora and tibiae of perinatal, juvenile, and adult dwarf *Candiacervus,* juvenile and adult specimens of *Procervulus praelucidus*, and a juvenile as well as two adult specimens of known-age *Dama dama* however indicate that no LAG is lost during ontogeny in femora and tibiae of these cervids. On the grounds of phylogenetic parsimony we consider it as justified to assume that in general bone resorption patterns are identical throughout cervids. This approach made retrocalculation techniques as performed for dinosaurs dispensable [12,59]. In order to make growth rate measurements comparable, we numbered the growth zones of adult specimens starting with two since the first growth zone is at least partially resorbed and not available for skeletochronology (Figure 3b,c,d).

Additionally, and in order to verify our observations made by growth zone counts and measurements, we followed [51] in determining how fast dwarf *Candiacervus, Megaloceros,* and *Procervulus* grew over a hypothetical 365 days growth period by assessing growth rates *sensu* Sander & Tückmantel and comparing them to the values observed in extant cervids. Although bone growth rates per day are always approximations, they allow comparison to and verification of known bone apposition rates in extant and fossil vertebrates [51,60].

In contrast to dwarfed forms of *Candiacervus* and to *Dama*, *Megaloceros* femora indicate up to five times higher growth rates, with the second growth zone yielding a rate of 7.69 μm/d, the third one 3.69 μm/d, and growth zones four to six between 2.04 – 1.35 μm/d (Figure 6a). The femora of *C. ropalophorus* indicated a growth rate of 2.19 μm/d to 1.81 μm/d in growth zones two to four (Figure 6a). In the following year the growth rate slightly decreased to 1.04 μm/d. The growth rate of *Candiacervus* sp. II decreased from 3.34 μm/d in growth zone two to 1.19 μm/d in growth zone four. In growth zones five to seven the growth rate ranged from 0.69 μm/d to 0.81 μm/d. The femoral growth rate of *Dama* is higher than that of *C. ropalophorus* and equal to that of *Candiacervus* sp. II in the second growth zone (3.34 μm/d). After that, growth rate strongly decreased below the rates of *C. ropalophorus* and sp. II (0.73 and 0.84 μm/d).

The growth rates recorded in the tibiae are similar to the ones obtained for the femora. *C. ropalophorus* grew in zone two at a rate of 2.47 μm/d, whereas *Candiacervus* sp. II only grew at 0.69 μm/d (Figure 6b). *D. dama*, at 2.54 μm/d, occupies an intermediate position between the dwarfed deer and *Megaloceros* (5.81 μm/d). Growth rate strongly decreases from zone two to zone three in most deer species sampled: 2.76 μm/d in *Procervulus*, 3.07 μm/d in *Megaloceros* but only 0.34 μm/d in *C.* sp. II. There is discrepancy among taxa, and *C. ropalophorus,* although the smallest species, shows about four times higher growth rate in the second growth zone (similar to *Dama*) compared to *Candiacervus* sp. II (Figure 6b). This demonstrates the diversity of life history parameters across morphotypes of *Candiacervus* in Crete during the Pleistocene [61,62].

Average growth rates of 0.46 μm/d (Figure 6c) in femora of *Procervulus* were the lowest measured for all the deer taxa sampled, lying below the lower limit of their 95% confidence interval. *Muntiacus*, *Capreolus*, *Dama* and dwarf *Candiacervus* show average to low growth rates around 1.4 μm/d, whereas *Cervus elaphus* (2.58 μm/d) had distinctly higher growth rates lying on the upper limit of the 95% confidence interval. *Alces alces* shows with 3.68 μm/d the highest average growth rates. In contrast, the absolute high growth rates (based on the growth zones preserved in the cortical bone tissue) of *Megaloceros* are relatively low given the regression (Figure 6c, average 3.23 μm/d), but still within the limits of the 95% confidence interval.

Growth rates *sensu* Sander & Tückmantel plotted against the anteroposterior bone diameter as a proxy for body mass indicate three groups (Figure 7): A group with high growth rates including *Megaloceros* (14.22 μm/d), *Cervus elaphus* (ZIUK 23517; 12.66 μm/d), *Alces* (ZMUZ

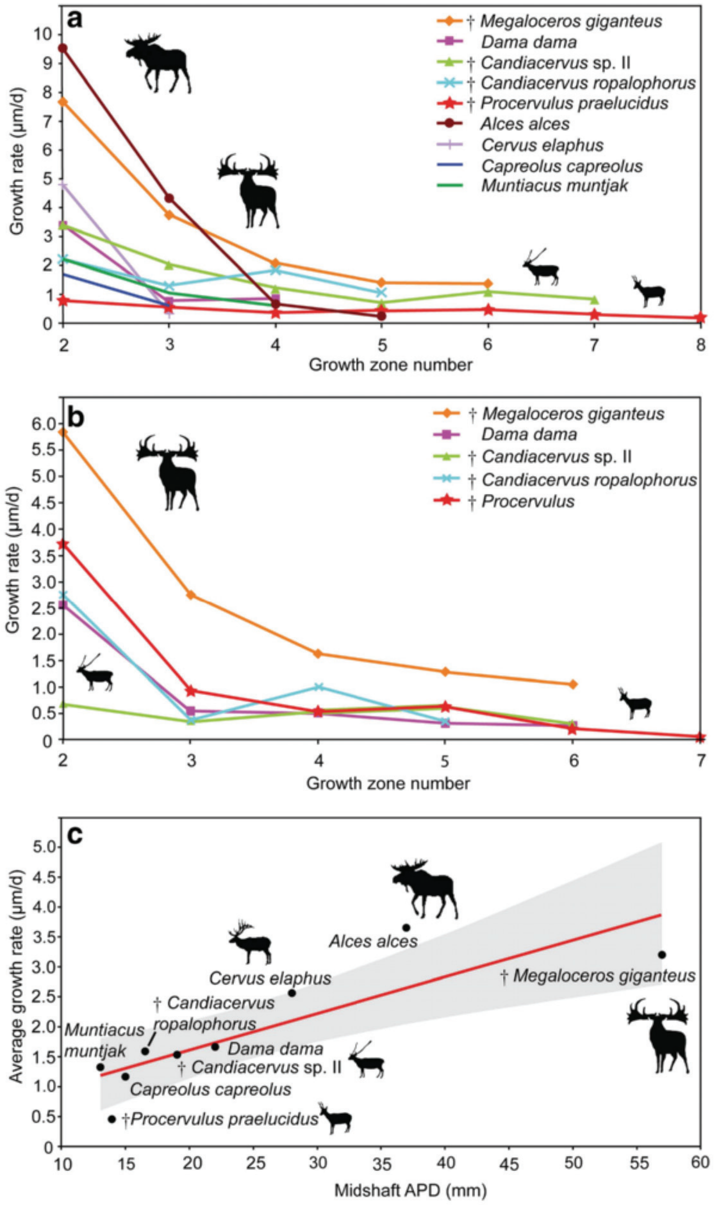

**Figure 6 Cervid growth rates. a)** Graph of growth zone measurements of cervid femora sampled. Points indicate sample means or measurements of single specimens (see also Additional file 2). Note exceptionally high growth rates in the first two growth zones of *Alces* and *Megaloceros* as well as exceptionally low rates of *Procervulus*. Growth zones numbered, starting with two for the innermost complete zone of the cortex. **b)** Graph of cervid tibiae sampled. Note the eight times higher growth rate in growth zone two of *Megaloceros* compared to *Candiacervus* sp. II (and still twice as high as in *C. ropalophorus*). **c)** Regression of average growth rates in cervid femora ($n = 12$, $r = 0.85111$, $p = 0.0036142$.). Shaded region represents the 95% confidence interval. Anteroposterior diameter (APD) of femoral midshaft region is taken as proxy for body mass.

20242; 12.58 µm/d), and *Dama* (12.35 µm/d); an intermediate group with *Capreolus* (ZIUK 9872; 6.79 µm/d) and *Muntiacus* (ZIUK 7994; 5.75 µm/d); and a group showing low growth rates, including *Candiacervus* sp. II (PIMUZ A/V 5218, 3.7 µm/d), and ranging from 4.16 µm/d in *Candiacervus ropalophorus* to 2.6 µm/d in *Procervulus* (Figure 7). *Dama* and *Cervus elaphus* plot above the upper limit of the 95% confidence interval whereas only *Candiacervus* sp. II lies well below the lower limit of the 95% confidence interval. All other cervids sampled show

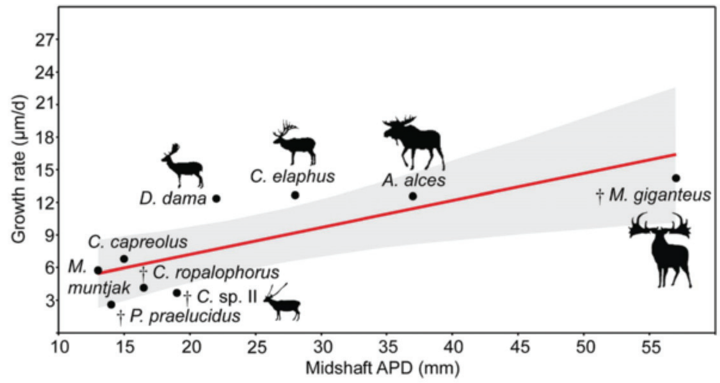

**Figure 7 Regression of growth rates *sensu* Sander & Tückmantel in cervid femora ($n = 12$, $r = 0.78168$, $p = 0.012835$).** Shaded region represents the 95% confidence interval. Anteroposterior diameter (APD) of femoral midshaft region is taken as proxy for body mass (see also Additional file 2).

growth rates within the 95% range given their body size (see also Additional file 1: Discussion).

### Skeletal maturity estimates

Examination of femora of extant cervid taxa revealed the occurrence of OCLs not coeval with the timing of sexual maturity, as reported for femora of antelopes [39]. An adult specimen of *Dama dama* (ZIUK 9630; Figure 3b) shows three LAGs before the OCL, in contrast to the onset of sexual maturity which has been reported to occur during the second year of life in *Dama dama* [63] (Figure 1a). These observations suggest that the transition of the fibrolamellar complex (FLC) to the OCL, which is not clearly definable in every specimen, is indicating cervid skeletal maturity *sensu* [64] and not sexual maturity. This is well in accordance with known data of skeletal maturity for *Dama* [30,31], and a recent study on growth marks in the bone tissue of ruminants that examined cervid bone histology in detail [41]. The bone cortex of dwarf *Candiacervus* femora indicates skeletal maturity at five to seven years whereas *Megaloceros* reached skeletal maturity at five to six years. One *Procervulus* specimen indicates attainment of skeletal maturity at seven years whereas *Cervus elaphus* (four to six years) ranges with its timing of skeletal maturity between *Megaloceros* and *Alces* (three years) [31].

### Cementum analysis and longevity

Tooth cementum analysis of first molars of *Candiacervus* provided an age of four years for a juvenile *Candiacervus* sp. II and an age of at least nine years for an adult specimen of *C. ropalophorus*. Two senile *Megaloceros giganteus* specimens revealed ages of 16 and 19 years (Figure 8a,b). Rest lines in two old *Candiacervus* specimens gave ages of 12 (dwarf *Candiacervus* sp.) and 18 years (*Candiacervus* sp. II, Figure 8c). Dwarf *Candiacervus* thus, in an allometric context, show an extended lifespan compared to other deer of similar body size such as *Mazama* with a maximum longevity of 12 years in the wild (Figure 1a). This is well in accordance with observations of a recent study on population structure and dynamics in dwarf *Candiacervus* [62].

A positive linear relationship between body mass and longevity has been demonstrated in bats and mammals in general [47,65], although this is difficult to assess in our cervid data set (Figure 1b) because of issues of comparability: for example, the 32-year maximum age of a captive specimen of *Cervus elaphus* [63], a farmed and extensively studied species, is probably anomalously high. Conversely, *Megaloceros* appears short-lived when body mass is taken into account (Figure 1b), although the sample size was small. Clearly, there is much diversity in life history across deer species, and examination of other populations of *Megaloceros* may reveal more diversity in the giant deer than we have recorded in our study [18,19].

## Conclusions

Our histological observations indicate lower growth rates in dwarf *Candiacervus* than in *Megaloceros*. The presence of laminar bone tissue in the middle and outer cortex of adults of small-sized deer (dwarf *Candiacervus, Procervulus* and *Muntiacus*) suggests lower growth rates, in contrast to the occurrence of plexiform bone in intermediate to large sized forms. Growth rates determined by growth zone measurements in femora and tibiae indicate comparable growth rates of intermediate sized and small deer species, with slower growth in the stem group cervid *Procervulus*. Growth rates in the two small *Candiacervus* morphotypes are different, underscoring the flexibility of growth strategies and the importance of a resolved phylogenetic framework to study heterochrony. Skeletal maturity data suggest late maturation for dwarf *Candiacerus* and *Procervulus* in comparison to a similarly

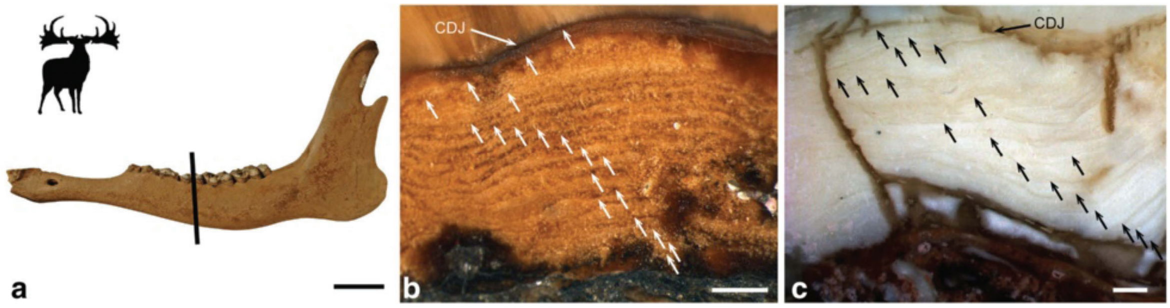

**Figure 8 Cervid tooth histology. a)** Senescent *Megaloceros* specimen PIMUZ A/V 2235. Left mandible in lateral view. Black bar indicates plane of sectioning. Scale bar, 50 mm. **b)** Tooth cementum of same specimen showing 19 rest lines (white arrows). Scale bar, 0.5 mm. **c)** Tooth cementum of the upper first molar of *Candiacervus* sp. II (PIMUZ A/V 5241) showing 18 rest lines (black arrows). CDJ = Cementum-dentine junction. Scale bar, 0.5 mm. Direction of cementum apposition to the bottom.

small cervid such as *Muntiacus* attaining skeletal maturity in two years [32].

The landmasses of islands have been hypothesized of being able to support only a limited number of primary producers affecting the energy flow at higher trophic levels. As a consequence, energy-poor islands are expected to be impoverished in competitors and predators making especially high growth rates and high reproductive rates dispensable to unnecessary [32,46,66-68]. A delay in the attainment of maturity was recorded for the dwarfed island bovid *Myotragus balearicus* [46], and was thought to be associated with synchronisation of metabolic requirements to fluctuating resource levels. The delay of attainment of maturity in the island cervid *Candiacervus* and the continental *Procervulus* demonstrates the variability of life history parameters in island as well as continental cervids. This might point towards fluctuating resource levels in the Late Pleistocene Crete, selecting for a growth pattern recalling that of the stem-cervid *Procervulus*.

The oldest individual seen in our cementum analysis of *Megaloceros* was 19 years, comparable to maximum longevity in extant *Dama*. This find extends an age based on cementum analysis [25] by five years and lies below another estimate [69] also based on cementum analysis, by four years. However, [69] did not illustrate cementum rest lines of the specimen studied. We therefore consider the result of our cementum analysis as the highest rest line count in *Megaloceros*. The oldest individual seen in our cementum analysis of *Candiacervus* was 18 years, indicating prolonged longevity for a deer of this body size.

The exact persistence time of the *Candiacervus* radiation on Crete is not known but was apparently much shorter, i.e., less than 0.5 myrs [5], compared to *Myotragus balearicus*, which dwelt on Majorca for 5.2 myrs [46]. The less extreme modification of bone tissue observed in dwarf *Candiacervus* could be related to shorter persistence time and perhaps to the larger size of Crete [3,8].

In life history theory, slow-developing long-lived species are typically associated with low fecundity and rapidly-developing short-lived species with high fecundity [36,70]. The condition found in *Candiacervus* has features in common with that of *Myotragus* [46], but is achieved with less far reaching modification of bone tissue, as indicated by the absence of lamellar-zonal bone throughout the cortex. Neither does the *Myotragus* pattern occur in the pygmy mammoth, *Mammuthus exilis*, from Santa Rosa Island, California, whose bone cortex is characterized by laminar fibrolamellar bone [71]. Therefore we suggest variable modes of life history and size evolution among island mammals in line with [65-68,72].

### Availability of supporting data

The data sets supporting the results of this article are included within the article (and its additional files).

High resolution versions of the histological figures provided in this article are available on MorphoBank [73], Project P2083 (http://www.morphobank.org/permalink/?P2083).

## Additional files

**Additional file 1:** **Includes Table S1, additional discussion on individual age estimates and growth rates, additional information on methods used in this study, additional references, and Figure S1.**

**Additional file 2:** **Primary data for growth rate analysis: Growth zone measurements, mean species growth rates, average species growth rates, bone diameter, OCL thickness, and number of non-OCL lines of arrested growth (for growth rates *sensu* Sander & Tückmantel).**

### Competing interests

The authors declare that they have no competing interests.

### Authors' contributions

CK and MRS-V designed the study and wrote the manuscript, CK, TMS, MAJS and CA collected and analysed histological data, JDV, AML, NTM, and GER provided materials and taxonomic/stratigraphical information, all authors contributed to the final interpretation and editing of the manuscript. All authors read and approved the final manuscript.

### Acknowledgments

We thank Naturalis Biodiversity Center, National Museum of Ireland, Natural History, Natural History Museum London (NHML), Bayerische Staatssammlung für Paläontologie und Geologie, Wildnispark Zürich, Frank Zachos (now Naturhistorisches Museum Wien), Heiner Luttmann, Zoologisches Institut der Universität Kiel, Marianne Haffner, Zoologisches Museum der Universität Zürich, Emma Bernard (NHML) and Heinz Furrer, Paläontologisches Institut und Museum der Universität Zürich (PIMUZ) for providing specimens for histological study, Alexandra van der Geer (Naturalis Biodiversity Center, Leiden) and two anonymous reviewers for constructive and improving criticism, as well as Vladimir Blagoderov, and Tony Wighton (NHML) for technical assistance. Vivien Jaquier, Fiona Straehl, Madeleine Geiger, James Neenan, Juan Carrillo, Sarah Bolliger, Markus Hebeisen, Rosi Roth and Jérôme Gapany (all PIMUZ) are thanked for various support and discussion. This work was funded by the SNSF (3100A0-133032/1 and 31003A-149605 to MRS-V; 31003A-149506 to TMS) and the Forschungskredit of the University of Zurich (No. 8264 to CK).

### Author details

[1]Paläontologisches Institut und Museum der Universität Zürich, Karl Schmid-Strasse 4, CH-8006 Zürich, Switzerland. [2]Department of Earth Sciences, The Natural History Museum, Cromwell Road, London SW7 5BD, UK. [3]Department of Animal and Vegetal Biology and Ecology, Faculty of Experimental Sciences, University of Jaén, Jaén 23071, Spain. [4]Naturalis Biodiversity Center, Postbus 9517, 2300 RA Leiden, The Netherlands. [5]Department of Integrative Zoology, IBL, Leiden University, Sylviusweg 72, Postbus 95052300 RA Leiden, The Netherlands. [6]Bayerische Staatssammlung für Paläontologie und Geologie, Richard-Wagner-Strasse 10, D-80333 München, Germany. [7]National Museum of Ireland-Natural History, Merrion Street, Dublin 2, Ireland.

Received: 22 July 2014 Accepted: 27 January 2015

### References

1. Foster JB. Evolution of mammals on islands. Nature. 1964;202:234–5.
2. Lomolino MV. Body size of mammals on islands: the island rule reexamined. Am Nat. 1985;125:310–6.
3. Lomolino MV, van der Geer AA, Lyras GA, Palombo MR, Sax DF, Rozzi R. Of mice and mammoths: generality and antiquity of the island rule. J Biogeogr. 2013;40:1427–39.
4. Lister AM. Rapid dwarfing of red deer on jersey in the last interglacial. Nature. 1989;342:539–42.
5. van der Geer A, Lyras G, de Vos J, Dermitzakis M. Evolution of Island Mammals. Adaptation and Extinction of Placental Mammals on Islands. Wiley-Blackwell: Sussex; 2010.
6. Quintana J, Köhler M, Moyà-Solà S. Nuragulus rex, gen. et sp. nov., an endemic insular giant rabbit from the Miocene of Minorca (Balearic Islands). J Vertebr Paleontol. 2011;31(2):231–40.
7. Palkovacs EP. Explaining adaptive shifts in body size on islands: a life history approach. Oikos. 2003;103:37–44.
8. Lomolino MV, Sax DF, Palombo MR, van der Geer A. Of mice and mammoths: evaluations of causal explanations for body size evolution in insular mammals. J Biogeogr. 2012;39:842–54.
9. Raia P, Meiri S. The island rule in large mammals: paleontology meets ecology. Evolution. 2006;60:1731–42.
10. Sander PM, Andrassy P. Lines of arrested growth and long bone histology in Pleistocene large mammals from Germany: what do they tell us about dinosaur physiology? Palaeontogr Abt A. 2006;277:143–59.
11. Sander PM, Christian A, Clauss M, Fechner R, Gee CT, Griebeler E-M, et al. Biology of the sauropod dinosaurs: the evolution of gigantism. Biol Rev. 2011;86(1):117–55.
12. Erickson GM, Curry Rogers K, Yerby SA. Dinosaurian growth patterns and rapid avian growth rates. Nature. 2001;412:429–33.
13. Erickson GM, Makovicky PJ, Currie PJ, Norell MA, Yerby SA, Brochu CA. Gigantism and comparative life history parameters of tyrannosaurid dinosaurs. Nature. 2004;430:772–5.
14. Chinsamy-Turan A (ed.): Forerunners of Mammals:Rradiation, Histology, Biology. Indiana: Indiana University Press;2012.
15. Huttenlocker AK, Botha-Brink J. Bone microstructure and the evolution of growth patterns in Permo-Triassic therocephalians (Amniota, Therapsida) of South Africa. PeerJ. 2014;2:e325.
16. de Vos J. The endemic Pleistocene deer of Crete. P K Ned Akad B. 1979;82(1):59–90.
17. de Vos J. The Endemic Pleistocene Deer of Crete, vol. 31. Amsterdam: North-Holland Publishing Company; 1984.
18. Vislobokova IA. Giant deer: origin, evolution, role in the biosphere. Paleontol J. 2012;46(7):643–775.
19. Vislobokova IA. Morphology, taxonomy, and phylogeny of megacerines (Megacerini, Cervidae, Artiodactyla). Palaeontol J. 2013;47(8):833–950.
20. Lister AM, Edwards CJ, Nock DAW, Bunce M, van Pijlen IA, Bradley DG, et al. The phylogenetic position of the 'giant deer' *Megaloceros giganteus*. Nature. 2005;438(7069):850–3.
21. Sickenberg O. Eine Säugetierfauna des tieferen Biharium aus dem Becken von Megalopolis (Peloponnes, Griechenland). Annales Géologiques des Pays Helléniques. 1975;27:25–73.
22. Gould GC, MacFadden BJ. Gigantism, dwarfism, and Cope's rule: "Nothing in evolution makes sense without a phylogeny". B Am Mus Nat Hist. 2004;285:219–37.
23. de Vos J. Pleistocene deer fauna in Crete: its adaptive radiation and extinction. Tropics. 2000;10(1):125–34.
24. de Vos J, Van der Geer A. Major patterns and processes in biodiversity: taxonomic diversity on islands explained in terms of sympatric speciation. In: WW H, EJ A, editors. World Islands in Prehistory, International Insular Investigations, V Deia International Conference of Prehistory. Oxford: British Archaeological Reports International Series; 2002. p. 395–405.
25. Chritz KL, Dyke GJ, Zazzo A, Lister AM, Monaghan NT, Sigwart JD. Palaeobiology of an extinct Ice Age mammal: Stable isotope and cementum analysis of giant deer teeth. Palaeogeogr Palaeocl. 2009;282(1–4):133–44.
26. Gould SJ. Positive allometry in antlers of the "Irish Elk", *Megaloceros giganteus*. Nature. 1973;244:375–6.
27. Woodman PC, McCarthy M, Monaghan NT. The Irish Quaternary fauna project. Quaternary Sci Rev. 1997;16:129–59.
28. Hughes S, Hayden TJ, Douady CJ, Tougard C, Germonpré M, Stuart A, et al. Molecular phylogeny of the extinct giant deer, *Megaloceros giganteus*. Mol Phylogenet Evol. 2006;40:285–91.
29. Rössner GE. Odontologische und schädelanatomische Untersuchungen an *Procervulus* (Cervidae, Mammalia). Münchner Geowissenschaftliche Abhandlungen (A). 1995;29:1–128.
30. McElligott AG, Mattiangeli V, Mattiello S, Verga M, Reynolds CA, Hayden TJ. Fighting tactics of fallow bucks *(Dama dama,* Cervidae): Reducing the risks of serious conflict. Ethology. 1998;104:789–803.
31. Habermehl K-H. Altersbestimmung bei Wild- und Pelztieren - Möglichkeiten und Methoden - Ein praktischer Leitfaden für Jäger, Biologen und Tierärzte. Verlag Paul Parey: Hamburg, Berlin; 1985.
32. Pei K. Post-natal growth of the Formosan Reeves' Muntjac *Muntiacus reevesi micrurus*. Zool Stud. 1996;35:111–7.
33. Palombo MR, Köhler M, Moya-Sola S, Giovinazzo C. Brain versus body mass in endemic ruminant artiodactyls: a case studied of *Myotragus balearicus* and smallest *Candiacervus* species from Mediterranean Islands. Quatern Int. 2008;182:160–83.
34. Gilbert C, Ropique A, Hassanin A. Mitochondrial and nuclear phylogenies of Cervidae (Mammalia, Ruminantia): Systematics, morphology, and biogeography. Mol Phylogenet Evol. 2006;40:101–17.
35. Hassanin A, Delsuc F, Ropiquet A, Hammer C, van Vuuren BJ, Matthee C, et al. Pattern and timing of diversification of Cetartiodactyla (Mammalia, Laurasiatheria), as revealed by a comprehensive analysis of mitochondrial genomes. C R Biol. 2012;335:32–50.
36. Stearns SC. The Evolution of Life Histories. Oxford: Oxford University Press; 1992.
37. Garcia-Martinez R, Marin-Moratalla N, Jordana X, Köhler M. The ontogeny of bone growth in two species of dormice: reconstructing life history traits. C R Palevol. 2011;10(5–6):489–98.

38. Chinsamy-Turan A. Microstructure of bones and teeth of nonmammalian therapsids. In Forerunners of Mammals: Radiation, Histology, Biology. Edited by Chinsamy-Turan A. Indiana: Indiana University Press; 2012;65–88.
39. Marin-Moratalla N, Jordana X, Köhler M. Bone histology as an approach to providing data on certain key life history traits in mammals: implications for conservation biology. Mamm Biol. 2013;78:422–9.
40. Castanet J, Croci S, Aujard F, Perret M, Cubo J, de Margerie E. Lines of arrested growth in bone and age estimation in a small primate: *Microcebus murinus*. J Zool. 2004;263:31–9.
41. Köhler M, Marín-Moratalla N, Jordana X, Aanes R. Seasonal bone growth and physiology in endotherms shed light on dinosaur physiology. Nature. 2012;487:358–61.
42. Woodward HN, Padian K, Lee AH. Skeletochronology. In Histology of Fossil Tetrapods - Advancing Methods, Analysis and Interpretation. Edited by Padian K, Lamm E-T. Berkeley, Los Angeles, London: University of California Press; 2013: 195–215.
43. Klevezal GA. Recording Structures of Mammals. Determination of Age and Reconstruction of Life History. A.A.Balkema: Rotterdam/Brookfield; 1996.
44. Azorit C, Munoz-Cobo J, Hervas J, Analla M. Aging through growth marks in teeth of Spanish red deer. Wildl Soc Bull. 2004;32(3):702–10.
45. Azorit C, Analla M, Hervas J, Carrasco R, Munoz-Cobo J. Growth marks observation: preferential techniques and teeth for ageing of Spanish red deer (*Cervus elaphus hispanicus*). Anat Histol Embryol-J Vet Med Ser C. 2002;31(5):303–7.
46. Köhler M, Moyà-Solà S. Physiological and life history strategies of a fossil large mammal in a resource-limited environment. P Natl Acad Sci USA. 2009;106(48):20354–8.
47. Calder WA. Size, Function, and Life History. Cambridge, Massachusetts, London: Harvard University Press; 1984.
48. Case TJ. On the evolution and adaptive significance of postnatal growth rates in the terrestrial vertebrates. Q Rev Biol. 1978;53(3):243–82.
49. Schmidt-Nielsen K. Scaling: Why is Animal Size so Important? Cambridge & New York: Cambridge University Press; 1984.
50. Stein K, Sander M. Histological core drilling: a less destrcutive method for studying bone histology. In: Methods in Fossil Preparation: Proceedings of the First Annual Fossil Preparation and Collections Symposium. Petrified Forest: Petrified Forest National Park; 2009. p. 69–80.
51. Sander PM, Tückmantel C. Bone lamina thickness, bone apposition rates, and age estimates in sauropod humeri and femora. Palaeontol Z. 2003;77(1):161–72.
52. Hammer Ø, Harper DAT, Ryan PD. PAST: Paleontological statistics software package for education and data analysis. Palaeontologia Electronica 2001;4(1): 9. http://palaeoelectronica.org/2001_1/past/issue1_01.htm
53. Ponton F, Elzanowski A, Castanet J, Chinsamy-Turan A, Margerie E, de Ricqlès A, et al. Variation of the outer circumferential layer in the limb bones of birds. Acta Ornithol. 2004;39(2):21–4.
54. Horner JR, Ricqlès AJD, Padian K. Variation in dinosaur skeletochronology indicators: implications for age assessment and physiology. Paleobiology. 1999;25:295–304.
55. van der Geer A, de Vos J, Lyras G, Dermitzakis M. New data on the Pleistocene Cretan deer *Candiacervus* sp. II (Cervinae, Mammalia). Cour Forsch Senck. 2006;256:131–7.
56. Stein K, Prondvai E. Rethinking the nature of fibrolamellar bone: an integrative biological revision of sauropod plexiform bone formation. Biol Rev. 2013;1–24
57. Francillon-Vieillot H, de Buffrénil V, Castanet J, Géraudie J, Meunier FJ, Sire JY, et al. Microstructure and mineralization of vertebrate skeletal tissues. In Skeletal Biomineralization: Patterns, Processes and Evolutionary Trends. Edited by Carter JG. New York: Van Nostrand Reinhold; 1990: 471–530.
58. Enlow DH, Brown SO. A comparative histological study of fossil and recent bone tissues. Part III Tex J Sci. 1958;10:187–230.
59. Horner JR, Padian K. Age and growth dynamics of *Tyrannosaurus rex*. P Roy Soc Lond B Bio. 2004;271:1875–80.
60. de Ricqlès A, Meunier FJ, Castanet J, Francillon-Vieillot H. Comparative microstructure of bone. In Bone Volume 3: Bone Matrix and Bone Specific Products. Edited by Hall BK. Boca Raton: CRC Press; 1991;1–78.
61. van der Geer A, Dermitzakis M, de Vos J. Relative growth of the metapodials in a juvenile island deer: *Candiacervus* (Mammalia, Cervidae) from the Pleistocene of Crete. Hell J Geosc. 2006;41:119–25.
62. van der Geer A, Lyras GA, MacPhee RDE, Lomolino MV, Drinia H. Mortality in a predator-free insular environment: the dwarf deer of Crete. Am Mus Novit. 2014;3807:1–26.
63. Tacutu R, Craig T, Budovsky A, Wuttke D, Lehmann G, Taranukha D, et al. Human ageing genomic resources: integrated databases and tools for the biology and genetics of ageing. Nucleic Acids Res. 2013;41(D1):D1027–33.
64. Huttenlocker AK, Woodward HN, Hall BK. The biology of bone. In Histology of Fossil Tetrapods - Advancing Methods, Analysis and Interpretation. Edited by Padian K, Lamm E-T. Berkeley, Los Angeles, London: University of California Press; 2013: 13–34.
65. Austad SN, Fischer KE. Mammalian aging, metabolism, and ecology: evidence from the bats and marsupials. J Gerontol. 1991;46(2):B47–53.
66. McNab B. Resource use and the survival of land and freshwater vertebrates on oceanic islands. Am Nat. 1994;144:643–60.
67. McNab BK. Minimizing energy expenditure facilitates vertebrate persistence on oceanic islands. Ecol Lett. 2002;5:693–704.
68. McNab BK. Geographic and temporal correlations of mammalian size reconsidered: a resource rule. Oecologia. 2010;164:13–23.
69. Aaris-Sorensen K, Liljegren R. Late Pleistocene remains of giant deer (*Megaloceros giganteus* Blumenbach) in Scandinavia: chronology and environment. Boreas. 2004;33:61–73.
70. Stearns SC. Life history evolution: successes, limitations, and prospects. Naturwissenschaften. 2000;87:476–86.
71. Curtin AJ, Macdowell AA, Schaible EG, Roth L. Noninvasive histological comparison of bone growth patterns among fossil and extant neonatal elephantids using synchrotron radiation X-ray microtomography. J Vertebr Paleontol. 2012;32(4):939–55.
72. Raia P, Barbera C, Conte M. The fast life of a dwarfed giant. Evol Ecol. 2003;17(3):293–312.
73. O'Leary, MA; Kaufman SG. MorphoBank 3.0: Web application for morphological phylogenetics and taxonomy. 2012; http://www.morphobank.org.

## SUPPLEMENTARY INFORMATION

# Growth in fossil and extant deer and implications for body size and life history evolution

Authors: Kolb C., Scheyer T. M., Lister A. M., Azorit C., de Vos J., Schlingemann M. A. J., Rössner G. E., Monaghan N. T., Sánchez-Villagra M. R.

**Additional file 1:** Includes Table S1, additional discussion on individual age estimates and growth rates, additional information on methods used in this study, additional references, and Figure S1.

**Additional file 2:** Primary data for growth rate analysis: Growth zone measurements, mean species growth rates, average species growth rates, bone diameter, OCL thickness, and number of non-OCL lines of arrested growth (for growth rates sensu Sander & Tückmantel).

## Additional file 1

**Table S1: Histological traits of cervid taxa sampled.** The terminology follows [57].

| Histological traits | Small body size | Intermediate/large body size |
|---|---|---|
| | | |
| Inner cortex (excl. inner cortical layer) | | |
| Primary bone | fibrolamellar | fibrolamellar |
| Vascularization | plexiform | plexiform |
| Lines of arrested growth | none | none |
| | | |
| Middle cortex | | |
| Primary bone | fibrolamellar | fibrolamellar |
| Vascularization | plexiform-laminar | plexiform/radiating |
| Lines of arrested growth | present | present |
| | | |
| Outer cortex (excl. outer circumf. layer) | | |
| Primary bone | fibrolamellar | fibrolamellar |
| Vascularization | laminar/avascular | plexiform/radiating/longitudinal |
| Lines of arrested growth | present | present |
| | | |
| Remodelling | strong | strong |
| Resorption/Endosteal bone | present | present |
| Haversian bone | normal to dense | normal to dense |

## Additional discussion

### *Individual age estimates*

In order to explore the issue of underestimation of individual ages by bone histological studies, we performed age determination based on both tooth cementum and bone histological analysis for two specimens of *Dama*. The growth record of an eight year old specimen (ZIUK 9630), of which the age was determined by cementum analysis, is represented by six LAGs in the bone tissue including LAGs in the OCL. Another eight year old specimen (PIMUZ A/V 5248) shows only two LAGs in total. This confirms that age estimates from growth marks in bone tissue variably underestimate the actual age.

*Growth rates*

Growth rates *sensu* Sander & Tückmantel give in some regards a different picture than average growth rates do (Figure 6c, Figure 7). *Alces* (ZMUZ 20242) lies well within the 95 % interval which is not the case in average growth rates. The fact that *Megaloceros* shows a slightly larger value compared to *Alces*, *Cervus elaphus* (ZIUK 23517) and *Dama* indicate the hypothetical nature of growth rates *sensu* Sander & Tückmantel and suggest the reflection of differences in number of LAGs and bone diameter but not actual patterns of growth. The same probably applies to the fact that *Muntiacus* (ZIUK 7994) shows much higher values in maximum growth rates than dwarf *Candiacervus*.

## Additional methods

Age classes in long bones have been determined by the state of epiphyseal fusion [31] and proximodistal length. For selection of aged specimens to be sampled for cementum analysis, we used known tooth eruption/wear state patterns in extant cervids [31, 74-76, Kolb & Azorit unpublished observations]. The bone tissue of perinatal, juvenile, and adult dwarf *Candiacervus* (*C. ropalophorus* and *Candiacervus* sp. II) are described. The observations are compared to the bone tissue of adult *Megaloceros giganteus* (extinct), juvenile as well as adult *Dama dama*, adult *Procervulus praelucidus* (extinct), *Muntiacus muntjak*, *Capreolus capreolus*, *Cervus elaphus*, and *Alces alces* specimens. The histological terminology used follows [57].

Due to differences in growth rates *C. ropalophorus* and *Candiacervus* sp. II were treated separately unlike our approach to bone tissue analysis. Points of growth zone measurements are based on one specimen each for *Candiacervus* sp. II, *Procervulus*, *Muntiacus*, *Capreolus*, and *Cervus* in the femora (Figure 6a, c). In the tibiae, points represent values of the mean of three specimens for *Megaloceros*, whereas *Candiacervus* sp. II, *Muntiacus*, *Capreolus*, and

*Cervus* are represented by one specimen each (Figure 6b). All other points represent mean values of two specimens.

Average growth rates represent average values of measured growth zones. Attained values of specimens have then been averaged in order to obtain an average value for each species. For attaining growth rates *sensu* Sander & Tückmantel [51] the radius of the bone was measured along the anterior quadrant of the bone (excluding the OCL) and divided by the number of LAGs excluding those in the OCL. This method assumes that the entire thickness of the bone from the center to the first growth line was formed within the first year of life. Prenatal bone apposition is not taken into account and, following [51], the OCL and contained LAGs are excluded. Since the original term "maximum growth rates" [51] might be misleading in the context of growth period estimates and their application for growth rate calculations, we use the "term growth rates *sensu* Sander & Tückmantel". After attaining growth rates *sensu* Sander & Tückmantel expressed as µm/d and assuming a yearlong growth period for each specimen, values have been averaged for attaining mean growth rates *sensu* Sander & Tückmantel of each species studied.

## Additional references

74. Chapman D, Chapman N: *Fallow deer - their history, distribution, and biology*. Machynlleth: Coch-y-bonddu books; 1997.
75. Azorit C, Analla M, Carrasco R, Calvo JA: **Teeth eruption pattern in red deer (Cervus elaphus hispanicus) in southern Spain**. *Anales de Biologia* 2002, **24**:107-114.
76. Azorit C, Analla M, Carrasco R, Munoz-Cobo J: **Determinación de edad por desgaste dental en el ciervo ibérico (Cervus elaphus hispanicus)**. *Bol R Soc Esp Hist Nat (Sec Biol)* 2003, **98**(1-4):123-134.

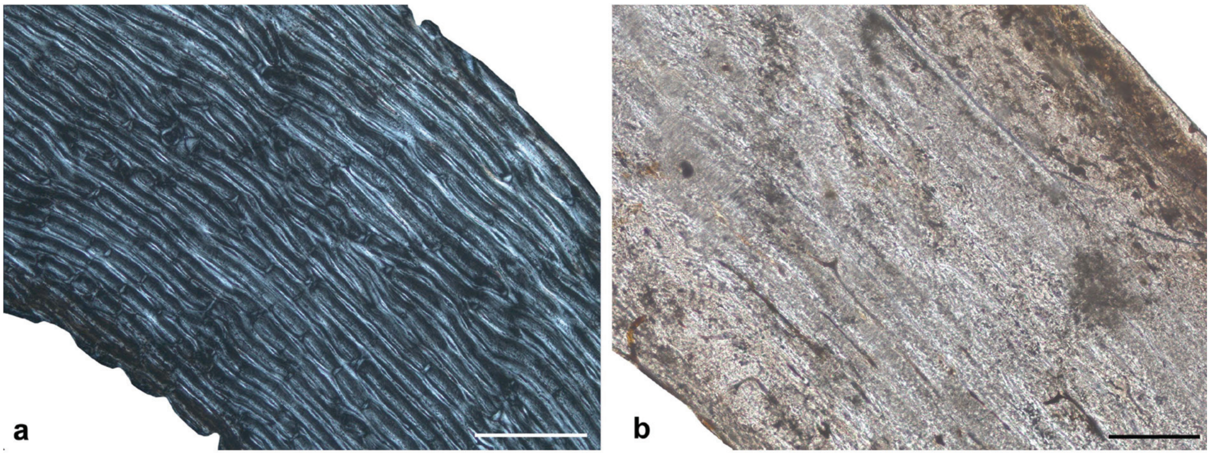

**Figure S1. Femoral bone cortex of *Dama* and *Procervulus*.** Typical plexiform bone tissue in a) juvenile *Dama* specimen PIMUZ A/V 5249 (xpl, scale bar 0.5 mm) and low amount of vascularisation in b) adult *Procervulus* specimen BSPG 1937 II 23226 (lpl, scale bar 0.2 mm). Brown and dark grey areas in the *Procervulus* specimen represent areas of recrystallisation. Bone surfaces at top right.

## Additional file 2

| **Femora** | Growth zone measurements (mm/a) | Species - Mean growth rates (mm/a) | Species - Mean growth rates (µ/d) - 365 days | Species - Growth rate interval (µ/d) - 275 - 245 days | Species - Mean growth rates (µ/d) - 260 days | Species - Average growth rate - 365 days (µ/d) | Species - Average growth rate interval (µ/d) - 275 - 245 days | Species - Average growth rate (µ/d) - 260 days | Anteroposterior diameter (mm) | OCL thickness (mm) used for growth rate analysis *sensu* Sander & Tückmantel | LAG number (OCL excluded) used for growth rate analysis *sensu* Sander & Tückmantel | Species - Mean growth rates *sensu* Sander & Tückmantel (µ/d) |
|---|---|---|---|---|---|---|---|---|---|---|---|---|
| *Megaloceros giganteus* NMING: F21306/13 | 1.79 | 2 | 5.48 | 7.27 - 8.16 | 7.69 | 2.3 | 3.05 - 3.43 | 3.23 | 57 | 0.14 | 6 | 14.22 |
| | 0.64 | 0.96 | 2.63 | 3.49 - 3.92 | 3.69 | | | | | | | |
| | 0.76 | 0.53 | 1.45 | 1.92 - 2.16 | 2.04 | | | | | | | |
| | 0.34 | 0.36 | 0.99 | 1.31 - 1.47 | 1.39 | | | | | | | |
| | 0.35 | 0.35 | 0.96 | 1.27 - 1.43 | 1.35 | | | | | | | |
| | | | | | | | | | | | | |
| *Megaloceros giganteus* NMING: F7937/4 | 2.2 | | | | | | | | 57 | 0.26 | 5 | |
| | 1.27 | | | | | | | | | | | |
| | 0.29 | | | | | | | | | | | |
| | 0.38 | | | | | | | | | | | |
| | | | | | | | | | | | | |
| *Dama dama* ZIUK 9630 | 0.67 | 0.87 | 2.38 | 3.16 - 3.55 | 3.34 | 1.17 | 1.55 - 1.74 | 1.64 | 23 | 0.07 | 3 | 12.35 |
| | 0.19 | 0.19 | 0.52 | 0.69 - 0.77 | 0.73 | | | | | | | |
| | 0.22 | 0.22 | 0.6 | 0.80 - 0.89 | 0.84 | | | | | | | |
| | | | | | | | | | | | | |
| *Dama dama* PIMUZ A/V 5248 | 1.07 | | | | | | | | 21 | 0.1 | 2 | |
| | | | | | | | | | | | | |
| *Candiacervus* sp. II PIMUZ A/V 5218 | 0.87 | 0.87 | 2.38 | 3.16 - 3.55 | 3.34 | 1.08 | 1.43 - 1.61 | 1.52 | 19 | 0.06 | 7 | 3.7 |
| | 0.52 | 0.52 | 1.42 | 1.88 - 2.12 | 1.99 | | | | | | | |
| | 0.31 | 0.31 | 0.85 | 1.13 - 1.27 | 1.19 | | | | | | | |
| | 0.18 | 0.18 | 0.49 | 0.65 - 0.73 | 0.69 | | | | | | | |
| | 0.28 | 0.28 | 0.77 | 1.02 - 1.15 | 1.08 | | | | | | | |
| | 0.21 | 0.21 | 0.58 | 0.77 - 0.86 | 0.81 | | | | | | | |

| **Femora** | Growth zone measure-ments (mm/a) | Species - Mean growth rates (mm/a) | Species - Mean growth rates (µ/d) - 365 days | Species - Growth rate interval (µ/d) - 275 - 245 days | Species - Mean growth rates (µ/d) - 260 days | Species - Average growth rate - 365 days (µ/d) | Species - Average growth rate interval (µ/d) - 275 - 245 days | Species - Average growth rate (µ/d) - 260 days | Anteropo-sterior diameter (mm) | OCL thickness (mm) used for growth rate analysis *sensu* Sander & Tückman-tel | LAG number (OCL excluded) used for growth rate analysis *sensu* Sander & Tückman-tel | Species - Mean growth rates *sensu* Sander & Tückman-tel (µ/d) |
|---|---|---|---|---|---|---|---|---|---|---|---|---|
| *Candiacervus ropalophorus* PIMUZ A/V 5195 | 0.48 | 0.57 | 1.56 | 2.07 - 2.32 | 2.19 | 1.12 | 1.49 - 1.67 | 1.57 | 17 | 1.19 | 5 | 4.16 |
| | 0.52 | 0.33 | 0.9 | 1.19 - 1.34 | 1.26 | | | | | | | |
| | 0.74 | 0.47 | 1.29 | 1.71 - 1.92 | 1.81 | | | | | | | |
| | 0.45 | 0.27 | 0.74 | 0.98 - 1.10 | 1.04 | | | | | | | |
| | | | | | | | | | | | | |
| *Candiacervus ropalophorus* PIMUZ A/V 5202 | 0.66 | | | | | | | | 16 | 0.14 | 5 | |
| | 0.14 | | | | | | | | | | | |
| | 0.19 | | | | | | | | | | | |
| | 0.08 | | | | | | | | | | | |
| | | | | | | | | | | | | |
| *Procervulus praelucidus* BSPG 1937 II 23227 | 0.21 | 0.21 | 0.58 | 0.77 - 0.86 | 0.81 | 0.33 | 0.44 - 0.49 | 0.46 | 14 | 0.38 | 7 | 2.6 |
| | 0.15 | 0.15 | 0.41 | 0.54 - 0.61 | 0.58 | | | | | | | |
| | 0.1 | 0.1 | 0.27 | 0.36 - 0.40 | 0.38 | | | | | | | |
| | 0.11 | 0.11 | 0.3 | 0.40 - 0.45 | 0.42 | | | | | | | |
| | 0.13 | 0.13 | 0.36 | 0.48 - 0.54 | 0.51 | | | | | | | |
| | 0.08 | 0.08 | 0.22 | 0.29 - 0.33 | 0.31 | | | | | | | |
| | 0.05 | 0.05 | 0.14 | 0.19 - 0.21 | 0.20 | | | | | | | |
| | | | | | | | | | | | | |
| *Alces alces* ZMUZ 20242 | 2.48 | 2.48 | 6.79 | 9.01 - 10.12 | 9.53 | 2.62 | 3.48 - 3.90 | 3.68 | 37 | 0.16 | 4 | 12.58 |
| | 1.11 | 1.11 | 3.04 | 4.03 - 4.53 | 4.27 | | | | | | | |
| | 0.17 | 0.17 | 0.47 | 0.62 - 0.70 | 0.66 | | | | | | | |
| | 0.06 | 0.06 | 0.16 | 0.21 - 0.24 | 0.22 | | | | | | | |
| | | | | | | | | | | | | |
| *Cervus elaphus* ZIUK 23517 | 1.26 | 1.26 | 3.45 | 4.58 - 5.14 | 4.84 | 1.84 | 2.44 - 2.74 | 2.58 | 28 | 0.07 | 3 | 12.66 |
| | 0.08 | 0.08 | 0.22 | 0.29 - 0.33 | 0.31 | | | | | | | |

| **Femora** | Growth zone measure-ments (mm/a) | Species - Mean growth rates (mm/a) | Species - Mean growth rates (µ/d) - 365 days | Species - Growth rate interval (µ/d) - 275 - 245 days | Species - Mean growth rates (µ/d) - 260 days | Species - Average growth rate - 365 days (µ/d) | Species - Average growth rate interval (µ/d) - 275 - 245 days | Species - Average growth rate (µ/d) - 260 days | Anteropo-sterior diameter (mm) | OCL thickness (mm) used for growth rate analysis *sensu* Sander & Tückman-tel | LAG number (OCL excluded) used for growth rate analysis *sensu* Sander & Tückman-tel | Species - Mean growth rates *sensu* Sander & Tückman-tel (µ/d) |
|---|---|---|---|---|---|---|---|---|---|---|---|---|
| *Capreolus capreolus* ZIUK 9872 | 0.44 | 0.44 | 1.21 | 1.61 - 1.80 | 1.70 | 0.83 | 1.10 - 1.24 | 1.17 | 15 | 0.05 | 3 | 6.79 |
| | 0.16 | 0.16 | 0.44 | 0.58 - 0.66 | 0.62 | | | | | | | |
| | | | | | | | | | | | | |
| *Muntiacus muntjak* ZIUK 7994 | 0.58 | 0.58 | 1.59 | 2.11 - 2.37 | 2.23 | 0.93 | 1.23 - 1.39 | 1.31 | 13 | 0.22 | 3 | 5.75 |
| | 0.28 | 0.28 | 0.77 | 1.02 - 1.15 | 1.08 | | | | | | | |
| | 0.16 | 0.16 | 0.44 | 0.58 - 0.66 | 0.62 | | | | | | | |
| | | | | | | | | | | | | |
| **Tibiae** | | | | | | | | | | | | |
| | | | | | | | | | | | | |
| *Megaloceros giganteus* F21306/14 | 1.94 | 1.51 | 4.14 | 5.49 - 6.17 | 5.81 | n.a. | n.a. | n.a. | 35 | n.a. | n.a. | n.a. |
| | 0.8 | 0.71 | 1.95 | 2.59 - 2.91 | 2.74 | | | | | | | |
| | 0.5 | 0.42 | 1.15 | 1.53 - 1.71 | 1.61 | | | | | | | |
| | 0.33 | 0.33 | 0.9 | 1.19 - 1.34 | 1.26 | | | | | | | |
| | 0.14 | 0.27 | 0.74 | 0.98 - 1.10 | 1.04 | | | | | | | |
| | | | | | | | | | | | | |
| *Megaloceros giganteus* F22534/5 | 0.93 | | | | | | | | 35 | n.a. | n.a. | |
| | 0.74 | | | | | | | | | | | |
| | 0.22 | | | | | | | | | | | |
| | 0.11 | | | | | | | | | | | |
| | | | | | | | | | | | | |
| *Megaloceros giganteus* F2655/34 | 1.67 | | | | | | | | 35 | n.a. | n.a. | |
| | 0.6 | | | | | | | | | | | |
| | 0.54 | | | | | | | | | | | |
| | 0.55 | | | | | | | | | | | |

| **Tibiae** | Growth zone measure-ments (mm/a) | Species - Mean growth rates (mm/a) | Species - Mean growth rates (µ/d) - 365 days | Species - Growth rate interval (µ/d) - 275 - 245 days | Species - Mean growth rates (µ/d) - 260 days | Species - Average growth rate - 365 days (µ/d) | Species - Average growth rate interval (µ/d) - 275 - 245 days | Species - Average growth rate (µ/d) - 260 days | Anteropo-sterior diameter (mm) | OCL thickness (mm) used for growth rate analysis *sensu* Sander & Tückman-tel | LAG number (OCL excluded) used for growth rate analysis *sensu* Sander & Tückman-tel | Species - Mean growth rates *sensu* Sander & Tückman-tel (µ/d) |
|---|---|---|---|---|---|---|---|---|---|---|---|---|
| | 0.4 | | | | | | | | | | | |
| | | | | | | | | | | | | |
| *Dama dama* ZIUK 9630 | 0.56 | 0.66 | 1.81 | 2.4 - 2.70 | 2.54 | n.a. | n.a. | n.a. | 18 | n.a. | n.a. | n.a. |
| | 0.21 | 0.14 | 0.38 | 0.5 - 0.57 | 0.53 | | | | | | | |
| | 0.09 | 0.13 | 0.36 | 0.48 - 0.54 | 0.51 | | | | | | | |
| | 0.05 | 0.08 | 0.22 | 0.29 - 0.33 | 0.31 | | | | | | | |
| | | 0.07 | 0.19 | 0.25 - 0.28 | 0.27 | | | | | | | |
| *Dama dama* PIMUZ A/V 5248 | 0.76 | | | | | | | | 16 | n.a. | n.a. | |
| | 0.07 | | | | | | | | | | | |
| | 0.04 | | | | | | | | | | | |
| | 0.11 | | | | | | | | | | | |
| | 0.07 | | | | | | | | | | | |
| | | | | | | | | | | | | |
| *Candiacervus* sp. II PIMUZ A/V 5222 | 0.18 | 0.18 | 0.49 | 0.65 - 0.73 | 0.69 | n.a. | n.a. | n.a. | 14 | n.a. | n.a. | n.a. |
| | 0.09 | 0.09 | 0.25 | 0.33 - 0.37 | 0.35 | | | | | | | |
| | 0.14 | 0.14 | 0.38 | 0.5 - 0.57 | 0.53 | | | | | | | |
| | 0.16 | 0.16 | 0.44 | 0.58 - 0.66 | 0.62 | | | | | | | |
| | 0.08 | 0.08 | 0.22 | 0.29 - 0.33 | 0.31 | | | | | | | |
| | | | | | | | | | | | | |
| *Candiacervus ropalophorus* PIMUZ A/V 5189 | 0.16 | 0.71 | 1.95 | 2.59 - 2.91 | 2.74 | n.a. | n.a. | n.a. | 13 | n.a. | n.a. | n.a. |
| | 0.09 | 0.095 | 0.26 | 0.35 - 0.39 | 0.37 | | | | | | | |
| | 0.31 | 0.26 | 0.71 | 0.94 - 1.06 | 1.00 | | | | | | | |
| | | 0.09 | 0.25 | 0.33 - 0.37 | 0.35 | | | | | | | |
| | | | | | | | | | | | | |
| | | | | | | | | | | | | |

| **Tibiae** | Growth zone measure-ments (mm/a) | Species - Mean growth rates (mm/a) | Species - Mean growth rates (µ/d) - 365 days | Species - Growth rate interval (µ/d) - 275 - 245 days | Species - Mean growth rates (µ/d) - 260 days | Species - Average growth rate - 365 days (µ/d) | Species - Average growth rate interval (µ/d) - 275 - 245 days | Species - Average growth rate (µ/d) - 260 days | Anteropo-sterior diameter (mm) | OCL thickness (mm) used for growth rate analysis *sensu* Sander & Tückman-tel | LAG number (OCL excluded) used for growth rate analysis *sensu* Sander & Tückman-tel | Species - Mean growth rates *sensu* Sander & Tückman-tel (µ/d) |
|---|---|---|---|---|---|---|---|---|---|---|---|---|
| *Candiacervus ropalophorus* PIMUZ A/V 5188 | 1.26 | | | | | | | | 13 | n.a. | n.a. | |
| | 0.1 | | | | | | | | | | | |
| | 0.21 | | | | | | | | | | | |
| | 0.09 | | | | | | | | | | | |
| | | | | | | | | | | | | |
| *Procervulus praelucidus* BSPG 1937 II 23230 | 0.61 | 0.96 | 2.63 | 3.49 - 3.92 | 3.69 | n.a. | n.a. | n.a. | 10 | n.a. | n.a. | n.a. |
| | 0.4 | 0.24 | 0.66 | 0.88 - 0.98 | 0.93 | | | | | | | |
| | 0.18 | 0.14 | 0.38 | 0.5 - 0.57 | 0.53 | | | | | | | |
| | 0.25 | 0.16 | 0.44 | 0.58 - 0.66 | 0.62 | | | | | | | |
| | 0.09 | 0.05 | 0.14 | 0.19 - 0.21 | 0.20 | | | | | | | |
| | | 0.04 | 0.04 | 0.05 - 0.06 | 0.06 | | | | | | | |
| | | | | | | | | | | | | |
| *Procervulus praelucidus* BSPG 1937 II 23231 | 1.31 | | | | | | | | 10 | n.a. | n.a. | |
| | 0.07 | | | | | | | | | | | |
| | 0.09 | | | | | | | | | | | |
| | 0.06 | | | | | | | | | | | |
| | 0.01 | | | | | | | | | | | |
| | 0.04 | | | | | | | | | | | |

# CHAPTER 4

## Growth and life history of Middle Miocene deer (Mammalia, Cervidae) based on bone histology

Authors: Amson E., Kolb C., Scheyer T. M., Sánchez-Villagra M. R.

Publication: 2015, *Comptes Rendus Palevol,* 14:637-645.

Contributions: EA, CK and MRS-V designed the study/experiments, EA performed the experiments and wrote the manuscript, EA, CK, and TMS, collected and analysed histological data, EA prepared figures/tables and took micrographs, and all authors contributed to the final interpretation and editing of the manuscript. All authors read and approved the final manuscript.

C. R. Palevol 14 (2015) 637–645

Contents lists available at ScienceDirect

Comptes Rendus Palevol

www.sciencedirect.com

General Palaeontology, Systematics and Evolution (Vertebrate Palaeontology)

# Growth and life history of Middle Miocene deer (Mammalia, Cervidae) based on bone histology

## *Croissance et histoire de vie de cervidés (Mammalia, Cervidae) du Miocène moyen (Mammalia, Cervidae) : apport de l'histologie osseuse*

Eli Amson , Christian Kolb , Torsten M. Scheyer , Marcelo R. Sánchez-Villagra*

*Paläontologisches Institut und Museum der Universität Zürich, Karl Schmid-Strasse 4, Zürich CH-8006, Switzerland*

ARTICLE INFO

*Article history:*
Received 21 April 2015
Accepted after revision 15 July 2015
Available online 1 October 2015

Handled by Michel Laurin

*Keywords:*
Bone histology
Cervidae
*Dicrocerus*
*Euprox*
Middle Miocene
Palaeohistology
Skeletochronology

ABSTRACT

Our knowledge of the histology of the Cervidae (deer) was recently expanded with a work describing long bone and tooth histology of various taxa (Kolb et al., 2015a). Included in this study was the Miocene *Procervulus*, an early cervid whose growth rate was found to be especially low. The present study examines further "stem-cervid" bone histology in describing that of other Miocene taxa, *Dicrocerus elegans* and *Euprox* sp. With their inclusion in the dataset of Kolb et al. (2015a), we estimate the ancestral growth rates among cervids, and studied its correlation with body size. The skeletochronology of *Dicrocerus* suggests a relatively high growth rate for its body size differing from the condition of *Procervulus* and *Euprox*, and hence, documenting diversity in the life history traits of Miocene cervids.

*Mots clés :*
Histologie osseuse
Cervidae
*Dicrocerus*
*Euprox*
Miocène moyen
Paléohistologie
Squelettochronologie

RÉSUMÉ

Notre connaissance de l'histologie des Cervidae a récemment été étendue grâce à une étude décrivant l'histologie osseuse et dentaire chez divers taxons (Kolb et al., 2015a). Cette précédente étude présentait *Procervulus*, un cervidé miocène dont le taux de croissance a été caractérisé comme particulièrement bas. Nous décrivons ici l'histologie osseuse de deux autres « stem-cervidés » miocènes, *Dicrocerus elegans* et *Euprox* sp. En les incorporant dans le jeu de données de Kolb et al. (2015a), nous estimons le taux de croissance ancestral au sein des cervidés, et étudions sa corrélation avec la taille corporelle. Les données squelettochronologiques chez *Dicrocerus* indiquent un taux de croissance relativement fort pour sa taille corporelle, contrastant avec ceux de *Procervulus* et *Euprox*, et documentant donc une diversité de traits d'histoire de vie chez les cervidés miocènes.

---

* Corresponding author.
*E-mail address:* m.sanchez@pim.uzh.ch (M.R. Sánchez-Villagra).

http://dx.doi.org/10.1016/j.crpv.2015.07.001

## 1. Introduction

The investigation of the palaeobiology of "stem-cervids" from the Miocene is necessary to understand the origin of the diverse life histories of deer. *Dicrocerus elegans* Lartet 1837, one of these early cervids (Azanza, 1993; Gentry, 1994), was originally described from the French locality of Sansan (local Helvetian age), which corresponds to the mammalian Neogene age MN6 [Middle Miocene, Langhian, *ca.* 15 Ma; (Peigné and Sen, 2012)]. *Dicrocerus*, of relatively intermediate body size [*ca.* 50 kg; (Costeur et al., 2012)], is characterized by its long pedicle and bifid "protoantler". It is known from numerous specimens, which have allowed, for instance, to propose that the female of *Dicrocerus*, like the extant *Rangifer* (Reindeer), were antlered, and that the species was marked by sexual dimorphism regarding size and shape of the antlers (Ginsburg and Azanza, 1991). However, different ontogenetic stages have been suggested as an alternative explanation (Gentry et al., 1999). The growth cycle of the "protoantler" comprises a shedding phase of the velvet-like skin and a phase with bare and dead bone tissue before casting (Azanza et al., 2012). Such a cycle appears to be an apomorphic feature grouping *Dicrocerus* with later cervids. However, the protoantlers of *Dicrocerus*, growing over a longer period than the annually deciduous antlers, may represent the ancestral condition for later cervids (DeMiguel et al., 2014). Although brachydont, *Dicrocerus* is considered to be a mixed feeder (Solounias and Moelleken, 1994).

*Euprox* is another cervid from the Middle Miocene of Europe (Gentry et al., 1999). Little is known about *Euprox*, hypothesized to be sister-taxon of other Muntiacini (Azanza, 1993), albeit this is controversial (Gentry et al., 1999).

*Procervulus praelucidus* (Obergfell 1957), known from the Early Miocene [MN3, Ginsburg (2011)], is regarded as being, with the rest of the Procervulinae, sister-group of all other cervids, including *Dicrocerus* (Azanza, 1993). This species was recently included in a study of long bone and dental histology concerned with cervids life history evolution in order to estimate skeletal maturity and growth rate (Kolb et al., 2015a). *Procervulus* distinguished itself in featuring the lowest estimated growth rate of all the cervids sampled in that study. We here investigate if such a condition is widespread in "stem-cervids". The bone histology and skeletochronology of *Dicrocerus* and *Euprox* will hence be investigated here to gain insight into life history traits in early cervids, as it was previously performed regarding feeding styles (DeMiguel et al., 2008).

## 2. Material and methods

For *Dicrocerus elegans*, eleven bones, comprising three humeri (MNHN.F.Sa7330, Sa7341, and Sa7343), three radii (MNHN.F.Sa2453, Sa2470, and Sa7063), two femora (MNHN.F.Sa6877, Sa6889), and three tibiae (MNHN.F.Sa6910, Sa6917, and Sa8163), were sampled. As indicated by epiphyseal closure, the specimens correspond to subadult to adult individuals. For *Euprox* sp., one femur from the locality of Steinheim (Germany), with epiphyseal lines still slightly visible, was sampled (NMB Sth.1281). Thin-sections were prepared following conventional procedure (Chinsamy-Turan, 2005; Kolb et al., 2015a; Padian and Lamm, 2013). The sections were taken as close as possible from the mid-diaphyseal level (see Appendix A for estimation of relative position of each thin-section). Observations were performed with a petrographic microscope (Leica DM 2500M®) under normal transmitted or cross-polarized light, in some cases with the use of a lambda compensator. Photographs were taken with a digital camera (Leica DFC 420C®) installed on the microscope. The quantification of the growth rate [annual growth rate with an estimated mean growth period of 260 days, as explained in Kolb et al. (2015a), and based on Köhler et al. (2012)], was performed following published methodology (Kolb et al., 2015a), using the Leica IM 50 Image Manager® software. Only the growth rate of the femur and tibia will be discussed, because these bones were considered by Kolb et al. (2015a) as the most informative. The growth zone measurements were taken in the anterior region of the bones, in order to be consistent with the data from Kolb et al. (2015a). The histological terminology follows Francillon-Vieillot et al. (1990). Regarding the definition of the OCL (necessary for the skeletal maturity estimation), we follow Ponton et al. (2004) in acknowledging its presence when parallel-fibred/lamellar and avascular tissue forms the external-most region of the cortex.

A timetree was used to perform phylogenetically-informed statistical tests. The relationships and divergence times in extant taxa are based on Hassanin et al. (2012). Regarding relationships and divergence times of extinct taxa, the following data were used (and see above for *Dicrocerus* and *Procervulus*). Megacerina *sensu* Vislobokova (2013) are here represented by the giant *Megaloceros giganteus* and *Sinomegaceros yabei*. *M. giganteus* is known from 0.4 Ma to 6 900 years BP (Stuart et al., 2004). The sampled specimen of *S. yabei* (OMNH QV-4067) comes from the Late Pleistocene (ca. 20–30,000 years) of Japan (Kolb et al., 2015b). Closely related to the Megacerina, the dwarf *Candiacervus* from Crete was also included (we consider the Megacerina to be included, along with *Candiacervus*, *Dama dama*, the Fallow deer, and *Cervus elaphus*, the Red deer, into the Cervini). Specimens of *C. ropalophorus* are known to be at least 43,600 years old in one locality, and dated at *ca.* 21,500 years in another (Vislobokova, 2013). *Candiacervus* sp. II is also well known from the Late Pleistocene (Van Der Geer et al., 2010, p. 333). The relationships among Megacerina, *Candiacervus*, and with their closest extant relative, *Dama* (Lister et al., 2005), are not well understood (A.M. Lister, pers. comm.). We hence prefer to leave a polytomy in the topology. The divergence times within the (Megacerina + *Candiacervus* + *Dama*) clade are based on Vislobokova (2013). Due to the age of the Megacerina fossils, the origin of the Cervini clade was pushed back when compared to the molecular dating of Hassanin et al. (2012). Since *Euprox* is found in MN6 (Gentry et al., 1999) and is hypothesized as sister-taxon of other Muntiacini (Azanza, 1993), the origins of Cervinae and crown-Cervidae were pushed back as well. However, this hypothesis should be treated with caution, because the phylogenetic position of *Euprox* is regarded as controversial (Gentry et al., 1999). A nexus file containing the timetree is given as Appendix A.

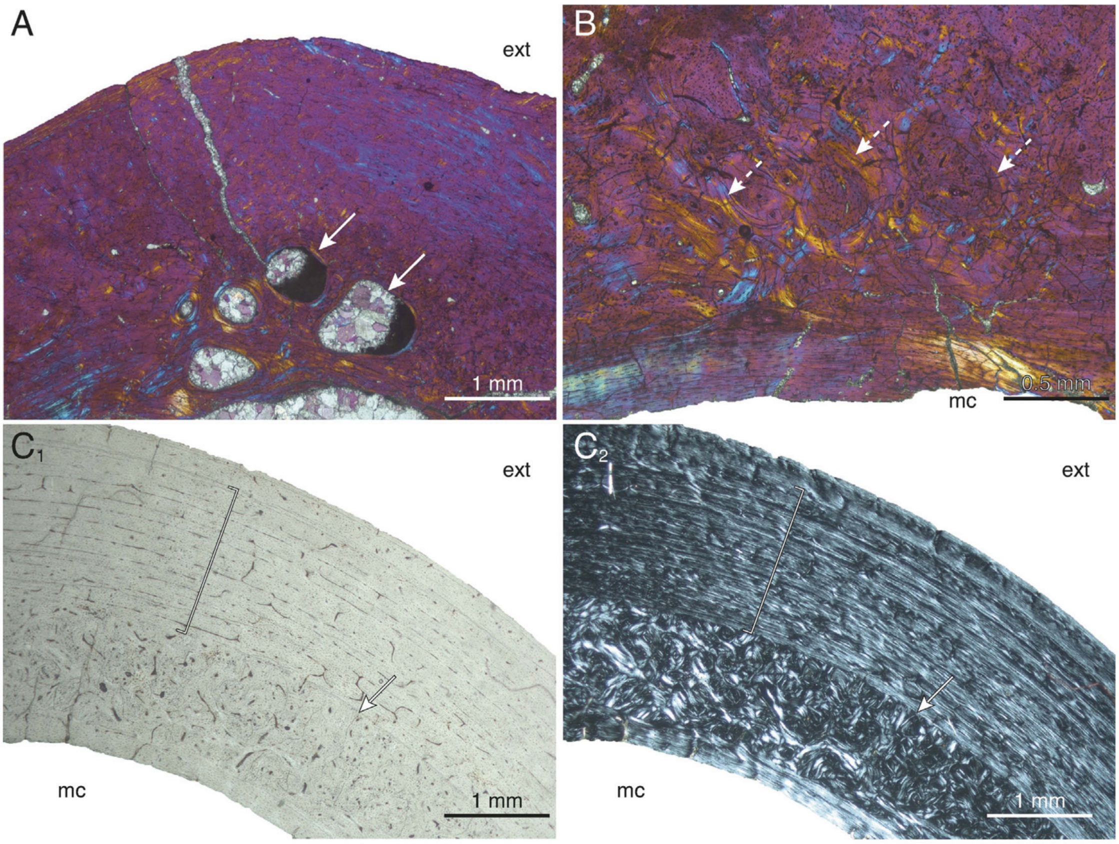

**Fig. 1.** (Color online). Histological features of the humerus of *Dicrocerus elegans*. A. Large resorption vacuities (white continuous arrows) seen under CPL-λ (anterior region; MNHN.F.Sa.7341). B. Secondary osteons of various orientations describing pseudo-circular patterns (white dashed arrows), seen under CPL-λ (anteromedial region; MNHN.F.Sa.7341). C. Fibrolamellar tissue (with a very low amount of fibrous tissue) with laminar to plexiform vascularization (white with black outline bracket) seen under NL ($C_1$) and CPL ($C_2$) (posterolateral region; MNHN.F.Sa.7343). Note the presence of a LAG (white with black outline continuous arrows) that sharply defines externally a strongly remodeled zone. Abbreviations: ext, exterior; mc, medullary cavity.

**Fig. 1.** (Couleur en ligne). Caractéristiques histologiques de l'humérus chez *Dicrocerus elegans*. A. Grandes cavités de résorption (flèches blanches en trait plein) vues sous CPL-λ (région antérieure; MNHN.F.Sa.7341). B. Ostéones secondaires d'orientations diverses formant des motifs pseudo-circulaires (flèches blanches en trait pointillé), observées sous CPL-λ (région antéromédiale; MNHN.F.Sa.7341). C. Tissu fibrolamellaire (à faible teneur en os fibreux) à vascularisation laminaire à plexiforme (crochet blanc à contour noir), observé sous NL ($C_1$) et CPL ($C_2$) (région postérolatérale; MNHN.F.Sa.7343). Noter la présence d'une LAG définissant nettement la limite externe d'une zone fortement remaniée. Abréviations : ext, extérieur ; mc, cavité médullaire.

A test for the presence of phylogenetic signal was performed for the growth rates and body size proxy (anteroposterior diameter of the section) using the Mesquite software (Maddison and Maddison, 2011) and a previously published procedure (Laurin, 2004; Quemeneur et al., 2013). It consists of the comparison of the squared length of the reconstructed parameter to those of 10,000 trees in which the terminal taxa were randomly reshuffled. The *P*-value of this test will be the number of trees (divided by 10,000) shorter than the initial tree. The ancestral character values were reconstructed using squared-change parsimony in Mesquite. The phylogenetically-informed linear regression of the growth rate against anteroposterior diameter of the section was performed using phylogenetically independent contrasts (PIC) analysis with the Mesquite software and its PDAP:PDTREE module (Midford et al., 2011).

Institutional abbreviations:

**NMB**, Naturhistorisches Museum Basel, Switzerland; **MNHN**, Muséum national d'Histoire naturelle, Paris, France; **OMNH**, Osaka Museum of Natural History, Japan; **ZIUK**, Zoologisches Institut der Universität Kiel, Germany.

Other abbreviations:

**CPL**, crossed polarized light; **CPL-λ**, crossed polarized light with the addition of a lambda compensator; **NL**, natural light; **OCL**, outer circumferential layer

## 3. Histological description

All sampled bones feature a free medullary cavity and a compact cortex. Except for a few minor instances, trabecular bone was not observed.

### 3.1. *Humerus of* Dicrocerus

A layer of endosteal lamellar bone of variable thickness is found on the whole circumference of the innermost cortex. Most of the inner region of the rest of the cortex is heavily remodeled in all three specimens, preventing

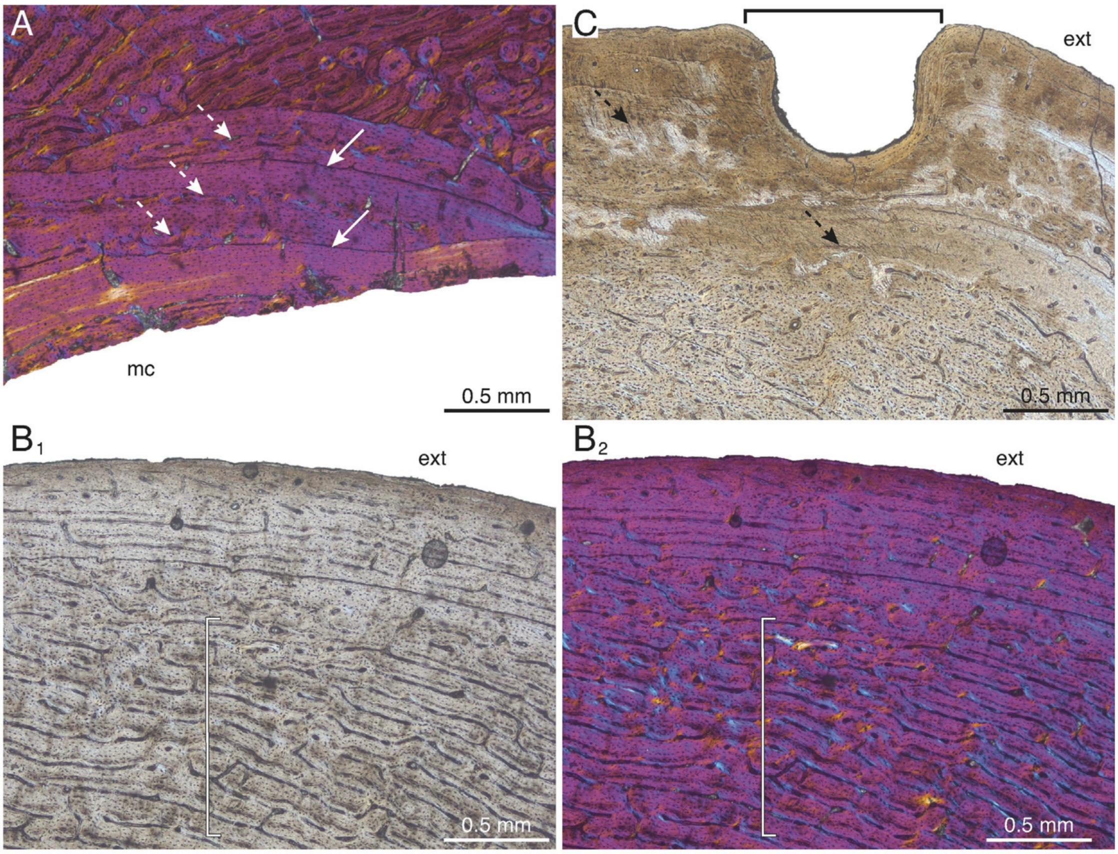

**Fig. 2.** (Color online). Histological features of the radius of *Dicrocerus elegans*. A. Lamellar endosteal deposit featuring cement lines (white continuous arrows) and vascular canals (white dashed arrows), seen under CPL-λ (anterolateral region; MNHN.F.Sa2470). B. Central region of the cortex formed by fibrolamellar bone with a plexiform to reticular vascularization (white with black outline bracket), seen under NL ($B_1$) and CPL-λ ($B_2$) (medial region; MNHN.F.Sa2470). C. Outer nutrient foramen (black bracket) with numerous Sharpey's fibre bundles (black dashed arrows), seen under NL (posterolateral region; MNHN.F.Sa7063). Abbreviations: ext, exterior; mc, medullary cavity.

**Fig. 2.** (Couleur en ligne). Caractéristiques histologiques du radius chez *Dicrocerus elegans*. A. Dépôt lamellaire endostéal présentant lignes cimentantes (flèches blanches en trait plein) et canaux vasculaires (flèches blanches en trait pointillé), observés sous CPL-λ (région antérolatérale; MNHN.F.Sa2470). B. Région centrale du cortex formée par de l'os fibrolamellaire à vascularisation plexiforme à réticulée (crochet blanc à contour noir), observée sous NL ($B_1$) et CPL-λ ($B_2$) (région médiale; MNHN.F.Sa2470). C. Foramen nourricier externe (crochet noir) cerné de nombreux paquets de fibres de Sharpey (flèches noires en trait pointillé). Abréviations : ext, extérieur ; mc, cavité médullaire.

the description of the primary structures. In one specimen (MNHN.F.Sa7341) large resorption vacuities, most likely related to a bone drift process, can be noted (Fig. 1A). These vacuities are surrounded by lamellar bone. The middle region of the cortex is either remodeled by longitudinal, oblique, and transverse secondary osteons (MNHN.F.Sa7330, MNHN.F.Sa7341, and part of MNHN.F.Sa7343) that can describe in some places pseudo-circular patterns (Fig. 1B), or be formed by fibrolamellar tissue, and with laminar to plexiform vascularization (Fig. 1C). In the outermost cortex, the vascularization is usually reduced to a few longitudinal vascular canals, and a clear OCL is found on two of the three specimens (MNHN.F.Sa7330; MNHN.F.Sa7341). Two specimens (MNHN.F.Sa7341 and MNHN.F.Sa7343) show a peculiar pattern of remodeling, in which most of the secondary osteons are restricted and almost entirely forming an area sharply defined externally by a line of arrested growth (LAG) (Fig. 1C).

### 3.2. *Radius of* Dicrocerus

In this bone, and when present, the endosteal deposit has a particularly irregular thickness, with sometimes several cement lines ("cementing line" *sensu* Francillon-Vieillot et al. (1990); Fig. 2A) and few longitudinal vascular canals. The rest of the cortex, either partially or entirely remodeled, is formed by fibrolamellar bone with a plexiform or reticular vascularization (Fig. 2B), and becomes poorly vascularized outwardly. One specimen (MNHN.F.Sa7063) corresponds to a section at the level of the outer nutrient foramen, as shown by the presence of a concavity in its posterolateral region. Numerous Sharpey's

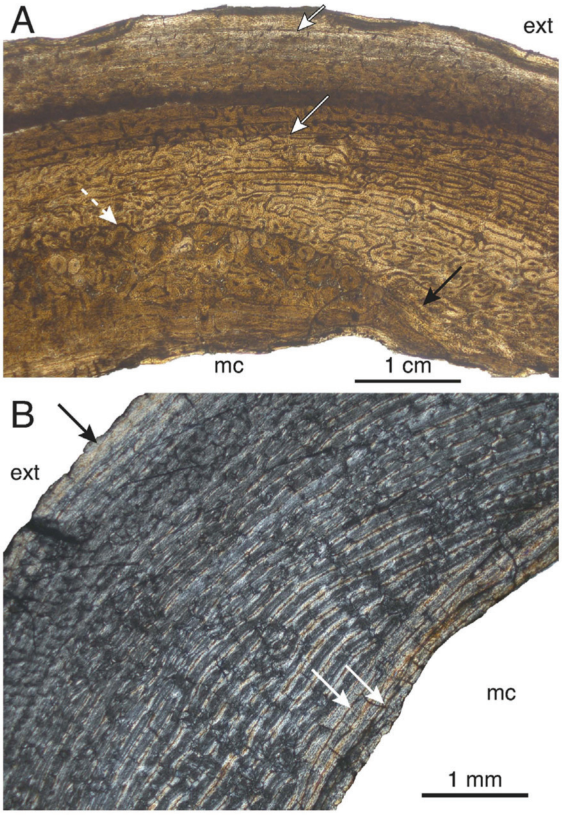

**Fig. 3.** (Color online). Histological features of the femur of *Dicrocerus elegans* and *Euprox* sp. A. Anterior region of *Dicrocerus elegans* (MNHN.F.Sa6877) seen under NL. Note the presence of a resorption line within the cortex (white dashed arrow) that is not found throughout the section, as shown by the presence of primary bone where it would have been found (black arrow); note also the two first LAGs (white with black outline continuous arrows; the first is a double LAG) delimiting the second growth zone. B. Anterior region of *Euprox* (NMB Sth.1281) seen under CPL. Note the cement lines in the endosteal deposit (white arrows), and a thin layer in the external-most cortex formed by lamellar bone (highly birefringent) without vascularization (black arrow). Abbreviations: ext, exterior; mc, medullary cavity.

**Fig. 3.** (Couleur en ligne). Caractéristiques histologiques du fémur de *Dicrocerus elegans* et *Euprox* sp. A. Région antérieure chez *Dicrocerus elegans* (MNHN.F.Sa6877), observée sous NL. Noter la présence d'une ligne de résorption au sein du cortex (flèche blanche en trait pointillé), qui n'est pas présente sur toute section, comme indiqué par la présence de tissu primaire (flèche noire) ; noter aussi les deux premières LAGs (flèches blanches en trait plein à contour noir) définissant la seconde zone de croissance. B. Région antérieure chez *Euprox* (NMB Sth. 1281), observée sous CPL. Noter la présence de lignes cimentantes dans le dépôt endostéal (flèches blanches) et celle, dans la région la plus externe du cortex, d'un fin dépôt formé par de l'os lamellaire sans vascularisation (flèche noire). Abréviations : ext, extérieur ; mc, cavité médullaire.

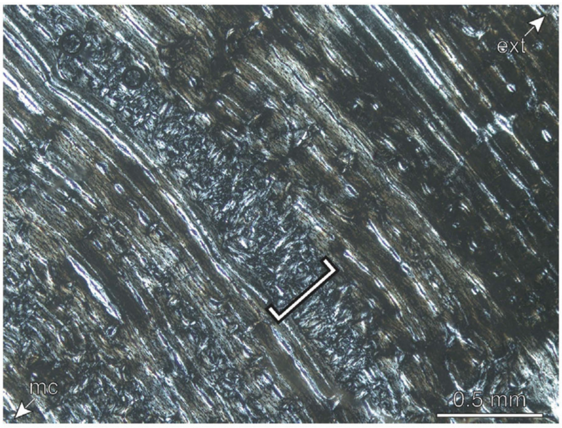

**Fig. 4.** (Color online). Histological features of the tibia of *Dicrocerus elegans*. Detail of a zone with reticular vascularization (white with black outline bracket) between laminae of the main plexiform vascularization, under CPL (posterior region; MNHN.F.Sa6910). Abbreviations: ext, exterior; mc, medullary cavity.

**Fig. 4.** (Couleur en ligne). Caractéristiques histologiques du tibia chez *Dicrocerus elegans*. Détail d'une zone à vascularisation réticulée (crochet blanc à contour noir) intercalée entre les lamines de vascularisation plexiforme principale, observée sous CPL (région postérieure, MNHN.F.Sa6910). Abréviations : ext, extérieur ; mc, cavité médullaire.

fibre bundles are seen in its vicinity (Fig. 2C). None of the specimens features a clear OCL.

### 3.3. *Femur of* Dicrocerus

A very narrow to absent layer of endosteal bone is observed. The middle part of the cortex is well remodeled in both available specimens. The secondary osteons are longitudinal and to a lesser extent oblique, and in some places describe pseudo-circular patterns. In the inner part of lateral region of MNHN.F.Sa6889, remnants of trabeculae are present. Where not entirely remodeled (especially in MNHN.F.Sa6889), the outermost cortex is weakly vascularized, with few, mostly longitudinal, vascular canals, and mainly consists of lamellar bone. One specimen (MNHN.F.Sa6877) shows a cement line that cannot be interpreted as a LAG, due to its irregular and wavy shape and because it is not present throughout the whole section (Fig. 3A). Based on a similar structure described by Klevezal (1996, fig. 9), we tentatively interpret it as a resorption line. Neither of the specimens features an OCL.

### 3.4. *Femur of* Euprox

Although rather thin, the layer of endosteal bone in the sampled specimen of *Euprox* sp. (NMB Sth.1281) features two cement lines (Fig. 3B). The cortex is mostly formed by plexiform fibrolamellar bone with a high amount of fibrous tissue. Externally the vascularization becomes reticular and is less present. Secondary osteons are extremely scarce. The external-most cortex is mostly formed by lamellar bone and does not show any vascularization (Fig. 3B). However, this concerns a very thin layer of bone, which prevents from securely recognizing an OCL.

### 3.5. *Tibia of* Dicrocerus

An endosteal lamellar layer of irregular thickness is found in all specimens. Most of the cortex is formed by fibrolamellar plexiform bone. Reticular vascularization is also observed, sometimes forming lenticular areas between laminae of the plexiform vascularization (Fig. 4). The outermost cortex is formed by avascular lamellar bone. The secondary osteons have a longitudinal, oblique, or radial

**Table 1**
Zone measurements and associated growth rates in the anterior region of long bones of *Dicrocerus elegans* and *Euprox* sp.
**Tableau 1**
Mesures des zones et taux de croissance associés dans la région antérieure des os longs chez *Dicrocerus elegans* et *Euprox* sp.

| | | LAG count | GZ number | GZ thickness (mm) | Mean GZ (mm/a) | Mean GR (μm/d) 260 d |
|---|---|---|---|---|---|---|
| ***Dicrocerus elegans*** | | | | | | |
| Femur | MNHN.F.Sa6877 | 2 (2) | 2nd | 0.98 | 0.98 | 3.77 |
| Tibia | MNHN.F.Sa6910 | 4 (4) | 2nd | 1.57 | 1.36 | 5.21 |
| | | | 3rd | 0.20 | 0.20 | 0.77 |
| | | | 4th | 0.12 | 0.12 | 0.46 |
| | MNHN.F.Sa6917 | 2 (6) | 2nd | 1.14 | | |
| | MNHN.F.Sa8163 | 1 (5) | | – | | |
| Humerus | MNHN.F.Sa7330 | 4 (7) | 2nd | 0.44 | 1.14 | 1.69 |
| | | | 3rd | 0.17 | 0.25 | 0.65 |
| | | | 4th | 0.06 | | 0.23 |
| | MNHN.F.Sa7343 | 3 (4) | 2nd | 1.84 | | 7.08 |
| | | | 3rd | 0.33 | | 1.27 |
| Radius | MNHN.F.Sa2453 | 2 (2) | 2nd | 0.44 | | 1.69 |
| | MNHN.F.Sa2470 | 2 (2) | 2nd | 0.65 | | 2.50 |
| | MNHN.F.Sa7063 | 3 (3) | 2nd | 0.28 | | 1.08 |
| | | | 3rd | 0.08 | | 0.31 |
| ***Euprox* sp.** | | | | | | |
| Femur | NMB Sth.1281 | 2 (2) | 2nd | 0.47 | | 1.81 |

**d**: days; **GR**: growth rate; **GZ**: growth zone; **LAG**: line of arrested growth in the anterior region of the bone used for the growth zone measurements and, between brackets, maximum number of LAGs found on the section.

orientation. The available specimens are weakly remodeled, with secondary osteons restricted to the inner half of the cortex. One specimen (MNHN.F.Sa6917) features an external deposit of avascular lamellar bone, but it is too thin to securely recognize it as an OCL.

## 4. Skeletochronology

When not obscured by secondary remodeling (especially the case in the sections farther away from the midshaft), all sampled bones feature at least one identifiable LAG. The LAG counts for each specimen (of which the count is not prevented by remodeling) are listed in Table 1. In *Dicrocerus*, for one specimen (MNHN.F.Sa7330; humerus) it was possible to conduct an estimation of skeletal maturity, thanks to its preservation of LAGs that are not obscured by secondary remodeling and of a clear OCL (Fig. 5). No LAG is lost (resorbed) during ontogeny in the femur and tibia of cervids (Kolb et al., 2015a). Based on the generally similar histomorphological pattern, it is also likely the case in the humerus and radius. With a count of five LAGs before the OCL, we hence hypothesize that the skeletal maturity in *Dicrocerus* was reached after five years. More specimens are required to make such an assertion for *Euprox* sp., because it was not possible to securely recognize an OCL in the available specimen.

The thickness of all zones and associated growth rates are given in Table 1. In *Dicrocerus*, and for the femur, only the second growth zone (between the first two LAGs) of one specimen could be measured (Fig. 3A). Being 0.98 mm thick, it corresponds to an annual growth rate of 3.77 μm per day. For the tibia, we were able to measure the thickness of the second growth zone on two specimens; in one of those specimens, we were also able to measure that of the second and third zones. The mean value of annual growth rate for the first three zones in the tibia is of 2.15 μm per day. In *Euprox*, the sampled femur yielded the first two LAGs defining a second growth zone that is 0.47 mm thick (Fig. 3B). This corresponds to an annual growth rate of 1.81 μm per day.

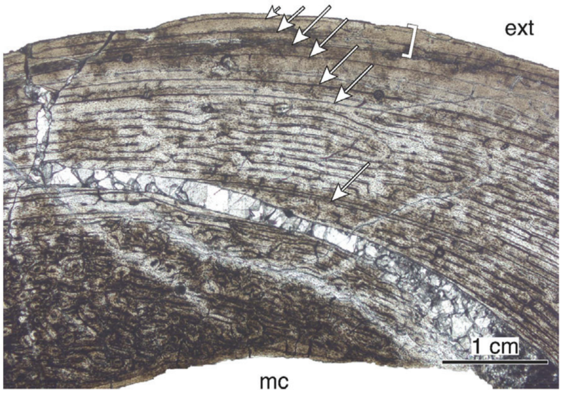

**Fig. 5.** (Color online). Seven lines of arrested growth (LAGs; indicated by arrows) and the OCL (outer circumferential layer; indicated by bracket) in the medial region of a humerus of *Dicrocerus elegans* (MNHN.F.Sa7330).
**Fig. 5.** (Couleur en ligne). Sept lignes d'arrêt de croissance (indiquées par des flèches) et l'OCL (système fondamental externe; indiqué par un crochet) dans la région médiale d'un humérus de *Dicrocerus elegans* (MNHN.F.Sa7330).

## 5. Discussion and conclusions

The free medullary cavity and compact cortex is a feature common to all cervids and more generally to most terrestrial amniotes (Laurin et al., 2011). The bone histology of *Dicrocerus* is on the whole consistent with that of other small to medium-sized cervids (Kolb et al., 2015a). Indeed, the primary bone tissue is mostly fibrolamellar and highly vascularized in the inner and middle cortex, with a mostly plexiform pattern, and the outer cortex is weakly

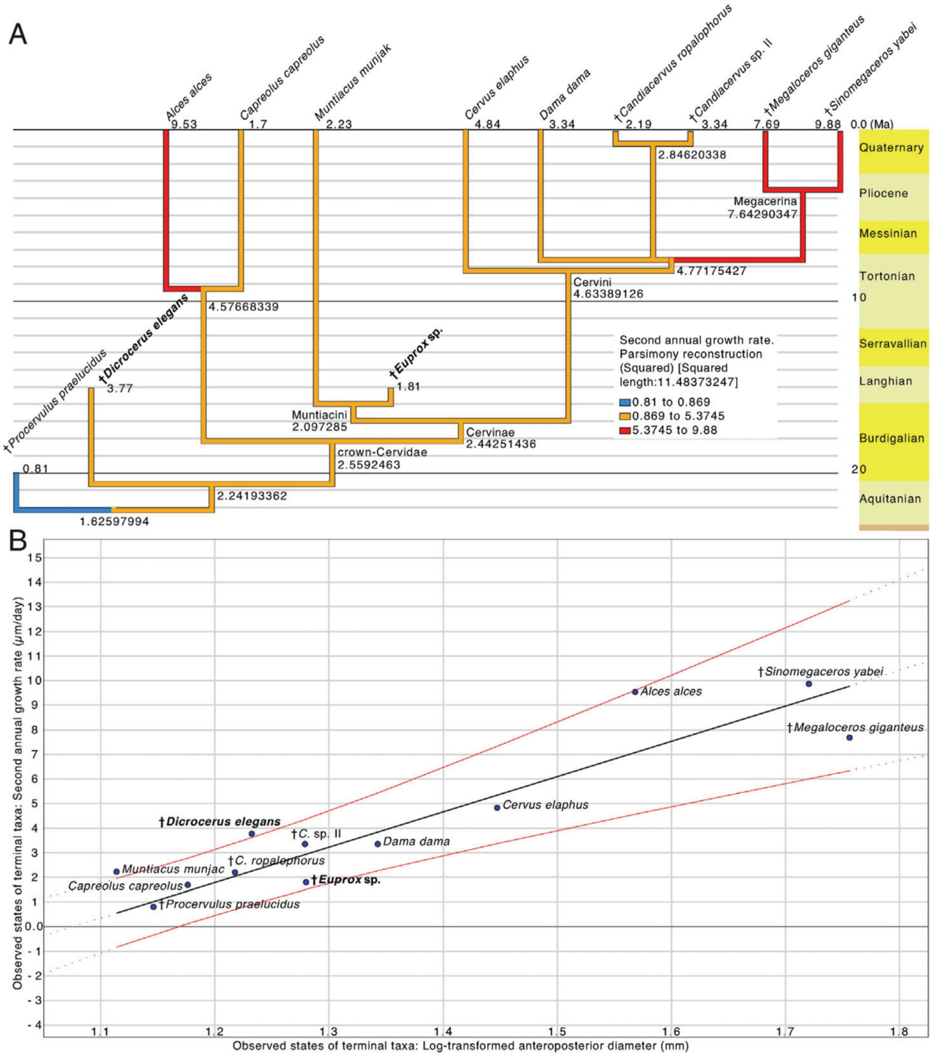

**Fig. 6.** (Color online). Phylogenetically-informed analysis of the relationship between femoral growth rate and body size in cervids. A. Timetree on which the second annual growth rate (260 days of growth) is mapped with Mesquite (Maddison and Maddison, 2011) and its stratigraphic tools module (Josse et al., 2006). The ancestral character states were reconstructed using squared-change parsimony. B. Independent contrasts least-squares linear regression (black line) of the second annual growth rate against the anteroposterior diameter of the section (body size proxy) mapped onto the original tip data space, performed with the PDAP:PDTREE module (Midford et al., 2011) of Mesquite. The red lines (see online version) represent the 95% confidence interval.

**Fig. 6.** (Couleur en ligne). Analyse prenant en compte la phylogénie de la relation entre le taux de croissance fémoral annuel et la taille corporelle chez les cervidés. A. Arbre phylogénétique calibré dans le temps, sur lequel le taux de croissance annuel (260 jours de croissance) de la deuxième année est plaqué grâce à Mesquite (Maddison et Maddison, 2011) et son module d'outils stratigraphiques (Josse et al., 2006). Les valeurs ancestrales ont été reconstruites grâce à l'algorithme de parcimonie (moindres carrés). B. Régression par méthode des moindres carrés des contrastes indépendants (droite noire) du taux de croissance annuel de la deuxième année sur le diamètre antéropostérieur de la section (proxy pour la masse corporelle) plaqué sur l'espace de données des branches terminales initiales, effectuée avec le module PDAP:PDTREE (Midford et al., 2011) de Mesquite. Les courbes rouges (voir la version en ligne) représentent l'intervalle de confiance à 95 %.

vascularized and formed by lamellar bone. The skeletal maturity, estimated in *Dicrocerus* to be reached after five years (during the sixth year of life), is reminiscent of that of *Cervus elaphus* (5-6 years old), *Megaloceros* (5–6 years old), and *Candiacervus* (5–7 years old; Kolb et al., 2015a).

The newly measured growth rates of *Dicrocerus* and *Euprox* were added to the dataset of Kolb et al. (2015a) in order to discuss them in the broader context of the Cervidae. A significant phylogenetic signal was found for the anteroposterior diameter of the section (*P*-value = 0.0163). For the second annual growth rate, a *P*-value of 0.0746 was obtained. Even though this is higher than the usual 5% threshold, we consider it as indicative of a pattern of biological significance. It should be noted that this value is at least partly explained by the fact that a high growth rate was independently acquired in *Alces*, the Elk, and the Megacerina clade (Fig. 6A). As a matter of fact, pruning *Alces* from the tree brings the *P*-value of this test to 0.0286. Furthermore, a phylogenetically-informed linear regression was performed. After trying all combination of log-transformation for each variable, the untransformed growth rate against log-transformed anteroposterior bone diameter obtained the greatest correlation coefficient ($R = 0.87$). Since a phylogenetic signal is also significantly present in the log-transformed anteroposterior bone diameter ($P$-value < 0.01), we used it for the rest of the analysis. The absence of significant correlation for both the growth rate and the log-transformed anteroposterior bone diameter in all diagnostic checks (absolute values of standardized contrasts against their standard deviations, or against their estimated nodal values, or against the heights of their base nodes, or the estimated nodal values against heights of the base nodes of the contrasts) allowed us to perform the PIC analysis (Midford et al., 2011). With a $R^2$ of 0.75 and a $P$-value lower than 0.0004, we find that the growth rate in cervids is strongly correlated with body size (Fig. 6B), confirming the results of Kolb et al. (2015a).

The growth rate corresponding to the femoral second zone is, in *Dicrocerus* (3.77 µm/day), close to that of *Dama* and *Candiacervus* sp. II (both at 3.34 µm/day), much lower than the large-sized *Megaloceros* (7.69 µm/day), *Sinomegaceros* (9.88 µm/day), and *Alces* (9.53 µm/day). However, *Dicrocerus* features a much greater second annual growth rate than *Procervulus* (0.81 µm/day) and *Euprox* sp. (1.81 µm/day). *Dicrocerus* falls slightly above the 95% confidence interval of the phylogenetically correct linear regression (Fig. 6B), indicating a relatively high growth rate for its size. The ancestral value reconstructed for all cervids is 1.63 µm/day (Fig. 6A). The ancestral state for the *Dicrocerus* plus crown-cervids clade is 2.24 µm/day, which is already much higher than that of the Early Miocene *Procervulus* and closer to that of *Dicrocerus*, and which will be roughly found as the ancestral value for the crown-cervids, the Muntiacini (here represented by *Muntiacus* and the Middle Miocene *Euprox*), and the Cervinae as well. A first departure from this value is found at the origin of the Capreolinae, here represented by *Alces* and *Capreolus capreolus* (Roe deer). But this result is likely an artefact, as *Alces*, much larger than *Capreolus*, was shown to lower the significance of the statistical test (see above). The increase of growth rate is more probably acquired in a more restricted taxon, and sampling extinct Alcini would clarify this question. A more documented increase of growth rate is found for the Cervini, with an ancestral growth rate of 4.63 µm/day. While the relationships between *Dama*, *Candiacervus*, and the large-sized Megacerina were left as unresolved, it can be emphasized that a reversion to a lower growth rate is found in *Candiacervus* (ancestral value for the genus of 2.85 µm/day), and a steep increase is found as the ancestral value for Megacerina, with a growth rate of 7.64 µm/day.

The bone histology of *Dicrocerus* is reminiscent of those of other small to medium-sized deer. The skeletochronological data suggest that *Dicrocerus* featured a higher growth rate than the other "stem-cervid" *Procervulus* and than the Middle Miocene *Euprox*. While growth rate was shown to be strongly correlated to body size, that of *Dicrocerus* was found as particularly high (slightly above the confidence interval of the phylogenetically-informed regression), documenting diversity in the early evolution of life history traits of the Cervidae.

## Acknowledgements

Christine Argot (MNHN), Loïc Costeur (NMB), and Shoji Hayashi and Hiroyuki Taruno (Osaka Museum of Natural History) are warmly thanked for granting access to the collections under their care and for their assistance. We thank Sergio Soares for his preliminary work on the *Dicrocerus* material. Finally, Loïc Costeur, Grégoire Métais, and a third anonymous reviewer are acknowledged, as well as the editor, Michel Laurin, for the improvement they brought the manuscript. This work was supported by Swiss National Fund SNF 31003A_149605 to M. R. Sánchez-Villagra and 31003A_149506 to T. M. Scheyer.

## Appendix A. Supplementary data

Supplementary data associated with this article can be found, in the online version, at http://dx.doi.org/10.1016/j.crpv.2015.07.001.

## References

Azanza, B., 1993. Sur la nature des appendices frontaux des cervidés (Artiodactyla, Mammalia) du Miocène inférieur et moyen. Remarques sur leur systématique et leur phylogénie. C. R. Acad. Sci. Paris, Ser. II 316, 1163–1169.

Azanza, B., DeMiguel, D., Andrés, M., 2012. The antler-like appendages of the primitive deer *Dicrocerus elegans*: morphology, growth cycle, ontogeny, and sexual dimorphism. Estud. Geol. 67, 579–602.

Chinsamy-Turan, A., 2005. The Microstructure of Dinosaur Bone: Deciphering Biology with Fine-scale Techniques. Hopkins University Press, Baltimore.

Costeur, L., Guérin, C., Maridet, O., 2012. Paléoécologie et paléoenvironnement du site miocène de Sansan. In: Mammifères de Sansan. Mem. Muséum National d'Histoire Naturelle, pp. 661–693.

DeMiguel, D., Azanza, B., Morales, J., 2014. Key innovations in ruminant evolution: a paleontological perspective. Integr. Zool. 9, 412–433.

DeMiguel, D., Fortelius, M., Azanza, B., Morales, J., 2008. Ancestral feeding state of ruminants reconsidered: earliest grazing adaptation claims a mixed condition for Cervidae. BMC Evol. Biol. 8, 13.

Francillon-Vieillot, H., Buffrénil, V., de Castanet, J., Géraudie, J., Meunier, F.J., Sire, J.-Y., Zylberberg, L., de Ricqlès, A., 1990. Microstructure and mineralization of vertebrate skeletal tissues. In: Carter, J.G. (Ed.), Skeletal Biomineralization: Patterns. Processes and Evolutionary Trends, 1. Van Nostrand Reinhold, New York, pp. 471–530.

Gentry, A.W., 1994. The Miocene differentiation of old world Pecora (Mammalia). Hist. Biol. 7, 115–158.

Gentry, A.W., Rössner, G.E., Heizmann, E.P.J., 1999. Suborder Ruminantia. In: Rössner, G.E., Heissig, K. (Eds.), The Miocene Land Mammals of Europe. Verlag Dr. Friedrich Pfeil, München, pp. 225–258.

Ginsburg, L., 2011. The Early Burdigalian (MN3; Miocene) large mammals from Estrepouy (Aquitaine basin, France): an updated faunal list. Estud. Geol. 67, 411–417.

Ginsburg, L., Azanza, B., 1991. Présence de bois chez les femelles du cervidé miocène *Dicrocerus elegans* et remarques sur le problème de l'origine du dimorphisme sexuel sur les appendices frontaux des Cervidés. C.R. Acad. Sci. Paris Ser.II 213, 121–126.

Hassanin, A., Delsuc, F., Ropiquet, A., Hammer, C., Jansen Van Vuuren, B., Matthee, C., Ruiz-Garcia, M., Catzeflis, F., Areskoug, V., Nguyen, T.T., Couloux, A., 2012. Pattern and timing of diversification of Cetartiodactyla (Mammalia, Laurasiatheria), as revealed by a comprehensive analysis of mitochondrial genomes. C.R. Biologies 335, 32–50.

Josse, S., Moreau, T., Laurin, M., 2006. Stratigraphic tools for Mesquite. http://mesquiteproject.org/packages/stratigraphicTools/.

Klevezal, G.A., 1996. Recording Structures of Mammals. Determination of Age and Reconstruction of Life History. Balkema Publishers, Rotterdam.

Kolb, C., Scheyer, T.M., Lister, A.M., Azorit, C., de Vos, J., Schlingemann, M.A., Rössner, G.E., Monaghan, N.T., Sánchez-Villagra, M.R., 2015a. Growth in fossil and extant deer and implications for body size and life history evolution. BMC Evol. Biol. 15, 1–15.

Kolb, C., Scheyer, T.M., Veitschegger, K., Forasiepi, A.M., Amson, E., van der Geer, A., Hayashi, S., van den Hoek Ostende, L.W., Sánchez-Villagra,

M.R., 2015b. Mammalian bone palaeohistology: new data and a survey. PeerJ Prepr. 3, e1405.
Köhler, M., Marín-Moratalla, N., Jordana, X., Aanes, R., 2012. Seasonal bone growth and physiology in endotherms shed light on dinosaur physiology. Nature 487, 358–361.
Laurin, M., 2004. The evolution of body size. Cope's rule and the origin of amniotes. Syst. Biol. 53, 594–622.
Laurin, M., Canoville, A., Germain, D., 2011. Bone microanatomy and lifestyle: a descriptive approach. C. R. Palevol 10, 381–402.
Lister, A.M., Edwards, C.J., Nock, D.A.W., Bunce, M., van Pijlen, I.A., Bradley, D.G., Thomas, M.G., Barnes, I., 2005. The phylogenetic position of the "giant deer" *Megaloceros giganteus*. Nature 438, 850–853.
Maddison, W.P., Maddison, D.R., 2011. Mesquite: a modular system for evolutionary analysis. Version 2. 75. http://mesquiteproject.org.
Midford, P., Garland Jr., T., Maddison, W., 2011. PDAP Package of Mesquite. Version 1.16. http://mesquiteproject.org/pdap_mesquite/index.html.
Padian, K., Lamm, E.-T., 2013. Bone histology of fossil tetrapods: advancing methods, analysis, and interpretation. University of California Press, Berkley.
Peigné, S., Sen, S., 2012. Mammifères de Sansan, 203. Mem. Muséum National d'Histoire Naturelle, Paris.
Ponton, F., Elzanowski, A., Castanet, J., Chinsamy, A., Margerie, E., de Ricqlès, A., de Cubo, J., 2004. Variation of the outer circumferential layer in the limb bones of birds. Acta Ornithol. 39, 137–140.
Quemeneur, S., Buffrénil, V., de Laurin, M., 2013. Microanatomy of the amniote femur and inference of lifestyle in limbed vertebrates. Biol. J. Linn. Soc. 109, 644–655.
Solounias, N., Moelleken, S.M.C., 1994. Differences in diet between two archaic ruminant species from Sansan, France. Hist. Biol. 7, 203–220.
Stuart, A.J., Kosintsev, P.A., Higham, T.F.G., Lister, A.M., 2004. Pleistocene to Holocene extinction dynamics in giant deer and woolly mammoth. Nature 431, 684–689.
Van Der Geer, A.A.E., Lyras, G., de Vos, J., Dermitzakis, M., 2010. Evolution of Island Mammals. Adaptation and Extinction of Placental Mammals on Islands. Blackwell publishing, Chichester.
Vislobokova, I.A., 2013. Morphology, taxonomy, and phylogeny of megacerines (Megacerini, Cervidae, Artiodactyla). Paleontol. J. 47, 833–950.

## SUPPLEMENTARY INFORMATION

# Growth and life history of Middle Miocene deer (Mammalia, Cervidae) based on bone histology

Authors: Amson E., Kolb C., Scheyer T. M., Sánchez-Villagra M. R.

- Estimations of relative position of each thin-section, using *Muntiacus muntjak* (ZIUK 7994) as basis for the cross-multiplications.

- Nexus file containing the timetree of the sampled cervids and associated data on their growth rates and femoral anteroposterior diameter (proxy for body size) is available

**Estimations of relative position of each thin-section, using *Muntiacus muntjak* (ZIUK 7994) as basis for the cross-multiplications.**

| ***Dicrocerus*** | | | | | | | | | |
|---|---|---|---|---|---|---|---|---|---|
| **Humerus** | Pr W | W at distal condyles | D just distal to head | Head to section L | Di trochlea to section | PD (head to distal trochlea) L | est. PD L | position from head to section | position from Di trochlea to section |
| Sa7341 | 34.03 | | | 49.81 | | | 132.02 | **0.38** | |
| Sa7343 | | | 34.84 | 63.50 | | | 156.72 | **0.41** | |
| Sa7330 | | 28.98 | | | 55.89 | | 131.81 | | **0.42** |
| | | | | | | | | | |
| *Muntiacus* (ZIUK 7994) | 26.32 | 22.45 | 22.70 | | | 102.11 | | | |
| | | | | | | | | | |
| **Radius** | Pr W | | | Pr end to section L | | PD (median plane) L | est. PD L | position from head to section | |
| Sa2470 | 26.79 | | | 53.82 | | | 129.78 | **0.41** | |
| Sa2453 | 27.57 | | | 70.14 | | | 133.55 | **0.53** | |
| Sa7063 | 25.59 | | | 40.47 | | | 123.96 | **0.33** | |
| | | | | | | | | | |
| *Muntiacus* (ZIUK 7994) | 19.77 | | | | | 95.77 | | | |
| | | | | | | | | | |
| **Femur** | L from fovea capitis to 3rd trochanter | W at distal condyles | | Head to section L | Di trochlea to section | PD (median plane) L | est. PD L | position from head to section | position from Di trochlea to section |
| Sa6877 | 41.91 | | | 97.85 | | | 177.91 | **0.55** | |
| Sa6889 | | 37.59 | | | 58.06 | | 175.51 | | **0.33** |
| | | | | | | | | | |
| *Muntiacus* (ZIUK 7994) | 29.18 | 26.53 | | | | 123.87 | | | |
| | | | | | | | | | |
| **Tibia** | D at tibial tuberosity | Di W | | Tibial tuberosity to section | Di trochlea to section | PD (median plane) L | est. PD L | position from head to section | position from Di trochlea to section |
| Sa6910 | 46.12 | | | 145.90 | | | 233.15 | **0.63** | |
| Sa8163 | | 30.15 | | | 76.67 | | 221.79 | | **0.35** |
| Sa6917 | | 30.00 | | | 73.25 | | 220.68 | | **0.33** |
| | | | | | | | | | |
| *Muntiacus* (ZIUK 7994) | 29.83 | 20.50 | | | | 150.80 | | | |

| ***Euprox*** | | | | | | | | | |
|---|---|---|---|---|---|---|---|---|---|
| **Femur** | L from fovea capitis to 3rd trochanter | W at distal condyles | | Head to section L | Di trochlea to section | PD (median plane) L | est. PD L | position from head to section | position from Di trochlea to section |
| Sth.1281 | 39.50 | | | 10.5 | | 20.97 | | 0.50 | |

Abbreviations: **D**, depth; **Di**, distal; **est**., estimated; **PD**, proximodistal; **Pr**, proximal; **W**, width.

**Nexus file containing the timetree of the sampled cervids and associated data on their growth rates and femoral anteroposterior diameter (proxy for body size).**

Available at:

http://www.sciencedirect.com/science/article/pii/S1631068315001244

# CHAPTER 5

## The constraint of size on the mid-diaphysis of long bones - the case of deer

Authors: Amson E. and Kolb C.
In preparation.
Contributions: EA and CK conceived and designed the study/experiments, EA performed the experiments, collected data, interpreted results, drafted the manuscript, and prepared figures/tables, CK collected data and interpreted results, both authors contributed to the final interpretation and editing of the manuscript. Both authors read and approved the final manuscript.

# The constraint of size on the mid-diaphysis of long bones - the case of deer

Eli Amson* and Christian Kolb

Paläontologisches Institut und Museum der Universität Zürich, Karl Schmid-Strasse 4,
Zürich, CH-8006, Switzerland

* Corresponding author: eli.amson@pim.uzh.ch

## ABSTRACT

How skeletal elements scale to size is a fundamental question in biology. Previous examinations have discovered general principles, using a broad sampling to encompass a wide range of body sizes. But to discover the scaling of bones it is necessary to consider the effect of confounding factors related to different lifestyles. Here, we study the mid-diaphyseal structure of limb long bones, focusing our comprehensive sampling on a mammalian clade that comprises various body sizes but a relatively uniform lifestyle, the Cervidae. None of the compactness parameters scaled allometrically in any of their bones. Positive allometry was found in femoral cross-sectional shape, indicating greater directional bending rigidity in large-sized taxa. Furthermore, the relative cortical thickness (P parameter) is more constrained in large-sized taxa. The values of this parameter being centred around a mass-saving biomechanical optimum, tubular bones of large-sized terrestrial animals are more intensively selected for an energy-saving mid-diaphyseal structure.

Keywords: Allometry; bone compactness; Cervidae; cortical thickness; cross-sectional shape; long bone.

## INTRODUCTION

Body size being one of the most influential parameters over the physiology and morphology of organisms, allometric studies have taken a central part in biology (Klingenberg, 1998). More particularly, in terrestrial vertebrates, an array of studies tackles the structure of the main supporting structures, i.e., long bones. These studies notably focused on bone general proportions (Alexander et al., 1979), curvature (Bertram and Biewener, 1992), cross-sectional geometry at mid-diaphysis (Currey and Alexander, 1985), and, more recently, architecture of the epiphyseal trabeculae (Doube et al., 2011; Swartz et al., 1998) and bone compactness parameters (Houssaye et al., 2016). These examples use extensive samplings of amniotes and are able to propose scaling patterns throughout broad groups. While the parameters used in those studies were shown to scale either isometrically or allometrically to body size, it was also emphasized that the animals' locomotor limb posture was of great importance to maintain viable locomotor stresses (Biewener, 1989).

Here we restrict our sample to deer, the Cervidae. In choosing this clade that comprises a wide range of body sizes [*ca.* 10 kg for *Pudu puda* (Molina, 1782), the Pudu (Tacutu et al., 2013), and up to *ca.* 600 kg for *Alces alces* (Linnaeus, 1758), the Elk (Franzmann, 1981)] but uniform lifestyle, we endeavour to control for potential functional adaptations that are known to correlate with bone microstructure and cross-sectional geometry of amniotes with different lifestyles, posture,and behaviour (e.g., Bertram and Biewener, 1992; Biknevicius, 1993; Houssaye et al., 2016; Meier et al., 2013; Quemeneur et al., 2013). In addition, the well-resolved phylogenetic relationships, rich fossil record and dates of origins within cervids allow taking into account phylogeny in our statistical approach.We are consequently able to propose a test for the presence of a relationship of body size itself with bone inner structure.

## MATERIAL AND METHODS

### Section acquisition

All five tribes and most widely recognized extant genera of cervids were sampled. We sampled the femur, tibia, humerus, and radius of skeletally mature individuals. Extinct taxa were sampled as well, bringing the number of species sampled to 25 and the number of elements sampled to 93 (Table S1). No method was used to define sample size a priori. Mid-diaphyseal cross-sections were acquired either by conventional thin-sectioning (Padian and

Lamm, 2013), or CT-scanning (UniversitätsSpital Zürich, Siemens SOMATOM Force, planar resolution of 0.098-0.480 mm depending on the size of the specimen). In the latter case, and for each bone, a raw DICOM stack was imported in the Fiji package (Schindelin et al., 2012) with the Bio-formats plugin (Linkert et al., 2010) and reoriented (using successive re-slicings) in order to obtain a transverse cross-section at mid-diaphysis.The sections were then binarized with Photoshop®.The maximum diameter of the sections were used as body size proxies (Quemeneur et al., 2013).

### Bone compactness parameters

In order to study bone inner structure, we used Bone Profiler 4.5.8 (Girondot and Laurin, 2003). This program characterizes cross-sections measuring values of long-studied parameters (global compactness, relative cortical thickness; see below), as well as new ones. The global compactness of a section (GC, or bone fraction) is simply obtained measuring the area occupied by bone and dividing it by the whole sectional area. Bone Profiler also captures other parameters related to bone internal structure indefining a compactness profile. By using a mean value calculated splitting the section in 51 zones and excluding outlying values (Girondot and Laurin, 2003), Bone Profiler is able to give for each parameter a representative value based on the whole cross-section. Furthermore, sections missing small fragments can be used as well. The compactness profile is computed as a sigmoidal function C, which gives the compactness according to d the distance from the centre (Girondot and Laurin, 2003):

$$C(d) = \frac{1}{1 + e^{\left({}^{1}/_{S}\right)(P-d)}}(Max - Min) + Min$$

where the compactness parameters are S, the reciprocal of the slope at the point of inflexion, P, the position of the curve inflection point on the x-axis, which is the distance to the centre,and Min and Max,the minimum and maximum asymptotes of the curve, respectively (Fig. 1). The S parameter reflects the relative width of the transition zone between the medulla and the cortical regions. P reflects the position of the transition area between the medulla and the cortex. P is exactly the same as the classical K parameter, i.e., the ratio between the radius of the whole bone and the medullary cavity thickness, defined by Currey and Alexander (1985), and used in numerous later studies (e.g., Bernáth et al., 2004; Demes et al., 1991; Margerie et al., 2005). The R/tparameter (Currey and Alexander, 1985), the ratio between the radius of the whole bone and the cortical thickness, has a proportional relationship with K and hence with P as well. Min and Max reflect the compactness at the centre and periphery, respectively.

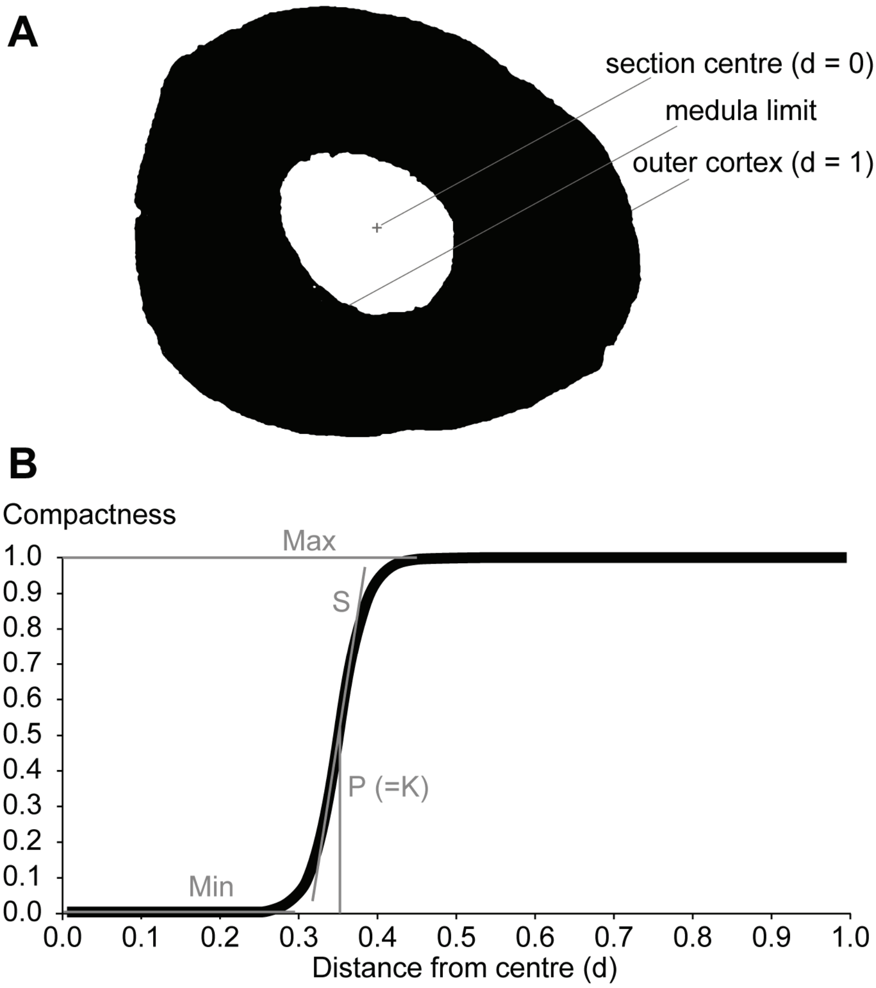

Figure 1. **Bone compactness parameters of a mid-diaphyseal section of the tibia of the extinct Cretan deer (*Candiacervus ropalophorus*, PIMUZ A/V 5188).** (A) Binarized section (black represents bone, and white the vacuities). Note the classical tubular structure consisting in a free medullary cavity and a compact cortex. (B) Compactness profile, a sigmoidal function describing the compactness along the radius of the bone section. In this example, the compactness parameters have the following values: S = 0.017; P = 0.35; Min = 0; Max = 1.

Section geometry

As second moment area provides an approximation of bending rigidity (Ruff et al., 2006), another relevant parameter for our study is the cross-sectional shape (CSS, or circularity index).We used the BoneJ plugin (Doube et al., 2010) of the Fiji package (Schindelin et al., 2012) to measure the second moment of areas of the section around its major and minor axes, respectively Imax and Imin. CSS is the ratio of Imax over Imin, and has therefore no dimension.

## Statistical analyses

In order to test for the presence of a significant phylogenetic signal, a timetree (a phylogenetic tree calibrated in time) was built (Fig.2) using a published one (Amson et al., 2015) augmented with several taxa according to published phylogeny and dates of origin of the clades (Hassanin et al., 2012; Vislobokova, 2013).

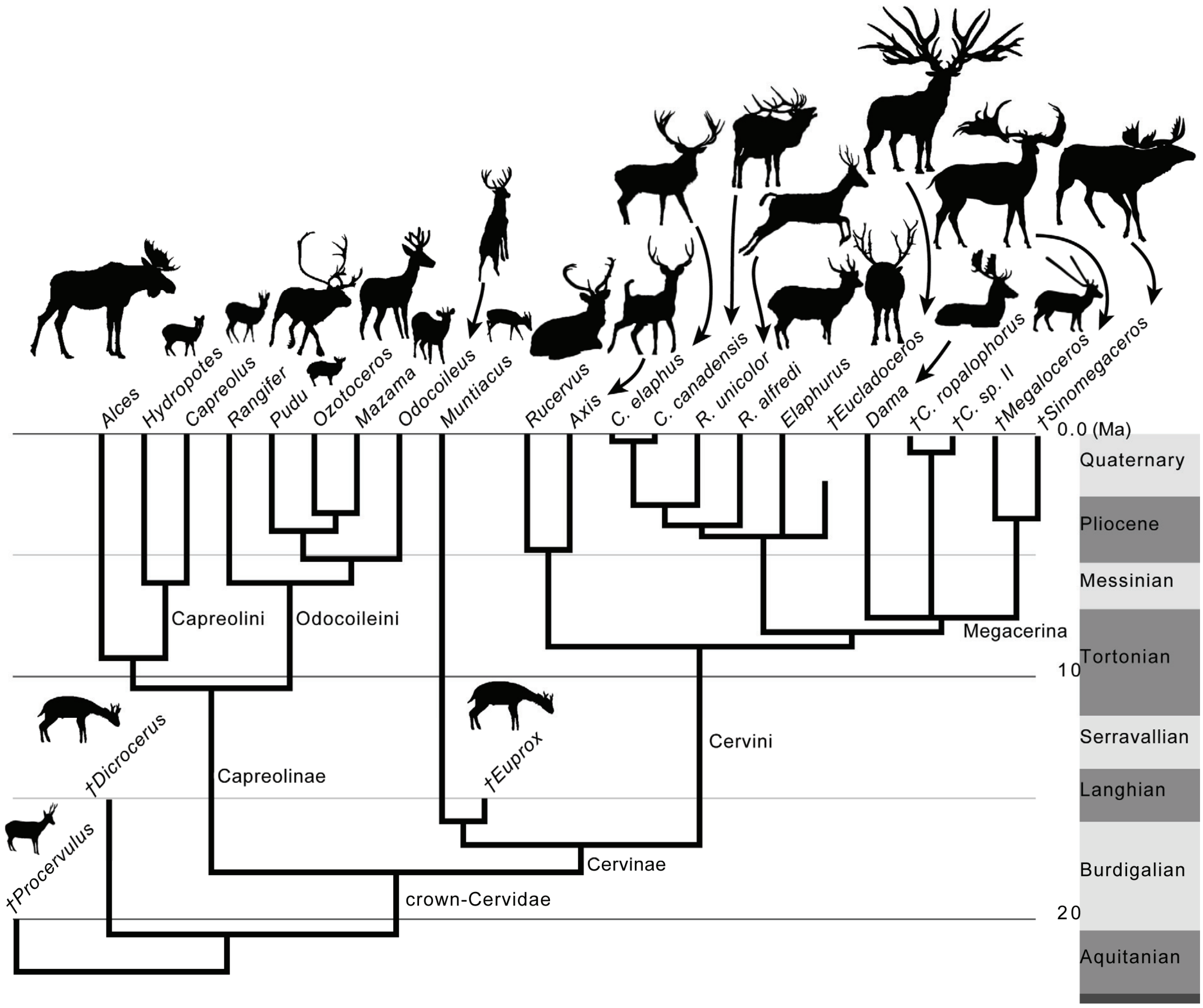

Figure 2. **Timetree of the cervids sampled for the present study.** The tree was elaborated with Mesquite 3.02 (Maddison and Maddison, 2011) and its Stratigraphic Tools module (Josse et al., 2006).

Nexus files containing the timetrees and matrices of bone compactness parameters and CSS (with in each case the associated bone maximum diameters) are given as SOM 1 and 2, respectively. Tests for the presence of a phylogenetic signal in the different parameters were performed using Mesquite 3.02 (Maddison and Maddison, 2011). According to previously published procedure (Laurin, 2004; Quemeneur et al., 2013), they consist in the comparison of the squared length of the reconstructed parameter to those of 10000 trees in which the terminal taxa were randomly reshuffled. The p-value of each test will be the number of trees shorter than the initial tree divided by 10000.As the CSS parameter can only be determined for complete sections, the tests for this parameter and the corresponding bone maximum diameters (used as a body size proxy) were performed with sub-trees excluding the fragmentary specimens.Phylogenetically uninformed tests were performed with Past 3.04 (Hammer et al., 2001).

## RESULTS AND DISCUSSION

All the bones sampled exhibit the classical tubular structure of terrestrial vertebrates, i.e., a free medullary cavity and a compact cortex (Fig. 1). The P parameter will therefore reflect the relative position of the inner limit of the cortex. Furthermore, the compactness at the centre, Min, will be close to zero, and the compactness at the periphery, Max, close to one. This is what is essentially featured by the parameters of all taxa. Because the spongiosa is virtually absent in the mid-diaphyseal region, the S parameter is close to zero in all taxa as well. For this reason, among bone compactness parameters, only the P parameter and GC are substantially variable in cervids, and will be further discussed. All the values of bone compactness parameters and section geometry parameters are given in SOM 3 and SOM 4, respectively.

We have tested for the presence of a phylogenetic signal in the maximum diameter (used as a body size proxy; for both the bone compactness parameter and section geometry datasets), P parameter, GC, and CSS of each of the bones studied. None of the tests concluded in the presence of a significant phylogenetic signal, except for the maximum diameter of the radius in the test on a sub-tree for the available CSS data (Tables S2, S3). This justifies the use of phylogenetically uninformed tests.

Cervids display quiet disparate values of the P parameter, ranging from 0.33 (two thirds of the sectional area is occupied by the cortex) to 0.73 (roughly one fourth of the sectional area is occupied by the cortex). None of the bones feature significant allometric scaling of their P parameter with the maximum diameter, used as the body size proxy (phylogenetically uninformed regressions, p-values > 0.05). Since there is no significant difference of the maximum diameter among the different bones (Kruskal-Wallis test, p-value > 0.8), all the values of the P parameter measured were grouped and plotted against the maximum diameter in order to describe the whole disparity of the cortical thickness within the Cervidae (Fig.3). Again, no significant allometric scaling can be found in the whole dataset. However, there is a decrease of the disparity in the large-sized cervids when compared to the smaller ones. This is shown by a comparison of the variances between two groups formed by the small-bodied half and the large-bodied half of the dataset. Of 0.011 and 0.005 respectively, the variances of the two groups are significantly different (Levene's test, p-value = 0.004 < Holm–Bonferroni six tests adjusted p-value$_{0.05}$ =0.008). However, the means of these groups, of 0.554 and 0.599 respectively, are not significantly different (Mann-Whitney U test, p-value = 0.064), the mean of the whole dataset being 0.577. A noteworthy large-bodied taxon outlying in having high values of P is *Alces*, the Elk (confirmed by the inclusion of two specimens, representing five bones; Fig. 3).In other words, it displays long bones with relatively thin cortices.

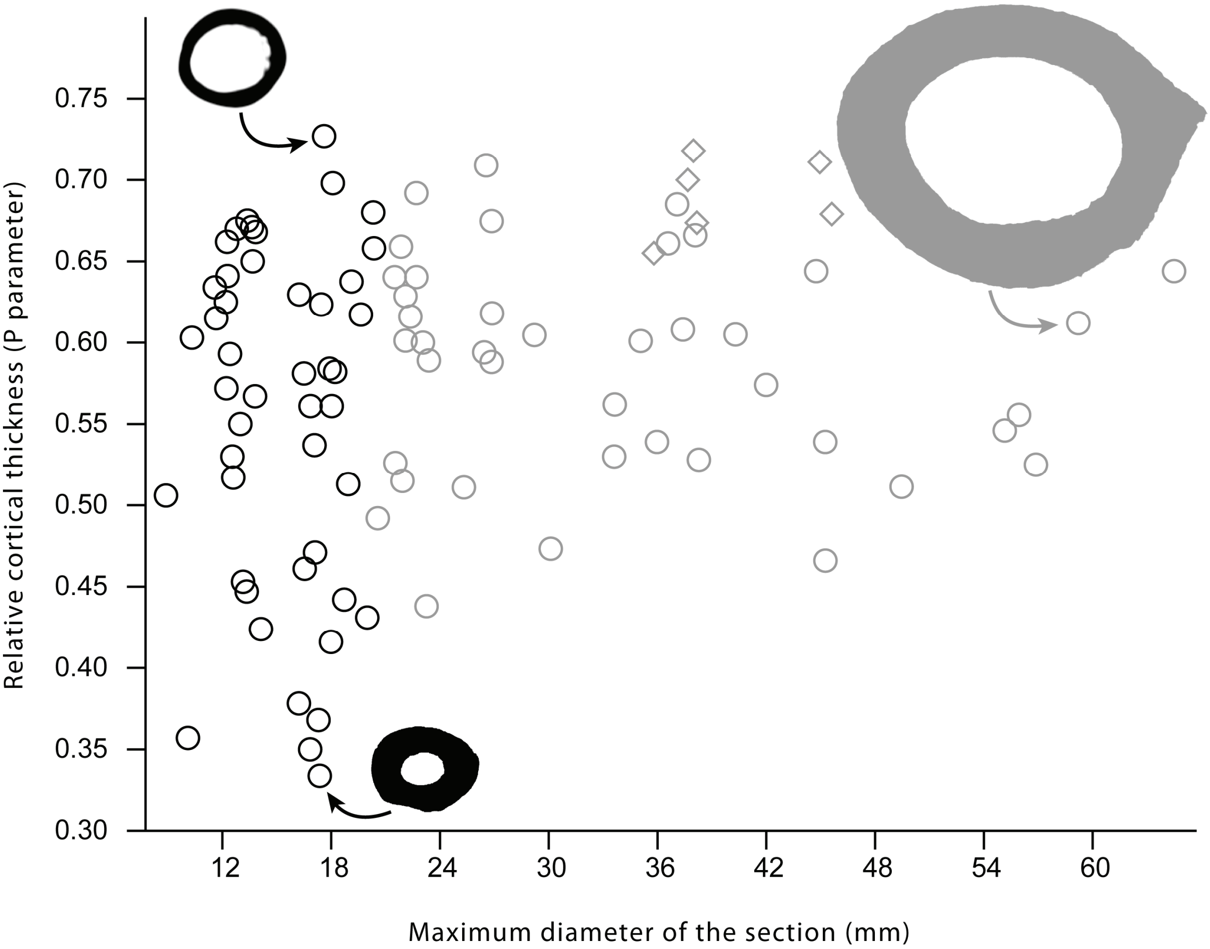

Figure 3. **Relative cortical thickness (P = K parameter) plotted against the maximum diameter (body size proxy).** The small-bodied half of the dataset is in black (n = 46), the large-bodied half is in grey (n = 47). The variances of the two groups are significantly different (Levene's test, p-value =

0.004). The data points of *Alces* (the Elk), a notable outlier, are figured as diamonds. Three examples of mid-diaphyseal cross-sections are shown to scale near their corresponding data points.

The GC values range from 0.47 to 0.88. As for the P parameter, none of the bones taken individually or the whole dataset feature significant allometric scaling of the GC with the maximum bone diameter (phylogenetically uninformed regressions, p-values > 0.05). Similarly, the small-bodied half of the dataset features a greater disparity (variance = 0.012) than the large-bodied half (variance = 0.007). However, the difference is not statistically significant (Levene's test, p-value = 0.052).

The mid-diaphyseal CSS varies from 1.04 (almost perfectly annular section) to 4.22 (strongly elliptical section). The CSS of the tibia, humerus, and radius were not found as significantly scaling to body size (phylogenetically uninformed regressions, p-values > 0.05). However, the CSS of the femur displays a small but significant positive correlation to body size (log-transformed values to comply to normality test, p-value < 0.001< Holm–Bonferroni 12 tests adjusted p-value$_{0.05}$ = 0.004). The slope of the regression is significantly different from zero (the expected coefficient denoting isometry for a dimensionless parameter), indicating that the mid-diaphyseal femoral CSS scales to body size with a slight positive allometry (a = 0.21, 95% bootstrapped confidence interval = 0.10–0.31).Large-sized deer hence have significantly more elliptical (less circular) femoral mid-diaphyseal cross-section. As terrestrial locomotion implies minor torsion loads at midshaft [(Biewener, 1991); but see Margerie et al.(2005)], a more strongly defined direction of bending rigidity in the mediolateral direction – that of the major axis of femoral mid-diaphyseal cross-section – is increasingly found in larger deer. While variability of directions of loading is considered as restricted by long bone longitudinal curvature, Bertram and Biewener(1992) found a decrease of the latter parameter with increasing size in the radius (and to a lesser extent in the tibia), indicative of greater load carrying capacity in large-sized taxa. The femora of deer showing the opposite pattern, it appears that directional loading in that case impacts more cross-sectional shape than pure load carrying. It is noteworthy that a study including a broad vertebrate sampling similarly found a positive significant allometry in the CSS of the femur and not in the other bones sampled (Houssaye et al., 2016). Since there is no significant difference of the maximum diameter among the different bones (Kruskal-Wallis test, p-value > 0.6), we have also tested for a difference of variance in the CSS of the whole dataset (no significant difference is found in the mean of the small-bodied and large-bodied groups either). As with the GC, the small-bodied half group has a greater variance than the large-bodied group (0.55 and 0.36, respectively), but the difference was not found as significant (Levene's test, p-value = 0.185).

Using a broad dataset of terrestrial mammals and birds, it was previously argued that the relative cortical thickness [referred to as the R/t ratio in the initial publication; (Currey and Alexander, 1985)] scales with significant negative allometry to body mass in the femur, metatarsal (or tarsometatarsus of birds), and metacarpal (or carpometacarpus of birds), but not in the tibia (or tibotarsus of birds) or other composite bones (Currey and Alexander, 1985). Regarding the bones in which allometry was demonstrated, we cannot draw a similar conclusion from our analysis of the relative cortical thickness in the Cervidae.This is unlikely due to our smaller sample size and the more restricted range of body sizes described by the sampled deer, because a recent analysis, which has used a broad sample of vertebrates, has found either no or a weak correlation of the compactness parameters in the bones sampled therein, namely the humerus, femur, and rib (Houssaye et al., 2016).

Nevertheless, our results do stand out in finding a relationship between body size and mid-diaphyseal cortical thickness in deer, a clade that combines a wide range of body sizes and a uniform lifestyle. Indeed, we found that the P parameter of large-sized cervids is significantly more constrained than that of the small-sized members of the clade.The sampled specimens of Elk are outliers, as a relatively thicker cortex is usually seen in deer of this body size. The Elk is long-legged, which is regarded as an adaptation for stilt-locomotion (Breda, 2008). The low cortical thickness of this taxon appears to reflect the elongation of the diaphyses of its long bones.The P parameter values of our whole dataset are centred around 0.577. Interestingly, the optimal value for impact loading (withstand a load suddenly applied) or ultimate strength (maximum stress that the bone can withstand before breaking) of this parameter was previously determined to be 0.55 in tubular bones of minimum mass [mentioned as K in the initial publication; (Currey and Alexander, 1985)]. The lower disparity found in large cervids suggests that mass saving is more intensively selected in those taxa than in small members of the clade. Even small differences in bone mass were argued to be selectively important, because they imply a non-negligible difference of energy cost (Currey, 2003; Currey and Alexander, 1985). It was previously argued that "the function of the skeleton is not purely mechanical, and therefore its mass and morphology represent a compromise between different physiological demands, of which mechanical competence is only one" (Ruff et al., 2006). Our results emphasize the importance of an energy-saving mechanical function in the tubular bones of large-sized cervids, which is most likely true for other terrestrial vertebrates as well.

## ACKNOWLEDGEMENTS

We thank Hatem Alkadhi (UniversitätsSpital Zürich) for performing the CT-scanning. Christine Argot, Christine Lefèvre, and Joséphine Lesur (Muséum national d'Histoire naturelle, Paris), Emma Bernard (Natural History Museum London), Christiane Funk (Museum für Naturkunde, Berlin),Loïc Costeur (Naturhistorisches Museum Basel), John de Vos (Naturalis Biodiversity Center, Leiden), Heinz Furrer, Christian Klug, and Winand Brinkmann (Paläontologisches Institut und Museum der Universität Zürich), Shoji Hayashi and Hiroyuki Taruno (Osaka Museum of Natural History), Renate Lücht and Heiner Luttmann (Zoologisches Institut der Universität Kiel), Nigel Monaghan (National Museum of Ireland, Natural History), Barbara Oberholzer (Zoologisches Museum der Universität Zürich), Gertrud E. Rössner (Bayerische Staatssammlung für Paläontologie und Geologie), Christian Stauffer (Wildnispark Zürich), and Frank Zachos and Alexander Bibl (Naturhistorisches Museum Wien) are acknowledged for granting us access to the collections under their care. Marcelo R. Sánchez-Villagra and Juan Carillo (PIMUZ) are thanked for fruitful discussions. Stephan Spiekman (Leiden University) and Philipp Münst (University of Zurich) are thanked for their preliminary data acquisition and analyses.We finally thank Andrew Biewener (Harvard University) for the substantial improvements he brought to the analysis and manuscript.

## COMPETING INTERESTS

No competing interests declared.

## AUTHOR CONTRIBUTIONS

E.A. and C.K. conceived and designed the study, EA collected data, interpreted results and drafted the manuscript; C.K. collected data and interpreted results. Both authors participated to the development of the manuscript and gave final approval for publication.

## FUNDING

Both authors were funded by the Swiss National Fund SNF 31003A_149605 granted to M. R. Sánchez-Villagra.

## REFERENCES

**Alexander, R. M., Jayes, A. S., Maloiy, G. M. O. and Wathuta, E. M.** (1979). Allometry of the limb bones of mammals from shrews (*Sorex*) to elephant (*Loxodonta*). *J. Zool.***189**, 305–314.

**Amson, E., Kolb, C., Scheyer, T. M. and Sánchez-Villagra, M. R.** (2015). Growth and life history of Middle Miocene deer (Mammalia, Cervidae) based on bone histology. *Comptes Rendus – Palevol***14**, 637–645.

**Bernáth, B., Suhai, B., Gerics, B., Csorba, G., Gasparik, M. and Horváth, G.** (2004). Testing the biomechanical optimality of the wall thickness of limb bones in the red fox (*Vulpes vulpes*). *J. Biomech.***37**, 1561–1572.

**Bertram, J. E. A. and Biewener, A. A.** (1992). Allometry and curvature in the long bones of quadrupedal mammals. *J. Zool.***226**, 455–467.

**Biewener, A. A.** (1989). Scaling body support in mammals: limb posture and muscle mechanics. *Science.***245**, 45–48.

**Biewener, A. A.** (1991). Musculoskeletal design in relation to body size. *J. Biomech.***24**, 19–29.

**Biknevicius, A. R.** (1993). Biomechanical scaling of limb bones and differential limb use in caviomorph rodents. *J. Mammal.***74**, 95–107.

**Breda, M.** (2008). Palaeoecology and palaeoethology of the Plio-Pleistocene genus *Cervalces* (Cervidae, Mammalia) in Eurasia. *J. Vertebr. Paleontol.***28**, 886–899.

**Currey, J. D.** (2003). How well are bones designed to resist fracture? *J. Bone Miner. Res.***18**, 591–598.

**Currey, J. D. and Alexander, R. M.** (1985). The thickness of the walls of tubular bones. *J. Zool.***206**, 453–468.

**Demes, B., Jungers, W. L. and Selpien, K.** (1991). Body size, locomotion, and long bone cross-sectional geometry in indriid primates. *Am. J. Phys. Anthropol.***86**, 537–547.

**Doube, M., Kłosowski, M. M., Arganda-Carreras, I., Cordelières, F. P., Dougherty, R. P., Jackson, J. S., Schmid, B., Hutchinson, J. R. and Shefelbine, S. J.** (2010). BoneJ: Free and extensible bone image analysis in ImageJ. *Bone***47**, 1076–1079.

**Doube, M., Klosowski, M. M., Wiktorowicz-Conroy, A. M., Hutchinson, J. R. and Shefelbine, S. J.** (2011). Trabecular bone scales allometrically in mammals and birds. *Proc. Biol. Sci.***278**, 3067–73.

**Franzmann, A. W.** (1981). *Alces alces*. *Mamm. Species***154**, 1–7.

**Girondot, M. and Laurin, M.** (2003). Bone profiler: a tool to quantify, model, and statistically compare bone-section compactness profiles. *J. Vertebr. Paleontol.***23**, 458–461.

**Hammer, Ø., Harper, D. A. T. and Ryan, P. D.** (2001). Paleontological statistics software package for education and data analysis. *Palaeontol. Electron.***4**, 1–9.

**Hassanin, A., Delsuc, F., Ropiquet, A., Hammer, C., Jansen Van Vuuren, B., Matthee, C., Ruiz-Garcia, M., Catzeflis, F., Areskoug, V., Nguyen, T. T., et al.** (2012). Pattern and timing of diversification of Cetartiodactyla (Mammalia, Laurasiatheria), as revealed by a comprehensive analysis of mitochondrial genomes. *C. R. Biol.***335**, 32–50.

**Houssaye, A., Waskow, K., Hayashi, S., Lee, A. H. and Hutchinson, J. R.** (2016). Biomechanical evolution of solid bones in large animals: a microanatomical investigation. *Biol. J. Linn. Soc.***117,** 350-371.

**Josse, S., Moreau, T. and Laurin, M.** (2006). Stratigraphic tools for Mesquite. Available at: http://mesquiteproject.org/packages/stratigraphicTools/.

**Klingenberg, C. P.** (1998). Heterochrony and allometry: the analysis of evolutionary change in ontogeny. *Biol. Rev.***73**, 79–123.

**Laurin, M.** (2004). The evolution of body size, Cope's rule and the origin of amniotes. *Syst. Biol.***53**, 594–622.

**Linkert, M., Rueden, C. T., Allan, C., Burel, J. M., Moore, W., Patterson, A., Loranger, B., Moore, J., Neves, C., MacDonald, D., et al.** (2010). Metadata matters: Access to image data in the real world. *J. Cell Biol.***189**, 777–782.

**Linnaeus, C. von** (1758). Systema Naturae, edition X, vol. 1 (Systema naturae per regna tria naturae, secundum classes, ordines, genera, species, cum characteribus, differentiis, synonymis, locis. Tomus I. Editio decima, reformata). *Holmiae Salvii***824**.

**Maddison, W. P. and Maddison, D. R.** (2011). Mesquite: a modular system for evolutionary analysis. Version 3.02. http://mesquiteproject.org.

**Margerie, E. de, Sanchez, S., Cubo, J. and Castanet, J.** (2005). Torsional resistance as a principal component of the structural design of long bones: Comparative multivariate evidence in birds. *Anat. Rec. - Part A***282A**, 49–66.

**Meier, P. S., Bickelmann, C., Scheyer, T. M., Koyabu, D. and Sánchez-Villagra, M. R.** (2013). Evolution of bone compactness in extant and extinct moles (Talpidae): exploring humeral microstructure in small fossorial mammals. *BMC Evol. Biol.***13**, 55.

**Molina, J. I.** (1782). Saggio sulla storia naturale del Chili. Stamperia di S. Tommaso d'Aquino. Bologna.

**Padian, K. and Lamm, E.-T.** (2013). Bone histology of fossil tetrapods : advancing methods, analysis, and interpretation.p. 285. Berkley: University of California Press.

**Quemeneur, S., Buffrénil, V. de and Laurin, M.** (2013). Microanatomy of the amniote femur and inference of lifestyle in limbed vertebrates. *Biol. J. Linn. Soc.***109**, 644–655.

**Ruff, C. B., Holt, B. and Trinkaus, E.** (2006). Who's afraid of the big bad Wolff?: "Wolff's law" and bone functional adaptation. *Am. J. Phys. Anthropol.***129**, 484–498.

**Schindelin, J., Arganda-Carreras, I., Frise, E., Kaynig, V., Longair, M., Pietzsch, T., Preibisch, S., Rueden, C., Saalfeld, S., Schmid, B., et al.** (2012). Fiji: an open-source platform for biological-image analysis. *Nat. Methods***9**, 676–682.

**Swartz, S. M., Parker, A. and Huo, C.** (1998). Theoretical and empirical scaling patterns and topological homology in bone trabeculae. *J. Exp. Biol.***201**, 573–590.

**Tacutu, R., Craig, C. T., Budovsky, A., Wuttke, D., Lehmann, G., Taranukha, D., Costa, J., Fraifeld, V. E. and De Magalhães, J.** (2013). Human Ageing Genomic Resources: Integrated databases and tools for the biology and genetics of ageing. *Nucleic Acids Res.***41**, D1027–D1033.

**Vislobokova, I. A.** (2013). Morphology, taxonomy, and phylogeny of megacerines (Megacerini, Cervidae, Artiodactyla). *Paleontol. J.***47**, 833–950.

## SUPPLEMENTARY INFORMATION

# The constraint of size on the mid-diaphysis of long bones - the case of deer

Authors: Amson E. and Kolb C.

## SUPPLEMENTARY TABLES

**Table S1.**List of specimens sampled.

**Table S2.**P-values of the tests for phylogenetic signal in bone compactness parameters.

**Table S3.** P-values of the tests for phylogenetic signal in the cross-sectional shape.

## SUPPLEMENTARY ONLINE MATERIAL

**SOM 1.**This nexus file comprises the matrices of data and timetree allowing to perform the phylogenetically-informed statistical tests on the compactness parameters and associated section diameter.

**SOM 2.** This nexus file comprises the matrices of data and timetree allowing to perform the phylogenetically-informed statistical tests on the cross-sectional shape and associated section diameter.

**SOM 3.**This MS excel file comprises all measured compactness parameters for the whole dataset.

**SOM 4.**This MS excel file comprises all measured slice geometry parameters for the whole dataset.

Table S1. List of specimens sampled.

| | Femur | Tibia | Humerus | Radius |
|---|---|---|---|---|
| *Cervus elaphus* | (Quemeneur et al., 2013) | (Kriloff et al., 2008) | (Canoville and Laurin, 2010) | (Germain and Laurin, 2005) |
| *Cervus canadensis* | MNHN.AC.1880-620 | MNHN.AC.1880-620 | MNHN.AC.1880-620 | MNHN.AC.1880-620 |
| *Dama dama* | (Quemeneur et al., 2013) | ZIUK 9630 | PIMUZ A/V 5248 | ZIUK 9630 |
| *Capreolus capreolus* | (Quemeneur et al., 2013) | (Kriloff et al., 2008) | (Canoville and Laurin, 2010) | (Germain and Laurin, 2005) |
| *Rangifer tarandus* | (Quemeneur et al., 2013) | PIMUZ A/V 5280 | (Canoville and Laurin, 2010) | - |
| *Muntiacus muntjak* | ZIUK 7994 | ZIUK 7994 | ZIUK 7994 | ZIUK 7994 |
| *Megaloceros giganteus* | NMING:F7937/4 | NMING:F22655/34 | NMING:F22655/37 | NMING:F22655/36 |
| *Candiacervus ropalophorus* | PIMUZ A/V 5195 | PIMUZ A/V 5188 | - | PIMUZ A/V 5186 |
| *Candiacervus* sp. II | PIMUZ A/V 5218 | PIMUZ A/V 5222 | PIMUZ A/V 5231 | PIMUZ A/V 5232 |
| *Sinomegaceros yabei* | OMNH QV-4068 | OMNH QV-4068 | - | - |
| *Alces alces* | ZMUZ 20242;<br>MNHN.AC.1980-74 | ZMUZ 20242 | ZMUZ 20242;<br>MNHN.AC.1980-74 | ZMUZ 20242 |
| *Pudu puda* | NMW 60135 | NMW 60135 | NMW 60135 | NMW 60135 |
| *Dicrocerus elegans* | MNHN.F.Sa6877 | MNHN.F.Sa6910 | MNHN.F.Sa7343 | MNHN.F.Sa2453 |
| *Procervulus praelucidus* | BSPG 1937 II 23226 | BSPG 1937 II 23230 | BSPG 1937 II 23234 | BSPG 1937 II 23235 |
| *Odocoileus virginianus* | ZMB_MAM8453 | ZMB_MAM8453 | ZMB_MAM8453 | ZMB_MAM8453 |
| *Ozotoceros bezoarticus* | ZMB_MAM2055 | ZMB_MAM2055 | ZMB_MAM2055 | ZMB_MAM2055 |
| *Rucervus eldii* | MNHN.AC.1937-157 | MNHN.AC.1937-157 | MNHN.AC.1937-157 | MNHN.AC.1937-157 |
| *Elaphurus davidianus* | MNHN.AC.1966-02 | MNHN.AC.1966-02 | MNHN.AC.1966-02 | MNHN.AC.1966-02 |

| | | | | |
|---|---|---|---|---|
| *Rusa alfredi* | MNHN.AC Ra-1 | MNHN.AC Ra-1 | MNHN.AC Ra-1 | MNHN.AC Ra-1 |
| *Rusa unicolor* | MNHN.AC.2013-28 | MNHN.AC.2013-28 | MNHN.AC.2013-28 | MNHN.AC.2013-28 |
| *Euprox* sp. | NMB Sth. 1281 | - | - | - |
| *Mazama gouazoubira* | NMW 1963-B 4196 | NMW 1963-B 4196 | NMW 1963-B 4196 | NMW 1963-B 4196 |
| *Eucladoceros* sp. | - | PIMUZ A/V 3311 | PIMUZ A/V 3312 | - |

**Canoville, A. and Laurin, M.** (2010). Evolution of humeral microanatomy and lifestyle in amniotes, and some comments on palaeobiological inferences. *Biol. J. Linn. Soc.***100**, 384–406.

**Germain, D. and Laurin, M.** (2005). Microanatomy of the radius and lifestyle in amniotes (Vertebrata, Tetrapoda). *Zool. Scr.***34**, 335–350.

**Kriloff, A., Germain, D., Canoville, A., Vincent, P., Sache, M. and Laurin, M.** (2008). Evolution of bone microanatomy of the tetrapod tibia and its use in palaeobiological inference. *J. Evol. Biol.***21**, 807–826.

**Quemeneur, S., Buffrénil, V. de and Laurin, M.** (2013). Microanatomy of the amniote femur and inference of lifestyle in limbed vertebrates. *Biol. J. Linn. Soc.***109**, 644–655.

Table S2. P-values of the tests for phylogenetic signal in bone compactness parameters and associated maximum diameter.

| **Femur** | p-values |
|---|---|
| Max. diameter | 0.1177 |
| P parameter | 0.6850 |
| Global compactness | 0.6368 |
| **Tibia** | |
| Max. diameter | 0.0894 |
| P parameter | 0.0595 |
| Global compactness | 0.2162 |
| **Humerus** | |
| Max. diameter | 0.7297 |
| P parameter | 0.2965 |
| Global compactness | 0.2979 |
| **Radius** | |
| Max. diameter | 0.1905 |
| P parameter | 0.4533 |
| Global compactness | 0.4647 |

Table S3. P-values of the tests for phylogenetic signal in the cross-sectional shape (CSS) and associated maximum diameter.

| **Femur** | p-values |
|---|---|
| Max. diameter | 0.1103 |
| CSS | 0.4188 |
| **Tibia** | |
| Max. diameter | 0.0206 |
| CSS | 0.6971 |
| **Humerus** | |
| Max. diameter | 0.0148 |
| CSS | 0.6009 |
| **Radius** | |
| Max. diameter | **0.0034** |
| CSS | 0.7643 |

Footnotes: After Holm–Bonferroni correction for multiple testing, only the maximum diameter of the radius features a significant phylogenetic signal (with an initial 0.05 threshold).

**SOM 1.**This nexus file comprises the matrices of data and timetree allowing to perform the phylogenetically-informed statistical tests on the compactness parameters and associated section diameter.

Available from the author of this dissertation: christian.kolb@pim.uzh.ch

**SOM 2.** This nexus file comprises the matrices of data and timetree allowing to perform the phylogenetically-informed statistical tests on the cross-sectional shape and associated section diameter.

Available from the author of this dissertation: christian.kolb@pim.uzh.ch

**SOM 3.** All measured compactness parameters for the whole dataset.

**FEMUR**

***Candiacervus ropalophorus***

| Parameter | Mean Global value | SE Global value | Mean Angular value | SD Angular value |
|---|---|---|---|---|
| Min | 1.25E-07 | 0 | 1.47E-08 | 1.48E-08 |
| Max | 0.9976082 | 0.0003216 | 0.999724 | 0.0007028 |
| S:1/Slope | 0.0175137 | 0.0002624 | 0.0035093 | 0.0020958 |
| P:transition | 0.6234761 | 0.0003595 | 0.6262197 | 0.03529 |

Global analysis

Maximum likelihood:-Ln L=608.7402

AIC=1225.48

r2=0.9987745

Observed compactness=0.602

Modeled compactness=0.602

Modeled compactness at the center=0

Modeled compactness at the periphery=0.998

R/t (Currey & Alexander 1985) : 2.6559

CDI (Castanet et al. 2000) : 0.3765

***Candiacervus* sp. II**

| Parameter | Mean Global value | SE Global value | Mean Angular value | SD Angular value |
|---|---|---|---|---|
| Min | 8.02E-08 | 4.52E-07 | 8.35E-09 | 7.68E-09 |
| Max | 0.999999 | 0 | 0.999999 | n.a. |
| S:1/Slope | 0.0132738 | 0.0001437 | 0.0032198 | 0.0015099 |
| P:transition | 0.6172567 | 0.0002306 | 0.6195051 | 0.0234126 |

Global analysis

Maximum likelihood:-Ln L=166.0431

AIC=340.0863

r2=0.9994829

Observed compactness=0.613

**TIBIA**

***Candiacervus ropalophorus***

| Parameter | Mean Global value | SE Global value | Mean Angular value | SD Angular value |
|---|---|---|---|---|
| Min | 0 | n.a. | 0 | 0 |
| Max | 1 | n.a. | 1 | 0 |
| S:1/Slope | 0.017 | n.a. | 0.003 | 0.001 |
| P:transition | 0.35 | n.a. | 0.352 | 0.032 |

Global analysis

Maximum likelihood:-Ln L=2 588.145

AIC=5 184.29

r2=0.999

Observed compactness=0.875

Modeled compactness=0.875

Modeled compactness at the center=0.

Modeled compactness at the periphery=1.

R/t (Currey & Alexander 1985) : 1.5386

CDI (Castanet et al. 2000) : 0.6499

***Candiacervus* sp. II**

| Parameter | Mean Global value | SE Global value | Mean Angular value | SD Angular value |
|---|---|---|---|---|
| Min | 2.64E-07 | 1.52E-06 | 3.70E-08 | 4.76E-08 |
| Max | 0.9998731 | 0.0000729 | 0.9999633 | 0.0002082 |
| S:1/Slope | 0.0172824 | 0.0002779 | 0.0027993 | 0.0014696 |
| P:transition | 0.3337881 | 0.0005038 | 0.336399 | 0.0303611 |

**Global analysis**

Maximum likelihood:-Ln L=60.39161

AIC=128.7832

r2=0.9997237

Observed compactness=0.843

**FEMUR**

Modeled compactness=0.613

Modeled compactness at the center=0

Modeled compactness at the periphery=1

R/t (Currey & Alexander 1985) : 2.6127

CDI (Castanet et al. 2000) : 0.3827

***Dama dama***

| Parameter | Mean Global value | SE Global value | Mean Angular value | SD Angular value |
|---|---|---|---|---|
| Min | 1.24E-07 | 0 | 8.12E-09 | 7.94E-09 |
| Max | 0.999999 | 0.0000133 | 0.999999 | n.a. |
| S:1/Slope | 0.0125854 | 0.0001139 | 0.0028196 | 0.0011762 |
| P:transition | 0.7324267 | 0.0002063 | 0.7337137 | 0.0212378 |

Global analysis

Maximum likelihood:-Ln L=252.5135

AIC=513.0271

r2=0.9992869

Observed compactness=0.453

Modeled compactness=0.453

Modeled compactness at the center=0

Modeled compactness at the periphery=1

R/t (Currey & Alexander 1985) : 3.7373

CDI (Castanet et al. 2000) : 0.2676

***Dicrocerus elegans***

| Parameter | Mean Global value | SE Global value | Mean Angular value | SD Angular value |
|---|---|---|---|---|
| Min | 2.54E-07 | 5.60E-06 | 2.00E-08 | 1.88E-08 |
| Max | 0.999999 | 0.0000124 | 0.999999 | n.a. |
| S:1/Slope | 0.0232462 | 0.0002102 | 0.0039082 | 0.0020738 |
| P:transition | 0.6375759 | 0.0003807 | 0.642213 | 0.0430781 |

Global analysis

**TIBIA**

Modeled compactness=0.843

Modeled compactness at the center=0.

Modeled compactness at the periphery=1.

R/t (Currey & Alexander 1985) : 1.6456

CDI (Castanet et al. 2000) : 0.6077

***Dama dama***

| Parameter | Mean Global value | SE Global value | Mean Angular value | SD Angular value |
|---|---|---|---|---|
| Min | 0 | 0 | 0 | 0 |
| Max | 1 | 0 | 1 | 0 |
| S:1/Slope | 0.011 | 0 | 0.003 | 0.001 |
| P:transition | 0.589 | 0 | 0.587 | 0.02 |

Global analysis

Maximum likelihood:-Ln L=397.133

AIC=802.266

r2=1

Observed compactness=0.648

Modeled compactness=0.648

Modeled compactness at the center=0.

Modeled compactness at the periphery=1.

R/t (Currey & Alexander 1985) : 2.4307

CDI (Castanet et al. 2000) : 0.4114

***Dicrocerus elegans***

| Parameter | Mean Global value | SE Global value | Mean Angular value | SD Angular value |
|---|---|---|---|---|
| Min | 0.00E+00 | n.a. | 0.00E+00 | 0.00E+00 |
| Max | 1 | n.a. | 1 | 0 |
| S:1/Slope | 0.025 | n.a. | 0.003 | 0.001 |
| P:transition | 0.513 | n.a. | 0.509 | 0.044 |

Global analysis

**FEMUR**

Maximum likelihood:-Ln L=227.5402

AIC=463.0804

r2=9993908

Observed compactness=0.586

Modeled compactness=0.586

Modeled compactness at the center=0

Modeled compactness at the periphery=1

R/t (Currey & Alexander 1985) : 2.7592

CDI (Castanet et al. 2000) : 0.3624

***Megaloceros giganteus***

| Parameter | Mean Global value | SE Global value | Mean Angular value | SD Angular value |
|---|---|---|---|---|
| Min | 0 | 0 | 0 | 0 |
| Max | 1 | 0 | 1 | 0 |
| S:1/Slope | 0.016 | 0 | 0.003 | 0.002 |
| P:transition | 0.644 | 0 | 0.646 | 0.025 |

Global analysis

Maximum likelihood:-Ln L=794.854

AIC=1597.71

r2=999

Observed compactness=0.578

Modeled compactness=0.578

Modeled compactness at the center=0

Modeled compactness at the periphery=1

R/t (Currey & Alexander 1985) : 2.8086

CDI (Castanet et al. 2000) : 0.356

***Sinomegaloceros yabei***

| Parameter | Mean Global value | SE Global value | Mean Angular value | SD Angular value |
|---|---|---|---|---|
| Min | 0.00E+00 | 0 | 0.00E+00 | 0.00E+00 |
| Max | 1 | 0.00E+00 | 1 | 0 |

**TIBIA**

Maximum likelihood:-Ln L=2 524.43

AIC=5 056.861

r2=0.997

Observed compactness=0.73

Modeled compactness=0.73

Modeled compactness at the center=0.

Modeled compactness at the periphery=1.

R/t (Currey & Alexander 1985) : 2.0555

CDI (Castanet et al. 2000) : 0.4865

***Megaloceros giganteus***

| Parameter | Mean Global value | SE Global value | Mean Angular value | SD Angular value |
|---|---|---|---|---|
| Min | 0.0059051 | 0.0004795 | 0.0106418 | 0.0436769 |
| Max | 0.9994955 | 0.0000945 | 0.9998357 | 0.0008859 |
| S:1/Slope | 0.0232726 | 0.0002391 | 0.004155 | 0.0042614 |
| P:transition | 0.5113519 | 0.0004147 | 0.5130364 | 0.0955564 |

Global analysis

Maximum likelihood:-Ln L=406.7238

AIC=821.4476

r2=0.9920947

Observed compactness=0.734

Modeled compactness=0.734

Modeled compactness at the center=0.006

Modeled compactness at the periphery=0.999

R/t (Currey & Alexander 1985) : 2.0465

CDI (Castanet et al. 2000) : 0.4886

***Sinomegaloceros yabei***

| Parameter | Mean Global value | SE Global value | Mean Angular value | SD Angular value |
|---|---|---|---|---|
| Min | 2.94E-07 | 1.63E-06 | 2.87E-08 | 2.07E-08 |
| Max | 0.9998731 | 0.0000478 | 0.9999256 | 0.0002855 |

**FEMUR**

| | | | | |
|---|---|---|---|---|
| S:1/Slope | 0.014 | 0 | 0.003 | 0.001 |
| P:transition | 0.612 | 0 | 0.612 | 0.024 |

Global analysis
Maximum likelihood:-Ln L=1953.54
AIC=3915.08
r2=999
Observed compactness=0.619
Modeled compactness=0.619
Modeled compactness at the center=0
Modeled compactness at the periphery=1
R/t (Currey & Alexander 1985) : 2.576
CDI (Castanet et al. 2000) : 0.3882

***Procervulus praelucidus***

| Parameter | Mean Global value | SE Global value | Mean Angular value | SD Angular value |
|---|---|---|---|---|
| Min | 0 | 0 | 0 | 0 |
| Max | 0.973 | 0 | 0.997 | 0.021 |
| S:1/Slope | 0.014 | 0 | 0.003 | 0.004 |
| P:transition | 0.65 | 0 | 0.724 | 0.134 |

Global analysis
Maximum likelihood:-Ln L=1 125.663
AIC=2 259.326
r2=0.999
Observed compactness=0.557
Modeled compactness=0.557
Modeled compactness at the center=0.
Modeled compactness at the periphery=0.973
R/t (Currey & Alexander 1985) : 2.8545
CDI (Castanet et al. 2000) : 0.3503

***Alces alces***

**TIBIA**

| | | | | |
|---|---|---|---|---|
| S:1/Slope | 0.0254475 | 0.0002174 | 0.003975 | 0.0016459 |
| P:transition | 0.5556484 | 0.0003937 | 0.5605821 | 0.0445927 |

Global analysis
Maximum likelihood:-Ln L=297.5604
AIC=603.1208
r2=0.9995317
Observed compactness=0.685
Modeled compactness=0.685
Modeled compactness at the center=0.
Modeled compactness at the periphery=1.
R/t (Currey & Alexander 1985) : 2.2505
CDI (Castanet et al. 2000) : 0.4444

***Procervulus praelucidus***

| Parameter | Mean Global value | SE Global value | Mean Angular value | SD Angular value |
|---|---|---|---|---|
| Min | 4.43E-07 | 2.70E-06 | 3.31E-08 | 3.59E-08 |
| Max | 0.999999 | 0 | 0.999999 | n.a. |
| S:1/Slope | 0.0165872 | 0.0002814 | 0.0033913 | 0.0019846 |
| P:transition | 0.5719002 | 0.0004614 | 0.5721727 | 0.0279227 |

Global analysis
Maximum likelihood:-Ln L=55.47604
AIC=118.9521
r2=0.99983
Observed compactness=0.668
Modeled compactness=0.668
Modeled compactness at the center=0.
Modeled compactness at the periphery=1.
R/t (Currey & Alexander 1985) : 2.3359
CDI (Castanet et al. 2000) : 0.4281

***Alces alces***

**FEMUR**

| Parameter | Mean Global value | SE Global value | Mean Angular value | SD Angular value |
|---|---|---|---|---|
| Min | 5.70E-08 | 5.61E-07 | 6.73E-09 | 7.76E-09 |
| Max | 0.999999 | 0.0000131 | 0.999999 | n.a. |
| S:1/Slope | 0.0093971 | 0.0001352 | 0.0027382 | 0.0012503 |
| P:transition | 0.6737111 | 0.000257 | 0.674972 | 0.0156757 |

Global analysis
Maximum likelihood:-Ln L=116.0101
AIC=240.0202
r2=0.9997789
Observed compactness=0.54
Modeled compactness=0.54
Modeled compactness at the center=0.
Modeled compactness at the periphery=1.
R/t (Currey & Alexander 1985) : 3.0648
CDI (Castanet et al. 2000) : 0.3263

***Cervus elaphus***

| Parameter | Mean Global value | SE Global value | Mean Angular value | SD Angular value |
|---|---|---|---|---|
| Min | 0 | 0 | 0 | 0 |
| Max | 1 | 0 | 1 | 0.001 |
| S:1/Slope | 0.012 | 0 | 0.003 | 0.001 |
| P:transition | 0.692 | 0 | 0.694 | 0.02 |

Global analysis
Maximum likelihood:-Ln L=263.531
AIC=535.061
r2=1
Observed compactness=0.514
Modeled compactness=0.514
Modeled compactness at the center=0.
Modeled compactness at the periphery=1.
R/t (Currey & Alexander 1985) : 3.2479

**TIBIA**

| Parameter | Mean Global value | SE Global value | Mean Angular value | SD Angular value |
|---|---|---|---|---|
| Min | 0 | n.a. | 0 | 0 |
| Max | 1 | n.a. | 1 | 0 |
| S:1/Slope | 0.012 | n.a. | 0.002 | 0.001 |
| P:transition | 0.655 | n.a. | 0.658 | 0.021 |

Global analysis
Maximum likelihood:-Ln L=22.715
AIC=53.43
r2=0.999
Observed compactness=0.565
Modeled compactness=0.565
Modeled compactness at the center=0.
Modeled compactness at the periphery=1.
R/t (Currey & Alexander 1985) : 2.9003
CDI (Castanet et al. 2000) : 0.3448

***Axis axis***

| Parameter | Mean Global value | SE Global value | Mean Angular value | SD Angular value |
|---|---|---|---|---|
| Min | 0 | 0 | 0 | 0 |
| Max | 1 | 0 | 1 | 0 |
| S:1/Slope | 0.017 | 0.001 | 0.002 | 0.001 |
| P:transition | 0.594 | 0.001 | 0.593 | 0.029 |

Global analysis
Maximum likelihood:-Ln L=28.087
AIC=64.175
r2=1
Observed compactness=0.641
Modeled compactness=0.641
Modeled compactness at the center=0.
Modeled compactness at the periphery=1.
R/t (Currey & Alexander 1985) : 2.4622

**FEMUR**

CDI (Castanet et al. 2000) : 0.3079

***Capreolus capreolus***

| Parameter | Mean Global value | SE Global value | Mean Angular value | SD Angular value |
|---|---|---|---|---|
| Min | 0 | n.a. | 0 | 0 |
| Max | 1 | n.a. | 1 | 0 |
| S:1/Slope | 0.014 | n.a. | 0.003 | 0.002 |
| P:transition | 0.681 | n.a. | 0.682 | 0.023 |

Global analysis

Maximum likelihood:-Ln L=143.931

AIC=295.862

r2=0.999

Observed compactness=0.529

Modeled compactness=0.529

Modeled compactness at the center=0.

Modeled compactness at the periphery=1.

R/t (Currey & Alexander 1985) : 3.1343

CDI (Castanet et al. 2000) : 0.319

***Muntiacus muntjak***

| Parameter | Mean Global value | SE Global value | Mean Angular value | SD Angular value |
|---|---|---|---|---|
| Min | 0 | 0 | 0 | 0 |
| Max | 1 | 0 | 1 | 0 |
| S:1/Slope | 0.014 | 0 | 0.003 | 0.002 |
| P:transition | 0.668 | 0 | 0.668 | 0.023 |

Global analysis

Maximum likelihood:-Ln L=89.537

AIC=187.075

r2=1

Observed compactness=0.547

**TIBIA**

CDI (Castanet et al. 2000) : 0.4061

***Elaphurus davidianus***

| Parameter | Mean Global value | SE Global value | Mean Angular value | SD Angular value |
|---|---|---|---|---|
| Min | 0 | n.a. | 0 | 0 |
| Max | 1 | n.a. | 1 | 0 |
| S:1/Slope | 0.032 | n.a. | 0.002 | 0.001 |
| P:transition | 0.53 | n.a. | 0.531 | 0.055 |

Global analysis

Maximum likelihood:-Ln L=79.577

AIC=167.154

r2=0.998

Observed compactness=0.709

Modeled compactness=0.709

Modeled compactness at the center=0.

Modeled compactness at the periphery=1.

R/t (Currey & Alexander 1985) : 2.1275

CDI (Castanet et al. 2000) : 0.47

***Hydropotes inermis***

| Parameter | Mean Global value | SE Global value | Mean Angular value | SD Angular value |
|---|---|---|---|---|
| Min | 0 | n.a. | 0 | 0 |
| Max | 1 | n.a. | 1 | 0 |
| S:1/Slope | 0.019 | n.a. | 0.001 | 0.001 |
| P:transition | 0.641 | n.a. | 0.641 | 0.034 |

Global analysis

Maximum likelihood:-Ln L=22.785

AIC=53.57

r2=0.999

Observed compactness=0.584

**FEMUR**

Modeled compactness=0.547

Modeled compactness at the center=0.

Modeled compactness at the periphery=1.

R/t (Currey & Alexander 1985) : 3.0122

CDI (Castanet et al. 2000) : 0.332

***Pudu puda***

| Parameter | Mean Global value | SE Global value | Mean Angular value | SD Angular value |
|---|---|---|---|---|
| Min | 0 | 0 | 0 | 0 |
| Max | 1 | 0 | 1 | 0 |
| S:1/Slope | 0.017 | 0 | 0.003 | 0.001 |
| P:transition | 0.662 | 0 | 0.664 | 0.029 |

Global analysis

Maximum likelihood:-Ln L=92.246

AIC=192.493

r2=1

Observed compactness=0.556

Modeled compactness=0.555

Modeled compactness at the center=0.

Modeled compactness at the periphery=1.

R/t (Currey & Alexander 1985) : 2.9558

CDI (Castanet et al. 2000) : 0.3383

***Elaphurus davidianus***

| Parameter | Mean Global value | SE Global value | Mean Angular value | SD Angular value |
|---|---|---|---|---|
| Min | 0 | 0 | 0 | 0 |
| Max | 1 | 0 | 1 | 0 |
| S:1/Slope | 0.025 | 0.001 | 0.003 | 0.002 |
| P:transition | 0.661 | 0.001 | 0.664 | 0.045 |

Global analysis

**TIBIA**

Modeled compactness=0.584

Modeled compactness at the center=0.

Modeled compactness at the periphery=1.

R/t (Currey & Alexander 1985) : 2.7845

CDI (Castanet et al. 2000) : 0.3591

***Muntiacus muntjak***

| Parameter | Mean Global value | SE Global value | Mean Angular value | SD Angular value |
|---|---|---|---|---|
| Min | 0 | n.a. | 0 | 0 |
| Max | 1 | n.a. | 1 | 0 |
| S:1/Slope | 0.027 | n.a. | 0.002 | 0.002 |
| P:transition | 0.593 | n.a. | 0.597 | 0.045 |

Global analysis

Maximum likelihood:-Ln L=57.376

AIC=122.751

r2=0.998

Observed compactness=0.64

Modeled compactness=0.64

Modeled compactness at the center=0.

Modeled compactness at the periphery=1.

R/t (Currey & Alexander 1985) : 2.458

CDI (Castanet et al. 2000) : 0.4068

***Odocoileus virginianus***

| Parameter | Mean Global value | SE Global value | Mean Angular value | SD Angular value |
|---|---|---|---|---|
| Min | 0 | n.a. | 0 | 0 |
| Max | 1 | n.a. | 1 | 0 |
| S:1/Slope | 0.023 | n.a. | 0.001 | 0.001 |
| P:transition | 0.561 | n.a. | 0.562 | 0.039 |

Global analysis

**FEMUR**

Maximum likelihood:-Ln L=56.867

AIC=121.734

r2=0.999

Observed compactness=0.554

Modeled compactness=0.554

Modeled compactness at the center=0.

Modeled compactness at the periphery=1.

R/t (Currey & Alexander 1985) : 2.9516

CDI (Castanet et al. 2000) : 0.3388

***Hydropotes inermis***

| Parameter | Mean Global value | SE Global value | Mean Angular value | SD Angular value |
|---|---|---|---|---|
| Min | 0 | n.a. | 0 | 0 |
| Max | 1 | n.a. | 1 | 0 |
| S:1/Slope | 0.015 | n.a. | 0.002 | 0.002 |
| P:transition | 0.671 | n.a. | 0.671 | 0.027 |

Global analysis

Maximum likelihood:-Ln L=20.811

AIC=49.622

r2=0.999

Observed compactness=0.543

Modeled compactness=0.543

Modeled compactness at the center=0.

Modeled compactness at the periphery=1.

R/t (Currey & Alexander 1985) : 3.0412

CDI (Castanet et al. 2000) : 0.3288

***Odocoileus virginianus***

| Parameter | Mean Global value | SE Global value | Mean Angular value | SD Angular value |
|---|---|---|---|---|
| Min | 0 | 0 | 0 | 0 |
| Max | 1 | 0 | 1 | 0 |

**TIBIA**

Maximum likelihood:-Ln L=38.073

AIC=84.147

r2=0.998

Observed compactness=0.68

Modeled compactness=0.68

Modeled compactness at the center=0.

Modeled compactness at the periphery=1.

R/t (Currey & Alexander 1985) : 2.278

CDI (Castanet et al. 2000) : 0.439

***Ozotoceros davidianus***

| Parameter | Mean Global value | SE Global value | Mean Angular value | SD Angular value |
|---|---|---|---|---|
| Min | 0 | 0 | 0 | 0 |
| Max | 1 | 0 | 1 | 0.003 |
| S:1/Slope | 0.025 | 0.001 | 0.001 | 0.001 |
| P:transition | 0.431 | 0.002 | 0.435 | 0.044 |

Global analysis

Maximum likelihood:-Ln L=52.765

AIC=113.531

r2=0.995

Observed compactness=0.808

Modeled compactness=0.808

Modeled compactness at the center=0.

Modeled compactness at the periphery=1.

R/t (Currey & Alexander 1985) : 1.7576

CDI (Castanet et al. 2000) : 0.5689

***Pudu puda***

| Parameter | Mean Global value | SE Global value | Mean Angular value | SD Angular value |
|---|---|---|---|---|
| Min | 0 | n.a. | 0 | 0 |
| Max | 1 | n.a. | 1 | 0 |

**FEMUR**

| | | | | |
|---|---|---|---|---|
| S:1/Slope | 0.013 | 0.001 | 0.002 | 0.002 |
| P:transition | 0.698 | 0.001 | 0.7 | 0.023 |

Global analysis

Maximum likelihood:-Ln L=19.546

AIC=47.092

r2=1

Observed compactness=0.511

Modeled compactness=0.511

Modeled compactness at the center=0.

Modeled compactness at the periphery=1.

R/t (Currey & Alexander 1985) : 3.3124

CDI (Castanet et al. 2000) : 0.3019

***Ozotoceros bezoarticus***

| Parameter | Mean Global value | SE Global value | Mean Angular value | SD Angular value |
|---|---|---|---|---|
| Min | 0 | 0 | 0 | 0 |
| Max | 1 | 0 | 1 | 0 |
| S:1/Slope | 0.013 | 0.001 | 0.001 | 0.001 |
| P:transition | 0.582 | 0.002 | 0.582 | 0.023 |

Global analysis

Maximum likelihood:-Ln L=17.329

AIC=42.658

r2=1

Observed compactness=0.656

Modeled compactness=0.656

Modeled compactness at the center=0.

Modeled compactness at the periphery=1.

R/t (Currey & Alexander 1985) : 2.3921

CDI (Castanet et al. 2000) : 0.418

***Rucervus eldii***

**TIBIA**

| | | | | |
|---|---|---|---|---|
| S:1/Slope | 0.02 | n.a. | 0.001 | 0.001 |
| P:transition | 0.357 | n.a. | 0.353 | 0.035 |

Global analysis

Maximum likelihood:-Ln L=30.647

AIC=69.294

r2=0.997

Observed compactness=0.868

Modeled compactness=0.868

Modeled compactness at the center=0.

Modeled compactness at the periphery=1.

R/t (Currey & Alexander 1985) : 1.5551

CDI (Castanet et al. 2000) : 0.643

***Rangifer* SN**

| Parameter | Mean Global value | SE Global value | Mean Angular value | SD Angular value |
|---|---|---|---|---|
| Min | 0 | 0 | 0 | 0 |
| Max | 1 | 0 | 1 | 0 |
| S:1/Slope | 0.042 | 0.001 | 0.003 | 0.003 |
| P:transition | 0.658 | 0.002 | 0.669 | 0.07 |

Global analysis

Maximum likelihood:-Ln L=105.009

AIC=218.018

r2=0.993

Observed compactness=0.561

Modeled compactness=0.561

Modeled compactness at the center=0.

Modeled compactness at the periphery=1.

R/t (Currey & Alexander 1985) : 2.9222

CDI (Castanet et al. 2000) : 0.3422

***Rucervus eldii***

**FEMUR**

| Parameter | Mean Global value | SE Global value | Mean Angular value | SD Angular value |
|---|---|---|---|---|
| Min | 0.001 | n.a. | 0 | 0 |
| Max | 1 | n.a. | 1 | 0 |
| S:1/Slope | 0.013 | n.a. | 0.002 | 0.003 |
| P:transition | 0.709 | n.a. | 0.708 | 0.022 |

Global analysis
Maximum likelihood:-Ln L=35.452
AIC=78.905
r2=1
Observed compactness=0.494
Modeled compactness=0.494
Modeled compactness at the center=0.001
Modeled compactness at the periphery=1.
R/t (Currey & Alexander 1985) : 3.4409
CDI (Castanet et al. 2000) : 0.2906

***Rusa alfredi***

| Parameter | Mean Global value | SE Global value | Mean Angular value | SD Angular value |
|---|---|---|---|---|
| Min | 0 | n.a. | 0 | 0 |
| Max | 1 | n.a. | 1 | 0 |
| S:1/Slope | 0.012 | n.a. | 0.001 | 0.001 |
| P:transition | 0.515 | n.a. | 0.515 | 0.021 |

Global analysis
Maximum likelihood:-Ln L=15.071
AIC=38.143
r2=1
Observed compactness=0.73
Modeled compactness=0.73
Modeled compactness at the center=0.
Modeled compactness at the periphery=1.
R/t (Currey & Alexander 1985) : 2.0631

**TIBIA**

| Parameter | Mean Global value | SE Global value | Mean Angular value | SD Angular value |
|---|---|---|---|---|
| Min | 0 | n.a. | 0 | 0 |
| Max | 1 | n.a. | 1 | 0 |
| S:1/Slope | 0.026 | n.a. | 0.002 | 0.003 |
| P:transition | 0.581 | n.a. | 0.587 | 0.043 |

Global analysis
Maximum likelihood:-Ln L=43.181
AIC=94.362
r2=0.998
Observed compactness=0.653
Modeled compactness=0.653
Modeled compactness at the center=0.
Modeled compactness at the periphery=1.
R/t (Currey & Alexander 1985) : 2.3847
CDI (Castanet et al. 2000) : 0.4193

***Rusa alfredi***

| Parameter | Mean Global value | SE Global value | Mean Angular value | SD Angular value |
|---|---|---|---|---|
| Min | 0 | n.a. | 0 | 0 |
| Max | 1 | n.a. | 1 | 0 |
| S:1/Slope | 0.014 | n.a. | 0.002 | 0.002 |
| P:transition | 0.442 | n.a. | 0.443 | 0.024 |

Global analysis
Maximum likelihood:-Ln L=30.179
AIC=68.357
r2=0.998
Observed compactness=0.801
Modeled compactness=0.801
Modeled compactness at the center=0.
Modeled compactness at the periphery=1.
R/t (Currey & Alexander 1985) : 1.7914

**FEMUR**

CDI (Castanet et al. 2000) : 0.4847

***Mazama gouazoubira***

| Parameter | Mean Global value | SE Global value | Mean Angular value | SD Angular value |
|---|---|---|---|---|
| Min | 0 | 0 | 0 | 0 |
| Max | 1 | 0 | 1 | 0 |
| S:1/Slope | 0.008 | 0.001 | 0.001 | 0.001 |
| P:transition | 0.55 | 0 | 0.55 | 0.015 |

Global analysis
Maximum likelihood:-Ln L=12.875
AIC=33.75
r2=1
Observed compactness=0.693
Modeled compactness=0.693
Modeled compactness at the center=0.
Modeled compactness at the periphery=1.
R/t (Currey & Alexander 1985) : 2.2215
CDI (Castanet et al. 2000) : 0.4502

***Euprox* sp.**

| Parameter | Mean Global value | SE Global value | Mean Angular value | SD Angular value |
|---|---|---|---|---|
| Min | 0 | 0 | 0 | 0 |
| Max | 1 | 0 | 1 | 0 |
| S:1/Slope | 0.016 | 0 | 0.004 | 0.002 |
| P:transition | 0.68 | 0 | 0.683 | 0.028 |

Global analysis
Maximum likelihood:-Ln L=510.57
AIC=1 029.14
r2=1
Observed compactness=0.531

**TIBIA**

CDI (Castanet et al. 2000) : 0.5582

***Mazama gouazoubira***

| Parameter | Mean Global value | SE Global value | Mean Angular value | SD Angular value |
|---|---|---|---|---|
| Min | 0 | 0 | 0 | 0 |
| Max | 1 | 0 | 1 | 0 |
| S:1/Slope | 0.014 | 0.001 | 0.001 | 0.001 |
| P:transition | 0.453 | 0.002 | 0.454 | 0.025 |

Global analysis
Maximum likelihood:-Ln L=24
AIC=56
r2=0.999
Observed compactness=0.789
Modeled compactness=0.789
Modeled compactness at the center=0.
Modeled compactness at the periphery=1.
R/t (Currey & Alexander 1985) : 1.8297
CDI (Castanet et al. 2000) : 0.5465

***Cervus canadensis***

| Parameter | Mean Global value | SE Global value | Mean Angular value | SD Angular value |
|---|---|---|---|---|
| Min | 0 | 0 | 0 | 0 |
| Max | 1 | 0 | 1 | 0 |
| S:1/Slope | 0.021 | 0.001 | 0.002 | 0.002 |
| P:transition | 0.528 | 0.002 | 0.533 | 0.039 |

Global analysis
Maximum likelihood:-Ln L=36.971
AIC=81.941
r2=0.998
Observed compactness=0.711

**FEMUR**

Modeled compactness=0.531

Modeled compactness at the center=0.

Modeled compactness at the periphery=1.

R/t (Currey & Alexander 1985) : 3.1262

CDI (Castanet et al. 2000) : 0.3199

***Cervus canadensis***

| Parameter | Mean Global value | SE Global value | Mean Angular value | SD Angular value |
|---|---|---|---|---|
| Min | 0 | n.a. | 0 | 0 |
| Max | 1 | n.a. | 1 | 0 |
| S:1/Slope | 0.018 | n.a. | 0.002 | 0.002 |
| P:transition | 0.605 | n.a. | 0.61 | 0.031 |

Global analysis

Maximum likelihood:-Ln L=28.723

AIC=65.445

r2=0.999

Observed compactness=0.625

Modeled compactness=0.625

Modeled compactness at the center=0.

Modeled compactness at the periphery=1.

R/t (Currey & Alexander 1985) : 2.5338

CDI (Castanet et al. 2000) : 0.3947

***Rusa unicolor***

| Parameter | Mean Global value | SE Global value | Mean Angular value | SD Angular value |
|---|---|---|---|---|
| Min | 0 | n.a. | 0 | 0 |
| Max | 1 | n.a. | 1 | 0 |
| S:1/Slope | 0.016 | n.a. | 0.002 | 0.003 |
| P:transition | 0.685 | n.a. | 0.688 | 0.026 |

Global analysis

**TIBIA**

Modeled compactness=0.711

Modeled compactness at the center=0.

Modeled compactness at the periphery=1.

R/t (Currey & Alexander 1985) : 2.1182

CDI (Castanet et al. 2000) : 0.4721

***Rusa unicolor***

| Parameter | Mean Global value | SE Global value | Mean Angular value | SD Angular value |
|---|---|---|---|---|
| Min | 0 | 0 | 0 | 0 |
| Max | 1 | 0 | 1 | 0 |
| S:1/Slope | 0.017 | 0.001 | 0.002 | 0.002 |
| P:transition | 0.562 | 0.001 | 0.567 | 0.028 |

Global analysis

Maximum likelihood:-Ln L=49.615

AIC=107.23

r2=0.998

Observed compactness=0.679

Modeled compactness=0.679

Modeled compactness at the center=0.

Modeled compactness at the periphery=1.

R/t (Currey & Alexander 1985) : 2.285

CDI (Castanet et al. 2000) : 0.4376

***Eucladoceros* sp.**

| Parameter | Mean Global value | SE Global value | Mean Angular value | SD Angular value |
|---|---|---|---|---|
| Min | 0 | n.a. | 0 | 0 |
| Max | 1 | n.a. | 1 | 0 |
| S:1/Slope | 0.024 | n.a. | 0.002 | 0.002 |
| P:transition | 0.466 | n.a. | 0.477 | 0.04 |

Global analysis

| **FEMUR** | **TIBIA** |
|---|---|
| Maximum likelihood:-Ln L=52.839 | Maximum likelihood:-Ln L=57.2 |
| AIC=113.679 | AIC=122.4 |
| r2=0.998 | r2=0.997 |
| Observed compactness=0.529 | Observed compactness=0.779 |
| Modeled compactness=0.529 | Modeled compactness=0.779 |
| Modeled compactness at the center=0. | Modeled compactness at the center=0. |
| Modeled compactness at the periphery=1. | Modeled compactness at the periphery=1. |
| R/t (Currey & Alexander 1985) : 3.1788 | R/t (Currey & Alexander 1985) : 1.8741 |
| CDI (Castanet et al. 2000) : 0.3146 | CDI (Castanet et al. 2000) : 0.5336 |

***Alces* sp.**

| Parameter | Mean Global value | SE Global value | Mean Angular value | SD Angular value |
|---|---|---|---|---|
| Min | 0 | 0 | 0 | 0 |
| Max | 1 | 0 | 0.999 | 0.004 |
| S:1/Slope | 0.013 | 0.001 | 0.002 | 0.002 |
| P:transition | 0.679 | 0.001 | 0.678 | 0.023 |

Global analysis

Maximum likelihood:-Ln L=18.717

AIC=45.433

r2=1

Observed compactness=0.536

Modeled compactness=0.536

Modeled compactness at the center=0.

Modeled compactness at the periphery=1.

R/t (Currey & Alexander 1985) : 3.1129

CDI (Castanet et al. 2000) : 0.3212

**HUMERUS**

***Candiacervus sp. II***

| Parameter | Mean Global value | SE Global value | Mean Angular value | SD Angular value |
|---|---|---|---|---|
| Min | 0 | 0 | 0 | 0 |
| Max | 1 | 0 | 1 | 0 |
| S:1/Slope | 0.022 | 0 | 0.004 | 0.002 |
| P:transition | 0.492 | 0 | 0.493 | 0.037 |

Global analysis
Maximum likelihood:-Ln L=433.244
AIC=874.488
r2=0.998
Observed compactness=0.752
Modeled compactness=0.752
Modeled compactness at the center=0.
Modeled compactness at the periphery=1.
R/t (Currey & Alexander 1985) : 1.9679
CDI (Castanet et al. 2000) : 0.5082

***Dama dama***

| Parameter | Mean Global value | SE Global value | Mean Angular value | SD Angular value |
|---|---|---|---|---|
| Min | 0 | 0 | 0 | 0 |
| Max | 1 | 0 | 1 | 0 |
| S:1/Slope | 0.014 | 0 | 0.003 | 0.001 |
| P:transition | 0.659 | 0 | 0.661 | 0.026 |

Global analysis
Maximum likelihood:-Ln L=425.93
AIC=859.859
r2=0.999
Observed compactness=0.559
Modeled compactness=0.559

**RADIUS**

***Dicrocerus elegans***

| Parameter | Mean Global value | SE Global value | Mean Angular value | SD Angular value |
|---|---|---|---|---|
| Min | 0 | n.a. | 0 | 0 |
| Max | 1 | n.a. | 1 | 0 |
| S:1/Slope | 0.011 | n.a. | 0.003 | 0.001 |
| P:transition | 0.461 | n.a. | 0.463 | 0.018 |

Global analysis
Maximum likelihood:-Ln L=67.165
AIC=142.33
r2=0.999
Observed compactness=0.784
Modeled compactness=0.784
Modeled compactness at the center=0.
Modeled compactness at the periphery=1.
R/t (Currey & Alexander 1985) : 1.8557
CDI (Castanet et al. 2000) : 0.5389

***Candiacervus ropalophorus***

| Parameter | Mean Global value | SE Global value | Mean Angular value | SD Angular value |
|---|---|---|---|---|
| Min | 0 | 0 | 0 | 0 |
| Max | 1 | 0 | 1 | 0 |
| S:1/Slope | 0.029 | 0 | 0.003 | 0.002 |
| P:transition | 0.368 | 0.001 | 0.379 | 0.052 |

Global analysis
Maximum likelihood:-Ln L=302.268
AIC=612.536
r2=0.998
Observed compactness=0.859
Modeled compactness=0.859

**HUMERUS**

Modeled compactness at the center=0.
Modeled compactness at the periphery=1.
R/t (Currey & Alexander 1985) : 2.93
CDI (Castanet et al. 2000) : 0.3413

***Dicrocerus elegans***

| Parameter | Mean Global value | SE Global value | Mean Angular value | SD Angular value |
|---|---|---|---|---|
| Min | 0 | 0 | 0 | 0 |
| Max | 1 | 0 | 1 | 0 |
| S:1/Slope | 0.016 | 0 | 0.003 | 0.001 |
| P:transition | 0.561 | 0 | 0.559 | 0.028 |

Global analysis
Maximum likelihood:-Ln L=232.852
AIC=473.703
r2=0.999
Observed compactness=0.678
Modeled compactness=0.678
Modeled compactness at the center=0.
Modeled compactness at the periphery=1.
R/t (Currey & Alexander 1985) : 2.2765
CDI (Castanet et al. 2000) : 0.4393

***Megaloceros giganteus***

| Parameter | Mean Global value | SE Global value | Mean Angular value | SD Angular value |
|---|---|---|---|---|
| Min | 0 | n.a. | 0 | 0 |
| Max | 1 | n.a. | 1 | 0.001 |
| S:1/Slope | 0.026 | n.a. | 0.007 | 0.007 |
| P:transition | 0.525 | n.a. | 0.531 | 0.044 |

Global analysis
Maximum likelihood:-Ln L=3 765.605

**RADIUS**

Modeled compactness at the center=0.
Modeled compactness at the periphery=1.
R/t (Currey & Alexander 1985) : 1.583
CDI (Castanet et al. 2000) : 0.6317

***Candiacervus sp. II***

| Parameter | Mean Global value | SE Global value | Mean Angular value | SD Angular value |
|---|---|---|---|---|
| Min | 0 | n.a. | 0 | 0 |
| Max | 1 | n.a. | 1 | 0 |
| S:1/Slope | 0.019 | n.a. | 0.004 | 0.003 |
| P:transition | 0.471 | n.a. | 0.479 | 0.033 |

Global analysis
Maximum likelihood:-Ln L=137.002
AIC=282.004
r2=0.999
Observed compactness=0.775
Modeled compactness=0.775
Modeled compactness at the center=0.
Modeled compactness at the periphery=1.
R/t (Currey & Alexander 1985) : 1.8917
CDI (Castanet et al. 2000) : 0.5286

***Dama dama***

| Parameter | Mean Global value | SE Global value | Mean Angular value | SD Angular value |
|---|---|---|---|---|
| Min | 0 | n.a. | 0 | 0 |
| Max | 1 | n.a. | 1 | 0 |
| S:1/Slope | 0.021 | n.a. | 0.003 | 0.002 |
| P:transition | 0.511 | n.a. | 0.502 | 0.037 |

Global analysis
Maximum likelihood:-Ln L=210.561

**HUMERUS**

AIC=7 539.211

r2=0.997

Observed compactness=0.718

Modeled compactness=0.718

Modeled compactness at the center=0.

Modeled compactness at the periphery=1.

R/t (Currey & Alexander 1985) : 2.1065

CDI (Castanet et al. 2000) : 0.4747

***Procervulus praelucidus***

| Parameter | Mean Global value | SE Global value | Mean Angular value | SD Angular value |
|---|---|---|---|---|
| Min | 0 | 0 | 0 | 0 |
| Max | 1 | 0 | 1 | 0 |
| S:1/Slope | 0.02 | 0 | 0.005 | 0.006 |
| P:transition | 0.67 | 0.001 | 0.67 | 0.033 |

Global analysis

Maximum likelihood:-Ln L=156.608

AIC=321.216

r2=0.999

Observed compactness=0.545

Modeled compactness=0.545

Modeled compactness at the center=0.

Modeled compactness at the periphery=1.

R/t (Currey & Alexander 1985) : 3.0305

CDI (Castanet et al. 2000) : 0.33

***Alces alces***

| Parameter | Mean Global value | SE Global value | Mean Angular value | SD Angular value |
|---|---|---|---|---|
| Min | 0 | 0 | 0 | 0 |
| Max | 1 | 0 | 1 | 0 |

**RADIUS**

AIC=429.121

r2=1

Observed compactness=0.729

Modeled compactness=0.729

Modeled compactness at the center=0.

Modeled compactness at the periphery=1.

R/t (Currey & Alexander 1985) : 2.0445

CDI (Castanet et al. 2000) : 0.4891

***Megaloceros giganteus***

| Parameter | Mean Global value | SE Global value | Mean Angular value | SD Angular value |
|---|---|---|---|---|
| Min | 0.031 | 0 | 0 | 0 |
| Max | 1 | 0 | 1 | 0 |
| S:1/Slope | 0.032 | 0 | 0.005 | 0.004 |
| P:transition | 0.546 | 0 | 0.549 | 0.064 |

Global analysis

Maximum likelihood:-Ln L=19 275.379

AIC=38 558.758

r2=0.996

Observed compactness=0.703

Modeled compactness=0.703

Modeled compactness at the center=0.031

Modeled compactness at the periphery=1.

R/t (Currey & Alexander 1985) : 2.2044

CDI (Castanet et al. 2000) : 0.4536

***Procervulus praelucidus***

| Parameter | Mean Global value | SE Global value | Mean Angular value | SD Angular value |
|---|---|---|---|---|
| Min | 0 | 0 | 0 | 0 |
| Max | 1 | 0 | 1 | 0 |

**HUMERUS**

| | | | | |
|---|---|---|---|---|
| S:1/Slope | 0.024 | 0.001 | 0.006 | 0.01 |
| P:transition | 0.718 | 0.001 | 0.72 | 0.036 |

Global analysis

Maximum likelihood:-Ln L=44.299

AIC=96.598

r2=0.999

Observed compactness=0.478

Modeled compactness=0.478

Modeled compactness at the center=0.

Modeled compactness at the periphery=1.

R/t (Currey & Alexander 1985) : 3.5509

CDI (Castanet et al. 2000) : 0.2816

***Elaphurus davidianus***

| Parameter | Mean Global value | SE Global value | Mean Angular value | SD Angular value |
|---|---|---|---|---|
| Min | 0.006 | n.a. | 0.001 | 0.006 |
| Max | 1 | n.a. | 1 | 0 |
| S:1/Slope | 0.035 | n.a. | 0.003 | 0.003 |
| P:transition | 0.608 | n.a. | 0.611 | 0.061 |

Global analysis

Maximum likelihood:-Ln L=169.16

AIC=346.32

r2=0.992

Observed compactness=0.624

Modeled compactness=0.624

Modeled compactness at the center=0.006

Modeled compactness at the periphery=1.

R/t (Currey & Alexander 1985) : 2.5498

CDI (Castanet et al. 2000) : 0.3922

***Hydropotes inermis***

**RADIUS**

| | | | | |
|---|---|---|---|---|
| S:1/Slope | 0.011 | 0 | 0.002 | 0.001 |
| P:transition | 0.517 | 0 | 0.517 | 0.019 |

Global analysis

Maximum likelihood:-Ln L=30.503

AIC=69.007

r2=1

Observed compactness=0.73

Modeled compactness=0.73

Modeled compactness at the center=0.

Modeled compactness at the periphery=1.

R/t (Currey & Alexander 1985) : 2.071

CDI (Castanet et al. 2000) : 0.4829

***Alces alces***

| Parameter | Mean Global value | SE Global value | Mean Angular value | SD Angular value |
|---|---|---|---|---|
| Min | 0 | n.a. | 0 | 0 |
| Max | 1 | n.a. | 1 | 0 |
| S:1/Slope | 0.011 | n.a. | 0.002 | 0.002 |
| P:transition | 0.7 | n.a. | 0.701 | 0.019 |

Global analysis

Maximum likelihood:-Ln L=14.902

AIC=37.804

r2=0.999

Observed compactness=0.503

Modeled compactness=0.503

Modeled compactness at the center=0.

Modeled compactness at the periphery=1.

R/t (Currey & Alexander 1985) : 3.336

CDI (Castanet et al. 2000) : 0.2998

***Axis axis***

**HUMERUS**

| Parameter | Mean Global value | SE Global value | Mean Angular value | SD Angular value |
|---|---|---|---|---|
| Min | 0 | n.a. | 0 | 0 |
| Max | 1 | n.a. | 1 | 0 |
| S:1/Slope | 0.015 | n.a. | 0.002 | 0.001 |
| P:transition | 0.625 | n.a. | 0.619 | 0.029 |

Global analysis
Maximum likelihood:-Ln L=14.173
AIC=36.347
r2=0.998
Observed compactness=0.61
Modeled compactness=0.61
Modeled compactness at the center=0.
Modeled compactness at the periphery=1.
R/t (Currey & Alexander 1985) : 2.6664
CDI (Castanet et al. 2000) : 0.375

***Muntiacus muntjak***

| Parameter | Mean Global value | SE Global value | Mean Angular value | SD Angular value |
|---|---|---|---|---|
| Min | 0 | 0 | 0 | 0 |
| Max | 1 | 0 | 1 | 0 |
| S:1/Slope | 0.013 | 0.001 | 0.002 | 0.001 |
| P:transition | 0.675 | 0.001 | 0.674 | 0.023 |

Global analysis
Maximum likelihood:-Ln L=27.067
AIC=62.134
r2=0.999
Observed compactness=0.536
Modeled compactness=0.536
Modeled compactness at the center=0.
Modeled compactness at the periphery=1.
R/t (Currey & Alexander 1985) : 3.0779

**RADIUS**

| Parameter | Mean Global value | SE Global value | Mean Angular value | SD Angular value |
|---|---|---|---|---|
| Min | 0 | 0 | 0 | 0 |
| Max | 1 | 0 | 1 | 0 |
| S:1/Slope | 0.025 | 0.001 | 0.003 | 0.004 |
| P:transition | 0.618 | 0.002 | 0.634 | 0.047 |

Global analysis
Maximum likelihood:-Ln L=52.027
AIC=112.055
r2=0.998
Observed compactness=0.612
Modeled compactness=0.612
Modeled compactness at the center=0.
Modeled compactness at the periphery=1.
R/t (Currey & Alexander 1985) : 2.6207
CDI (Castanet et al. 2000) : 0.3816

***Elaphurus davidianus***

| Parameter | Mean Global value | SE Global value | Mean Angular value | SD Angular value |
|---|---|---|---|---|
| Min | 0.01 | 0.004 | 0 | 0 |
| Max | 0.988 | 0.002 | 0.991 | 0.05 |
| S:1/Slope | 0.026 | 0.002 | 0.003 | 0.003 |
| P:transition | 0.601 | 0.002 | 0.608 | 0.049 |

Global analysis
Maximum likelihood:-Ln L=160.202
AIC=328.404
r2=0.995
Observed compactness=0.627
Modeled compactness=0.627
Modeled compactness at the center=0.01
Modeled compactness at the periphery=0.988
R/t (Currey & Alexander 1985) : 2.5067

**HUMERUS**

CDI (Castanet et al. 2000) : 0.3249

***Odocoileus virginianus***

| Parameter | Mean Global value | SE Global value | Mean Angular value | SD Angular value |
|---|---|---|---|---|
| Min | 0 | n.a. | 0 | 0 |
| Max | 1 | n.a. | 1 | 0 |
| S:1/Slope | 0.017 | n.a. | 0.002 | 0.002 |
| P:transition | 0.727 | n.a. | 0.727 | 0.03 |

Global analysis
Maximum likelihood:-Ln L=40.176
AIC=88.351
r2=0.998
Observed compactness=0.466
Modeled compactness=0.466
Modeled compactness at the center=0.
Modeled compactness at the periphery=1.
R/t (Currey & Alexander 1985) : 3.6608
CDI (Castanet et al. 2000) : 0.2732

***Ozotoceros bezoarticus***

| Parameter | Mean Global value | SE Global value | Mean Angular value | SD Angular value |
|---|---|---|---|---|
| Min | 0 | n.a. | 0 | 0 |
| Max | 1 | n.a. | 1 | 0 |
| S:1/Slope | 0.017 | n.a. | 0.002 | 0.002 |
| P:transition | 0.537 | n.a. | 0.536 | 0.029 |

Global analysis
Maximum likelihood:-Ln L=26.996
AIC=61.992
r2=0.999
Observed compactness=0.707

**RADIUS**

CDI (Castanet et al. 2000) : 0.3989

***Hydropotes inermis***

| Parameter | Mean Global value | SE Global value | Mean Angular value | SD Angular value |
|---|---|---|---|---|
| Min | 0 | n.a. | 0 | 0 |
| Max | 1 | n.a. | 1 | 0 |
| S:1/Slope | 0.021 | n.a. | 0.002 | 0.003 |
| P:transition | 0.634 | n.a. | 0.625 | 0.04 |

Global analysis
Maximum likelihood:-Ln L=16.743
AIC=41.487
r2=0.998
Observed compactness=0.601
Modeled compactness=0.601
Modeled compactness at the center=0.
Modeled compactness at the periphery=1.
R/t (Currey & Alexander 1985) : 2.7318
CDI (Castanet et al. 2000) : 0.3661

***Muntiacus muntjak***

| Parameter | Mean Global value | SE Global value | Mean Angular value | SD Angular value |
|---|---|---|---|---|
| Min | 0 | n.a. | 0 | 0 |
| Max | 1 | n.a. | 1 | 0 |
| S:1/Slope | 0.016 | n.a. | 0.002 | 0.002 |
| P:transition | 0.567 | n.a. | 0.576 | 0.027 |

Global analysis
Maximum likelihood:-Ln L=21.9
AIC=51.799
r2=1
Observed compactness=0.677

## HUMERUS

Modeled compactness=0.707

Modeled compactness at the center=0.

Modeled compactness at the periphery=1.

R/t (Currey & Alexander 1985) : 2.1609

CDI (Castanet et al. 2000) : 0.4628

***Pudu puda***

| Parameter | Mean Global value | SE Global value | Mean Angular value | SD Angular value |
|---|---|---|---|---|
| Min | 0 | 0 | 0 | 0 |
| Max | 1 | 0 | 1 | 0 |
| S:1/Slope | 0.011 | 0.001 | 0.002 | 0.001 |
| P:transition | 0.615 | 0.001 | 0.615 | 0.02 |

Global analysis

Maximum likelihood:-Ln L=21.681

AIC=51.362

r2=0.999

Observed compactness=0.616

Modeled compactness=0.616

Modeled compactness at the center=0.

Modeled compactness at the periphery=1.

R/t (Currey & Alexander 1985) : 2.597

CDI (Castanet et al. 2000) : 0.3851

***Rucervus eldii***

| Parameter | Mean Global value | SE Global value | Mean Angular value | SD Angular value |
|---|---|---|---|---|
| Min | 0 | 0 | 0 | 0 |
| Max | 1 | 0 | 1 | 0 |
| S:1/Slope | 0.025 | 0.001 | 0.002 | 0.003 |
| P:transition | 0.616 | 0.002 | 0.619 | 0.042 |

Global analysis

## RADIUS

Modeled compactness=0.677

Modeled compactness at the center=0.

Modeled compactness at the periphery=1.

R/t (Currey & Alexander 1985) : 2.31

CDI (Castanet et al. 2000) : 0.4329

***Odocoileus virginianus***

| Parameter | Mean Global value | SE Global value | Mean Angular value | SD Angular value |
|---|---|---|---|---|
| Min | 0 | n.a. | 0 | 0 |
| Max | 1 | n.a. | 1 | 0 |
| S:1/Slope | 0.025 | n.a. | 0.002 | 0.003 |
| P:transition | 0.584 | n.a. | 0.582 | 0.047 |

Global analysis

Maximum likelihood:-Ln L=45.746

AIC=99.492

r2=0.996

Observed compactness=0.656

Modeled compactness=0.656

Modeled compactness at the center=0.

Modeled compactness at the periphery=1.

R/t (Currey & Alexander 1985) : 2.4028

CDI (Castanet et al. 2000) : 0.4162

***Ozotoceros bezoarticus***

| Parameter | Mean Global value | SE Global value | Mean Angular value | SD Angular value |
|---|---|---|---|---|
| Min | 0 | n.a. | 0 | 0 |
| Max | 1 | n.a. | 1 | 0 |
| S:1/Slope | 0.026 | n.a. | 0.002 | 0.002 |
| P:transition | 0.416 | n.a. | 0.412 | 0.045 |

Global analysis

**HUMERUS**

Maximum likelihood:-Ln L=43.448

AIC=94.896

r2=0.997

Observed compactness=0.614

Modeled compactness=0.614

Modeled compactness at the center=0.

Modeled compactness at the periphery=1.

R/t (Currey & Alexander 1985) : 2.6044

CDI (Castanet et al. 2000) : 0.384

***Rusa alfredi***

| Parameter | Mean Global value | SE Global value | Mean Angular value | SD Angular value |
|---|---|---|---|---|
| Min | 0 | 0 | 0 | 0 |
| Max | 1 | 0 | 1 | 0 |
| S:1/Slope | 0.022 | 0.001 | 0.001 | 0.001 |
| P:transition | 0.526 | 0.002 | 0.523 | 0.041 |

Global analysis

Maximum likelihood:-Ln L=35.806

AIC=79.611

r2=0.999

Observed compactness=0.72

Modeled compactness=0.72

Modeled compactness at the center=0.

Modeled compactness at the periphery=1.

R/t (Currey & Alexander 1985) : 2.1095

CDI (Castanet et al. 2000) : 0.4741

**Mazama gouazoubira**

| Parameter | Mean Global value | SE Global value | Mean Angular value | SD Angular value |
|---|---|---|---|---|
| Min | 0 | 0 | 0 | 0 |
| Max | 1 | 0 | 1 | 0 |

**RADIUS**

Maximum likelihood:-Ln L=54.217

AIC=116.434

r2=0.997

Observed compactness=0.823

Modeled compactness=0.823

Modeled compactness at the center=0.

Modeled compactness at the periphery=1.

R/t (Currey & Alexander 1985) : 1.7136

CDI (Castanet et al. 2000) : 0.5836

***Pudu puda***

| Parameter | Mean Global value | SE Global value | Mean Angular value | SD Angular value |
|---|---|---|---|---|
| Min | 0 | 0 | 0 | 0 |
| Max | 1 | 0 | 1 | 0 |
| S:1/Slope | 0.014 | 0.001 | 0.001 | 0.002 |
| P:transition | 0.506 | 0.001 | 0.507 | 0.03 |

Global analysis

Maximum likelihood:-Ln L=26.449

AIC=60.899

r2=0.998

Observed compactness=0.738

Modeled compactness=0.738

Modeled compactness at the center=0.

Modeled compactness at the periphery=1.

R/t (Currey & Alexander 1985) : 2.0262

CDI (Castanet et al. 2000) : 0.4935

***Rucervus eldii***

| Parameter | Mean Global value | SE Global value | Mean Angular value | SD Angular value |
|---|---|---|---|---|
| Min | 0 | 0 | 0 | 0 |
| Max | 1 | 0 | 1 | 0 |

**HUMERUS**

| | | | | |
|---|---|---|---|---|
| S:1/Slope | 0.017 | 0.001 | 0.001 | 0.001 |
| P:transition | 0.53 | 0.001 | 0.527 | 0.031 |

Global analysis

Maximum likelihood:-Ln L=24.797

AIC=57.594

r2=1

Observed compactness=0.712

Modeled compactness=0.712

Modeled compactness at the center=0.

Modeled compactness at the periphery=1.

R/t (Currey & Alexander 1985) : 2.1289

CDI (Castanet et al. 2000) : 0.4697

***Cervus canadensis***

| Parameter | Mean Global value | SE Global value | Mean Angular value | SD Angular value |
|---|---|---|---|---|
| Min | 0 | 0 | 0 | 0 |
| Max | 1 | 0 | 1 | 0.001 |
| S:1/Slope | 0.02 | 0.001 | 0.003 | 0.003 |
| P:transition | 0.644 | 0.001 | 0.647 | 0.035 |

Global analysis

Maximum likelihood:-Ln L=53.883

AIC=115.766

r2=0.998

Observed compactness=0.58

Modeled compactness=0.58

Modeled compactness at the center=0.

Modeled compactness at the periphery=1.

R/t (Currey & Alexander 1985) : 2.8074

CDI (Castanet et al. 2000) : 0.3562

***Rusa unicolor***

**RADIUS**

| | | | | |
|---|---|---|---|---|
| S:1/Slope | 0.019 | 0.001 | 0.002 | 0.003 |
| P:transition | 0.6 | 0.002 | 0.6 | 0.031 |

Global analysis

Maximum likelihood:-Ln L=23.082

AIC=54.164

r2=1

Observed compactness=0.633

Modeled compactness=0.633

Modeled compactness at the center=0.

Modeled compactness at the periphery=1.

R/t (Currey & Alexander 1985) : 2.5021

CDI (Castanet et al. 2000) : 0.3997

***Rusa alfredi***

| Parameter | Mean Global value | SE Global value | Mean Angular value | SD Angular value |
|---|---|---|---|---|
| Min | 0 | 0 | 0 | 0 |
| Max | 1 | 0 | 1 | 0 |
| S:1/Slope | 0.024 | 0.001 | 0.003 | 0.006 |
| P:transition | 0.438 | 0.002 | 0.444 | 0.039 |

Global analysis

Maximum likelihood:-Ln L=26.342

AIC=60.684

r2=0.999

Observed compactness=0.804

Modeled compactness=0.804

Modeled compactness at the center=0.

Modeled compactness at the periphery=1.

R/t (Currey & Alexander 1985) : 1.7794

CDI (Castanet et al. 2000) : 0.562

***Mazama gouazoubira***

**HUMERUS**

| Parameter | Mean Global value | SE Global value | Mean Angular value | SD Angular value |
|---|---|---|---|---|
| Min | 0 | 0 | 0 | 0 |
| Max | 1 | 0 | 1 | 0 |
| S:1/Slope | 0.021 | 0.001 | 0.002 | 0.003 |
| P:transition | 0.666 | 0.001 | 0.669 | 0.037 |

Global analysis
Maximum likelihood:-Ln L=44.37
AIC=96.741
r2=0.998
Observed compactness=0.553
Modeled compactness=0.553
Modeled compactness at the center=0.
Modeled compactness at the periphery=1.
R/t (Currey & Alexander 1985) : 2.9897
CDI (Castanet et al. 2000) : 0.3345

***Alces* sp.**

| Parameter | Mean Global value | SE Global value | Mean Angular value | SD Angular value |
|---|---|---|---|---|
| Min | 0 | 0 | 0 | 0 |
| Max | 1 | 0 | 1 | 0 |
| S:1/Slope | 0.034 | 0.001 | 0.003 | 0.004 |
| P:transition | 0.711 | 0.002 | 0.717 | 0.057 |

Global analysis
Maximum likelihood:-Ln L=109.891
AIC=227.782
r2=0.987
Observed compactness=0.493
Modeled compactness=0.493
Modeled compactness at the center=0.
Modeled compactness at the periphery=1.
R/t (Currey & Alexander 1985) : 3.4551

**RADIUS**

| Parameter | Mean Global value | SE Global value | Mean Angular value | SD Angular value |
|---|---|---|---|---|
| Min | 0 | 0 | 0 | 0 |
| Max | 1 | 0 | 1 | 0 |
| S:1/Slope | 0.016 | 0.001 | 0.001 | 0.001 |
| P:transition | 0.447 | 0.001 | 0.449 | 0.029 |

Global analysis
Maximum likelihood:-Ln L=27.868
AIC=63.736
r2=0.999
Observed compactness=0.796
Modeled compactness=0.796
Modeled compactness at the center=0.
Modeled compactness at the periphery=1.
R/t (Currey & Alexander 1985) : 1.8099
CDI (Castanet et al. 2000) : 0.5525

***Cervus canadensis***

| Parameter | Mean Global value | SE Global value | Mean Angular value | SD Angular value |
|---|---|---|---|---|
| Min | 0 | 0 | 0 | 0 |
| Max | 1 | 0 | 1 | 0 |
| S:1/Slope | 0.019 | 0.001 | 0.003 | 0.003 |
| P:transition | 0.574 | 0.001 | 0.579 | 0.035 |

Global analysis
Maximum likelihood:-Ln L=26.218
AIC=60.437
r2=1
Observed compactness=0.666
Modeled compactness=0.666
Modeled compactness at the center=0.
Modeled compactness at the periphery=1.
R/t (Currey & Alexander 1985) : 2.3496

**HUMERUS**

CDI (Castanet et al. 2000) : 0.2894

***Eucladoceros* sp.**

| Parameter | Mean Global value | SE Global value | Mean Angular value | SD Angular value |
|---|---|---|---|---|
| Min | 0 | n.a. | 0 | 0 |
| Max | 1 | n.a. | 1 | 0 |
| S:1/Slope | 0.027 | n.a. | 0.002 | 0.002 |
| P:transition | 0.539 | n.a. | 0.539 | 0.048 |

Global analysis
Maximum likelihood:-Ln L=101.237
AIC=210.475
r2=0.995
Observed compactness=0.704
Modeled compactness=0.704
Modeled compactness at the center=0.
Modeled compactness at the periphery=1.
R/t (Currey & Alexander 1985) : 2.1683
CDI (Castanet et al. 2000) : 0.4612

**RADIUS**

CDI (Castanet et al. 2000) : 0.4256

***Rusa unicolor***

| Parameter | Mean Global value | SE Global value | Mean Angular value | SD Angular value |
|---|---|---|---|---|
| Min | 0 | n.a. | 0 | 0 |
| Max | 1 | n.a. | 1 | 0 |
| S:1/Slope | 0.024 | n.a. | 0.002 | 0.003 |
| P:transition | 0.539 | n.a. | 0.553 | 0.039 |

Global analysis
Maximum likelihood:-Ln L=29.853
AIC=67.707
r2=0.999
Observed compactness=0.702
Modeled compactness=0.702
Modeled compactness at the center=0.
Modeled compactness at the periphery=1.
R/t (Currey & Alexander 1985) : 2.1686
CDI (Castanet et al. 2000) : 0.4611

**Castanet, J., Rogers, K. C., Cubo, J., and Jacques-Boisard, J.** (2000). Periosteal bone growth rates in extant ratites (ostriche and emu). Implications for assessing growth in dinosaurs. C.R. Acad. Sci. III-Vie.***323*(6)**, 543-550.

**Currey, J. D. and Alexander, R. M.** (1985). The thickness of the walls of tubular bones. *J. Zool.***206**, 453–468.

**SOM 4.** All measured slice geometry parameters for the whole dataset.

| | CSA (mm^2) | X cent. (mm) | Y cent. (mm) | Density | wX cent. (mm) | wY cent. (mm) | Theta (rad) | R1 (mm) | R2 (mm) | Imin (mm^4) | Imax (mm^4) | Ipm (mm^4) | Zmax (mm^3) | Zmin (mm^3) | Zpol (mm^3) | Feret Min (mm) | Feret Max (mm) | Feret Angle (rad) | Perime-ter (mm) | Max Thick 2D (mm) | Mean Thick 2D (mm) | SD Thick 2D (mm) |
|---|---|---|---|---|---|---|---|---|---|---|---|---|---|---|---|---|---|---|---|---|---|---|
| **Tibia adults** | | | | | | | | | | | | | | | | | | | | | | |
| | | | | | | | | | | | | | | | | | | | | | | |
| ***Alces alces*** | 483.92 | 19.28 | 20.96 | 1.80 | 19.28 | 20.96 | 1.09 | 14.97 | 18.67 | 36271.17 | 58026.63 | 63.63 | 3108.76 | 2422.33 | 4935.86 | 29.17 | 37.09 | 2.29 | 110.64 | 7.23 | 6.03 | 0.82 |
| ***Axis axis*** | 296.46 | 19.09 | 18.28 | 1.80 | 19.09 | 18.28 | -0.20 | 11.01 | 13.33 | 12407.96 | 16905.82 | 1.91 | 1268.74 | 1126.67 | 2189.89 | 21.70 | 26.61 | 2.91 | 81.33 | 6.37 | 5.18 | 0.53 |
| ***Candiacervus ropalophorus*** | 160.31 | 10.58 | 9.11 | 1.80 | 10.58 | 9.11 | 0.30 | 6.98 | 8.75 | 2088.63 | 3166.44 | 2.35 | 362.00 | 299.11 | 600.72 | 13.81 | 16.99 | 2.46 | 54.30 | 6.43 | 5.40 | 0.72 |
| ***Candiacervus* sp. II** | 160.02 | 8.51 | 10.47 | 1.80 | 8.51 | 10.47 | -1.53 | 7.03 | 8.92 | 2177.86 | 3553.19 | 26.63 | 398.49 | 309.88 | 635.05 | 13.74 | 17.58 | 1.67 | 52.82 | 5.67 | 4.93 | 0.46 |
| ***Cervus canadensis*** | 726.99 | 21.73 | 23.30 | 1.80 | 21.73 | 23.30 | 1.08 | 17.29 | 19.54 | 63150.88 | 88363.04 | 93.78 | 4521.26 | 3652.74 | 7259.15 | 32.43 | 39.04 | 2.47 | 121.16 | 11.93 | 9.23 | 1.65 |
| ***Dama dama*** | 218.30 | 16.55 | 11.73 | 1.80 | 16.55 | 11.73 | -0.24 | 9.05 | 12.09 | 5916.05 | 10342.34 | 2.03 | 855.46 | 653.45 | 1340.36 | 17.78 | 23.74 | 0.32 | 70.58 | 5.08 | 4.34 | 0.44 |
| ***Dicrocerus elegans*** | 170.76 | 9.62 | 8.16 | 1.80 | 9.62 | 8.16 | -0.46 | 7.72 | 9.79 | 3228.42 | 4934.16 | 5.59 | 503.86 | 418.36 | 832.80 | 15.27 | 19.21 | 0.58 | 58.42 | 4.73 | 4.25 | 0.32 |
| ***Elaphurus davidianus*** | 557.44 | 19.54 | 19.31 | 1.80 | 19.54 | 19.31 | 1.25 | 14.55 | 18.25 | 36894.39 | 52953.34 | 83.62 | 2901.38 | 2535.34 | 4920.93 | 28.20 | 35.11 | 1.16 | 106.71 | 10.93 | 8.10 | 1.64 |
| ***Eucladoceros* sp.** | 1091.10 | 27.12 | 24.90 | 1.80 | 27.12 | 24.90 | 1.21 | 21.54 | 24.90 | 118700.66 | 188007.41 | 159.70 | 7551.51 | 5510.43 | 12187.59 | 38.31 | 47.88 | 2.12 | 144.97 | 16.91 | 12.75 | 2.84 |
| ***Hydropotes inermis*** | 60.50 | 8.29 | 8.93 | 1.80 | 8.29 | 8.93 | -0.61 | 6.06 | 6.47 | 572.82 | 820.53 | 3.30 | 126.87 | 94.58 | 213.86 | 10.98 | 12.97 | 0.55 | 38.39 | 2.65 | 2.21 | 0.25 |
| ***Mazama gouazoubira*** | 101.60 | 8.95 | 9.03 | 1.80 | 8.95 | 9.03 | 1.57 | 6.16 | 6.46 | 1205.46 | 1274.92 | 16.93 | 197.27 | 195.81 | 361.33 | 12.31 | 13.27 | 0.89 | 42.21 | 3.95 | 3.67 | 0.19 |
| ***Muntiacus muntjak*** | 67.86 | 8.23 | 7.65 | 1.80 | 8.23 | 7.65 | -0.92 | 5.86 | 6.79 | 618.92 | 962.98 | 7.16 | 141.78 | 105.71 | 231.80 | 10.54 | 13.14 | 1.29 | 39.39 | 3.56 | 2.61 | 0.52 |
| ***Odocoileus virginianus*** | 130.12 | 10.40 | 10.02 | 1.80 | 10.40 | 10.02 | 1.01 | 7.50 | 8.69 | 2224.07 | 2969.86 | 15.57 | 341.68 | 296.53 | 584.09 | 14.35 | 17.03 | 2.42 | 52.48 | 4.76 | 3.74 | 0.56 |
| ***Ozotoceros bezoarticus*** | 198.60 | 13.81 | 15.72 | 1.80 | 13.81 | 15.72 | -1.24 | 8.26 | 10.29 | 3558.55 | 5863.22 | 29.62 | 569.87 | 430.62 | 909.70 | 15.75 | 20.69 | 1.16 | 59.77 | 7.06 | 5.49 | 1.00 |
| ***Procervulus praelucidus*** | 68.74 | 7.95 | 6.09 | 1.80 | 7.95 | 6.09 | -0.14 | 5.23 | 6.40 | 616.41 | 893.68 | 0.24 | 139.54 | 117.76 | 233.77 | 10.23 | 12.49 | 0.50 | 39.17 | 3.07 | 2.57 | 0.30 |
| ***Pudu puda*** | 60.48 | 8.27 | 7.11 | 1.80 | 8.27 | 7.11 | 1.55 | 4.13 | 5.17 | 304.32 | 464.66 | 10.08 | 89.93 | 73.62 | 147.95 | 8.20 | 10.31 | 1.35 | 31.42 | 3.46 | 3.13 | 0.19 |
| ***Rangifer tarandus*** | 159.24 | 15.80 | 12.86 | 1.80 | 15.80 | 12.86 | 1.24 | 10.24 | 11.29 | 4136.28 | 6252.90 | 23.76 | 554.07 | 404.03 | 891.45 | 17.88 | 21.09 | 2.26 | 65.43 | 6.21 | 3.90 | 1.42 |
| ***Rucervus eldii*** | 255.05 | 16.09 | 16.86 | 1.80 | 16.09 | 16.86 | -0.66 | 11.41 | 12.83 | 8579.50 | 12579.82 | 15.90 | 980.41 | 752.05 | 1643.52 | 20.79 | 25.06 | 0.61 | 74.88 | 7.26 | 5.25 | 1.13 |
| ***Rusa unicolor*** | 495.95 | 21.54 | 21.88 | 1.80 | 21.54 | 21.88 | -1.37 | 13.79 | 17.93 | 29503.46 | 47641.77 | 79.27 | 2657.45 | 2139.89 | 4298.70 | 26.42 | 34.86 | 1.15 | 102.98 | 9.73 | 7.32 | 1.39 |
| ***Rusa alfredi*** | 199.52 | 13.60 | 11.15 | 1.80 | 13.60 | 11.15 | 1.57 | 8.57 | 10.18 | 4154.10 | 5471.55 | 33.25 | 537.40 | 484.94 | 936.62 | 16.74 | 19.98 | 1.07 | 60.50 | 5.79 | 5.29 | 0.55 |
| ***Sinomegaloceros yabei*** | 905.16 | 24.71 | 21.89 | 1.80 | 24.71 | 21.89 | -0.23 | 19.90 | 25.11 | 105945.03 | 150848.61 | 7.75 | 6006.46 | 5325.06 | 10209.63 | 38.58 | 45.84 | 0.26 | 178.66 | 12.17 | 9.61 | 2.01 |
| | | | | | | | | | | | | | | | | | | | | | | |
| **Femur adults** | | | | | | | | | | | | | | | | | | | | | | |
| | | | | | | | | | | | | | | | | | | | | | | |
| ***Alces alces* (1980-74)** | 622.37 | 33.25 | 32.50 | 1.80 | 33.25 | 32.50 | -0.45 | 16.72 | 23.92 | 57679.54 | 115265.96 | 19.24 | 4818.86 | 3449.44 | 7215.90 | 33.55 | 46.31 | 0.39 | 129.33 | 8.27 | 6.51 | 0.98 |
| ***Alces alces* (ZMUZ 20242)** | 496.34 | 20.93 | 17.73 | 1.80 | 20.93 | 17.73 | -0.27 | 15.60 | 20.18 | 40681.75 | 66830.34 | 5.78 | 3312.15 | 2608.59 | 5289.97 | 30.49 | 38.74 | 0.18 | 116.03 | 6.83 | 5.72 | 0.71 |
| ***Candiacervus ropalophorus*** | 129.52 | 8.74 | 10.00 | 1.80 | 8.74 | 10.00 | -1.41 | 8.20 | 8.93 | 2695.16 | 3413.23 | 21.06 | 382.28 | 328.84 | 651.06 | 15.17 | 17.78 | 0.96 | 60.98 | 3.55 | 3.21 | 0.37 |

| | CSA (mm^2) | X cent. (mm) | Y cent. (mm) | Density | wX cent. (mm) | wY cent. (mm) | Theta (rad) | R1 (mm) | R2 (mm) | Imin (mm^4) | Imax (mm^4) | Ipm (mm^4) | Zmax (mm^3) | Zmin (mm^3) | Zpol (mm^3) | Feret Min (mm) | Feret Max (mm) | Feret Angle (rad) | Perime-ter (mm) | Max Thick 2D (mm) | Mean Thick 2D (mm) | SD Thick 2D (mm) |
|---|---|---|---|---|---|---|---|---|---|---|---|---|---|---|---|---|---|---|---|---|---|---|
| ***Candiacervus* sp. II** | 172.26 | 12.09 | 12.71 | 1.80 | 12.09 | 12.71 | -1.50 | 9.67 | 9.80 | 5084.10 | 5366.26 | 28.55 | 547.46 | 526.03 | 1041.16 | 18.69 | 19.59 | 1.73 | 64.25 | 4.24 | 3.72 | 0.45 |
| ***Capreolus capreolus*** | 94.45 | 9.55 | 8.66 | 1.80 | 9.55 | 8.66 | -1.19 | 7.63 | 7.63 | 1876.17 | 1958.52 | 13.51 | 256.84 | 245.77 | 488.33 | 14.70 | 15.25 | 1.74 | 50.12 | 2.88 | 2.49 | 0.26 |
| ***Cervus canadensis*** | 710.85 | 29.54 | 21.53 | 1.80 | 29.54 | 21.53 | -0.12 | 17.21 | 20.49 | 70441.55 | 102413.38 | 1.56 | 4998.39 | 4094.19 | 8060.96 | 33.95 | 41.14 | 0.53 | 125.53 | 10.45 | 8.15 | 1.44 |
| ***Cervus elaphus*** | 311.86 | 20.97 | 17.15 | 1.80 | 20.97 | 17.15 | 0.21 | 16.09 | 19.43 | 19880.94 | 24291.91 | 2.31 | 1250.11 | 1235.95 | 2261.27 | 26.74 | 31.02 | 2.81 | 107.49 | 5.00 | 4.31 | 0.55 |
| ***Dama dama*** | 177.61 | 12.71 | 17.33 | 1.80 | 12.71 | 17.33 | -1.10 | 11.50 | 12.23 | 7889.04 | 8700.51 | 23.58 | 711.47 | 686.02 | 1344.86 | 21.54 | 23.68 | 1.22 | 74.76 | 3.75 | 3.02 | 0.34 |
| ***Dicrocerus elegans*** | 133.24 | 9.93 | 10.96 | 1.80 | 9.93 | 10.96 | 1.39 | 7.96 | 9.65 | 2795.98 | 3990.68 | 21.51 | 413.48 | 351.18 | 702.41 | 15.61 | 19.00 | 1.78 | 57.44 | 4.19 | 3.23 | 0.54 |
| ***Elaphurus davidianus*** | 486.60 | 27.36 | 19.59 | 1.80 | 27.36 | 19.59 | -0.16 | 15.68 | 17.49 | 41787.78 | 53873.46 | 2.01 | 3079.52 | 2665.84 | 4809.31 | 30.43 | 37.27 | 0.65 | 111.68 | 7.47 | 6.09 | 0.94 |
| ***Euprox* sp.** | 154.90 | 11.46 | 10.75 | 1.80 | 11.46 | 10.75 | 1.20 | 9.72 | 10.96 | 4730.23 | 5794.65 | 22.48 | 528.95 | 486.86 | 941.01 | 18.51 | 20.66 | 2.15 | 66.03 | 3.88 | 3.17 | 0.50 |
| ***Hydropotes inermis*** | 62.21 | 8.86 | 8.84 | 1.80 | 8.86 | 8.84 | 0.80 | 5.46 | 7.20 | 649.67 | 965.94 | 5.34 | 134.18 | 118.91 | 221.49 | 10.83 | 13.79 | 2.48 | 39.74 | 2.33 | 2.10 | 0.21 |
| ***Mazama gouazoubira*** | 86.39 | 7.74 | 8.70 | 1.80 | 7.74 | 8.70 | -1.47 | 6.13 | 6.54 | 1029.67 | 1158.21 | 14.25 | 177.21 | 167.95 | 327.62 | 12.04 | 13.11 | 2.12 | 41.55 | 3.30 | 2.95 | 0.20 |
| ***Megaloceros giganteus*** | 1301.98 | 32.77 | 26.00 | 1.80 | 32.77 | 26.00 | 0.25 | 25.55 | 32.56 | 252641.05 | 426301.91 | 13.69 | 13094.79 | 9890.19 | 20565.07 | 48.05 | 63.94 | 2.87 | 195.15 | 14.20 | 9.86 | 2.05 |
| ***Muntiacus muntjak*** | 73.00 | 9.86 | 8.58 | 1.80 | 9.86 | 8.58 | -0.21 | 6.37 | 7.28 | 1030.36 | 1182.67 | 0.53 | 162.39 | 161.66 | 300.12 | 12.57 | 14.26 | 0.43 | 43.90 | 2.55 | 2.23 | 0.19 |
| ***Odocoileus virginianus*** | 104.58 | 10.01 | 10.92 | 1.80 | 10.01 | 10.92 | 0.79 | 7.75 | 9.78 | 2122.27 | 2911.06 | 8.82 | 297.67 | 273.95 | 513.11 | 15.35 | 18.19 | 2.27 | 53.76 | 3.17 | 2.62 | 0.34 |
| ***Ozotoceros bezoarticus*** | 146.04 | 10.64 | 11.29 | 1.80 | 10.64 | 11.29 | -0.94 | 8.34 | 9.45 | 3027.93 | 3822.85 | 15.98 | 404.41 | 362.92 | 722.85 | 16.23 | 18.45 | 0.96 | 55.79 | 4.39 | 3.71 | 0.34 |
| ***Procervulus praelucidus*** | 39.30 | 6.03 | 6.32 | 1.80 | 6.03 | 6.32 | -0.99 | 5.67 | 6.49 | 449.59 | 599.10 | 4.57 | 92.30 | 79.31 | 161.28 | 11.07 | 12.27 | 0.94 | 39.32 | 1.59 | 1.32 | 0.23 |
| ***Pudu puda*** | 70.21 | 8.64 | 7.94 | 1.80 | 8.64 | 7.94 | -0.95 | 6.24 | 7.02 | 934.11 | 1059.33 | 7.68 | 150.83 | 149.78 | 281.26 | 12.20 | 13.33 | 0.75 | 42.35 | 2.66 | 2.26 | 0.29 |
| ***Rucervus eldii*** | 207.55 | 16.49 | 15.15 | 1.80 | 16.49 | 15.15 | -0.49 | 10.72 | 14.20 | 8493.30 | 12016.21 | 7.72 | 846.46 | 792.57 | 1429.77 | 21.41 | 26.88 | 0.56 | 76.84 | 3.97 | 3.52 | 0.28 |
| ***Rusa unicolor*** | 468.03 | 27.04 | 26.09 | 1.80 | 27.04 | 26.09 | -0.95 | 16.76 | 19.61 | 42049.77 | 53309.72 | 51.74 | 2719.04 | 2509.56 | 4767.28 | 31.67 | 37.98 | 1.02 | 113.35 | 7.15 | 5.58 | 0.70 |
| ***Rusa alfredi*** | 236.99 | 15.37 | 16.38 | 1.80 | 15.37 | 16.38 | -0.51 | 9.66 | 10.90 | 6815.16 | 8543.63 | 9.34 | 783.96 | 705.57 | 1315.73 | 19.06 | 22.32 | 0.80 | 68.03 | 5.87 | 5.08 | 0.36 |
| ***Sinomegaloceros yabei*** | 1254.49 | 24.76 | 30.24 | 1.80 | 24.76 | 30.24 | -1.52 | 23.52 | 31.27 | 222272.16 | 342999.30 | 208.62 | 10968.89 | 9449.27 | 17709.93 | 45.88 | 59.97 | 1.63 | 183.23 | 12.23 | 10.06 | 1.28 |
| | | | | | | | | | | | | | | | | | | | | | | |
| Radius adults | | | | | | | | | | | | | | | | | | | | | | |
| | | | | | | | | | | | | | | | | | | | | | | |
| ***Alces alces (ZMUZ 20242)*** | 372.58 | 21.41 | 28.52 | 1.80 | 21.41 | 28.52 | -0.13 | 12.85 | 19.27 | 21355.14 | 46621.62 | 0.98 | 2419.87 | 1661.87 | 3474.97 | 25.11 | 38.07 | 0.36 | 104.71 | 6.69 | 4.92 | 0.85 |
| ***Axis axis*** | 217.24 | 14.88 | 17.23 | 1.80 | 14.88 | 17.23 | -0.04 | 8.97 | 13.23 | 5235.17 | 13913.23 | 0.04 | 1052.08 | 583.63 | 1354.84 | 16.87 | 27.37 | 0.30 | 77.09 | 6.69 | 4.48 | 1.26 |
| ***Candiacervus ropalophorus*** | 178.75 | 10.68 | 8.85 | 1.80 | 10.68 | 8.85 | -0.15 | 10.35 | 11.81 | 5874.87 | 7969.59 | 0.67 | 674.69 | 567.45 | 998.07 | 17.25 | 26.55 | 2.43 | 74.78 | 11.94 | 7.68 | 3.27 |
| ***Candiacervus* sp. *II*** | 115.58 | 7.72 | 10.79 | 1.80 | 7.72 | 10.79 | 1.56 | 5.55 | 8.86 | 1040.87 | 2744.83 | 19.26 | 309.66 | 187.55 | 424.97 | 10.97 | 17.53 | 1.64 | 50.97 | 5.72 | 4.02 | 1.15 |
| ***Cervus canadensis*** | 573.63 | 19.61 | 23.79 | 1.80 | 19.61 | 23.79 | -1.10 | 12.22 | 21.18 | 30167.20 | 87768.98 | 76.23 | 4143.85 | 2469.77 | 5472.62 | 24.73 | 42.75 | 0.92 | 116.74 | 9.93 | 7.53 | 1.62 |
| ***Dama dama*** | 213.69 | 9.23 | 12.19 | 1.80 | 9.23 | 12.19 | 1.18 | 8.13 | 13.11 | 3730.86 | 10431.77 | 30.49 | 795.61 | 459.03 | 1072.15 | 15.55 | 25.43 | 2.00 | 68.48 | 6.46 | 4.78 | 0.89 |
| ***Dicrocerus elegans*** | 106.85 | 7.94 | 10.98 | 1.80 | 7.94 | 10.98 | 1.53 | 5.30 | 8.35 | 883.01 | 2231.22 | 17.78 | 267.27 | 166.50 | 366.54 | 10.34 | 16.67 | 1.46 | 46.17 | 5.03 | 3.81 | 0.80 |

| | CSA (mm^2) | X cent. (mm) | Y cent. (mm) | Density | wX cent. (mm) | wY cent. (mm) | Theta (rad) | R1 (mm) | R2 (mm) | Imin (mm^4) | Imax (mm^4) | Ipm (mm^4) | Zmax (mm^3) | Zmin (mm^3) | Zpol (mm^3) | Feret Min (mm) | Feret Max (mm) | Feret Angle (rad) | Perime- ter (mm) | Max Thick 2D (mm) | Mean Thick 2D (mm) | SD Thick 2D (mm) |
|---|---|---|---|---|---|---|---|---|---|---|---|---|---|---|---|---|---|---|---|---|---|---|
| ***Elaphurus davidianus*** | 456.30 | 21.67 | 23.54 | 1.80 | 21.67 | 23.54 | 0.58 | 15.76 | 17.54 | 29808.14 | 44907.87 | 22.65 | 2559.83 | 1890.91 | 3877.94 | 27.41 | 35.32 | 2.97 | 107.96 | 8.25 | 6.21 | 1.22 |
| ***Hydropotes inermis*** | 39.98 | 7.64 | 6.44 | 1.80 | 7.64 | 6.44 | -0.27 | 3.61 | 6.07 | 165.36 | 491.27 | 0.46 | 80.97 | 45.79 | 107.92 | 6.91 | 12.01 | 0.33 | 32.29 | 2.44 | 1.84 | 0.33 |
| ***Mazama gouazoubira*** | 69.42 | 6.19 | 8.96 | 1.80 | 6.19 | 8.96 | -1.57 | 4.16 | 6.68 | 358.30 | 932.00 | 11.57 | 139.48 | 86.10 | 187.06 | 8.13 | 13.50 | 1.45 | 36.87 | 4.19 | 3.15 | 0.65 |
| ***Muntiacus muntjak*** | 47.79 | 8.24 | 6.12 | 1.80 | 8.24 | 6.12 | 0.15 | 3.37 | 7.00 | 170.21 | 718.85 | 0.17 | 102.77 | 50.47 | 125.70 | 6.65 | 13.94 | 2.91 | 34.95 | 3.34 | 2.25 | 0.66 |
| ***Odocoileus virginianus*** | 91.03 | 11.13 | 11.47 | 1.80 | 11.13 | 11.47 | -1.29 | 5.39 | 9.22 | 759.61 | 2380.49 | 14.04 | 258.20 | 140.98 | 335.41 | 10.12 | 18.11 | 1.19 | 47.82 | 4.27 | 2.90 | 0.70 |
| ***Ozotoceros bezoarticus*** | 126.05 | 7.47 | 10.29 | 1.80 | 7.47 | 10.29 | -1.42 | 5.51 | 9.03 | 1085.84 | 2965.20 | 20.56 | 328.54 | 197.03 | 448.58 | 10.77 | 18.05 | 1.36 | 48.89 | 6.02 | 4.41 | 1.03 |
| ***Procervulus praelucidus*** | 53.50 | 9.53 | 5.63 | 1.80 | 9.53 | 5.63 | 0.05 | 3.62 | 6.76 | 210.65 | 741.03 | 0.03 | 109.66 | 58.13 | 138.55 | 7.12 | 13.56 | 3.05 | 35.01 | 3.36 | 2.53 | 0.64 |
| ***Pudu puda*** | 38.60 | 8.05 | 8.47 | 1.80 | 8.05 | 8.47 | -1.15 | 3.37 | 5.02 | 131.46 | 301.53 | 5.37 | 60.03 | 38.99 | 85.92 | 6.81 | 9.97 | 1.06 | 28.05 | 2.62 | 2.13 | 0.31 |
| ***Rucervus eldii*** | 152.93 | 11.49 | 13.67 | 1.80 | 11.49 | 13.67 | -1.36 | 6.91 | 11.56 | 2304.88 | 6581.26 | 24.42 | 569.10 | 333.51 | 767.22 | 13.40 | 23.28 | 1.28 | 61.39 | 5.58 | 3.80 | 0.94 |
| ***Rusa unicolor*** | 390.82 | 29.45 | 36.32 | 1.80 | 29.45 | 36.32 | 0.34 | 10.96 | 18.64 | 12210.73 | 40815.17 | 7.03 | 2189.18 | 1114.57 | 2801.77 | 19.92 | 36.17 | 2.92 | 96.83 | 10.25 | 6.91 | 2.10 |
| ***Rusa alfredi*** | 181.69 | 20.43 | 13.46 | 1.80 | 20.43 | 13.46 | -0.12 | 6.98 | 11.72 | 2123.54 | 7435.64 | 0.42 | 634.70 | 304.14 | 799.56 | 13.27 | 23.66 | 0.07 | 63.53 | 6.68 | 4.86 | 1.15 |
| | | | | | | | | | | | | | | | | | | | | | | |
| **Humerus adults** | | | | | | | | | | | | | | | | | | | | | | |
| | | | | | | | | | | | | | | | | | | | | | | |
| ***Alces alces* (1980-74)** | 704.47 | 30.11 | 25.36 | 1.80 | 30.11 | 25.36 | 0.77 | 21.40 | 23.65 | 104061.03 | 125628.71 | 57.18 | 5311.20 | 4863.91 | 9553.14 | 39.68 | 45.75 | 2.88 | 140.60 | 11.19 | 7.19 | 2.22 |
| ***Alces alces* (ZMUZ 20242)** | 475.60 | 22.17 | 23.62 | 1.80 | 22.17 | 23.62 | 1.37 | 17.35 | 20.07 | 46593.65 | 62558.30 | 75.99 | 3117.51 | 2685.26 | 5430.87 | 32.38 | 38.40 | 1.44 | 116.57 | 6.83 | 5.02 | 1.12 |
| ***Candiacervus* sp. II** | 197.61 | 9.69 | 12.11 | 1.80 | 9.69 | 12.11 | 1.42 | 8.65 | 10.57 | 4103.33 | 6313.17 | 32.14 | 597.54 | 474.62 | 978.27 | 16.78 | 20.77 | 1.71 | 62.05 | 5.87 | 4.86 | 0.77 |
| ***Cervus canadensis*** | 749.43 | 26.84 | 22.39 | 1.80 | 26.84 | 22.39 | -0.41 | 18.66 | 22.69 | 85845.05 | 128675.89 | 19.74 | 5672.20 | 4600.01 | 9203.60 | 36.89 | 45.28 | 0.50 | 134.18 | 9.86 | 7.81 | 1.42 |
| ***Dama dama*** | 187.34 | 11.19 | 11.62 | 1.80 | 11.19 | 11.62 | -1.34 | 9.77 | 11.08 | 6192.46 | 7997.71 | 29.59 | 721.92 | 634.01 | 1243.88 | 19.40 | 22.10 | 1.29 | 69.45 | 4.10 | 3.65 | 0.41 |
| ***Dicrocerus elegans*** | 299.80 | 16.20 | 15.37 | 1.80 | 16.20 | 15.37 | 0.50 | 10.69 | 13.58 | 10979.18 | 16906.45 | 11.47 | 1244.71 | 1026.80 | 2028.38 | 21.23 | 26.97 | 2.62 | 86.86 | 6.14 | 5.27 | 0.61 |
| ***Elaphurus davidianus*** | 572.17 | 26.21 | 23.29 | 1.80 | 26.21 | 23.29 | -0.13 | 16.44 | 18.80 | 47722.52 | 63158.40 | 1.51 | 3359.85 | 2903.70 | 5804.26 | 31.27 | 37.88 | 0.28 | 114.25 | 10.23 | 7.48 | 1.89 |
| ***Eucladoceros* sp.** | 875.67 | 28.80 | 23.90 | 1.80 | 28.80 | 23.90 | 0.10 | 18.00 | 22.76 | 83880.37 | 140466.65 | 1.44 | 6172.35 | 4659.72 | 9728.74 | 34.77 | 45.68 | 3.00 | 132.23 | 11.82 | 9.72 | 1.53 |
| ***Hydropotes inermis*** | 49.51 | 7.78 | 9.04 | 1.80 | 7.78 | 9.04 | 1.53 | 4.24 | 6.02 | 303.88 | 590.73 | 8.24 | 98.11 | 71.62 | 147.81 | 8.53 | 12.32 | 1.72 | 33.82 | 2.19 | 2.03 | 0.09 |
| ***Mazama gouazoubira*** | 71.32 | 8.56 | 6.70 | 1.80 | 8.56 | 6.70 | -0.19 | 5.10 | 6.49 | 570.78 | 889.89 | 0.44 | 137.12 | 111.94 | 225.07 | 10.10 | 12.69 | 0.18 | 37.44 | 3.02 | 2.72 | 0.19 |
| ***Megaloceros giganteus*** | 1513.32 | 30.00 | 24.09 | 1.80 | 30.00 | 24.09 | -0.12 | 24.43 | 29.27 | 262612.36 | 384721.58 | 3.46 | 13143.35 | 10750.99 | 22045.25 | 47.62 | 57.51 | 0.09 | 173.24 | 14.91 | 12.22 | 2.66 |
| ***Muntiacus muntjak*** | 64.82 | 8.48 | 6.94 | 1.80 | 8.48 | 6.94 | 0.18 | 5.77 | 6.94 | 728.49 | 1051.50 | 0.36 | 151.42 | 126.16 | 255.18 | 11.18 | 13.85 | 2.94 | 40.75 | 2.69 | 2.11 | 0.26 |
| ***Odocoileus virginianus*** | 104.28 | 12.38 | 9.28 | 1.80 | 12.38 | 9.28 | -0.23 | 8.07 | 9.16 | 2564.54 | 2863.03 | 0.86 | 312.61 | 317.63 | 588.54 | 15.89 | 17.80 | 0.35 | 54.79 | 2.90 | 2.46 | 0.27 |
| ***Ozotoceros bezoarticus*** | 142.12 | 12.98 | 11.73 | 1.80 | 12.98 | 11.73 | -0.43 | 7.56 | 8.72 | 2518.77 | 3238.65 | 4.04 | 371.46 | 333.12 | 656.02 | 15.18 | 17.34 | 0.42 | 52.68 | 4.62 | 3.93 | 0.48 |
| ***Procervulus praelucidus*** | 57.01 | 6.68 | 7.59 | 1.80 | 6.68 | 7.59 | -1.14 | 5.17 | 6.54 | 536.53 | 844.83 | 7.82 | 129.21 | 103.74 | 207.91 | 10.28 | 13.07 | 1.07 | 39.87 | 2.28 | 1.93 | 0.26 |
| ***Pudu puda*** | 52.13 | 7.06 | 6.32 | 1.80 | 7.06 | 6.32 | 0.15 | 4.75 | 6.08 | 372.96 | 595.47 | 0.19 | 97.96 | 78.50 | 159.30 | 9.27 | 11.82 | 3.01 | 34.44 | 2.66 | 2.11 | 0.27 |

| | CSA (mm^2) | X cent. (mm) | Y cent. (mm) | Density | wX cent. (mm) | wY cent. (mm) | Theta (rad) | R1 (mm) | R2 (mm) | Imin (mm^4) | Imax (mm^4) | Ipm (mm^4) | Zmax (mm^3) | Zmin (mm^3) | Zpol (mm^3) | Feret Min (mm) | Feret Max (mm) | Feret Angle (rad) | Perimeter (mm) | Max Thick 2D (mm) | Mean Thick 2D (mm) | SD Thick 2D (mm) |
|---|---|---|---|---|---|---|---|---|---|---|---|---|---|---|---|---|---|---|---|---|---|---|
| ***Rucervus eldii*** | 205.58 | 14.78 | 14.11 | 1.80 | 14.78 | 14.11 | -0.29 | 9.72 | 11.27 | 6271.29 | 8418.48 | 2.70 | 747.04 | 645.56 | 1283.39 | 19.04 | 22.57 | 0.27 | 67.87 | 5.37 | 4.26 | 0.67 |
| ***Rusa unicolor*** | 554.75 | 26.28 | 26.35 | 1.80 | 26.28 | 26.35 | -0.19 | 17.32 | 19.73 | 54950.35 | 68770.51 | 3.24 | 3485.95 | 3172.04 | 6242.31 | 33.03 | 38.06 | 3.04 | 118.01 | 8.55 | 6.47 | 1.20 |
| ***Rusa alfredi*** | 225.07 | 13.99 | 13.77 | 1.80 | 13.99 | 13.77 | -0.34 | 9.89 | 11.17 | 6107.65 | 8091.01 | 4.16 | 724.55 | 617.55 | 1265.51 | 18.48 | 22.26 | 0.37 | 66.59 | 5.69 | 4.91 | 0.53 |

# CHAPTER 6

# CONCLUSIONS AND FUTURE PERSPECTIVES

# 6 Conclusions and future perspectives

This dissertation contains much documentation on the histology of hard tissues in extant and extinct mammals, and the implications of these new data for body size and life history evolution are discussed based on different kinds of analyses. In section 1.7 of chapter 1 and chapter 2, it is shown that synapsid bone displays a large variety of bone tissue and vascularisation patterns. Tissue types observed in bone are lamellar, parallel-fibred, fibrolamellar, and woven-fibred bone, depending on taxon and individual age. Large bodied cynodont and mammalian species typically show plexiform to laminar vascularisation. Deposition of secondary Haversian bone in synapsids is common. Only "basal" synapsids such as edaphosaurids and sphenacodontids exhibit little or no remodelling. In chapter 3, histological observations in extinct and extant cervids revealed the presence of laminar bone tissue in the middle and outer cortex of adults of small-sized deer (dwarf *Candiacervus*, *Procervulus* and *Muntiacus*) suggesting lower growth rates, in contrast to the occurrence of plexiform bone in intermediate to large sized forms. Measured growth rates from femora and tibiae revealed relatively low rates in dwarf *Candiacervus*, whereas the giant deer *Megaloceros* shows high rates. Intermediate sized and small cervids show comparable growth rates with the slowest growth in the stem-cervid *Procervulus*. Dwarf *Candiacervus* and *Procervulus* skeletally matured late in comparison to similar sized extant cervids such as *Muntiacus*, demonstrating the variability of life history parameters in island as well as continental cervids. The oldest individual of *Megaloceros* recorded in our cementum analysis was 19 years, whereas the oldest individual of dwarfed *Candiacervus* was 18 years, indicating prolonged longevity for a deer of this body size. The condition found in *Candiacervus*, i.e. the overall absence of lamellar-zonal bone tissue, has features in common with that of the island bovid *Myotragus* (Köhler et al. 2009), but is achieved with less far reaching modification of bone tissue. Therefore, various modes of bone histological modification and mammalian life history evolution in island mammals in comparison with mainland ones, as likely determined by factors such as island size, distance from mainland, climate, phylogeny, and time of evolution, are suggested (Lomolino et al. 2012, 2013). Chapter 4 shows the bone cortex of *Dicrocerus* to be consistent with that of other small cervids. *Dicrocerus* reached its skeletal maturity after five years (during the sixth year of life), similar to *Cervus elaphus*, *Megaloceros*, and dwarf *Candiacervus*. A phylogenetic signal was found for the anteroposterior diameter of the bone section. *Alces* and the Megacerina (here represented by *Megaloceros* and *Sinomegaceros*) independently acquired a high growth rate. A phylogenetically informed linear regression shows that the growth rate in cervids strongly correlates with body size, confirming the results of chapter 3. Second annual growth rates of *Procervulus* and *Euprox* are much lower than those of *Dicrocerus*, which fall slightly above the 95 % confidence interval of the phylogenetically corrected linear regression, indicating a relatively high growth rate for its size. The reconstruction of an ancestral growth rate value for all cervids is 1.63 µm/day and reversion to a lower ancestral growth rate in dwarf *Candiacervus* as well as an increase in Megacerina was found. The particularly high growth rates in *Dicrocerus* in comparison to other stem-cervids from the Miocene document diversity in the early life history evolution of the Cervidae. In chapter 5, compactness parameters in cervid long bones indicate the relative thickness of the bone cortex to be more constrained in large-sized taxa, suggesting more intense selection for an energy-saving mid-diaphyseal structure. Pointing towards greater directional bending rigidity in large-sized taxa, femoral cross-sectional shape exhibits positive allometry.

By using bone and tooth histological methods, this dissertation advanced the knowledge on life history, body size, and island evolution of mammals and especially cervids, but much can still be learnt. Sampling of more specimens and species for further bone histological examinations of fossil insular endemics and their mainland relatives within an ontogenetic framework would significantly improve our knowledge of the ecology of past ecosystems. It would be essential to sample long bones of the extinct rhinocerotoid *Paraceratherium* for understanding the life history of the largest terrestrial mammal that ever lived. In the case of *Leithia*, the extinct island rodent, sampling of more specimens would help to put into context its special bone histology, i.e. the occurrence of a high amount of compact coarse cancellous bone, and deduce possible island modifications. More actualistic studies of the bone histology of mammals would help to improve our knowledge of life history signals in bone, i.e. essentially speed of growth, timing of sexual/skeletal maturity, and longevity. This could be achieved not only by invasive thin section techniques but as well via non-invasive virtual imaging and new statistical/computational methods.

### References

Köhler, M., and S. Moyà-Solà 2009. Physiological and life history strategies of a fossil large mammal in a resource-limited environment. Proceedings of the National Academy of Sciences of the United States of America 106(48):20354-20358.

Lomolino, M. V., D. F. Sax, M. R. Palombo, and A. van der Geer. 2012. Of mice and mammoths: evaluations of causal explanations for body size evolution in insular mammals. Journal of Biogeography 39:842-854.

Lomolino, M. V., A. A. van der Geer, G. A. Lyras, M. R. Palombo, D. F. Sax, and R. Rozzi. 2013. Of mice and mammoths: generality and antiquity of the island rule. Journal of Biogeography 40:1427–1439.

# APPENDIX 1

## The palaeohistology of the basal ichthyosaur *Mixosaurus* Baur, 1887 (Ichthyopterygia, Mixosauridae) from the Middle Triassic: Palaeobiological implications

Authors: Kolb C., Sánchez-Villagra M. R., Scheyer T. M.
Publication: 2011, *Comptes Rendus Palevol,* 10:403-411.
Contributions: CK and TMS designed the study/experiments and wrote the manuscript, collected and analysed histological data, prepared figures and took micrographs, CK performed the experiments, and all authors contributed to the final interpretation and editing of the manuscript. All authors read and approved the final manuscript.

C. R. Palevol 10 (2011) 403–411

Contents lists available at ScienceDirect

Comptes Rendus Palevol

www.sciencedirect.com

Systematic palaeontology (Vertebrate palaeontology)

# The palaeohistology of the basal ichthyosaur *Mixosaurus* Baur, 1887 (Ichthyopterygia, Mixosauridae) from the Middle Triassic: Palaeobiological implications

## *La paléohistologie de l'ichthyosaure basal Mixosaurus Baur, 1887 (Ichthyopterygia, Mixosauridae) du Trias moyen : implications paléobiologiques*

Christian Kolb, Marcelo R. Sánchez-Villagra, Torsten M. Scheyer*

*Paläontologisches Institut und Museum der Universität Zürich, Karl Schmid-Strasse 4, 8006 Zürich, Switzerland*

ARTICLE INFO

*Article history:*
Received 25 August 2010
Accepted after revision 23 October 2010
Available online 8 January 2011

Written on invitation of the Editorial Board

*Keywords:*
Ichthyopterygia
Mixosaur
Bone histology
Ontogenetic series
Monte San Giorgio
Microstructure

*Mots clés :*
Ichthyopterygia
Mixosaure
Histologie osseuse
Série ontogénétique
Monte San Giorgio
Microstructure

ABSTRACT

Here, we provide the first bone histological examination of an ontogenetic series of the basal ichthyosaur *Mixosaurus* encompassing postnatal to large adult specimens. Growth marks are present in sampled humeri, a femur, a fibula, as well as in other skeletal elements (gastral ribs). Ontogenetic changes are traceable throughout stylo- and zeugopodial development, but interior remodelling and resorption deleted part of the internal growth record in the primary cortex. *Mixosaurus* humeri started as flat structures consisting of a core of endochondral woven bone and residual calcified cartilage, whereas growth continued by deposition of periosteal fibrolamellar and parallel-fibred bone. Unlike the fast-growing post-Triassic ichthyosaurs that lack growth marks, microstructural and life history data are now becoming available for a basal ichthyosaur. The high growth rate of *Mixosaurus* may indicate that higher metabolic rates characterised small, non-thunniform ichthyosaurs, as had been suggested already for post-Triassic, cruising forms.

RÉSUMÉ

Nous rapportons ici la première étude ostéohistologique d'une série ontogénétique quasi-complète (spécimens postnataux à adultes) de l'ichthyosaure basal *Mixosaurus*. Des stries de croissance sont visibles sur les humérus échantillonnés, ainsi que sur un fémur, un péroné et d'autres éléments du squelette (côtes gastriques). On peut suivre les changements ontogénétiques au cours du développement des stylo- et zeugopodes, mais le remodelage interne et la résorption ont en partie effacé l'enregistrement de la croissance interne dans le cortex primaire. Les humérus de *Mixosaurus* sont initialement des structures plates consistant en un noyau d'os endochondral en « sucre mouillé » et de cartilage calcifié rémanent. La croissance continue

---

* Corresponding author.
*E-mail addresses:* christian.kolb@pim.uzh.ch (C. Kolb), m.sanchez@pim.uzh.ch (M.R. Sánchez-Villagra), tscheyer@pim.uzh.ch (T.M. Scheyer).

1631-0683/$ – see front matter © 2010 Académie des sciences. Published by Elsevier Masson SAS. All rights reserved.
doi:10.1016/j.crpv.2010.10.008

par dépôt d'os périostique fibrolamellaire et à fibres parallèles. Contrairement aux ichthyosaures post-triasiques à croissance rapide, qui ne présentent pas de stries de croissance, des données microstructurelles et d'histoire de vie sont maintenant disponibles pour un taxon basal du groupe. Le haut taux de croissance de *Mixosaurus* pourrait indiquer que les petits ichthyosaures non thunniformes étaient caractérisés par des taux métaboliques élevés, comme cela fut déjà suggéré pour les formes migrantes post-triasiques.

## 1. Introduction

The ichthyosaurs are a group of extinct reptiles with a strongly re-shaped body outline, showing numerous adaptations to a marine lifestyle. Because of their abundance and excellent fossil preservation, this lineage offers unique possibilities to get insights into the palaeobiology of a long extinct group of specialized marine vertebrates, which lacks any modern descendants (Sander, 2000). Ichthyosaurs are generally characterised by a fish- or dolphin-like body shape, a long snout and large eyes, but to date, the origins of ichthyosaurs within the amniote tree of life are still controversial (Motani, 1999). In more recent cladistic analyses, Ichthyopterygia have been repeatedly recovered as diapsid reptiles, possibly as sister group to Sauria, the clade which encompasses Lepidosauromorpha and Archosauromorpha (Motani et al., 1998; Müller, 2004).

Among Mixosauridae (Fig. 1), the genus *Mixosaurus,* erected by Baur (1887) based on the type species *Mixosaurus cornalianus* (Bassani, 1886), represents a particularly successful group of small to medium-sized ichthyosaurs (< 2 m body length) restricted to the Middle Triassic (Motani, 1999). McGowan and Motani (2003) recognise five species of *Mixosaurus*, including *Mixosaurus atavus* (Quenstedt, 1852), *Mixosaurus nordenskioeldii* (Hulke, 1873), *M. cornalianus* (Bassani, 1886), *Mixosaurus fraasi* (Merriam, 1910), and *Mixosaurus kuhnschnyderi* (Brinkmann, 1998), of which *M. cornalianus* and *M. kuhnschnyderi* are well known from the Middle Triassic of the Besano region, Italy, and from the Besano Formation of the Monte San Giorgio locality, Switzerland.

The impact of the general adaptation to the marine environment is clearly observable in the bone histology of ichthyosaurs. Whilst studies on bone histology of fossil reptiles have been done by many researchers in the past (Scheyer et al., 2010), the bone histology of marine reptiles, and especially of ichthyosaurs, is not well examined. Among others, Gross (1934), Kiprijanoff (1881) and Seitz (1907) already made useful detailed observations on the bone histology of post-Triassic ichthyosaurs (Fig. 1), such as *Ichthyosaurus, Ophthalmosaurus* and *Platypterygius*. In these works, the peculiar spongy nature of the bones was already noted. Especially Seitz (1907), who because of preservational restrictions analysed only thin-sections of ribs (and also restudied Kiprijanoff's original sections), mentioned that the primary bone tissue houses not only primary vascular canals and osteons but is also subject to secondary remodelling. Gross (1934) further encountered primary and secondary osteons and larger resorption bays in a section of a lower jaw of *Ichthyosaurus* sp. and in the rib of *Ophthalmosaurus icenicus*. More recently, de Buffrénil and Mazin (1990) gave a comparative account on the bone histology of the ichthyosaurs *Stenopterygius* and *Ichthyosaurus*, as well as the Early Triassic *Omphalosaurus*, an enigmatic taxon whose systematic position is still under debate (Motani, 2000; Sander and Faber, 2003). de

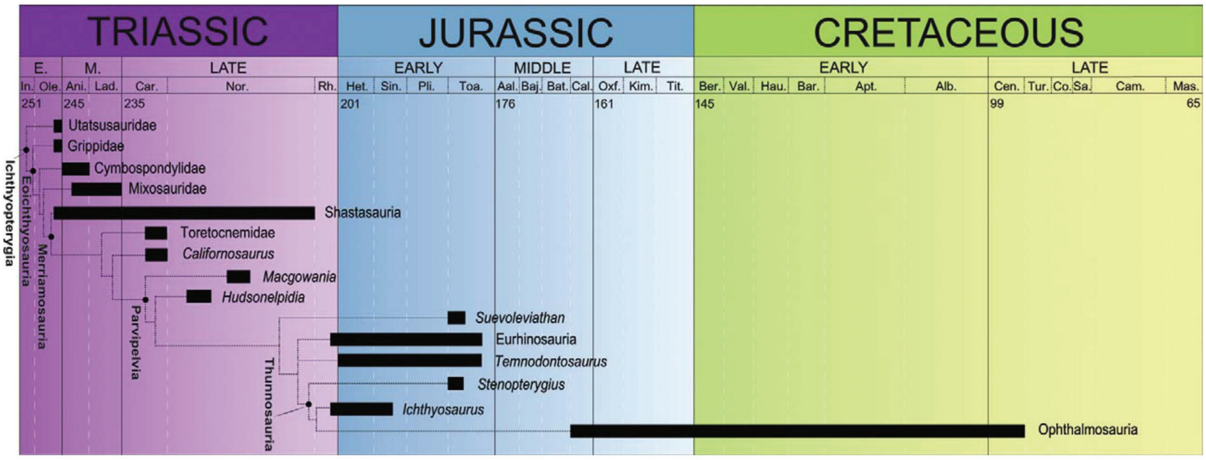

**Fig. 1.** Simplified time-calibrated cladogram (modified from McGowan and Motani, 2003; Motani, 2005; Walker and Geissman, 2009 [GSA 2009 Geologic Time Scale]) showing the interrelationships of the Ichthyopterygia and the position of the Mixosauridae within the clade.

**Fig. 1.** Cladogramme simplifié (d'après McGowan et Motani, 2003 ; Motani, 2005 ; Walker and Geissman, 2009 [GSA 2009 Geologic Time Scale]) montrant les relations entre les Ichthyopterygia et position des Mixosauridae au sein du clade.

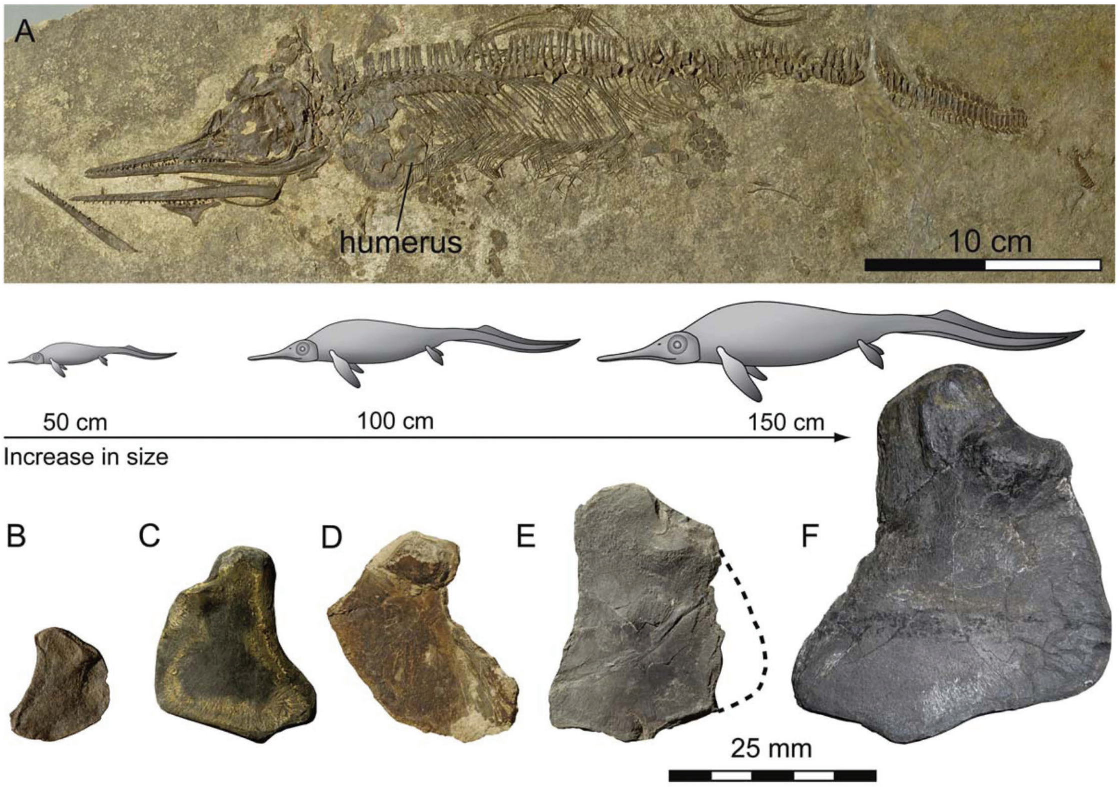

**Fig. 2.** Sampled humeri of *Mixosaurus* (Middle Triassic, Monte San Giorgio, Switzerland). Mark the arrow (time line) and mixosaur sketches showing the increase in body size of the sampled specimens. Note that the sketches do not show allometric changes throughout ontogeny. A. Smallest sampled individual of *Mixosaurus* (PIMUZ T 77). B. Small left humerus, ventral view (PIMUZ T 77). C. Right humerus, ventral view (PIMUZ T 2046). D. Distorted and crushed left humerus, dorsal view (PIMUZ T 1296). E. Distorted and crushed left humerus, ventral view (PIMUZ T 2388). Note that the anterior flange has broken off prior to sampling. F. Large left humerus, ventral view (PIMUZ T 5844).

**Fig. 2.** Humérus échantillonnés de *Mixosaurus* (Trias moyen, Monte San Giorgio, Suisse). Remarquez la flèche (axe temporel) et les croquis indiquant l'augmentation de taille des spécimens étudiés. Notez que les croquis ne montrent pas de changements allométriques pendant toute l'ontogenèse. A. Plus petit individu de *Mixosaurus* échantillonné (PIMUZ T 77). B. Petit humérus gauche, vue ventrale (PIMUZ T 77). C. Humérus droit, vue ventrale (PIMUZ T 2046). D. Humérus gauche tordu et écrasé, vue dorsale (PIMUZ T 1296). E. Humérus gauche tordu et écrasé, vue ventrale (PIMUZ T 2388). Notez que le flanc antérieur s'est brisé avant l'échantillonnage. F. Gros humérus gauche, vue ventrale (PIMUZ T 5844).

Buffrénil and Mazin (1990) showed that in bones of juvenile specimens of these ichthyosaur taxa, woven-fibred tissue was predominately deposited as well vascularised spongy bone. More compact primary bone was then subsequently deposited in older specimens before being extensively remodelled into cancellous tissue. *Mixosaurus*, on the other hand, a taxon which due to its intermediate body plan (sensu Motani, 2005) between the more basal (Early-Middle Triassic) eel-shaped and the clade of younger (post-Triassic) dolphin-shaped ichthyosaurs represents a key taxon of ichthyosaur evolution, had not been studied yet.

In this present work we describe and interpret the histological structures observed in the bones of *Mixosaurus* in comparison with that of post-Triassic ichthyosaurs. Conclusions are drawn on the implications of the observed microstructures for the palaeobiology of these highly adapted marine reptiles.

## 2. Material and methods

Various bones of the well identifiable genus *Mixosaurus* from the collections of the Palaeontological Institute and Museum of the University of Zurich were sampled. All specimens were recovered from the Middle Triassic series of Monte San Giorgio, Ticino, Switzerland. First, a series of five humeri of *Mixosaurus* was sectioned, including a humerus belonging to a very small, presumably postnatal individual (PIMUZ T 77) of about 50 cm in body length (Fig. 2A, B), three intermediate-sized specimens of 100–120 cm body length (PIMUZ T 1296, T 2046, T 2388; Figs. 2C-E), as well as a large specimen of about 150 cm body length (PIMUZ T 5844; Fig. 2F). Estimates of body length, i.e. snout-tail length, are based on comparisons with complete skeletons of *Mixosaurus* housed in the Palaeontological Museum of the University of Zurich. Moreover, various bones of the zeugo- and autopodium of PIMUZ T 2046 could be sampled. These include a femur, a fibula, an ischium, one ulna, as well as two phalanges. Additionally, it was possible to section one scapula (PIMUZ T 5844) along with rib- and gastral rib fragments (PIMUZ T 1296, T 2046).

After formatting of the bone-bearing rock samples, thin sections were produced. Following standard procedures, the samples were coated and impregnated with epoxy resin (Araldite) prior to sawing and grinding. The long bones,

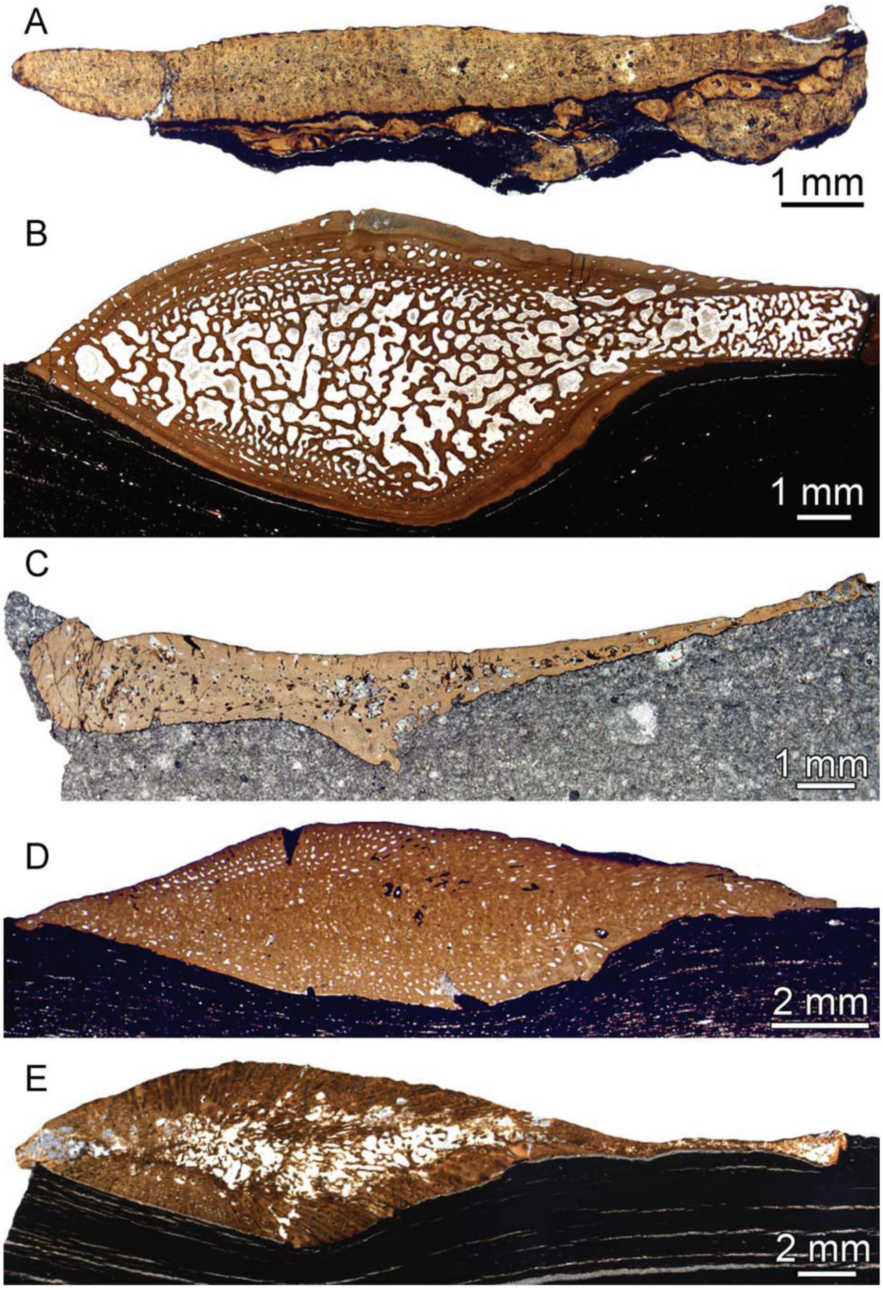

**Fig. 3.** General aspects of transverse thin-sections of humeral shafts. A. PIMUZ T 77. B. PIMUZ T 2046. C. PIMUZ T 1296. D. PIMUZ T 2388. E. PIMUZ T 5844. Note the good preservation of T 2046 (B), in contrast to the compacted specimens PIMUZ T 1296 (C) and PIMUZ T 2388 (D). Anterior is to the right.

**Fig. 3.** Aspect général des lames minces transverses des fûts huméraux. A. PIMUZ T 77. B. PIMUZ T 2046. C. PIMUZ T 1296. D. PIMUZ T 2388. E. PIMUZ T 5844. Notez la bonne préservation de T 2046 (B), a contrario des spécimens compactés PIMUZ T 1296 (C) et PIMUZ T 2388 (D). La face antérieure est à droite.

the ulna and the phalanges were transversely sectioned in the middle of the shaft whereas the ischium was sectioned along its smallest width. Sections were observed by standard light microscopy (normal transmitted and polarized light) using a Leica DM2500 M composite microscope. A Leica DFC 420 °C digital camera was used for taking micrographs. Specimens and sections are housed in the collections of the Palaeontological Institute and Museum of the University of Zurich.

### 2.1. *Institutional abbreviations*

**PIMUZ**: Paläontologisches Institut und Museum, Universität Zürich, Switzerland.

**SMNS**: Staatliches Museum für Naturkunde Stuttgart, Germany.

## 3. Results

In the following part, the main observations in the bone histology of *Mixosaurus* will be described. The histology of the ontogenetic series of humeri will be described first from the smallest to the largest specimen, followed by the histological description of the additionally sampled skeletal elements. Besides the histological features, several outer anatomical and microstructural ontogenetic changes characterise humeral growth in *Mixosaurus*. These changes include an overall increase of periosteal bone leading to a smoother bone surface, a decrease of internal vascular patterns being visible externally, and the development of a more angular bone shape with more distinct articulation facets. The length to width ratio, on the other hand, stays nearly constant throughout humeral growth.

### *3.1. Histological description of developmental series of humeri*

All sampled humeri (Fig. 3) show cortical fibrolamellar bone locally substituted with parallel-fibred bone. Osteocyte lacunae with a mostly long-oval outline are present in internal woven bone as well as in the cortex. The primary osteons, which can be best observed in the primary matrix of fibrolamellar bone, show a concentric arrangement of lamellar bone which is, however, not clearly visible in every case.

The humerus of the postnatal specimen PIMUZ T 77 (Fig. 3A) has a proximodistal length of 14 mm. It shows a core of endochondral woven bone with residual calcified cartilage, which is surrounded by periosteal fibrolamellar bone (Fig. 4A). Towards the anterior flange, the amount of calcified tissue appears to increase interiorly, because of the reduced thickness of the surrounding cortical bone. The rim of the flange is capped by calcified cartilage. Vascularisation of the bone is generally low. It was possible to identify one line of arrested growth (LAG) basically encompassing the woven bone core, indicating that the specimen was in its second year of life.

Humerus PIMUZ T 2046 (Fig. 3B) has a proximodistal length of 24 mm. It is the best preserved specimen sampled, which shows almost no compaction. In the main shaft region, the cortex consists of fibrolamellar bone. Nine to ten LAGs are countable in the cortical tissue (Fig. 4B). However, approximately three LAGs have been lost due to resorption and remodelling processes. Towards the anterior flange, the cortex is composed of parallel-fibred bone (Fig. 4C). The interior of the bone shows strong resorption in its deeper parts, whereas the trabeculae are at various stages of remodelling into secondary lamellar bone (Fig. 4D). Locally, remains of woven-fibred bone associated with calcified cartilage are still observable between the resorption bays. The anterior margin of the anterior flange shows a cap of cartilage (Fig. 4E, F).

Humerus PIMUZ T 1296 (Fig. 3C), having a proximodistal length of 23 mm, is strongly crushed and distorted and does not show a good growth record. This specimen histologically resembles PIMUZ T 2046, but it has a condensed core of crushed trabecular bone surrounded by cortical fibrolamellar bone. Sharpey's fibres are present in some areas of the dorsal part of the cortex (Fig. 4G).

The proximodistal length of PIMUZ T 2388 (Fig. 3D) with 32 mm indicates a specimen of at least intermediate to large size. Strikingly, the diaphyseal shaft region of the bone appears almost compact in cross section. However, this "compactness" results from severely crushed cancellous bone, visible as small irregularly arranged trabecular fragments of lamellar bone, filling up most of the endosteal vascular spaces. Due to this compaction the overall dorsoventral thickness of the shaft of PIMUZ T 2388 (max. 3.8 mm) measures only about 65 % of the shaft thickness of PIMUZ T 2046 (max. 5.8 mm). The outer cortex of the main shaft region is composed of fibrolamellar bone (Fig. 4H) with radially arranged primary osteons, whereas the compacta of the anterior flange consists of parallel-fibred bone. Sharpey's fibres are most prominent in the ventral compacta of the posterior shaft region.

The largest specimen is PIMUZ T 5844 (Fig. 3E); with a proximodistal length of 47 mm it has a dorsoventral thickness of the shaft of max. 6.3 mm, indicating that this specimen is also strongly compacted, as is confirmed by the histology of the specimen. The interior cancellous parts of the bone appear again quite compact, because of collapsed trabeculae filling up the vascular spaces. Otherwise this humerus shares histological features with PIMUZ T 2388, including the radial arrangement of primary osteons, the distribution of fibrolamellar and parallel-fibred tissues in the cortex, as well as the presence of Sharpey's fibres in the ventral cortex of the posterior shaft region. LAGs (Fig. 4I) are only locally preserved in the cortical tissue and hard to trace, which makes a reliable count difficult. However, taking a conservative approach, it was still possible

**Fig. 4.** Bone histology of the *Mixosaurus* humeri sampled. A. Close-up of the bone centre of PIMUZ T 77 in polarized (left) and normal light (right). White arrows mark the interior core of woven bone and calcified cartilage (lighter colour), surrounded by fibrolamellar bone. B. Close-up of the tip of the humerus PIMUZ T 2046 showing centripetally progression of erosion bays (EB) and lines of arrested growth in the cortical bone. C. Primary cortex of PIMUZ T 2046 in polarized light showing parallel-fibred bone between primary osteons. D. Cancellous and compact bone of PIMUZ T 2046 with areas of parallel-fibred bone (lower half of the image) and woven-fibred, as well as secondary lamellar bone (upper half of the image). E. Cartilage cap at the anterior flange margin of PIMUZ T 2046 in normal light. F. Cartilage cap of PIMUZ T 2046 in polarized light with lambda compensator. Note that the photograph shown in (E) and (F) was rotated 90 degrees anti-clockwise compared to Fig. 3B for technical reasons. G. Posterior region of diaphysis (PIMUZ T 1296) in polarized light with lambda compensator. The white arrow to the left indicates the crushed area of the bone. The arrow to the right indicates Sharpey's fibres (Shf, blue colours) inserting into the compact bone (yellow-orange colours). H. Cortex of PIMUZ T 2388 in polarized light consisting of fibrolamellar bone. I. Primary cortex of PIMUZ T 5844 showing typical features of the cortex of *Mixosaurus* humeri as fibrolamellar bone, primary osteons, and LAGs (lines of arrested growth) as indicated by white arrows. J. Anterior region of PIMUZ T 5844 in normal light, showing a close-up of the flange region and the cartilage cap. Note that internal bone structures have largely collapsed.

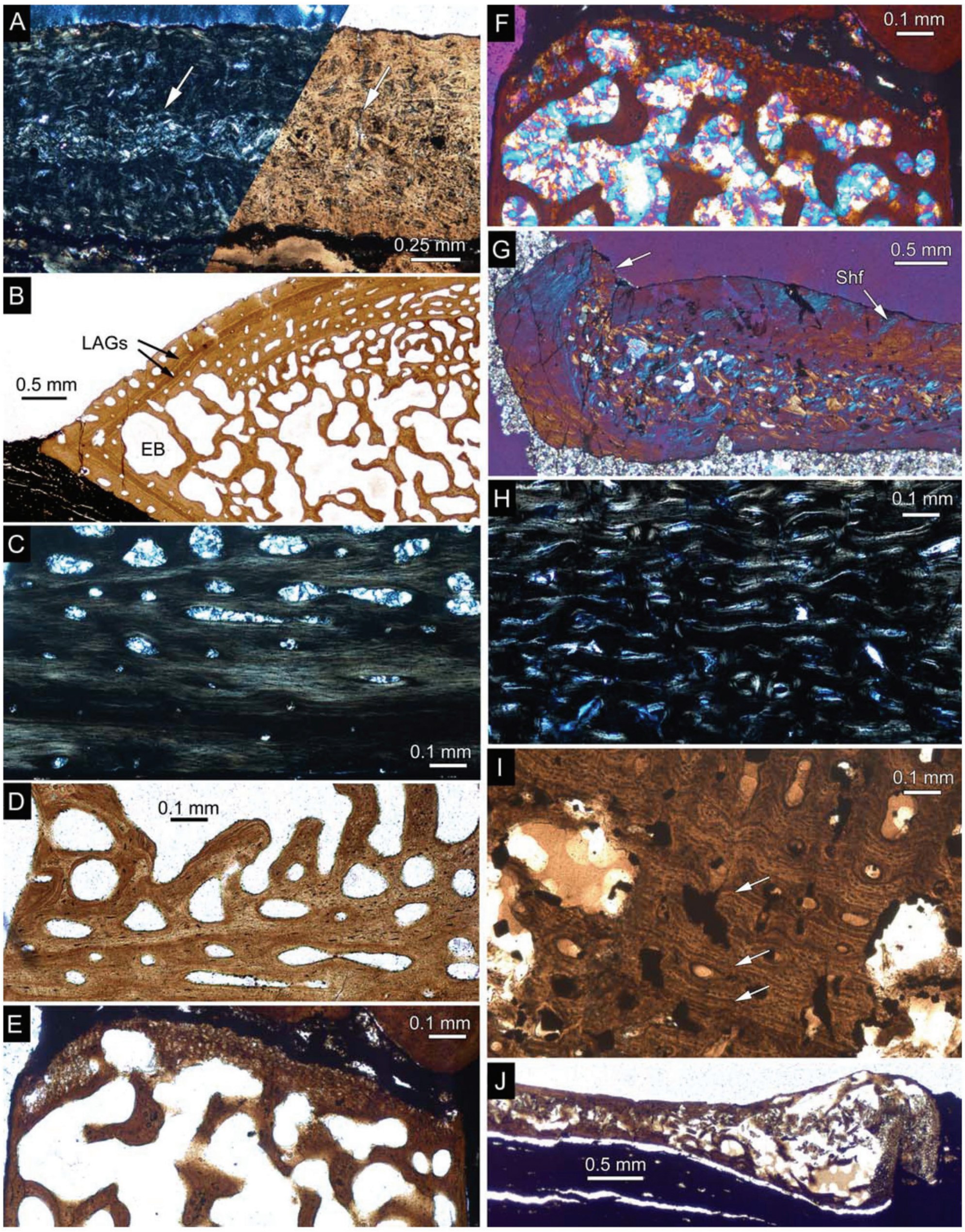

**Fig. 4.** Histologie osseuse des humérus échantillonnés de *Mixosaurus*. A. Vue rapprochée du centre osseux de PIMUZ T 77 en lumière polarisée (gauche) et naturelle (droite). Les flèches blanches marquent le noyau interne d'os en 'sucre mouillé' et de cartilage calcifié (couleur plus claire), entouré d'os fibrolamellaire. B. Vue rapprochée de la tête de l'humérus PIMUZ T 2046 montrant la progression centripète des baies d'érosion (EB) et des lignes d'arrêt de croissance dans la corticale. C. Cortex primaire de PIMUZ T 2046 en lumière polarisée montrant l'os à fibres parallèles entre les ostéons primaires. D. Os spongieux et compact de PIMUZ T 2046 avec des zones d'os à fibres parallèles (partie basse de l'image), d'os fibreux, ainsi que des zones d'os lamellaire secondaire (partie haute). E. Bouchon cartilagineux sur le bord du flanc antérieur de PIMUZ T 2046 en lumière naturelle. F. Bouchon cartilagineux de PIMUZ T 2046 en lumière polarisée avec compensateur lambda. Notez que, pour des raisons techniques, la photo a été tournée de 90 degrés. G. Région postérieure de la diaphyse (PIMUZ T 1296) en lumière polarisée avec compensateur lambda. La flèche blanche sur la gauche indique la zone écrasée de l'os. La flèche sur la droite indique les fibres de Sharpey (Shf, en bleu) s'insérant dans l'os compact (en jaune-orange). H. Cortex d'os fibrolamellaire de PIMUZ T 2388 en lumière polarisée. I. Cortex primaire de PIMUZ T 5844 montrant les attributs typiques du cortex des humérus de *Mixosaurus* : os fibrolamellaire, ostéons primaires, et lignes d'arrêt de croissance (LAGs) tels qu'indiqués par les flèches blanches. J. Région antérieure de PIMUZ T 5844 en lumière naturelle, montrant une vue rapprochée du flanc et du bouchon cartilagineux. Notez que les structures osseuses internes sont en grande partie effondrées.

to count 12 LAGs in the dorsal and ventral cortices of the mid-diaphyseal shaft region of the humerus. Taking into account that zones might have been larger in the faster growing juveniles, it is assumed that three to four LAGs have been lost through internal remodelling and resorption. Based on these assumptions, the largest individual investigated might have reached an age between 15 and 16 years. The cartilage cap (Fig. 4J) in the anterior flange is strongly developed in this humerus.

### *3.2. Histological description of additional skeletal elements*

With the exception of a scapula, which belongs to PIMUZ T 5844, all of the additional specimens sampled come from PIMUZ T 2046. Based on convergent morphologies, especially of their semi-circular shaft areas, the microstructures of the femur, fibula and scapula will be described together in one section. Similarly, the flat bone morphology of the ulna and the ischium exhibit very similar histologies.

The femur (Fig. 5A) and the fibula (Fig. 5B) have a proximodistal length of 11 mm, whereas the femur shaft is slightly larger in diameter. The deeper cortical layers of both bones show fibrolamellar bone tissue, whereas the more superficial cortical layers are composed of parallel-fibred bone. The cortex of the scapula (PIMUZ T 5844) is essentially similar to that of the femur and fibula but is more variable in thickness. Osteocyte lacunae are more round-shaped in the fibrolamellar bone, whereas they are more flattened in the parallel-fibred tissue of the outer cortex. Sharpey's fibres extend extensively into all parts of the cortices, often obscuring the primary periosteal bone tissues. Primary osteons are arranged in radial rows in the outer parts of the cortices. The interior parts of the bones are strongly cancellous, with the trabeculae showing various stages of resorption and remodelling. The trabeculae in the fibula can be extremely thin. The primary bone tissue between the resorption bays consists of woven-fibred bone and residual calcified cartilage. Similar to the growth record count in the humerus, about 10 LAGs are visible in the cortices of both the femur and fibula.

The ulna (Fig. 5C) has a proximodistal length of 16 mm; the ischium (Fig. 5D) only 12 mm. Both elements have a compact cortex of parallel-fibred bone, variable in thickness, surrounding cancellous bone. In the ulna, the cortical bone, which is vascularised by scattered primary osteons, is thickest at the anterior margin and wedges out towards the posterior rim of the bone, which itself is capped by calcified cartilage. In the ischium, the anteromedial margin is concave in cross-section and also composed of calcified cartilage. In both bones, Sharpey's fibres are most conspicuous in the thickened cortical parts, where they inserted mostly perpendicularly into the primary bone tissue. Ten LAGs are countable throughout the cortex in both bones. Isolated larger erosion bays and scattered secondary osteons are found especially in the anterior part of the cortex. The cancellous bone consists of thin trabeculae, which often preserve a core of primary cartilaginous tissue.

The two phalanges sampled show periosteal parallel-fibred bone dorsally and ventrally at the bone centre, whereas the anterior and posterior parts of the bone are cancellous, consisting of primary trabeculae, which are successively remodelled (Fig. 5E). The anterior and posterior margins are covered by calcified cartilage caps. The growth record is best preserved at the cortex of the bone centre, showing nine to 10 LAGs.

Several small circular, semi-circular or bean-shaped bones, interpreted to be either ribs or gastral ribs, were sampled. Especially the gastralia, which usually lack a central marrow cavity or vascularisation, are well suited for growth record counts. The cores of the gastralia consist of a small amount of woven bone and calcified cartilage, surrounded by layers of parallel-fibred or lamellar-zonal bone. In the case of a gastral rib lying adjacent to the humerus of PIMUZ T 2046, 13 LAGs were counted (Fig. 5F). In the ribs, a large central marrow cavity is present, making them less suitable in this regard.

## 4. Discussion and conclusions

As revealed by the new data on *Mixosaurus*, the bone histology of the different bone samples is rather uniform, with changes in bone tissue types being mostly related to the different dimensions and shapes of the samples. Differences in the bone deposition rates thus appear to correlate with the overall size of the bone, in that the thickest and largest bones (i.e., humeri) show extensive woven and fibrolamellar tissue. Other limb elements (e.g. femur, fibula) show less fibrolamellar and prevalently parallel-fibred tissue, whereas the thinnest elements (e.g. ribs and gastralia) exclusively show parallel-fibred or lamellar-zonal tissue. The well-documented presence of parallel and coarse Sharpey's fibres in the ventral compacta of the posterior humeral shaft further indicates a strong muscular or tendinous region of insertion, presumably used for front limb retraction in steering.

New data on *Temnodontosaurus* (Fig. 5G; SMNS 50329) are consistent with data of de Buffrénil and Mazin (1990) that long bones of geologically younger thunniform ichthyosaurs overall show spongy cancellous tissue, as is typically encountered in vertebrates adapted to open marine conditions (Ricqlès and de Buffrénil, 2001). Unlike the geologically younger ichthyosaur clade, however, all *Mixosaurus* bones sampled reveal a good growth record (i.e. LAGs) in their cortical bone tissue. Similarly to the condition in *Mixosaurus*, LAGs appear to be present in the basal ichthyosaur *Utatsusaurus* from the Lower Triassic Osamu Formation of Japan (Nakajima, 2009) and in *Omphalosaurus* from the Lower Triassic of Spitsbergen (de Buffrénil and Mazin, 1990). An external fundamental system, i.e. a closely spaced series of LAGs at the periosteal margin indicating cessation of growth, as was briefly noted for most bones of *Utatsusaurus* by Nakajima (2009), was not found in *Mixosaurus*.

The compacta of *Mixosaurus* bones remain usually well developed throughout life, because the imbalance between bone absorption and deposition, especially the high remodelling rates of older individuals found in cruising post-Triassic ichthyosaurs, is not pronounced. As such, the bone histology fits with other morphological

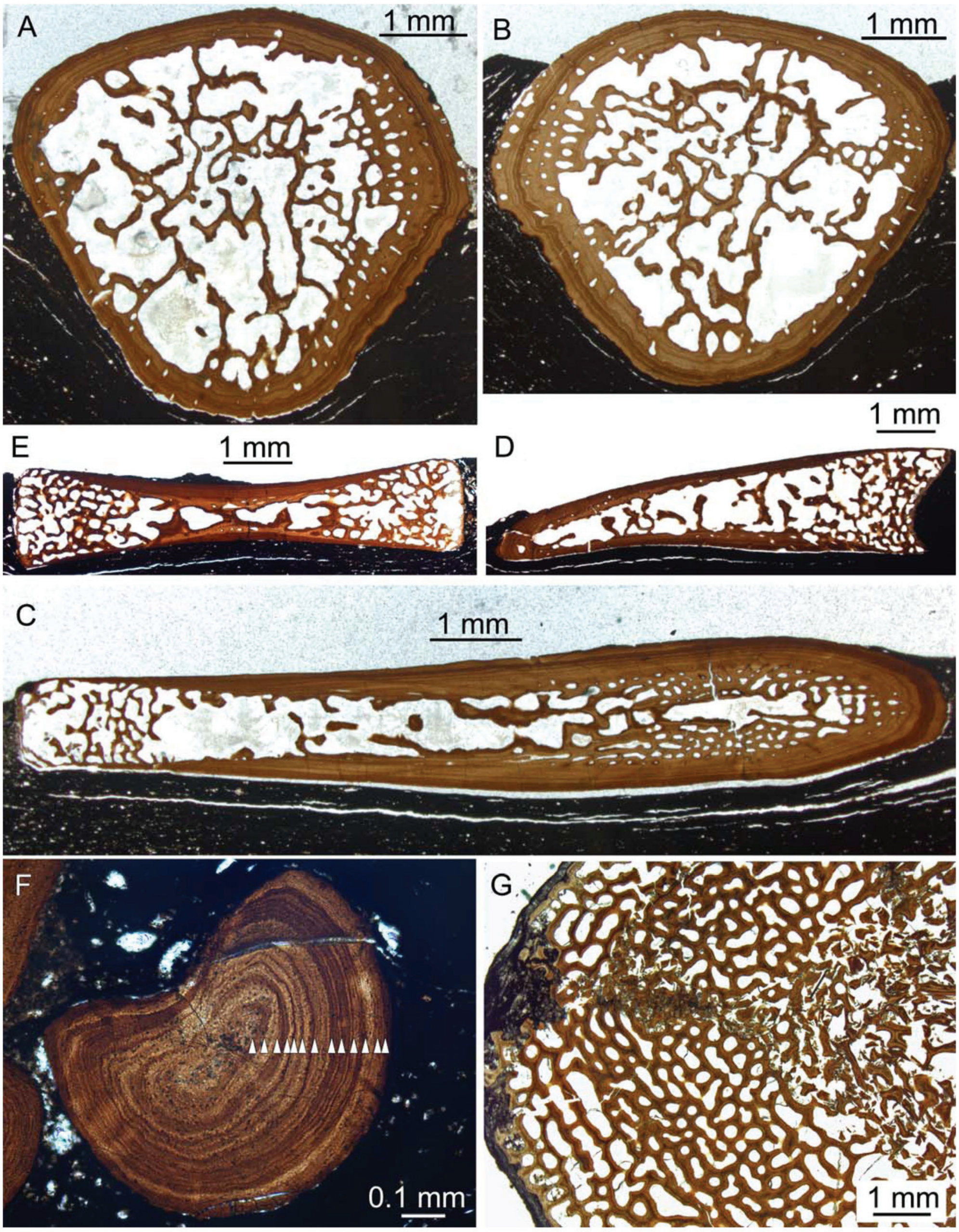

**Fig. 5.** General aspects of transverse sections of additional sampled bones of *Mixosaurus*. Specimens in (A–F) belong to PIMUZ T 2046. A. Femur. B. Fibula. C. Ulna. D. Ischium. E. Phalanx. F. Gastral rib showing 13 incremental growth circles (white triangles) consisting of zones of bone growth, annuli and LAGs. G. General texture of the cortex of *Temnodontosaurus* (Lower Jurassic, Holzmaden, Germany) in humerus SMNS 50329 showing collapse structures of the cancellous bone tissue in its centre.

**Fig. 5.** Aspect général de sections transverses d'autres os de *Mixosaurus*. Les spécimens (A–F) appartiennent à PIMUZ T 2046. A. Fémur. B. Fibula. C. Ulna. D. Ischion. E. Phalange. F. Côte gastrique montrant 13 cercles de croissance incrémentale (triangles blancs) correspondant aux zones de croissance osseuse, aux annulus et aux LAGs. G. Texture générale du cortex de *Temnodontosaurus* (Jurassique inférieur, Holzmaden, Allemagne) dans l'humérus SMNS 50 329 présentant des structures d'effondrement du tissu de l'os spongieux en son centre.

traits (i.e., non-thunniform body shape lacking well developed back – and tail fins; retention of five-fingered limbs modified in paddles with moderate polyphalangy) which characterise *Mixosaurus* as a near-shore or shelf dweller that did not venture frequently into open or deep marine environments. Note, however, that *Mixosaurus* lacks histological specialisations such as osteosclerosis or pachyostosis (Houssaye, 2009), which occur frequently in tetrapods living in shallow-water or near-shore habitats.

Caldwell (1997, 2002) pointed out that there is a proximal to distal and postaxial to preaxial perichondral bone loss in ichthyosaurs and plesiosaurians. Showing the forelimb of *M. cornalianus*, he noted the loss to occur first at the postaxial margin of the ulna, followed by the postaxial margin of the fifth metacarpal (continued by the postaxial margins of the proximal phalanges of the fifth digit) prior to the loss at the preaxial and postaxial margins of the first metacarpal (continued by the preaxial margins of the proximal phalanges of the first digit). However, as can be seen here in the histological description of the developmental series of humeri of *Mixosaurus*, the margin of the anterior (= preaxial) flange of the humeri is always capped by cartilage only, indicating also a perichondral bone loss at this position. While the proximodistal direction of bone reduction appears to be retained, the postaxial to preaxial shift proposed by Caldwell (1997, 2002) is not found in *Mixosaurus*. Therefore, *Mixosaurus*, at least in the forelimb, seems to show a divergent pattern of periosteal bone reduction, in comparison to the other ichthyosaurs.

To better understand the evolution of the dolphin-like body plan of the cruising post-Triassic ichthyosaurs (i.e., the ichthyosaur “crown”), it is important to study the palaeobiology and ecology of the more basal taxa (i.e., “stem” ichthyosaurs), to elucidate how traits evolved in this lineage. In summary, both the outer morphology and the bone microstructures of *Mixosaurus* show an intermediate state between the eel-shaped utatsusaurids or other basal eoichthyosaurians, and the more highly nested parvipelvian ichthyosaurs (Fig. 1). The *Mixosaurus* data confirm the presence of high growth rates, as expressed by the deposition of fibrolamellar bone tissue, at least in the larger, massive skeletal elements, such as the humeri, throughout ontogeny. It seems thus plausible that higher metabolic rates (as precondition for homeothermy), which were postulated to be present already in the large post-Triassic cruising ichthyosaurs and in *Omphalosaurus* (de Buffrénil and Mazin, 1990; Motani, 2010), were also present in the small non-thunniform *Mixosaurus*.

## Acknowledgments

Winand Brinkmann, Heinz Furrer (PIMUZ), and Rainer Schoch (SMNS) are thanked for providing specimens for histological study and discussions. Markus Hebeisen, Jasmina Hugi and Rosi Roth (PIMUZ) are thanked for their various helps in preparing sections and photographs. Thanks also go to Nicolas Goudemand (PIMUZ) for translating parts of the manuscript into French and to Kevin Padian (UCMP) for comments on a previous version of the manuscript. Volume Editors Jorge Cubo and Michel Laurin (CNRS), as well as two anonymous reviewers are thanked for additional helpful comments. This work was partly funded by the SNSF (No. 31003A_127053/1 to TMS) and the DAAD (D/09/46969 to CK).

## References

Bassani, F., 1886. Sui fossili e sull’età degli schisti bituminosi triasici di Besano in Lombardia. Communicazione preliminare. Atti della Società Italiana di Scienze Atti Soc. ital. Sci. nat. Museo civ. Stor. nat. Milano 29, 15–17.

Baur, G., 1887. Ueber den Ursprung der Extremitäten der Ichthyopterygia. Berichte über die Versammlungen des Oberrheinischen Geologischen Vereines 20, 17–20.

Brinkmann, W., 1998. *Sangiorgiosaurus* n. g. - eine neue Mixosaurier-Gattung (Mixosauridae, Ichthyosauria) mit Quetschzähnen aus der Grenzbitumenzone (Mitteltrias) des Monte San Giorgio (Schweiz, Kanton Tessin). N. Jb. Geol. Paläont., Abh. 207, 125–144.

de Buffrénil, V., Mazin, J.M., 1990. Bone histology of the ichthyosaurs: comparative data and functional interpretation. Paleobiology 16, 435–447.

Caldwell, M.W., 1997. Modified perichondral ossification and the evolution of paddle-like limbs in ichthyosaurs and plesiosaurs. J. Vert. Paleont. 17, 534–547.

Caldwell, M.W., 2002. From fins to limbs to fins: limb evolution in fossil marine reptiles. Am. J. Med. Genet. 112, 236–249.

Gross, W., 1934. Die Typen des mikroskopischen Knochenbaues bei fossilen Stegocephalen und Reptilien. Z. Anat. Entwicklungsgesch. 203, 731–764.

Houssaye, A., 2009. Pachyostosis” in aquatic amniotes: a review. Integr. Zool. 4, 325–340.

Hulke, J.W., 1873. Memorandum on some fossil vertebrate remains collected by the Swedish expedition to Spitzbergen in 1864 and 1868, Bihang till K. Svenska Vetenskapskademiens Handlinger, I. Afdelning IV 9, 1–11.

Kiprijanoff, W., 1881. Studien über die fossilien Reptilien Russlands. I. Theil, Gattung *Ichthyosaurus* König. Mémoires de l’Académie des Sciences de St.-Pétersbourg VII$^{e}$ Série Tome XXVIII (8), 1–103.

McGowan, C., Motani, R., 2003. Ichthyopterygia. Handbuch der Paläoherpetologie [Handbook of Paleoherpetology] Part 8, 1–173.

Merriam, J.C., 1910. The skull and dentition of a primitive ichthyosaurian from the Middle Triassic. University of California Publications. Bulletin of the Department of Geology 5/24, 381–390.

Motani, R., 1999. Phylogeny of Ichthyopterygia. J. Vert. Paleont. 19, 473–496.

Motani, R., 2000. Is *Omphalosaurus* ichthyopterygian?– A phylogenetic perspective. J. Vert. Paleont. 20, 295–301.

Motani, R., 2005. Evolution of fish-shaped reptiles (Reptilia: Ichthyopterygia) in their physical environments and constraints. Annu. Rev. Earth Planet. Sci. 33, 395–420.

Motani, R., 2010. Warm-blooded “sea dragons”? Science 328, 1361–1362.

Motani, R., Minoura, N., Ando, T., 1998. Ichthyosaurian relationships illuminated by new primitive skeletons from Japan. Nature 393, 255–257.

Müller, J., 2004. The relationships among diapsid reptiles and the influence of taxon selection. In: Arratia, G., Wilson, M.V.H., Cloutier, R. (Eds.), Recent Advances in the Origin and Early Radiation of Vertebrates. Verlag Dr. Friedrich Pfeil, München, pp. 379–408.

Nakajima, Y., 2009. Paleoecology of primitive ichthyopterygians suggested by bone histology, Japan Geoscience Union Meeting 2009. Abstract Issue, B102-012.

Quenstedt, F.A., 1852. Handbuch der Petrefaktenkunde, H. Laupp. Tübingen, 792.

Ricqlès, A.de, Buffrénil, V.de, 2001. Bone histology, heterochronies and the return of tetrapods to life in water: were are we? In: Mazin, J.M., Buffrénil, V.de (Eds.), Secondary Adaptations of Tetrapods to Life in Water. Verlag Dr. Friedrich Pfeil, München, pp. 289–310.

Sander, P.M., 2000. Ichthosauria: their diversity, distribution, and phylogeny. Paläont. Z. 74, 1–35.

Sander, P.M., Faber, C., 2003. The Triassic marine reptile *Omphalosaurus*: osteology, jaw anatomy, and evidence for ichthyosaurian affinities. J. Vert. Paleont. 23, 799–816.

Scheyer, T.M., Klein, N., Sander, P.M., 2010. Developmental palaeontology of Reptilia as revealed by histological studies. In: Sánchez-Villagra, M.R. (Ed.), Developmental Vertebrate Palaeontology. Semin. Cell Dev. Biol., 21, pp. 462–470.

Seitz, A.L.L., 1907. Vergleichende Studien über den mikroskopischen Knochenbau fossiler und rezenter Reptilien, und dessen Bedeutung für das Wachstum und Umbildung des Knochengewebes im allgemeinen. Nova Acta, Abh. der Kaiserl. Leop.-Carol. Deutschen Akademie der Naturforscher 87, 230–370.

Walker, J.D., Geissman, J.W., 2009. (Compilers). Geologic Time Scale: Geological Society of America, doi:10.1130/2009.CTS004R2C© 2009. The Geological Society of America.

# APPENDIX 2

## A new look at ichthyosaur long bone microanatomy and histology: implications for their adaptation to an aquatic life

Authors: Houssaye A., Scheyer T. M., Kolb C., Fischer V., Sander P. M.
Publication: 2014, *PLoS ONE,* 9(4):e95637.
Contributions: AH and PMS conceived and designed the study/experiments, AH performed the experiments, AH and PMS analysed the data, AH, CK, PMS, TMS, and VF contributed reagents/materials/analysis tools, AH wrote the manuscript, and AH, CK, PMS, TMS, and VF critically reviewed the manuscript.

OPEN ACCESS Freely available online

PLOS | ONE

# A New Look at Ichthyosaur Long Bone Microanatomy and Histology: Implications for Their Adaptation to an Aquatic Life

**Alexandra Houssaye[1]*, Torsten M. Scheyer[2], Christian Kolb[2], Valentin Fischer[3], P. Martin Sander[1]**

**1** Steinmann-Institut für Geologie, Mineralogie und Paläontologie, Universität Bonn, Bonn, Germany, **2** Paläontologisches Institut und Museum der Universität Zürich, Zürich, Switzerland, **3** Geology department, University of Liège, Liège, Belgium

## Abstract

***Background:*** Ichthyosaurs are Mesozoic reptiles considered as active swimmers highly adapted to a fully open-marine life. They display a wide range of morphologies illustrating diverse ecological grades. Data concerning their bone microanatomical and histological features are rather limited and suggest that ichthyosaurs display a spongious, "osteoporotic-like" bone inner structure, like extant cetaceans. However, some taxa exhibit peculiar features, suggesting that the analysis of the microanatomical and histological characteristics of various ichthyosaur long bones should match the anatomical diversity and provide information about their diverse locomotor abilities and physiology.

***Methodology/Principal Findings:*** The material analyzed for this study essentially consists of mid-diaphyseal transverse sections from stylopod bones of various ichthyosaurs and of a few microtomographic (both conventional and synchrotron) data. The present contribution discusses the histological and microanatomical variation observed within ichthyosaurs and the peculiarities of some taxa (*Mixosaurus*, *Pessopteryx*). Four microanatomical types are described. If *Mixosaurus* sections differ from those of the other taxa analyzed, the other microanatomical types, characterized by the relative proportion of compact and loose spongiosa of periosteal and endochondral origin respectively, seem to rather especially illustrate variation along the diaphysis in taxa with similar microanatomical features. Our analysis also reveals that primary bone in all the ichthyosaur taxa sampled (to the possible exception of *Mixosaurus*) is spongy in origin, that cyclical growth is a common pattern among ichthyosaurs, and confirms the previous assumptions of high growth rates in ichthyosaurs.

***Conclusions/Significance:*** The occurrence of two types of remodelling patterns along the diaphysis, characterized by bone mass decrease and increase respectively is described for the first time. It raises questions about the definition of the osseous microanatomical specializations bone mass increase and osteoporosis, notably based on the processes involved, and reveals the difficulty in determining the true occurrence of these osseous specializations in ichthyosaurs.

**Citation:** Houssaye A, Scheyer TM, Kolb C, Fischer V, Sander PM (2014) A New Look at Ichthyosaur Long Bone Microanatomy and Histology: Implications for Their Adaptation to an Aquatic Life. PLoS ONE 9(4): e95637. doi:10.1371/journal.pone.0095637

**Editor:** Andrew A. Farke, Raymond M. Alf Museum of Paleontology, United States of America

**Received** January 23, 2014; **Accepted** March 27, 2014; **Published** April 21, 2014

**Funding:** AH acknowledges financial support from the Alexander von Humboldt Foundation, TMS from the Swiss National Science Foundation (grant no. 31003A 146440), and CK from the DAAD (D/09/46969). The funders had no role in study design, data collection and analysis, decision to publish, or preparation of the manuscript.

**Competing Interests:** The authors have declared that no competing interests exist.

* E-mail: houssaye@mnhn.fr

## Introduction

Ichthyosaurs represent one of the most successful groups of Mesozoic marine reptiles, as shown by their cosmopolitan distribution and their extensive fossil record [1–3]. They lived from the Early Triassic to the early Late Cretaceous, *i.e.* from about 245 to 90 million years ago. Ichthyosaurs are among the first air-breathing vertebrates that adapted to a pelagic life style [3]. These latter forms are considered as the reptiles most strongly morphologically adapted to a fully open-marine life. Among extant aquatic amniotes, only cetaceans are as highly modified for a pelagic lifestyle as ichthyosaurs were. Ichthyosaurs appear thus as a particularly interesting group to understand the evolutionary processes involved in secondary adaptation to an aquatic life.

Although ichthyosaurs are very often represented as dolphin-like or tuna-shaped, they display a wide range of morphologies illustrating diverse ecological grades. The earliest forms, showing a long, slender body with a straight and long tail (cf. *Utatsusaurus*), were probably anguilliform swimmers [4]. Conversely, most of the post-Triassic forms display a fusiform stiff body with an upright bilobate (fish-like) tail on a narrow peduncle (cf. *Stenopterygius*) and are considered as thunniform swimmers [5], whereas the Middle Triassic taxon *Mixosaurus* displays an intermediary pattern [4]. Several additional intermediary morphologies between these two 'extremes' (with differences for example in body size, shape, elongation and flexibility) were illustrated (e.g., [6,7]).

Bone microanatomical organization mainly relies on the biomechanical constraints undergone by organisms (e.g., [8–12]). The analysis of the microanatomical characteristics of various ichthyosaur long bones should thus provide information about their locomotor abilities. Data concerning ichthyosaur bone microanatomical and histological features consist only of a few long bone, vertebra and rib sections (except for *Mixosaurus*, for which more bones were analyzed; see [13]) of *Utatsusaurus*, *Mixosaurus*, *Pessopteryx*, *Caypullisaurus*, *Mollesaurus*, *Stenopterygius*, *Ichthyosaurus* and *Platypterygius* (misidentified as *Ichthyosaurus* by Kiprijanoff, [14]) [13,15–24]. Although representing several genera, the data are too heterogeneous to permit significant intrageneric comparisons, as well as homologous intergeneric ones.

A comment on *Pessopteryx* is in order here because it is noteworthy that this material was assigned to *Omphalosaurus* in earlier histological studies [18,19]. *Pessopteryx* is a taxon erected by Wiman [25] for cranial and limb material found together in the Lower Triassic of Spitsbergen. The cranial part of this material is now assigned to the possible ichthyosaur *Omphalosaurus* [26], whereas the limb material is considered to pertain to an ichthyosaur for which the name *Pessopteryx nisseri* seems most appropriate [2,27,28]. However, the possibility cannot be excluded that the limb bones do belong to the same taxon as the cranial material, after all. In addition, the systematic affinities of *Omphalosaurus* remain controversial because it is either one of the most primitive ichthyosaurs [26,29] or the sister group of Ichthyosauria [30]. Inclusion of *Pessopteryx* in this study seems justified because its histology will be informative under either phylogenetic hypothesis and because of the important earlier work that was done on its histology under the ichthyosaur affinity hypothesis [18,19].

Based on the data available, it is currently generally considered that ichthyosaurs display a spongious, 'osteoporotic-like' bone inner structure, *i.e.* that their inner bone structure is characterized by a loss of bone, a pattern exemplified by extant cetaceans [31–33]. It must be pointed out that this broad statement relies on the analysis of only a few sections and has been generalized for all ichthyosaurs. Buffrénil and Mazin [19] described differences in the limb microanatomy between *Pessopteryx* (*Omphalosaurus* in their study) on the one hand and *Ichthyosaurus* and *Stenopterygius* on the other hand, notably consisting of the occurrence of a small free medullary cavity and of cyclical growth in *Pessopteryx*. It should also be noted that the '*Ichthyosaurus*' humerus of the study of Buffrénil and Mazin [19] is Kimmeridgian in age and actually closely resembles the humerus of ophthalmosaurine ophthalmosaurids, a clade of highly derived ichthyosaurs [34]. Moreover Kolb et al. [13] observed a relatively higher inner compactness in *Mixosaurus*, as compared to the other ichthyosaurs, which they interpreted as a possible characteristic of a near-shore or shelf habitat. Bone microanatomy appears thus to confirm the diversity observed based on anatomical features within ichthyosaurs.

The aim of this study is to discuss these various hypotheses based on the analysis of new material (and of previously analyzed sections) encompassing various ichthyosaur taxa. It discusses the histological and microanatomical variations observed within ichthyosaurs, notably along the diaphysis, but also the peculiarities of some taxa.

## Materials and Methods

We are very thankful to R. Schoch (Staatliches Museum für Naturkunde Stuttgart, Stuttgart, Germany), H. Furrer (Paläontologisches Institut und Museum der Universität, Zurich, Switzerland), R. Hauff (Urwelt-Museum Hauff, Holzmaden, Germany), and S. Stuenes (Paleontological Museum of Uppsala University, Uppsala, Sweden) for the loan of specimens and permission to section, to O. Dülfer and R. Hofmann (Steinmann-Institut, Universität Bonn, Bonn, Germany) for the preparation of casts and thin sections, and to J. Lindgren (Lund University, Sweden) for the loan of some sections.

The material essentially consists of sections from humeri and femora (Table 1) because stylopodial bones have a stronger ecological signal than zeugopodial ones [35,36]. Material from various ichthyosaurs could be accessed for histological investigations and was thus analyzed: *Mixosaurus*, *Temnodontosaurus*, *Ichthyosaurus*, *Stenopterygius*, and *Ophthalmosaurus*, as well as *Pessopteryx* (Table 1). The six taxa sampled encompass the breadth of ichthyosaurian phylogeny, with all major lineages being represented.

Some sections were already made for previous studies [13,19]; see Table 1. All sections are mid-diaphyseal transverse sections and were processed using standard procedures (see [13]). Prior to sectioning, most new specimens were photographed and cast. Sections were observed under a Leica DM 2500 compound polarizing microscope equipped with a Leica DFC 420C digital camera, scanned at high resolution (i.e., between 6400 and 12800 dpi) using an Epson V750-M Pro scanner and transformed into binary images using Photoshop CS3 (where black and white represent bone and cavities respectively). Compactness was calculated by means of the software ImageJ [37]. However, for several sections, compactness was difficult to estimate because the bone underwent some crushing during fossilization. This process is naturally more intense in the less compact parts of the bone. Taking into consideration this crushing, approximate compactness indices were calculated as an estimate. The bone maximal diameter was measured directly on the sections.

In addition, three humeri (*Ichthyosaurus* IPB R222, IPB R 216 and *Ophthalmosaurus* ULg 2013-11-19) and one femur (*Stenopterygius* IPB R 633) were scanned using a high-resolution helical CT scanner (GEphoenix|X-ray v|tome|xs, resolution between 40.7 and 77.1 µm) at the Division of Paleontology, Steinmann Institute for Geology, Mineralogy, and Paleontology, University of Bonn (Germany). Moreover, in order to obtain a better contrast between bone and the infilling sediment, the *Ophthalmosaurus* ULg 2013-11-19 humerus was scanned using phase contrast at the European Synchrotron Radiation Facility (ESRF, Grenoble, France) on the beamline BM5 (resolution: 28.4 µm, reconstructions performed using a phase retrieval approach based on Paganin's algorithm; see [38]). Image segmentation and visualization were performed using VG-Studio Max (Volume Graphics) version 2.0. and 2.2.

## Results

### (a) Microanatomical features

All bones analyzed are spongious without a medullary cavity (except for already published sections of *Pessopteryx*). However, distinct microanatomical patterns occur between taxa, but also within a single taxon and even within a single bone.

**Humeri.** *Mixosaurus* sections differ from those of the other taxa analyzed. The sections essentially consist of a loose spongiosa surrounded by a layer of compact cortical bone (Microanatomical Type [MiT] 0; see [13]; Fig. 1A). This rather compact cortical bone, its thickness and the looseness of the spongiosa (i.e., few trabeculae surrounding rather large intertrabecular spaces) differ from what is observed in the other taxa (notably the thinner and more numerous trabeculae surrounding smaller and more numerous intertrabecular spaces).

Concerning the other taxa, variation also occurs: Some sections almost exclusively consist of a relatively loose spongiosa with randomly shaped (especially in the medullary region) intertrabecular spaces, surrounded by a relatively thin compact peripheral layer exhibiting rather small cavities (Fig. 1F). Conversely, other

**Table 1.** List of the material analyzed in this study.

| Taxon | Coll. Nb. | Locality/Stratigraphy | B | C | MD | MiT |
|---|---|---|---|---|---|---|
| *Ichthyosaurus* | PIMUZ A/III 843 | No information | H | 68.0 | 15 | - |
| | IPB R222 | Lyme Regis, Dorset, England | H | 68.5 | 29 | 2 |
| | | Lower Jurassic | | | | |
| | SMNS Unnumbered | Lyme Regis, Dorset, England | H | 83.3 | 39 | 1 |
| | | Lower Jurassic | | 87.5 | | |
| | LO 11904t | Lyme Regis, Dorset, England | F | 68.3 | 16 | 2 |
| | | Lower Jurassic | | | | |
| | SMNS Unnumbered | Holzmaden, Baden Wurttemberg, Germany | F | 51.3 | 9 | 2 |
| | | Lower Jurassic | | | | |
| | IPB R216 | Lyme Regis, Dorset, England | F | | 34 | 1 |
| | | Lower Jurassic | | | | |
| *Mixosaurus* | PIMUZ T5844 [13] | Monte San Giorgio, Ticino, Switzerland | H | 73.3 | - | 0 |
| | | Middle Triassic | | 78.1 | | |
| | PIMUZ T2046 [13] | Monte San Giorgio, Ticino, Switzerland | H | 60.9 | - | 0 |
| | | Middle Triassic | | 62.4 | | |
| | | | F | 52.4 | | |
| *Pessopteryx* | PMU uncatalogued | Spitsbergen | E | 60.5 | 35 | 2 |
| | | Lower Triassic | | 54.0 | | |
| *Ophthalmosaurus* | SMNS 10170 | Lower Oxford Clay, England | H | 78.1 | 85 | 1 |
| | | Peterborough Member, Middle Jurassic | | 76.5 | | |
| | ULg 2013-11-19 | Kimmeridgian, Dorset, England | H | - | 43 | - |
| | | Kimmeridge Clay Fm. | | | | |
| *Stenopterygius* | SMNS 81194 | Staatswald Ohmden, Kirschmann quarry, Germany | H | 73.7 | 31 | 1–2 |
| | | Early/Lower Toarcian, Lower Jurassic | | 79.6 | | |
| | SMNS A [19] | Holzmaden, Baden-Wurttemberg, Germany | H | 55.3 | 42 | 3 |
| | SMNS 50093 | Lower Jurassic | H | 71.5 | 24 | - |
| | SMNS 50328 | | H | 58.1 | - | 2 |
| | SMNS B [19] | | F | 63.6 | 22 | 2 |
| | IPB R633 | Holzmaden, Baden-Wurttemberg, Germany | F | - | - | - |
| | | Lower Jurassic | | | | |
| *Temnodontosaurus* | PIMUZ SMNS 50329 | No information | H | 57.3 | 53 | 2 |
| | | | | 56.4 | | |
| | | | F | - | 44 | 2 |

B: bone, H: humerus, F: femur, E: epipodial indet.; C: compactness (in %), MD: maximal diameter (in mm), MiT: microanatomical type. The included references refer to papers where some sections, which were reanalyzed in the present study, were previously described. IPB: Institute for Paleontology, University of Bonn, Germany; LO: Lund Original, Department of Geology, Lund University, Sweden; PIMUZ: Paläontologisches Institut und Museum, Universität Zürich, Switzerland; SMNS: Staatliches Museum für Naturkunde Stuttgart, Germany; ULg: Palaeontological Collections, Université de Liège, Belgium.

doi:10.1371/journal.pone.0095637.t001

sections correspond to a relatively compact spongiosa with small cavities (even in the core of the section) displaying a circumferential organization in the outer and inner cortex and being randomly shaped and oriented in the core (Fig. 1B–C). Various sections are intermediate between these two 'extremes' with a variable percentage of the medullary region consisting of a relatively loose poorly organized spongiosa, whereas the surrounding spongiosa exposes a rather laminar organization (Fig. 1D–E).

These various patterns are usually observed within a single genus and are thus not correlated with taxonomy. Moreover, they are correlated neither with species size, nor with ontogeny (size being estimated from section maximal diameter; see Table 1). Observation of two sections taken at a very short distance at bone mid-diaphysis highlighted already significant differences in the respective proportion of the unorganized versus laminar spongiosae and thus suggested important variability along the diaphysis. Indeed, if all sections are mid-diaphyseal, they probably do not all exactly correspond to the same homologous plane. The reference plane, or 'perfect' mid-diaphyseal section, is the one intercepting the point where growth originated and where all the bone originally consisted of periosteal bone. Virtual longitudinal and transverse sections from the specimens scanned highlighted the important difference in the thickness of the compact bone layer of periosteal origin along the diaphysis and the important resulting differences in microanatomical organization (Fig. 2). The parts

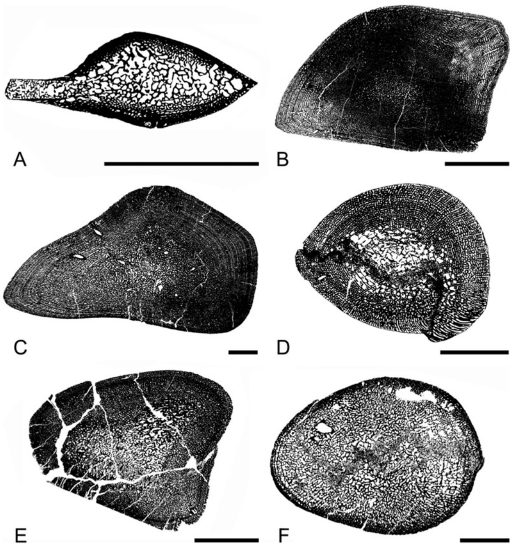

**Figure 1. Schematic drawings illustrating the microanatomical types observed in ichthyosaur humeri.** A, *Mixosaurus* PIMUZ T 2046; B, *Ichthyosaurus* SMNS Unnumbered; C, *Ophthalmosaurus* SMNS 10170; D, *Ichthyosaurus* IPB R222; E, *Stenopterygius* SMNS 81194; F, *Stenopterygius* SMNS A; A: Microanatomical type (MiT) 0; B–C: MiT1; D–E: MiT2; F: MiT3. Scale bars equal 10 mm.
doi:10.1371/journal.pone.0095637.g001

where the spongiosa is looser are naturally less resistant during diagenesis and, as a result, are often crushed.

Compactness indices for the humerus vary from 55.3% in the *Stenopterygius* section SMNS A to 87.5% in the *Ichthyosaurus* section SMNS Unnumbered A.

**Femora.** The organization of the few femora available appears similar to that observed in the humeri and the same variations seem to occur (Fig. 3A–B). Compactness indices range from 51.3 to 68.3%.

**Epipodials.** *Pessopteryx* epipodials show an organization similar to that observed in the humeri analyzed (except *Mixosaurus*; Fig. 3C). Compactness indices were estimated between 54.0% and 60.5%.

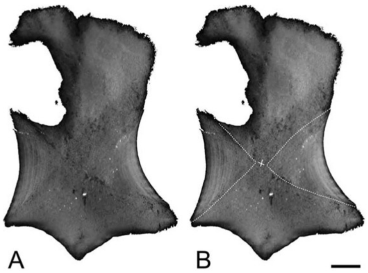

**Figure 2. Virtual longitudinal sections of the humerus of *Ophthalmosaurus* ULg 2013-11-19I.** The dotted lines indicate the transition between the osseous tissues of periosteal (left-right) and endochondral (top-bottom) origin. Note the visible LAGs on the primary periosteal bone. The cross indicates the point of origin of growth. Scale bars equal 10 mm.
doi:10.1371/journal.pone.0095637.g002

### (b) Histological features

Various histological features are observed depending on the sections. As differences between the different types of bones appear rather inconsequential, all bones are hereafter described together.

We first focus on the most compact sections, with no or almost no central area of rather loose spongiosa, which are therefore considered to expose only spongiosa of periosteal origin (MiT 1; e.g., *Ichthyosaurus* SMNS Unnumbered, *Ophthalmosaurus* SMNS 10170; see Table 1). In these sections, cortical bone consists of fibro-lamellar bone, i.e., a matrix of woven-fibered bone – as shown by the isotropy of the tissue and by the large irregularly shaped and randomly oriented osteocyte lacunae – with numerous primary osteons (Fig. 4A–B). The primary osteons are longitudinally oriented and organized in circumferential layers. Numerous anastomoses occur; they are, depending on the position on the section, essentially circular, or circular and radial, thus characterizing a laminar or plexiform tissue (see [39]; Fig. 4B). Locally, primary osteons can also be essentially radially oriented, thus characterizing radiating fibro-lamellar bone. Primary bone can also locally consist of 'unusual parallel-fibered bone' sensu [40] that is parallel-fibered bone with large, randomly shaped and oriented osteocyte lacunae (Fig. 4C). Resorption is limited in the outermost cortex, so that remains of primary bone are abundant (Fig. 4B), but increases toward the core of the section. Remodelling is generally important; secondary bone essentially consists of parallel-fibered bone. Numerous secondary osteons occur. Important centripetal bone deposits of lamellar or parallel-fibered bone fill the vascular and intertrabecular spaces, so that the spongiosa is secondarily compacted (Fig. 4D–E). As a result, most of the section almost exclusively consists of a dense network of primary and secondary bone in the outer cortex and of secondary bone with interstitial remains of woven-fibered bone in its core (Fig. 4D–E).

In sections with a significant area of loose spongiosa, i.e. of supposed endochondral spongiosa (MiT 2; e.g., *Ichthyosaurus* R222; *Pessopteryx* epipodial; Table 1; Fig. 1D–E), primary bone also essentially consists of fibro-lamellar bone (Fig. 4F–H). However, the laminar or plexiform organization, as well as radiating fibro-lamellar bone, only occur in the outer cortex (Fig. 4F–G), i.e. in the spongiosa of periosteal origin. Important remains of primary woven bone are observed in the core of the trabeculae (Fig. 4H). As in MiT 1, parallel-fibered bone (or unusual parallel-fibered bone) also locally occurs (Fig. 4I–J). In the periphery, some vascular spaces are not yet filled with lamellar bone deposits and thus do not yet consist of primary osteons (Fig. 4J). In the core of the section, i.e., in the spongiosa of endochondral origin, remodelling is intense and characterized by an imbalance between bone resorption and reconstruction with a resorption prevalence. As a result, the deep spongiosa, where trabeculae are almost exclusively made of secondary lamellar bone, is loose. Secondary osteons occur in both areas.

In some sections (MiT 3; *Stenopterigius* SMNS A; Table 1; Fig. 1F), the circumferential organization is absent or only occurs in the outermost cortex (Fig. 5A,E). The cortex is very thin and consists of primary woven-fibered bone with primary and secondary osteons rather randomly distributed and with random size and shapes (Fig. 5B). Remains of primary bone quickly diminish away from the bone periphery and are absent in the core of the section (Fig. 5C–D). Remodelling is very intense, even in the outer (but not outermost) cortex. In the *Ichthyosaurus* section PIMUZ A/III 843, the outer cortex essentially displays primary and numerous secondary osteons and restricted remains of

**Figure 3. Sections of ichthyosaur long bones.** A–B, *Ichthyosaurus* femora; A, LO 11904t; B, SMNS Unnumbered. C, *Pessopteryx* epipodial PMU uncatalogued. Scale bars equal 10 mm.
doi:10.1371/journal.pone.0095637.g003

primary bone (Fig. 5F). The latter diminish centripetally and are almost absent in the core of the section, where remodelling is characterized by a resorption prevalence, and which is thus much looser than the cortex (Fig. 5G–H). The core of the section corresponds to Haversian tissue. Such sections are considered as essentially exposing spongiosa of endochondral origin, surrounded by a very thin layer of periosteal bone. The outermost cortex is mostly compact, with areas deprived of any vascularization.

Several sections (see Fig. 6) display evidence of cyclical bone deposition. Indeed, some layers with large intertrabecular spaces alternate with layers characterized by spaces of much lower size, thus probably illustrating a slowing in growth (Fig. 6A). These features are rarely observable on the whole section. They are generally localized, probably as a result of bone remodelling, which prevents their use for skeletochronological analyses. Some sections display in their outer cortex a vascularized layer deposited after an avascular one, which clearly suggests that growth resumed after a slow-down (Fig. 6B).

## Discussion

### (a) Histological features

The cortical spongiosa of *Ichthyosaurus* and *Stenopterygius* was described as resulting from the inner resorption of primary compact tissues, and thus as being secondary in origin, as opposed to that of *Pessopteryx*, which was assumed to be of primary origin [19]. Our study shows that primary bone in all the ichthyosaurian taxa sampled (to the possible exception of *Mixosaurus*, whose microanatomical organization appears peculiar within ichthyosaurs) is spongy in origin.

The presence of highly vascularized fibrolamellar bone confirms the previous observations to suggest high growth rates in ichthyosaurs (see [41] for details).

### (b) Microanatomical variation along the diaphysis

Our analysis reveals an important diversity in microanatomical organization among ichthyosaur long bones, which is not correlated with size. The analysis of virtual longitudinal sections of the long bones scanned (see Material and Methods section) revealed an important change in microanatomy along the diaphysis, which probably explains the variations observed.

The transition from the rather compact to the looser spongiosa illustrates the transition between the spongiosa of periosteal and endochondral origin respectively. Such a variation in proportion, along the diaphysis, between the two types of spongiosa, exhibiting important differences in compactness, was already described in *Pessopteryx* [18]. However, even the periosteal spongiosa was not previously described as particularly compact.

The denser sections, exhibiting only a spongiosa of periosteal origin (MiT 1), are considered to correspond to the 'perfect' mid-diaphyseal sectional plane, i.e. the one intersecting the point of origin of growth. In these sections, remodelling is active, especially in the medullary area, and characterized by excessive secondary bone deposits filling the intertrabecular spaces, coupled with a slight inhibition in primary bone resorption, notably in the outer cortex, conferring to the whole section a high compactness. In the sections that are considered the further away from the 'perfect' mid-diaphyseal sectional plane (MiT 3), and which are assumed to essentially consist of a spongiosa of endochondral origin, remodelling is active and characterized, notably in the medullary area, by a reconstruction deficit, so that the spongiosa is more loosely organized. Bone remodelling varies thus strongly locally along the diaphysis, as these two transverse sectional planes are close in the ichthyosaur bones, which characteristically exhibit a short diaphysis.

A deficit in secondary bone deposits during remodelling generally characterizes what has been called an osteoporotic-like pattern, responsible for a decrease in bone mass [32]. Conversely, additional deposits filling the intertrabecular spaces correspond to one pattern of osteosclerosis, engendering bone mass increase (cf. [42]). Various bones from a single skeleton can display these two types of osseous specializations (e.g., bone mass increase in the rostrum of *Mesoplodon*; probably bone lightening in its long bones; [43]). However, the two types of remodelling patterns have never been described in a single bone yet. Our study thus raises questions about the definition of these specializations, notably based on the processes involved.

Based on MiT 3 sections, it was previously suggested that ichthyosaurs, like modern cetaceans, displayed osteoporotic-like bones [19,32]. The lowest compactness indices obtained in our sample are slightly above 50% (51.3 and 52.4% in *Ichthyosaurus* and *Mixosaurus* femora, 54% in a *Pessopteryx* epipodial and 55.3% in a *Stenopterygius* humerus; see Table 1). These values, although among the lowest values within amniotes, are not particularly low, as several amniote taxa display similar compactness indices in their humeri and femora (cf. [44]). These bones thus do not seem to illustrate a true osteoporotic-like pattern. They are indeed not really characterized by a loss in bone mass, but rather by a spongious organization, with the absence of a medullary cavity. The highest compactness indices in the sections studied, range around 80–85% (83.3 and 87.5% in *Ichthyosaurus*, 78.1% in *Mixosaurus*, 78.1 and 76.5% in *Ophthalmosaurus*). These values are

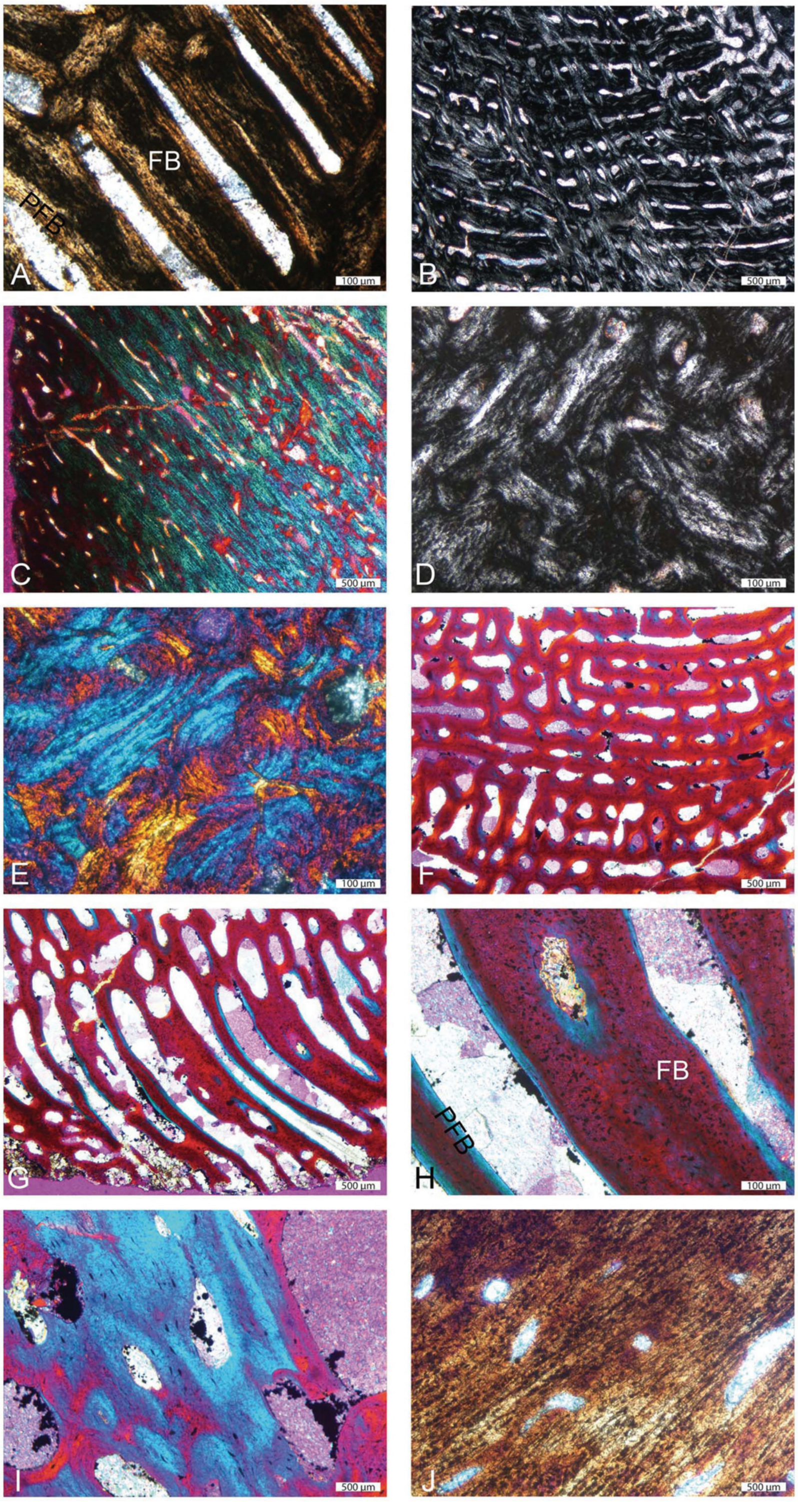

**Figure 4. Histological features of ichthyosaur humeral sections.** A–C and D–E, *Ichthyosaurus* SMNS Unnumbered outer and inner parts of the section respectively. A, primary fibrolamellar bone (FLB) in natural light (NL); note the isotropic nature of the primary fibrous bone (FB); B, FLB in polarized light (PL) illustrating the variable orientations of the primary osteons; C, 'unusual parallel-fibered bone' (UPFB) in PL with gypsum filter; D–E, extremely compact core of the section made of almost exclusively secondary bone in PL and PL with gypsum filter. F–I, *Ichthyosaurus* IPB R222 outer

cortex. J, *Ichthyosaurus* SMNS Unnumbered outer cortex. F–H, primary FLB in PL with gypsum filter; F, laminar organization; G, radiating FLB; H, important amount of primary FB in the osseous trabeculae. I–J, UPFB in I, PL with gypsum filter and J, NL respectively; note the occurrence of simple vascular canals. FB: fibrous bone; PFB: parallel-fibered bone.
doi:10.1371/journal.pone.0095637.g004

rather high within amniotes (cf. [44]) but, again, bones that are clearly osteosclerotic usually display much higher values (cf. [44]).

As a consequence, if based on one or another type of diaphyseal section it would be tempting to attribute an osteoporotic-like or osteosclerotic state to these bones, this would probably be a mistake. It would appear logical to determine the possible occurrence of a microanatomical specialization based on the whole bone general organization. Mid-diaphyseal sections are used as reference planes for long bones as they typically reflect the three-dimensional organization. However, this does not seem to be the case in ichthyosaurs, which complicates the understanding of their microanatomical specialization.

In ichthyosaurs, except in some specimens of *Pessopteryx* [18,19], the long bones have clearly lost the medullary cavity. The general organization appears thus spongious, with no layer of highly compact bone, with the exception of a very thin one in the bone periphery of some specimens. If the spongiosa is much compacted in the 'perfect' mid-diaphyseal plane, it is much looser farther away from this plane.

Remodelling in the periosteal and endochondral areas appears thus characterized by an increase and decrease in bone compactness respectively. These antagonistic processes impede the attribution of a general type of specialization to the whole bone. It seems thus more cautious not to try to name this atypical microanatomy based on the specializations already described in other taxa.

As opposed to the condition described above, the microanatomical organization is overall homologous along the diaphysis in most amniotes, even in other efficient swimmers like cetaceans ([45,46,47]; A.H. pers. obs.). However, it must be pointed out that such a change also seems to occur in a few taxa, like the sea otter *Enhydra lutris* [47] or some plesiosaurs [48]. A compacted mid-shaft usually results from either an inhibition of primary periosteal bone resorption or from increased secondary bone deposition during remodelling. However, it is usually associated with an increase in compactness of the spongiosa of endochondral origin, which is not the case in ichthyosaurs. Our study reveals the interest of analyzing the possible occurrence of variations in microanatomical organization along the diaphysis in active swimmers characterized by short shafts, and notably the processes involved, in order to see if this phenomenon is specific to ichthyosaurs or not.

Bone microanatomy is generally considered to reflect the physical constraints of locomotion (see e.g., [8,10,11,49]. Bone mass increase is considered to be an adaptation for hydrostatic buoyancy and body trim control in poorly active swimmers living in shallow water environments [42], whereas a spongious light organization generally characterizes active swimmers relying on a hydrodynamic control of buoyancy and body trim and requiring good manoeuvrability and acceleration abilities [32,42]. A spongious organization with a compacted central area has never been described in any extant or extinct taxon so far. As a consequence, it appears too early to try to infer any specifically associated functional requirement.

### (c) Specificity of *Pessopteryx*

All long bones of *Pessopteryx* (humerus, femur, tibia) were described as displaying a small medullary cavity [18,19], which was interpreted as a specificity of this taxon among Ichthyosauria. However, we did not observe a medullary cavity in the epipodial bone of *Pessopteryx* analyzed.

Remodelling was described as relatively limited in *Pessopteryx*, as compared to the more derived *Ichthyosaurus* and *Stenopterygius* [19]. However, our analysis shows a high degree of remodelling in *Pessopteryx* epipodial bones, as in the other ichthyosaurs.

In addition, the bones of *Pessopteryx* were described as showing histological evidence of cyclic growth, which were considered absent in *Ichthyosaurus* and *Stenopterygius* [19]. The evidence of cyclic growth is suggested in sections of several ichthyosaurs, although the cycles are generally not continuous and thus cannot be used in skeletochronology (like the LAGs in *Mixosaurus* sections; see below, [13]). These observations nevertheless reveal that cyclical growth is a common pattern among ichthyosaurs but, as it is only observable in the primary spongiosa of periosteal origin, it is not seen in all sections, which probably resulted in this misinterpretation.

The absence of a marked difference between the histology of *Pessopteryx* and that of the other taxa in this study would be consistent with either a very basal position of this taxon among ichthyosaurs or with this taxon being a sister-group of Ichthyosauria (see above).

### (d) Specificity of *Mixosaurus*

Our study also highlights the clear difference in microanatomical organization between *Mixosaurus* on the one hand, and the other ichthyosaurs from our sample on the other hand. Morphologically, *Mixosaurus* humeri characteristically show an anterior flange, as in many other Triassic ichthyosaurs [50]. But they also differ in their microanatomy. *Mixosaurus* long bones show a peripheral layer of compact cortex clearly distinct from the remainder of the section, which consists of a loose spongiosa [13]. Although it is not clear because of intense distortion, *Utatsusaurus* long bones seem to suggest a microanatomical organization closer to that of the non-*Mixosaurus* ichthyosaurs [23]. Further investigations are required to check the absence of a compacted mid-shaft area in *Mixosaurus* long bones. Another specificity of *Mixosaurus* is that it is the only taxon for which remains of calcified cartilage are observed in the core of sections of presumably new born and juvenile specimens. However, no specimen of similar ontogenetic stage has been analyzed for another taxa yet, so that this peculiarity should be interpreted with caution. Moreover, it is the only taxon showing LAGs [13], which remains unexplained.

It must be pointed out that Kolb et al. [13] described the inner compactness in *Mixosaurus* long bones as relatively high (essentially as a result of the compact outer cortex) and interpreted it as a possible characteristic of a near-shore form or shelf dweller. However, our study shows that *Mixosaurus* bones do not display a higher compactness than the other ichthyosaurs, which challenges this earlier interpretation. The peculiarity of *Mixosaurus* microanatomical features could nevertheless reflect some differences in locomotion mode, which needs further investigations to be specified.

## Conclusions

(1) Important variations are observed between the various ichthyosaur sections. The various patterns do not correlate with taxonomy (except maybe for *Mixosaurus*), species size, or

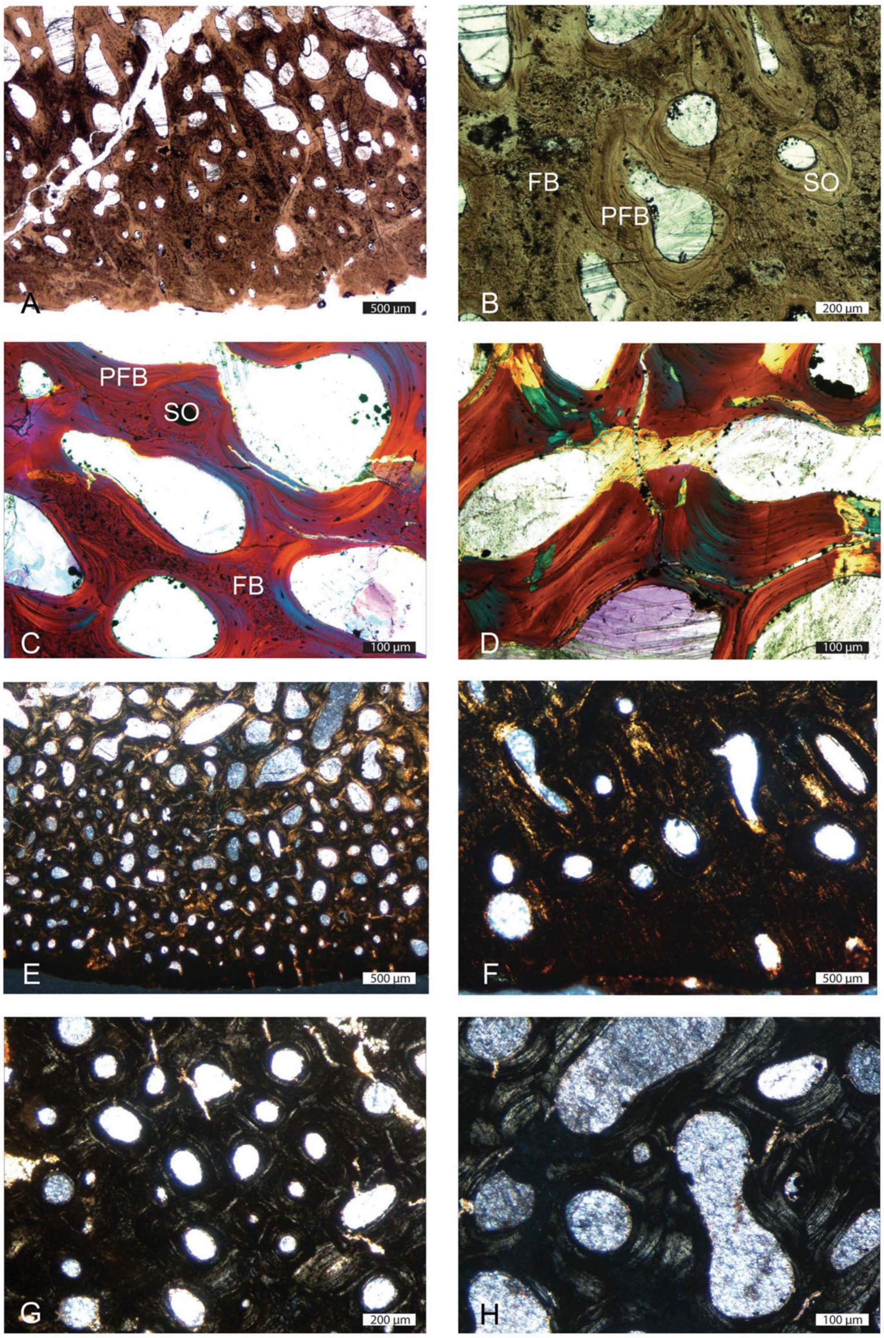

**Figure 5. Histological features of ichthyosaur humeral sections.** A–D, *Stenopterygius* SMNS A; E–H, *Ichthyosaurus* Unnumbered. A,B,E,F outer cortex in natural light with numerous primary and secondary osteons. C, trabeculae slightly away from the bone periphery; note the remains of primary fibrous bone and the secondary lamellar and parallel-fibered bone; D, core of the section; the trabeculae are entirely secondary in origin. G–H, Haversian tissue in the core of the section. FB: fibrous bone; PFB: parallel-fibered bone; SO: secondary osteon.
doi:10.1371/journal.pone.0095637.g005

ontogeny but seem to essentially illustrate a strong variability along the diaphysis.

(2) Two types of remodelling patterns occur along the diaphysis, characterized by bone mass decrease and increase respectively, which has never been described in a single bone before. This result raises questions about the definition of the osseous specializations bone mass increase and osteoporosis, notably based on the processes involved. It suggests that none of these

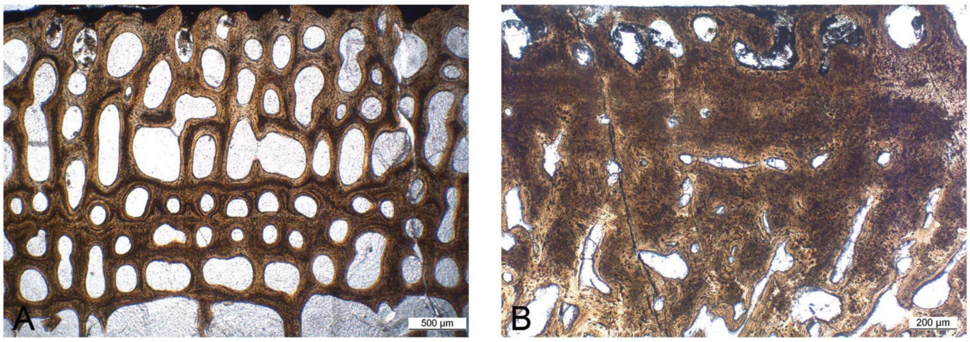

**Figure 6. Cyclicity features in some ichthysaur humeri.** A, *Temnodontosaurus* PIMUZ SMNS 50329; note the alternation of layers with large and small intertrabecular spaces respectively; B, *Stenopterygius* SMNS 50093; note the vascularized layer at the bone periphery (top) following an almost avascular layer.
doi:10.1371/journal.pone.0095637.g006

specializations truly occurs in ichthyosaur long bones and reveals the importance of analyzing the possible occurrence of variations in microanatomical organization along the diaphysis in other active swimmers, in order to see if this peculiarity is specific to ichthyosaurs or not.

(3) Our study shows that primary bone in all the ichthyosaur taxa sampled (to the possible exception of *Mixosaurus*) is spongy in origin and that cyclical growth is a common pattern among these taxa.

(4) Highly vascularized fibrolamellar bone is in accordance with previous assumptions of high growth rates in ichthyosaurs.

## Acknowledgments

We thank N. Bardet (Museum National d'Histoire Naturelle, Paris, France) and M. Talevi (Universidad Nacional de Río Negro, Argentina) for fruitful comments that improved the manuscript, the Steinmann Institut (University of Bonn, Germany) and the European Synchrotron and P. Tafforeau (ESRF, Grenoble, France) for providing beamtime and support, and the Steinmann Institut and UMR 7207 CR2P MNHN CNRS UPMC-Paris6 for 3D imaging facilities.

## Author Contributions

Conceived and designed the experiments: AH PMS. Performed the experiments: AH. Analyzed the data: AH PMS. Contributed reagents/materials/analysis tools: AH CK PMS TMS VF. Wrote the paper: AH. Critical revision of the manuscript: AH CK PMS TMS VF.

## References

1. Sander MP (2000) Ichthyosauria: their diversity, distribution, and phylogeny. Paläont Z 74: 1–35.
2. McGowan C, Motani R (2003) Handbook of Paleoherpetology. Part 8. Ichthyopterygia. Dr. Freidrich Pfeil Verlag, Munich.
3. Motani R (2009) The evolution of marine reptiles. Evo Edu Outreach 2: 224–235.
4. Motani R, You H, McGowan C (1996) Eel-like swimming in the earliest ichthyosaurs. Nature 382: 347–348.
5. Lingham-Soliar T (1998) Taphonomic evidence for fast tuna-like swimming in Jurassic and Cretaceous ichthyosaurs. N Jb Geol Paläont Abh 207: 171–183.
6. Motani R (2008) Combining uniformitarian and historical data to intrepret how earth environment influenced the evolution of ichthyopterygia. In: Kelley PH, Bambach RK, editors. From Evolution to Geobiology: Research Questions Driving Paleontology at the Start of a New Century: Paleontological Society Papers. pp. 147–164.
7. Buchholtz EA (2001) Swimming styles in Jurassic ichthyosaurs. J Vertebr Paleontol 21: 61–73.
8. Turner CH (1998) Three rules for bone adaptation to mechanical stimuli. Bone 23: 399–407.
9. Huiskes R (2000) If bone is the answer, then what is the question? J Anat 197: 145–156.
10. Ruimerman R, Hilbers P, Rietbergen Bv, Huiskes R (2005a) A theoretical framework for strain-related trabecular bone maintenance and adaptation. J Biomech 38: 931–941.
11. Ruimerman R, Rietbergen Bv, Hilbers P, Huiskes R (2005b) The effects of trabecular-bone loading variables on the surface signaling potential for bone remodeling and adaptation. Ann Biomed Engin 33: 71–78.
12. Chappard D, Baslé MF, Legrand E, Audran M (2008) Trabecular bone microarchitecture: A review. Morphologie 92: 162–170.
13. Kolb C, Sánchez-Villagra MR, Scheyer TM (2011) The palaeohistology of the basal ichthyosaur *Mixosaurus* Baur, 1887 (Ichthyopterygia, Mixosauridae) from the Middle Triassic: palaeobiological implications. C R Palevol 10: 403–411.
14. Kiprijanoff AV (1881–83) Studien Fiber die Fossilen Reptilien Russlands. Mémoires de l'Académie Impériale des Sciences, St Petersbourg 7, 1–144.
15. Fraas E (1891) Die Ichthyosaurier der süddeutschen Trias- und Jura-Ablagerungen. Laupp, Tübingen 1–81.
16. Seitz ALL (1907) Vergleichende Studien über den mikroskopischen Knochenbau fossiler und rezenter Reptilien, und dessen Bedeutung für das Wachstum und Umbildung des Knochengewebes im allgemeinen. Nova Acta, Abh. der Kaiserl. Leop.-Carol. Deutschen Akademie der Naturforscher 87: 230–370.
17. Gross W (1934) Die Typen des mikroskopischen Knochenbaues bei fossilen Stegocephalen und Reptilien. Z Anat Entwicklungsgesch 203: 731–764.
18. Buffrénil Vd, Mazin J-M, Ricqlès Ad (1987) Caractères structuraux et mode de croissance du fémur d'*Omphalosaurus nisseri*, ichthyosaurien du trias moyen du Spitzberg. Ann Paléontol 73: 195–216.
19. Buffrénil Vd, Mazin J-M (1990) Bone histology of the ichthyosaurs: comparative data and functional interpretation. Paleobiology 16: 435–447.
20. Talevi M, Fernandez M (2012) Unexpected skeletal histology of an ichthyosaur from the Middle Hurassic of Patagonia: implications for evolution of bone microstructure among secondary aquatic tetrapods. Naturwissenschaften 99: 241–244.
21. Talevi M, Fernandez M, Salgado L (2012) Variacion ontogenetica en la histologia osea de *Caypullisaurus bonapartei* Fernandez, 1997 (Ichthyosauria: Ophthalmosauridae). Ameghiniana 49: 38–46.
22. Maxwell EE, Scheyer TM, Fowler DA (2014) An evolutionary and developmental perspective on the loss of regionalization in the limbs of derived ichthyosaurs. Geol Mag 151: 29–50. (In press)
23. Fernandez M, Talevi M (2014) Ophthalmosaurian (Ichthyosauria) records from the Aalenian–Bajocian of Patagonia (Argentina): an overview Geol Mag 151: 49–59
24. Nakajima J, Houssaye A, Endo H (2014) Osteohistology of *Utatsusaurus hataii* (Reptilia: Ichthyopterygia): Implications for early ichthyosaur biology. Acta Palaeontol Pol. doi: 10.4202/app.2012.0045. (In press)
25. Wiman C (1910) Ichthyosaurier aus der Trias Spitzbergens. Bull Geol Instit Univ Uppsala 10: 124–148.
26. Sander PM, Faber C (2003) The Triassic marine reptile *Omphalosaurus*: osteology, jaw anatomy, and evidence for ichthyosaurian affinities. J Vert Paleontol 23: 799–816.
27. Maisch MW (2010) Phylogeny, systematics, and origin of the Ichthyosauria – the state of the art. Palaeodiv 3:151–214.
28. Maxwell EE, Kear BP (2013) Triassic ichthyopterygian assemblages of the Svalbard archipelago: a reassessment of taxonomy and distribution. GFF 135: 85–94.

29. Sander MP, Faber C (1998) New finds of *Omphalosaurus* and a review of triassic ichthyosaur paleobiogeography. Paläont Z 72: 149–162.
30. Motani R (2000) Is *Omphalosaurus* ichthyopterygian? - A phylogenetic perspective. J Vertebr Paleontol 20: 295–301.
31. Buffrénil Vd, Schoevaert D (1988) On how the periosteal bone of the delphinid humerus becomes cancellous: ontogeny of a histological specialization. J Morphol 198: 149–164.
32. Ricqlès Ad, de Buffrénil V (2001) Bone histology, heterochronies and the return of Tetrapods to life in water: where are we? In: Mazin JM, de Buffrénil V, editors. Secondary Adaptation of Tetrapods to life in Water. München. pp. 289–310.
33. Dumont M, Laurin M, Jacques F, Pellé E, Dabin W, et al. (2013) Inner architecture of vertebral centra in terrestrial and aquatic mammals: a two-dimensional comparative study. J Morphol 274: 570–584.
34. Fischer V, Maisch MW, Naish D, Kosma R, Liston J, et al. (2012) New ophthalmosaurid ichthyosaurs from the European Lower Cretaceous demonstrate extensive ichthyosaur survival across the jurassic-Cretaceous boundary. Plos One 7(1): e29234.
35. Canoville A, Laurin M (2010) Evolution of humeral microanatomy and lifestyle in amniotes, and some comments on palaeobiological inferences. Biol J Linn Soc 100: 384–406.
36. Quemeneur S, Buffrénil Vd, Laurin M (2013) Microanatomy of the amniote femur and inference of lifestyle in limbed vertebrates. Biol J Linn Soc 109: 644–655.
37. Abramoff MD, Magelhaes PJ, Ram SJ (2004) Image Processing with ImageJ. Biophoton Int 11: 36–42.
38. Sanchez S, Ahlberg PE, Trinajstic K, Mirone A, Tafforeau P (2012) Three dimensional synchrotron virtual paleohistology: a new insight into the world of fossil bone microstructures. Microsc Microanal 18: 1095–1105.
39. Francillon-Vieillot H, de Buffrénil V, Castanet J, Geraudie J, Meunier FJ, et al. (1990) Microstructure and Mineralization of Vertebrate Skeletal Tissues. In: Carter JG, editor. Skeletal Biomineralization: Patterns, Processes and Evolutionary Trends. New York. pp. 471–529.
40. Houssaye A, Lindgren J, Pellegrini R, Lee AH, Germain D, et al. (2013) Microanatomical and histological features in the long bones of mosasaurine mosasaurs (Reptilia, Squamata) – Implications for aquatic adaptation and growth rates. Plos One 8(10): e76741.
41. Houssaye A (2013) Bone histology of aquatic reptiles: what does it tell us about secondary adaptation to an aquatic life. Biol J Linn Soc 108: 3–21.
42. Houssaye A (2009) "Pachyostosis" in aquatic amniotes: a review. Integrative Zool 4: 325–340.
43. Buffrenil Vd, Casinos A (1995) Observations histologiques sur le rostre de *Mesoplodon densirostris* (Mammalia, Cetacea, Ziphiidae): le tissu osseux le plus dense connu. Ann Sci Nat, Zool 16: 21–32.
44. Hayashi S, Houssaye A, Nakajima Y, Chiba K, Inuzuka N, et al. (2013) Bone histology suggests increasing aquatic adaptations in Desmostylia (Mammalia, Afrotheria). Plos One 8(4): e59146.
45. Wall WP (1983) The correlation between high limb-bone density and aquatic habits in recent mammals. J Paleontol 57: 197–207.
46. Stein BR (1989) Bone density and adaptation in semiaquatic mammals. J Mammal 70: 467–476.
47. Madar SI (1998) Structural Adaptations of Early Archaeocete Long Bones. In: Thewissen JGM, editor. The Emergence of Whales. New York: Plenum Press. pp. 353–378.
48. Liebe L, Hurum JH (2012) Gross internal structure and microstructure of plesiosaur limb bones from the Late Jurassic, central Spitsbergen. Norwegian J Geol 92: 285–309.
49. Liu XS, Bevill G, Keaveny TM, Sajda P, Guo XE (2009) Micromechanical analyses of vertebral trabecular bone based on individual trabeculae segmentation of plates and rods. J Biomech 42: 249–256.
50. Motani R (1999) Phylogeny of the Ichthypterygia. J Vertebr Paleontol 19: 473–496.

# Curriculum vitae

*Address*
Christian Kolb
Paläontologisches Institut und Museum
Universität Zürich
Karl-Schmid-Strasse 4
8006 Zürich
Switzerland

Phone: +41 (0) 446 34 22 69
Mobile: +41 (0) 774 28 83 05

E-mail: christian.kolb@pim.uzh.ch

## Personal information

| | |
|---|---|
| Birthdate: | August 9, 1979 |
| Birthplace: | Nuremberg, Germany |
| Nationality: | German |
| Family status: | Married, one daughter |

## Education

| | |
|---|---|
| 4/2002–6/2006 | **Diploma in Geology/Palaeontology**<br>University of Bonn, Germany<br>Title of diploma thesis: “Redescription of the Lower Cretaceous ichthyosaur *Platypterygius hercynicus*”; title of diploma mapping project: “Geologische Kartierung im Monte-Rosa-Gebiet und dem obersten Gressoney-Tal” (Italy) |
| 10/1999 –3/2002 | **Intermediate Diploma in Geology/Palaeontology**<br>University of Erlangen-Nuremberg, Germany |
| 9/1990 – 7/1999 | Secondary school – Sigena-Gymnasium in Nuremberg. „Abitur“– diploma qualifying for university admission |

## Academic positions

| | |
|---|---|
| 11/2014 | **Scientific Assistant / PhD student,** Palaeontological Institute and Museum of the University of Zurich, Switzerland |
| 10/2010 | **PhD student**, Palaeontological Institute and Museum of the University of Zurich, Switzerland<br>Title of PhD thesis: “Bone and tooth microstructure in extinct and extant mammals and implications for growth and life history evolution, with an emphasis on cervids as a case study” |
| 5/2010 – 10/2010 | **Scientific Assistant**, Palaeontological Institute and Museum of the University of Zurich, Switzerland |
| 1/2010 – 4/2010 | **DAAD Guest Researcher**, Palaeontological Institute and Museum of the University of Zurich, Switzerland |
| 6/2009 – 12/2009 | **Scientific Assistant**, Palaeontological Institute and Museum of the University of Zurich, Switzerland |
| 9/2008 – 4/2009 | **Scientific Assistant**, General Department of Cultural Heritage Rhineland Palatinate, Mainz, Germany |
| 9/2006– 8/2008 | **Wissenschaftlicher Volontär (Internship, Conservational Assistant)**, General Department of Cultural Heritage Rhineland Palatinate, Mainz |
| 9-11/2001 | **Student Assistant**, Institute for Geology and Mineralogy of the University of Erlangen-Nuremberg |

## Fundraising

| | |
|---|---|
| 10/2012 – 9/2013 | **Forschungskredit** of the University of Zurich |
| 1/2010 – 4/2010 | **DAAD** grant (Deutscher Akademischer Austauschdienst) |

## Honorary activities

| | |
|---|---|
| 10/2002 – 5/2006 | Student representative in the examination board of the geology/palaeontology department of the University of Bonn |
| 7/2002 – 7/2003 | Assistant cash auditor of the students council of the geology/palaeontology department of the University of Bonn |

## Special skills

- Geoscientific preparation (thin sections and air stylus)
- Scientific drawing
- EDP: Microsoft Office®, Adobe Illustrator®, Adobe Photoshop®, Corel Draw®, Corel Photo-Paint®, ImageJ®, Mesquite©, PGIS©
- Languages: German (first language), English (business fluent), French and Latin (school knowledge)
- Driving licence class 3

## Teaching

| | |
|---|---|
| 2012-2014 | “Practical at the museum”/“Integument of vertebrates” (BIO 121, supervision of students), Palaeontological Institute and Museum, University of Zurich |
| 2011-2014 | “Evolutionary Morphology of Vertebrates– Issues and Methods” (BIO 262, co-lecturer and student project supervisor), Palaeontological Institute and Museum, University of Zurich |
| 2012 | Bachelor thesis co-supervision: Schlingemann, M. A. J. 2012. Bone histological growth patterns in fallow deer (*Dama dama*) and extinct deer: implications for island evolution. Leiden University, University of Zurich. |

## Outreach activities (selected)

| | |
|---|---|
| 10/12/2015 | Science trail at the Palaeontological Institute and Museum, University of Zurich (presentation) |
| 2009-2014 | Lange Nacht der Museen (guided tours and other activities), Palaeontological Museum, University of Zurich |
| 2012-2014 | Guided tour: „Fossillagerstätte Monte San Giorgio.” Palaeontological Museum, University of Zurich |
| 2012-2013 | Guided tour (Sonntagsführung): „Urzeitliche Liebe – Geschlechtsunterschiede und Fortpflanzung im Fossilbericht.“ Palaeontological Museum, University of Zurich |
| 13/04/2011 | Talk: „Fischsaurier – Was uns Fossilbericht und Knochenstrukturen über deren Leben erzählen.“ Palaeontological Museum of the University of Zurich |
| 09/2009 | Exhibition: „Auf welchem Ast sitzen wir? Der Baum des Lebens: Vielfalt und Einheit - Darwin year ’09 in RailCity Zürich by UZH/ETH Zürich“ (participation) |

## Field work (selected activities)

| | |
|---|---|
| 10/2009 | Palaeontological fieldwork: Devonian of Morocco (3 weeks) |
| 2008 | Palaeontological excavation: Late Oligocene of Haiger-Langenaubach. General Direction of Cultural Heritage Rhineland Palatinate, Section Geological History of the Earth, Mainz, Germany (2 weeks, leading position) |
| 2007-2008 | Palaeontological excavation: Late Oligocene of Enspel, Germany. General Direction of Cultural Heritage Rhineland Palatinate, Section Geological History of the Earth, Mainz, Germany (8 weeks in total) |
| 07/2005-08/2005 | Palaeontological excavation: Middle Triassic of Winterswijk, The Netherlands. Steinmann Institute of the University of Bonn (10 days) |
| 07/2004-08/2004 | Geological fieldwork: Gressoney valley (Italian Alps). Diploma mapping. Steinmann Institute of the University of Bonn (4 weeks) |

## List of publications

**Kolb C.**, Scheyer T. M., Veitschegger K., Forasiepi A. M., Amson E., van der Geer A. A. E, van den Hoek Ostende L. W., Hayashi S., and M. R. Sánchez-Villagra. 2015. Mammalian bone palaeohistology: a survey and new data with emphasis on island forms. PeerJ 3:e1358. DOI 10.7717/peerj.1358.

Amson, E., **Kolb, C.**, Scheyer, T. M., and M. R. Sánchez-Villaga. 2015. Growth and life history of Middle Miocene deer (Mammalia, Cervidae) based on bone histology. C. R. Palevol (14): 637-645. DOI 10.1016/j.crpv.2015.07.001.

**Kolb, C.**, Scheyer, T. M., Lister, A. M., Azorit, C., de Vos, J., Schlingemann, M. A. J., Rössner, G. E., Monaghan, N. T., and M. R. Sánchez -Villagra. Growth in fossil and extant deer and implications for body size and life history evolution. BMC Evolutionary Biology: 15: 19. DOI: 10.1186/s12862-015-0295-3.

Naglik, C., Monnet, C., Goetz, S., **Kolb, C.**, de Baets, K., Tajika, A., and C. Klug. 2014. Growth trajectories of some major ammonoid sub-clades revealed by serial grinding tomography data. Lethaia 48 (1): 29–46. DOI: 10.1111/let.12085.

Houssaye, A., Scheyer, T. M., **Kolb, C.**, Fischer, V., and P. M. Sander. 2014. A new look at ichthyosaur long bone microanatomy and histology: Implications for their adaptation to an aquatic life. Plosone 9 (4): 1-10, e95637.

**Kolb, C.**, M. R. Sánchez-Villagra, and T. M. Scheyer. 2011. The palaeohistology of the basal ichthyosaur *Mixosaurus* Baur, 1887 (Ichthyopterygia, Mixosauridae) from the Middle Triassic: palaeobiological implications. C. R. Palevol 10 (5-6): 403-411.

**Kolb, C.** and Sander, P. M. 2009. Redescription of the ichthyosaur *Platypterygius hercynicus* (KUHN, 1946) from the Lower Cretaceous of Salzgitter (Lower Saxony, Germany). Palaeontographica A 288: 151-192.

*Conference abstracts/talks*

**Kolb, C.** 2014. Bone and tooth growth in fossil and recent deer and implications for body size and life history evolution. Program and Abstracts of the 74th Meeting of the Society of Vertebrate Paleontology in Berlin, Germany:161. Romer Prize Session.

Veitschegger, K., **Kolb, C.**, Azorit, C. and M. R. Sánchez-Villagra. 2014. Eruption patterns and dental histology in artiodactyls as markers of postnatal growth and life history evolution. Programme and Abstracts of the 4th International Palaeontological Congress in Mendoza, Argentina.

Veitschegger K., **Kolb, C.**, Azorit, C. and M. R. Sánchez-Villagra. 2014. Eruption patterns and dental histology in artiodactyls as markers of postnatal growth and life history evolution. Programme and Abstracts of the 12th Annual Meeting of the European Association of Vertebrate Palaeontologists in Torino, Italy.

**Kolb, C.** 2013. Growth in fossil and recent deer and implications for island evolution. Programme and Abstracts of the 10th International Congress of Vertebrate Morphology in Barcelona, Spain, Anatomical Record (Special Feature) 296:155.

**Kolb, C.**, Schlingemann, M. A. J., Scheyer, T. M., Azorit, C., De Vos, J., and N. T. Monaghan. 2012. Bone and tooth histological growth patterns in fossil and recent deer and their implications for island evolution. Programme and Abstracts of the 60th Annual Symposium of Vertebrate Palaeontology and Comparative Anatomy in Oxford, UK:15.

**Kolb, C.**, de Vos, J., Azorit, C., Scheyer, T. M., and M. R. Sánchez-Villagra. 2012. Knochen- und zahnhistologische Wachstumsmuster der verzwergten Inselhirsches *Candiacervus* aus dem oberen Pleistozän von Kreta. 39. Treffen des Arbeitskreises Wirbeltierpaläontologie, Neustadt, Germany.

**Kolb, C.** 2011. Growth patterns deduced from bone histology of the dwarfed island deer *Candiacervus* from the Late Pleistocene of Crete. Abstract Volume 9th Swiss Geoscience Meeting in Zurich, Switzerland: 312.

**Kolb, C.**, de Vos, J., Scheyer, T. M., and M. R. Sánchez-Villagra.2011. The ontogeny of bone histology in the dwarfed island deer *Candiacervus* from the Late Pleistocene of Crete. Programme and Abstracts of the 9th Annual Meeting of the European Association of Vertebrate Palaeontologists in Heraklion, Greece: 31-32.

**Kolb, C.**, T. M. Scheyer, and M. R. Sánchez-Villagra. 2010. The palaeohistology of the basal ichthyosaur *Mixosaurus* Baur, 1887 (Ichthyopterygia, Mixosauridae) from the Middle Triassic: palaeobiological implications. Programm und Kurzfassungen der 80. Jahrestagung der Paläontologischen Gesellschaft in Munich, Germany, Zitteliana B 29: 62.

**Kolb, C.** 2006. Die Diversität von Ichthyosauriern in der deutschen Kreide – Revision von *Platypterygius hercynicus* KUHN, 1946 (Ichthyosauria: Ophthalmosauridae). 33. Treffen des Arbeitskreises Wirbeltierpaläontologie, Greifswald, Germany.

*Outreach articles/press*

Schindler, T. und **C. Kolb**. 2009. Paläontologische Notbergung in einer Tongrube im Lahn-Dill-Kreis. Pflanzen, Fische und Kaulquappen aus tertiären Vulkanablagerungen. hessenARCHÄOLOGIE 2009: 19-20.

**Kolb, C.** 2009. Museumsportrait: Das "Devonium Waxweiler". Fossilien 6/09: 333-336.

**20 Minuten.** 2015. Knochen verraten die Lebensweise von Urzeit-Tieren, 30.10.2015.

*Exhibition*

**Kolb, C.**, P. Schaefers, T. Bizer, and M. Wuttke. 2008. Der Stöffel-Park - Zukunftsentwicklung im Westerwald. Travelling exhibition of the General Direction of Cultural Heritage Rhineland Palatinate, Section Geological History of the Earth, Mainz, Germany (associated with press releases in local newspapers).